BioMed Research International

Recent Trends in Pharmaceutical Radiochemistry for Molecular PET Imaging

Guest Editors: Olaf Prante, Roland Haubner, and Patrick Riss

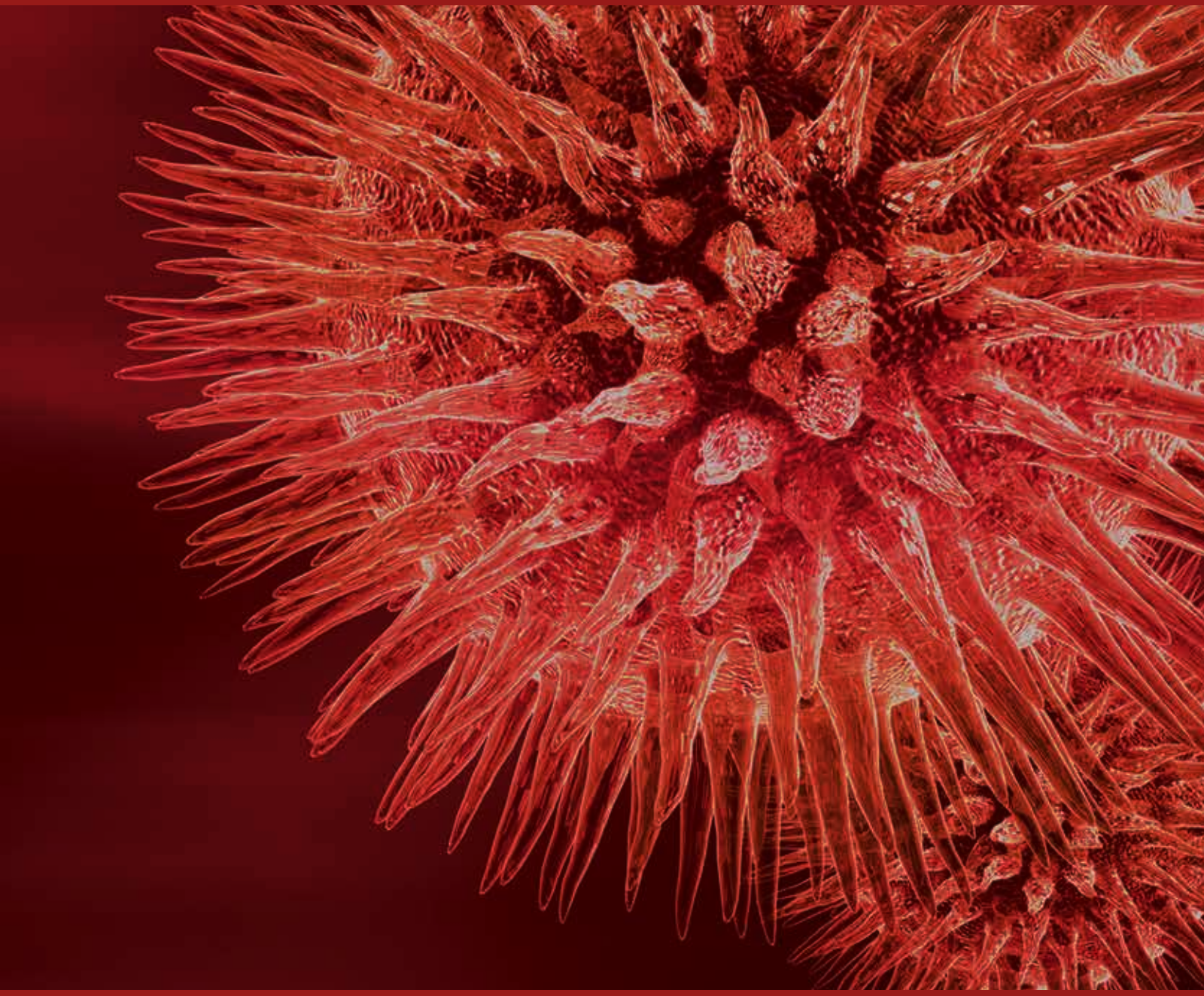

Recent Trends in Pharmaceutical Radiochemistry for Molecular PET Imaging

BioMed Research International

Recent Trends in Pharmaceutical Radiochemistry for Molecular PET Imaging

Guest Editors: Olaf Prante, Roland Haubner, and Patrick Riss

Contents

Hindawi Publishing Corporation
BioMed Research International
Volume 2014, Article ID 890540, 3 pages
http://dx.doi.org/10.1155/2014/890540

Editorial

Recent Trends in Pharmaceutical Radiochemistry for Molecular PET Imaging

Olaf Prante,[1] Roland Haubner,[2] Patrick Riss,[3] and Bernd Neumaier[4]

[1] *Molecular Imaging and Radiochemistry, Department of Nuclear Medicine, Friedrich-Alexander University Erlangen-Nürnberg (FAU), Erlangen, Germany*
[2] *Department of Nuclear Medicine, Medical University Innsbruck, Innsbruck, Austria*
[3] *Department of Chemistry, University Oslo, Oslo, Norway*
[4] *Institute of Radiochemistry and Experimental Molecular Imaging, University Clinic Cologne and Max Planck Institute of Metabolic Research, Cologne, Germany*

Correspondence should be addressed to Olaf Prante; olaf.prante@uk-erlangen.de

Received 10 July 2014; Accepted 10 July 2014; Published 24 July 2014

This Special Issue is dedicated to Professor Heinz H. Coenen on the occasion of his 65th birthday

In the field of radiopharmaceutical research, the development of new radiochemistry methods has been one of the major driving forces for positron emission tomography (PET) imaging during the past decade. The use and availability of the positron emitters C-11, F-18, Ga-68, Cu-64, or Zr-89, to name a few, have enormously increased and, especially in terms of chemoselectivity and radiolabeling efficacy, significant progress has been made. In the field of F-18 chemistry, various click chemistry-based labeling methods, the use of the silicon-fluoride acceptor reagents, and Al-F-NOTA complexes offer an even more simplified strategy to introduce F-18 into biomolecules. These techniques facilitate the syntheses of radiotracers for PET imaging studies and thus accelerate their pronounced use in preclinical studies and even clinical trials. A similar situation is seen in the field of metallic positron emitters, where additional strategies have been developed to extend and to improve radiometal chemistry, for example, by introducing Zr-89 for the labeling of antibodies and long-term imaging studies.

The field of radiopharmaceutical sciences has been mainly influenced by its founders and their pioneering work. One of the scientific pioneers of modern radiochemistry for imaging by PET, Professor Heinz H. Coenen, is celebrating his 65th birthday the same time this special issue was published. He is highly recognized in the field of radiochemistry and molecular imaging and one of the authors of the most cited paper in the field of nuclear medicine and molecular imaging. He has been director of the German Research Center in Jülich for more than 15 years and has been international president of the largest radiopharmaceutical society (Society of Radiopharmaceutical Sciences, SRS).

This special issue describes many important and recent research advancements in PET chemistry that have been influenced by the pioneering work of Professor Heinz H. Coenen. Additionally, this special issue is thought to create awareness of multiple imaging applications of newly developed radiotracers and thereby encourages young researchers to expand their projects and developments by applying these modern techniques. However, it is clearly impossible in an issue of this size to cover all recent developments in PET chemistry.

We do not pretend to be infallible in collecting review papers with such a wide variety of topics. Some of the articles in this special issue were written by former Ph.D. degree students of Professor Coenen and we are sure that especially these research topics were significantly inspired

and motivated by their early scientific work together with Professor Heinz H. Coenen.

We were pleased that Professor Bernd Neumaier, whose scientific mentor has been Professor Heinz H. Coenen, agreed to perform some comments on the different contributions in this special issue.

Olaf Prante
Roland Haubner
Patrick Riss

Foreword by Bernd Neumaier (Institute of Radiochemistry and Experimental Molecular Imaging and Max Planck Institute for Neurological Research, Cologne, Germany)

Broad application of noninvasive imaging techniques, especially positron emission tomography (PET) and related hybrid methods (PET/CT and PET/MR), in clinical practice has significantly contributed to a considerabe increase of accuracy in clinical diagnostics. PET offers quantitative 3D-visualization of physiological and pathological processes *in vivo* using probes labeled with positron-emitting nuclides. Moreover, PET represents a powerful tool for drug development which allows precise assessment and validation of their pharmacological properties at a molecular level. Furthermore, novel PET-tracers enable monitoring the success of anticancer treatment. The consistent growth of PET is accompanied by a large unmet need for the development of novel PET-probes including labeling techniques for the visualization of suitable targets of various diseases.

The starting point of modern PET imaging was the introduction of 2-[^{18}F]fluoro-2-deoxy-D-glucose ([^{18}F]FDG) in clinical practice (1976). However, highly sophisticated preparation procedures prevented its widespread application. This situation changed entirely after the introduction of an efficient stereospecific synthesis of n.c.a. [^{18}F]FDG using aminopolyether supported nucleophilic ^{18}F-substitution proposed by Kurt Hamacher, Heinz H. Coenen, and Gerhard Stöcklin in 1986. The novel radiosynthesis enabled obtaining [^{18}F]FDG in amounts allowing its broad clinical application. Moreover, this radiofluorination method has an enormous impact on ^{18}F-chemistry until today. That is one of the numerous trend-setting works of Professor Heinz H. Coenen, whose concepts influenced radiochemistry substantially. Although his scientific work covers different aspects of nuclear chemistry his achievements in modern ^{18}F-labeling chemistry are of exceptional importance. His work on the preparation of ^{18}F-PET-tracers from iodonium salts as well as the production of ^{18}F-labeled amino and fatty acids and their application for tumor imaging are definitely further highlights of his work. Accordingly, the present issue is dedicated to Professor Heinz H. Coenen on the occasion of his 65th birthday. Not surprisingly, in this issue excerpts of his pioneering works can be found.

The majority of papers in this issue deal with ^{18}F radiolabeling chemistry reflecting the outstanding potential of ^{18}F in PET imaging. The exceptional position of this radioisotope is based on its favorable nuclear properties (half-life and β^+-decay) and easy accessibility in >50 GBq quantities.

In recent years copper-catalyzed azide-alkyne click reactions have become a convenient method to introduce ^{18}F under mild reaction conditions. Further developments make use of more reactive 1,3-dipoles beyond azide and/or exploit strain-promoted metal-free click chemistry to prepare radiofluorinated compounds. This topic is reviewed by K. Kettenbach et al.

Recently, the silicon-fluoride-acceptor isotopic exchange (SIFA-IE) was established for ^{18}F-labeling. This novel approach gives rise to objective advantages such as no need for separation of radiolabeled product from precursor and very mild reaction conditions. The works in this field are covered by the contribution of V. Bernard-Gauthier et al.

Further, this issue provides a deeper insight into the radiosynthesis of small ^{18}F-molecules as intermediates for modular build-up syntheses. A plethora of labeling methods for the synthesis of ^{18}F-labeled building blocks for the construction of radiofluorinated complex molecules is reviewed by J. Ermert.

The CF_3 moiety is present in a large number of pharmaceuticals and drug candidates. The introduction of the trifluoromethyl group is often applied to improve pharmacological properties of lead structures. Consequently, several methods for introduction of 2-[^{18}F]fluoro-2,2-difluoroethyl group in target molecules have been proposed. They are presented in detail by V. T. Lien and P. J. Riss.

Chemoselective ^{18}F-fluoroglycosylation, for example, via azide-alkyne click reactions or via oxime formation allows preparing structurally defined ^{18}F-labeled glycoconjugates which often display improved *in vivo* kinetics and increased metabolic stability compared to parent compounds. S. Maschauer and O. Prante give a brief overview of the developments in this emerging field.

^{18}F-Chemistry is topped off with a review on 6-L-[^{18}F]FDOPA, the most popular PET-neurotracer with an exceptionally broad spectrum of applications. The paper of M. Pretze et al. summarizes the developments in the field of [^{18}F]F-DOPA syntheses using electrophilic synthesis pathways as well as recent developments of nucleophilic syntheses of 6-L-[^{18}F]FDOPA and compares the different synthesis strategies regarding the accessibility and applicability of the products for human *in vivo* PET tumor imaging.

Radiolabeled RGD peptides are of great importance for tumor detection since overexpression of definite integrins is frequently associated with tumor-induced angiogenesis and tumor metastasis. The contribution of R. Haubner et al. deals with different labeling techniques for the production of radiolabeled RGD-peptides. Beside different ^{18}F-labeling methods, an overview of other opportunities to efficiently label RDG peptides is provided. Furthermore, novel sequences targeting other integrin subgroups such as $\alpha_5\beta_1$ are described.

Owing to very slow blood clearance and metabolism of antibodies conventional PET emitters are unsuitable for PET measurements. This problem can be overcome, for example, by using the long-lived positron emitter ^{89}Zr. Strategies for

^{89}Zr-labeling of antibodies and use of ^{89}Zr-labeled antibodies for PET-imaging are outlined by F. C. J. van de Watering et al.

Since the introduction of microfluidics into PET-chemistry in 2004 syntheses of numerous PET-tracers based on different microfluidic setups have been described. This method comprises numerous advantages. The most important one, especially for the preparation of PET-tracers labeled with very short-lived isotopes such as ^{11}C, ^{13}N, and ^{15}O, is the reduced reaction time. The review presented by L. Brichard et al. deals with the production of ^{11}C-tracers using microfluidics.

Hybrid imaging technologies which combine different imaging modalities can provide additional clinical advantages. Some of them such as PET/CT and PET/MR are already widely applied in clinics. Despite its great potential, the combination of PET with optical imaging (OI) still remains in the phase of preclinical development. The paper authored by U. Seibold et al. is devoted to the preparation of and preclinical feasibility studies with bimodal agents for PET/OI imaging.

The current issue has not been designed to be comprehensive but, instead, to demonstrate the versatility, dynamics, and challenges of modern PET-chemistry. The efforts in this fast growing field aim at a steady improvement of existing and development of novel radiolabeling procedures in order to actively implement the "from bench to bedside" approach and, ultimately, to improve patient care.

Bernd Neumaier

Hindawi Publishing Corporation
BioMed Research International
Volume 2014, Article ID 454503, 20 pages
http://dx.doi.org/10.1155/2014/454503

Review Article

^{18}F-Labeled Silicon-Based Fluoride Acceptors: Potential Opportunities for Novel Positron Emitting Radiopharmaceuticals

Vadim Bernard-Gauthier,[1] Carmen Wängler,[2] Esther Schirrmacher,[3] Alexey Kostikov,[3] Klaus Jurkschat,[4] Bjoern Wängler,[5] and Ralf Schirrmacher[3,6]

[1] *Division of Experimental Medicine, Department of Medicine, McGill University, 1110 Pine Avenue West, Montreal, QC, Canada H3A 1A3*
[2] *Biomedical Chemistry, Department of Clinical Radiology and Nuclear Medicine, Medical Faculty Mannheim of Heidelberg University, 68167 Mannheim, Germany*
[3] *McConnell Brain Imaging Centre, Montreal Neurological Institute, McGill University, 3801 University Street, Montreal, QC, Canada H3A 2B4*
[4] *Department of Inorganic Chemistry II, Faculty of Chemistry, TU Dortmund, Otto-Hahn-Straße 6, 44221 Dortmund, Germany*
[5] *Molecular Imaging and Radiochemistry, Department of Clinical Radiology and Nuclear Medicine, Medical Faculty Mannheim of Heidelberg University, 68167 Mannheim, Germany*
[6] *Department of Oncology, University of Alberta, 11560 University Avenue, Edmonton, AB, Canada T6G 1Z2*

Correspondence should be addressed to Vadim Bernard-Gauthier; vadim.bernard-gauthier@mail.mcgill.ca and Ralf Schirrmacher; schirrma@ualberta.ca

Received 19 February 2014; Revised 7 April 2014; Accepted 8 April 2014; Published 24 July 2014

Academic Editor: Olaf Prante

Background. Over the recent years, radiopharmaceutical chemistry has experienced a wide variety of innovative pushes towards finding both novel and unconventional radiochemical methods to introduce fluorine-18 into radiotracers for positron emission tomography (PET). These "nonclassical" labeling methodologies based on silicon-, boron-, and aluminium-^{18}F chemistry deviate from commonplace bonding of an [^{18}F]fluorine atom (^{18}F) to either an aliphatic or aromatic carbon atom. One method in particular, the silicon-fluoride-acceptor isotopic exchange (SiFA-IE) approach, invalidates a dogma in radiochemistry that has been widely accepted for many years: the inability to obtain radiopharmaceuticals of high specific activity (SA) via simple IE. *Methodology.* The most advantageous feature of IE labeling in general is that labeling precursor and labeled radiotracer are chemically identical, eliminating the need to separate the radiotracer from its precursor. SiFA-IE chemistry proceeds in dipolar aprotic solvents at room temperature and below, entirely avoiding the formation of radioactive side products during the IE. *Scope of Review.* A great plethora of different SiFA species have been reported in the literature ranging from small prosthetic groups and other compounds of low molecular weight to labeled peptides and most recently affibody molecules. *Conclusions.* The literature over the last years (from 2006 to 2014) shows unambiguously that SiFA-IE and other silicon-based fluoride acceptor strategies relying on $^{18}F^-$ leaving group substitutions have the potential to become a valuable addition to radiochemistry.

1. Introduction

Radiopharmaceutical chemistry, besides the medicinal rationale, is undoubtedly the driving force behind tracer development for in vivo molecular imaging. Devising new radiochemical methodologies to introduce radioisotopes into organic molecules of various molecular weights and chemical nature has been a continuing strife throughout the history of radioactive probe development. In principle, almost any organic compound can be radioactively labeled depending on the nuclide, the acceptable level of derivatization which is necessary particularly in radiometal labeling, and of course

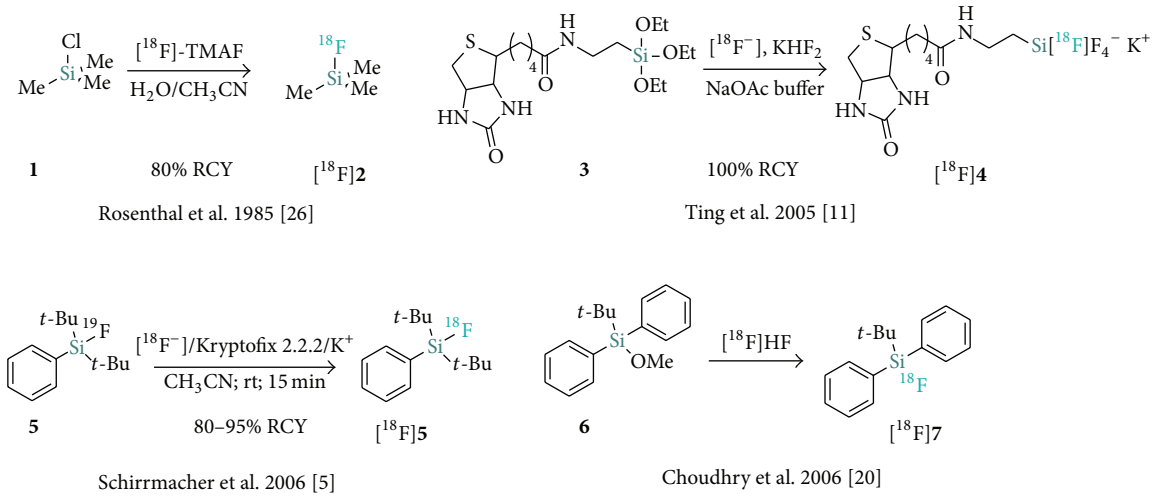

Scheme 1: Early developments of silicon-[^{18}F]fluorine-based compounds.

the position of the label itself. With the contingent of existing labeling methods, it is possible to label nearly all compounds in sufficient radiochemical yields (RCYs); however, sometimes the required great technical effort can prevent clinical routine production. Currently, only radiochemistries based on coordinating radiometals such as technetium-99m (^{99m}Tc), which accounts for the majority of all radiopharmaceuticals produced for single-photon emission computed tomography (SPECT), as well as indium-111 (^{111}In, for SPECT), gallium-68 (^{68}Ga), and copper-64 (^{64}Cu) both for positron emission tomography (PET) proceeds in a kit-like manner [1–4]. In particular, ^{99m}Tc radiochemistry evolved over decades into fully GMP compliant (Good Manufacturing Practice) labeling kits where a simple addition of the radionuclide in the chemical form of its pertechnetate ($^{99m}TcO_4^-$) followed by very few simple steps yields the tracer. For other radiometals, final HPLC purification is sometimes inevitable and the operators in the laboratory have to possess a certain degree of technical proficiency and equipment in order to deliver an injectable solution that complies with GMP regulations.

Additional obstacles exist for radiolabeling with the most extensively used PET isotope ^{18}F. The interest towards the development of ^{18}F-radiopharmaceuticals ensues essentially from the low positron energy (635 KeV) and the most suitable half-life (109.7 min) of this radioisotope. As a consequence, ^{18}F is ideal for numerous PET imaging applications involving tracers of low molecular weight as well as various biomolecules with a suitable kinetic profile. In particular, the successful and widespread use of [^{18}F]2-fluoro-2-deoxy-D-glucose ([^{18}F]FDG) has ignited the interest in new ^{18}F-tracers but despite its favorable nuclear properties, ^{18}F-radiochemistry remains often associated with relatively cumbersome and lengthy labeling procedures. Indeed, ^{18}F-labeling normally involves relatively large precursor quantities and often requires high reaction temperatures as well as the presence of activating reagents (e.g., strong bases plus cryptands) leading to unwanted radioactive and chemical side products, which need to be thoroughly separated from the desired ^{18}F-labeled tracer. Consequently, there are only few examples published in the literature where the radiochemical labeling procedure does not require a final HPLC purification. This is problematic due to the need for fully GMP compliant synthesis modules, which led manufacturers to search for solid phase based purifications to circumvent HPLC procedures [5–7]. Moreover, the classical use of harsh reaction conditions precludes a direct ^{18}F-radiolabeling of complex biomolecules not able to withstand those reaction conditions. In such cases, the use of ^{18}F-carbon-based prosthetic groups is often necessary, imposing further equipment challenges in addition to the time-consuming aspects.

The recent development of comparatively simple, efficient, and innovative labeling approaches based on silicon-^{18}F [5, 8–10] and boron-^{18}F [11–14] bond formation as well as aluminium-^{18}F [14–19] chelation scaffolds each address in part some of the major drawbacks associated with conventional nucleophilic ^{18}F-labeling on a carbon atom. Particularly, silicon-^{18}F labeling methods have been increasingly exploited in recent years due to their inherent simplicity and efficiency compared to conventional labeling strategies. The organosilicon-based fluoride acceptor (SiFA) ^{18}F-labeling strategy was initially coined in reference to the isotopic exchange (IE) approach introduced by Schirrmacher et al. [5] (Scheme 1). A more inclusive definition of SiFAs also comprises the alkoxysilane leaving group approach introduced by Choudhry et al. [20] which was expanded to hydrosilanes and silanols by the group of Ametamey [21]. The current review will detail and discuss the technical developments and applications which have led to the current status of [^{18}F]-SiFA radiochemistry as a simplified approach towards new radiopharmaceuticals for PET imaging.

2. SiFA Labeling Chemistry

Formation of Si–F bonds is driven by the strong affinity between silicon and fluorine as exemplified by the high

corresponding bond energy (565 kJ mol^{-1} for Si–F versus 485 kJ mol^{-1} for C–F and 318 kJ mol^{-1} for Si–C). Simple organofluorosilanes display poor kinetic stability and may be cleaved under mild conditions in the presence of fluoride or other silophiles due to the high polarization of Si–F bonds which is also true for Si–O bonds. Tetravalent silicon readily reacts with Lewis bases to form hypervalent species (both 5- and 6-coordinate) as a consequence of vacant low energy d-orbitals. Moreover, the greater covalent radius of silicon versus carbon contributes to the enhanced propensity of organosilanes to undergo nucleophilic substitutions at the silicon atom compared to their carbon-centered counterparts. Those characteristics build the foundation of various nonradioactive organosilicon chemistries and are also central to the development of [^{18}F]organofluorosilanes for PET imaging.

The synthesis of ^{18}F-labeled silicon tetrafluoride (Si[^{18}F]F_4) via metallic hexafluoridosilicate formation from metallic fluorides and SiF_4 has been known for more than half a century in radiochemistry [22–24]. [^{18}F]Fluorotrimethylsilane ([^{18}F]**2**) was also reported as a hypothetical intermediate from hexamethylsiloxane reaction with [^{18}F]HF as early as 1978 [25]. The first in vivo evaluation of silicon-^{18}F building blocks was introduced by Rosenthal et al. with the radiosynthesis of the volatile species [^{18}F]**2** from chlorotrimethylsilane (**1**; Scheme 1) [26]. The labeling proceeded efficiently delivering [^{18}F]**2** using no-carrier-added (nca) tetramethylammonium-[^{18}F]fluoride ([^{18}F]TMAF, 80% radiochemical yield (RCY) decay-corrected); however, upon inhalation by rats extensive bone uptake was observed as a result of defluorination (anionic ^{18}F– is rapidly taken up by the bone apatite). This result paralleled the observed poor hydrolytic in vitro profile of [^{18}F]**2** which led the authors at the time to suggest that bulkier groups at the silicon atom may be necessary in order to generate hydrolytically stable ^{18}F-silicon building blocks. This original contribution was followed by the development of variations of [^{18}F]fluorotrimethylsilane-based release of dry nca $^{18}F^-$ for the use in nucleophilic radiofluorination [27, 28].

In a more recent study, the group of Perrin provided an innovative approach towards ^{18}F-silicon building blocks, synthesizing the biotin-linked alkyl tetrafluorosilicate [^{18}F]**4** via near-quantitative carrier added radiofluorination (from KHF_2) [11]. A typical reaction procedure involved reacting alkyl triethoxysilane **3** with a preformed mixture of 440 μCi of $^{18}F^-/H_2O$ from target water ([^{18}O]H_2O) along with 130 mM KHF_2 (4.4 equiv.) in 200 mM NaOAc (pH 4.5). This important development also constituted the first efficient $^{18}F^-$ aqueous labeling and provided, despite hydrolytic stability concerns, the groundwork for ^{18}F-silicon radiochemistry developments.

In 2006, Schirrmacher et al. convincingly demonstrated that [^{18}F]SiFA building blocks could be generated in high RCYs and specific activity (SA) by means of a IE from the corresponding- and chemically identical-^{19}F-precursors [5]. Conversion of [^{19}F]-tBu$_2$PhSiF (**5**) to the radiolabeled [^{18}F]-tBu$_2$PhSiF ([^{18}F]**5**) proceeded in 80–95% RCYs in the presence [^{18}F]$^-$/Kryptofix 2.2.2/K^+ in acetonitrile (100 μL) with minimal precursor quantity (1 μg). The prototypical di-*tert*-butylphenyl-bearing SiFA [^{18}F]**5** was obtained in SAs of 2.7–27 Ci μmol^{-1} and the methodology was also applied to direct, unprotected labeling of SiFA-aminooxy-derivatized Tyr^3-octreotate at room temperature (see Section 4). This work validated that IE at the silicon atom (SiFA-IE) constitutes an effective and mild methodology towards new ^{18}F-labeled compounds. The authors also reported an early stability study of a series of labeled SiFA derivatives (*vide infra*). This result was reported almost simultaneously with the important contribution of Choudhry et al. establishing a silicon-leaving group approach to the radiosynthesis of [^{18}F]SiFA starting from an alkoxy-substituted acceptor precursor [20]. The reaction proceeded directly from aqueous $^{18}F^-$ and allowed for the efficient conversion of *tert*-butyldiphenylmethoxysilane (**6**) to [^{18}F]*tert*-butyldiphenylfluorosilane ([^{18}F]**7**) at room temperature in 5 minutes.

The leaving group methodology currently constitutes one of the two extensively exploited strategies towards [^{18}F]SiFAs—the other one being the SiFA-IE. Both approaches were shown to deliver [^{18}F]SiFA in high RCYs and SAs (Figure 1(a)). Yet, important distinctions exist between the two techniques, one of which resides in the fact that the IE typically proceeds at room temperature or below while the Si-leaving group approach, like aliphatic and aromatic ^{18}F-carbon radiochemistry in general, necessitates elevated temperatures which may be detrimental when direct labeling of biomolecules is considered.

The efficiency of the IE, even at low temperatures, can be attributed to the low energy barrier for the $^{19}F^-$ isoenergetic replacement with $^{18}F^-$ in acetonitrile via the formation of a trigonal bipyramidal siliconate anion intermediate ($\Delta G_{IE} \approx 0$; negligible isotopic effect; Figure 2). Indeed, DFT calculations in condensed phase (acetonitrile) on model SiFAs of the type $R_3SiF_2^-$ indicated that $\Delta G^\ddagger$ values associated with the formation of siliconate intermediates from those precursors range from 5 to 10 kcal mol^{-1} (Figure 1(b), upper path) [29]. On the other hand, in the gas phase, values of $\Delta G^\ddagger$ of −50 to −40 kcal mol^{-1} were calculated in agreement with the expected formation of thermodynamically stable organofluorosiliconates (Figure 1(b), lower path) [30, 31]. Those energetic differences ensue from the diminished Lewis basicity of the fluoride anion in acetonitrile compared to that in the gas phase, suggesting that in the former case equilibrium is rapidly reached leading to the fast and near-irreversible formation of [^{18}F]SiFA species as a consequence of stoichiometric leverage. Kostikov et al. also experimentally determined a characteristically low activation energy (E_a = 15.7 kcal mol^{-1}) and exceptionally low preexponential factor ($A = 7.9\times10^{13}$ M^{-1} s^{-1}) for the SiFA-IE from the corresponding Arrhenius plot [32]. These results are in contrast with the values gained from a comparable carbon-^{18}F bond formation reaction, namely, the ^{18}F-fluorination of ethyleneglycol-di-*p*-tosylate (E_a = 17.0 kcal mol^{-1} and $A = 2.9 \times 10^9$ M^{-1} s^{-1}), and support the experimental observation that SiFA-IE

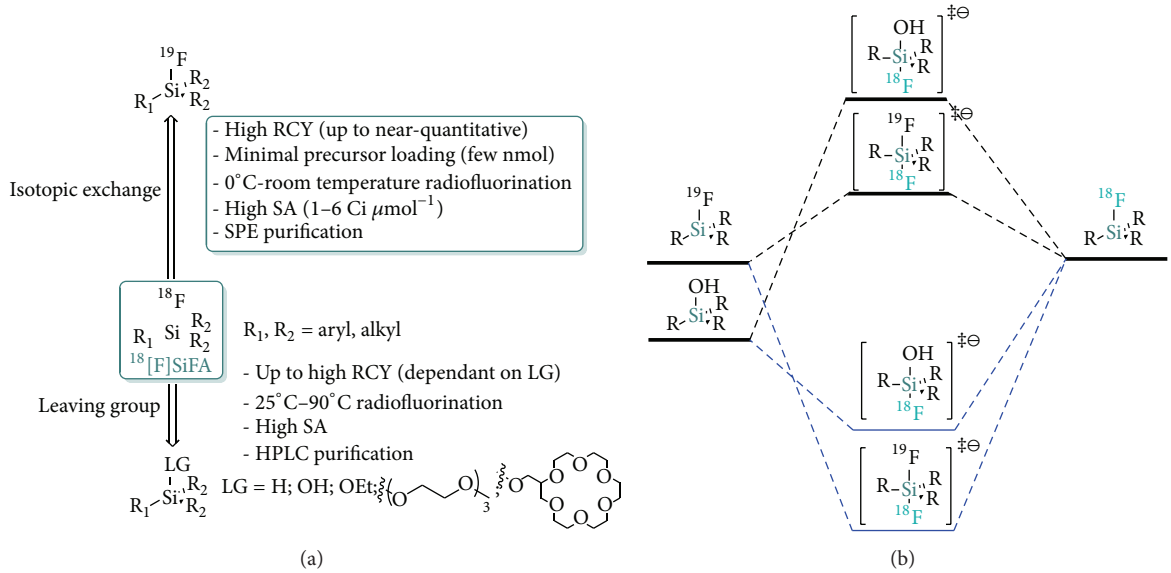

Figure 1: (a) Approaches towards [^{18}F]SiFA compounds for PET; [^{18}F]SiFA can be obtained by either isotopic exchange or leaving group substitution from the suitable organosilane precursors. (b) Comparison of simplified reaction coordinates for IE and leaving group radiofluorination (from hydroxysilane in the absence of acid catalyst). Simple hypothetical siliconates intermediates are depicted. (Gas phase = dash blue lines, MeCN = dash black lines.)

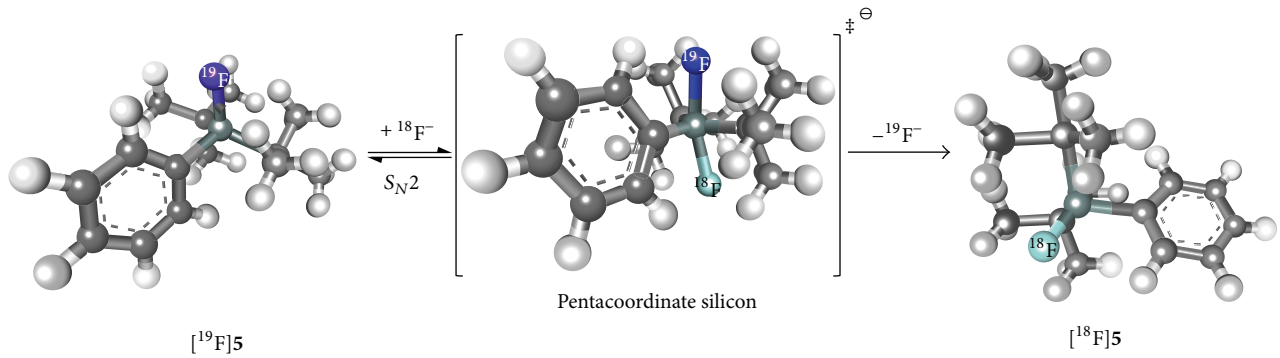

Figure 2: Formation of a trigonal bipyramid siliconate anion intermediate leading to formation of [^{18}F]**5** from [^{19}F]**5** (gray = carbon; dark green = silicon; blue = fluorine-19; cyan = fluorine-18; white = hydrogen).

proceeds quasi-quantitatively in many instances even at low temperatures [32]. In contrast, ^{18}F-radiofluorination of more stable silanol precursors [33] (or other leaving group bearing silanes) should be endergonic ($\Delta G > 0$) and associated with less stable hydrosiliconate intermediates in both gaseous and condense phases as expected from bond dissociation energies (BDEs).

An additional important distinction between IE and the leaving group method relates to purification techniques. Since the IE involves chemically identical entities and proceeds under mild conditions that do not lead to side products, HPLC purification can often be avoided and purification can be limited to solid phase cartridge extraction (SPE). This approach is feasible irrespective of the nature of the tracer (e.g., small fragments or biomolecules). In contrast, HPLC purification constitutes a prerequisite of the leaving group approach as chemically distinct precursors and ^{18}F-radiolabeled products have to be carefully separated. Nevertheless, this method has been thoroughly developed and adapted frequently by the radiochemistry community. Since the initial contribution of Choudhry et al., the group of Ametamey and coworkers has further extended the silicon-leaving group approach methodology to hydride, hydroxy, and alkoxy leaving groups.

Mu et al. exemplified this method with the radiosynthesis of a series of fluorosilanes bearing alkyl ([^{18}F]**10**, [^{18}F]**11**) or aryl ([^{18}F]**15**, [^{18}F]**16**) Si-linked fragments containing various R groups (Scheme 2) [21]. Few compounds such as the dimethyl- (**8**) and diisopropylethoxysilane (**9**) reacted readily at 30°C whereas most substrates necessitated elevated temperatures (65°C–90°C) in order to react with the ^{18}F$^-$. Compounds [^{18}F]**15** and [^{18}F]**16** were obtained in moderate to high RCYs from the corresponding silanol and silanes (SA of [^{18}F]**16** = 1.73 Ci μmol^{-1}). As expected, adding acetic acid significantly influenced incorporation yields in the presence

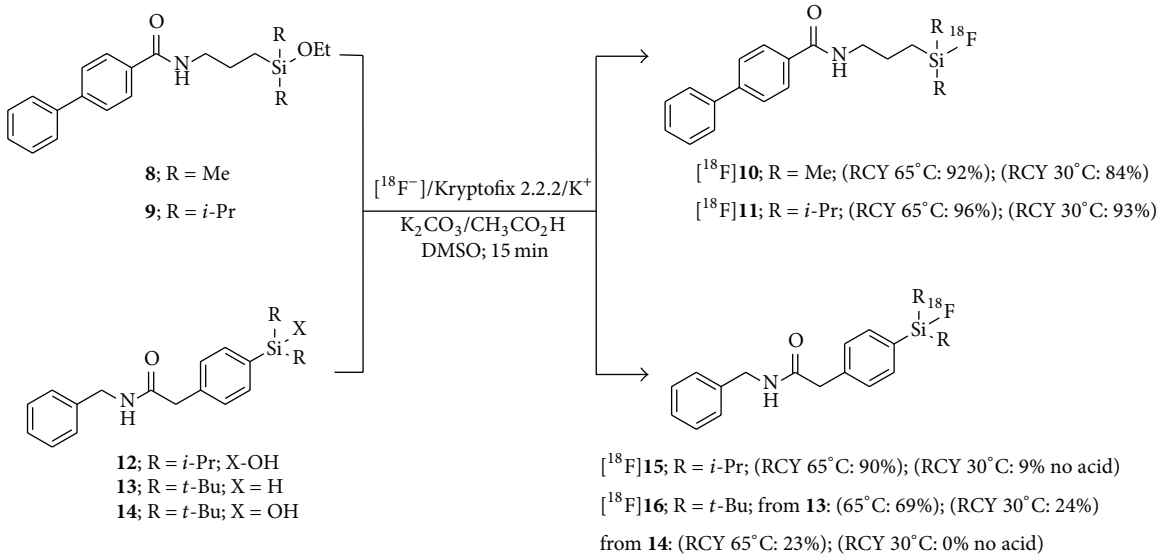

Scheme 2: Synthesis of ^{18}F-labeled silicon-containing model compounds with alkyl and aryl linkers by Mu et al.

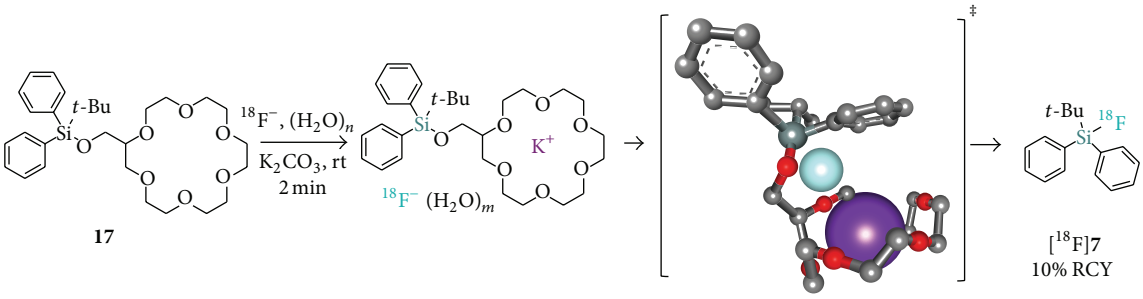

Scheme 3: Postulated mechanism for rate enhancement in silicon fluorination using a crown ether leaving group by Al-huniti et al. conditions (gray = carbon; red = oxygen; dark green = silicon; cyan = fluoride; purple = potassium; hydrogen omitted for simplicity).

of *O*-bearing leaving groups but did not modify hydride rate departure from precursor **13**.

In a recent study, the leaving group SiFA methodology was combined with the nucleophile assisting leaving group (NALG) strategy to generate Si-appended potassium-chelating SiFA-based leaving groups [34, 35]. In the absence of added Kryptofix 2.2.2, the facilitation of ^{18}F-fluorination in the presence of cyclic crown ethers such as in **17** compared to acyclic polyethers or alkoxide leaving groups was clearly established. Unfortunately, the RCYs were undermined by the limited solubility (1–5%) of nca K^{18}F in the reaction media. This issue was partially addressed by water addition (up to 0.5% v/v) leading to an increased K^{18}F solubility (31%), but further addition subsequently diminished the observed RCYs. Consequently, upon optimized conditions, [^{18}F]**7** was obtained in overall 10% RCY (Scheme 3). Thus, despite being conceptually elegant and promising, this approach is significantly hampered by ^{18}F$^-$ solubility issues which will possibly be addressed in the future to establish this methodology as a practical alternative to the simpler and straightforward SiFA-leaving group method or IE methodology.

3. SiFA Lipophilicity and Hydrolytic Stability

Stability investigations of a series of phenyl- and *tert*-butyl-bearing [^{18}F]SiFAs ([^{18}F]**5**, [^{18}F]**7**, and [^{18}F]**18**) early on established the importance of the *tert*-butyl substituents at the silicon atom in order to achieve sufficient in vivo stability for potential in vivo PET applications (Figure 3) [5]. Compound [^{18}F]**18** displayed poor in vitro stability in human serum at 37.4°C ($t_{1/2}$ = 5 min) while both [^{18}F]**5** and [^{18}F]**7** were found to be persistently stable under those conditions. However, only [^{18}F]-*t*Bu$_2$PhSiF ([^{18}F]**5**) showed satisfactory in vivo stability as demonstrated by the limited ^{18}F$^-$ bone uptake observed upon injection into Sprague Dawley rats. The stability trend originates from steric hindrance in combination with the diminished silicon Lewis acidity in the presence of *tert*-butyl fragments. Unfortunately, this substitution pattern comes at the price of a significant increase in lipophilicity which, when chemically linked to biomolecules, may substantially impact metabolism and biodistribution, generating unspecific uptake and leading to poor PET imaging quality. This issue has been addressed by

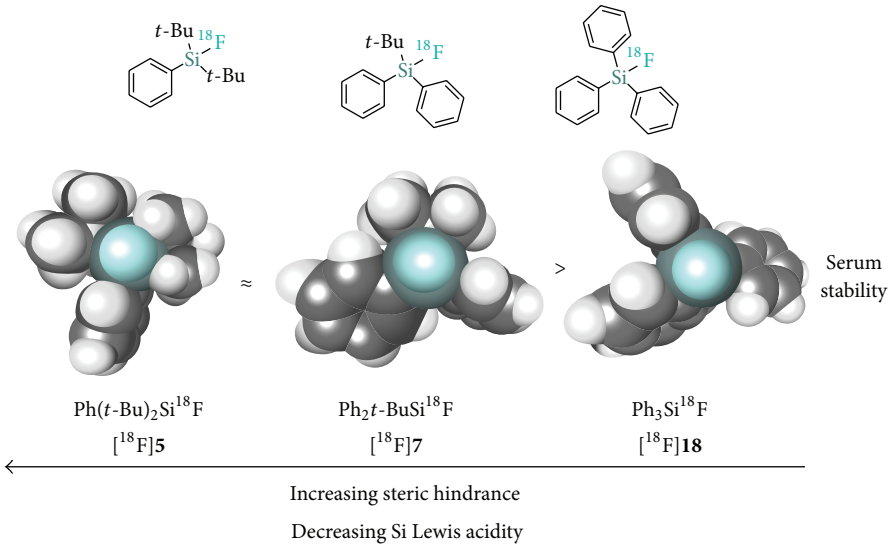

Figure 3: In vitro hydrolytic stability of [^{18}F]fluorosilanes in human serum.

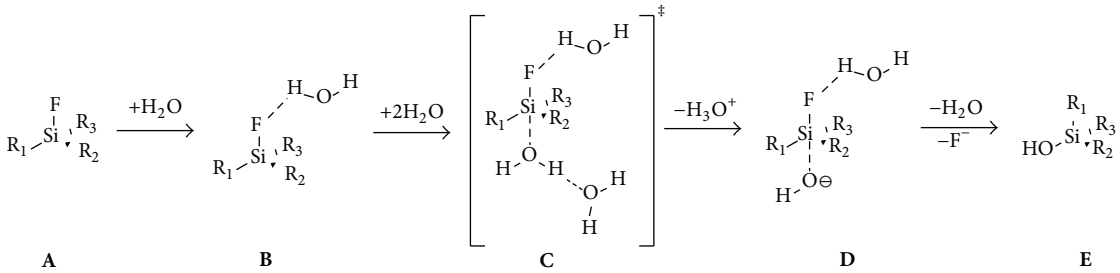

Scheme 4: Mechanism for the hydrolysis of organofluorosilanes as suggested by Höhne et al.

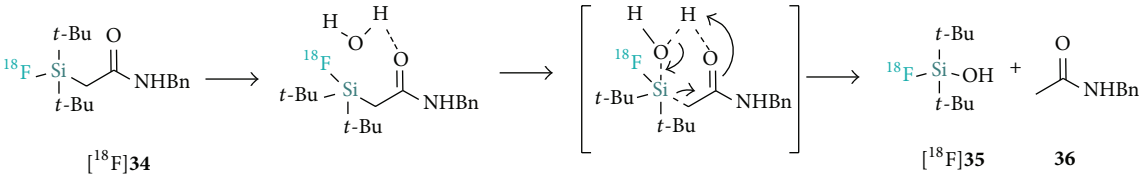

Scheme 5: Suggested mechanism for the hydrolysis of [^{18}F]SiFA β-acetamide [^{18}F]**34**.

the development of lipophilicity-reducing auxiliaries which will be discussed in Section 4.

Further confirmation of the importance of sterically demanding SiFA substituents was provided by the detailed and systematic investigation on hydrolytic stability led by Höhne et al. (Table 1) [33].

The observed trends strongly correlate with the steric nature of the silicon substituents. In particular, the presence of bulky *tert*-butyl groups, combined with an aryl linker moiety, result in remarkable stability whereas smaller alkyl substituents progressively enhance the hydrolysis rate. Furthermore, the authors also provided a detailed hydrolysis mechanism (Scheme 4) as well as a theoretical model based on the difference in Si–F bond lengths ($\Delta_{(\mathrm{Si-F})}$) between the starting SiFA structures (**A**) and the DFT optimized intermediate structure (**D**) (where $\Delta_{(\mathrm{Si-F})} \geq 0.19$ Å corresponds to hydrolytically unstable SiFAs).

In a recent study, the group of Ametamey attempted the radiosynthesis of a β-acetamide [^{18}F]SiFA ([^{18}F]**34**) from the corresponding hydrosilane precursor but instead isolated di-*tert*-butyl-[^{18}F]fluorosilanol ([^{18}F]**35**) (Scheme 5) [36]. They suggested that this conversion proceeds with an analogous mechanism to the one encountered in the hydrolysis of β-ketosilanes following treatment with water [37]. This interestingly constitutes the first example of a SiFA hydrolytic stability issue involving the cleavage of the silicon-carbon bond.

4. [^{18}F]SiFA Labeling of Peptides

The labelling of peptides for PET imaging has traditionally been achieved via multistep strategies involving ^{18}F-S$_N$2 reactions at carbon centers and ^{18}F-labeled prosthetic groups. This strategy succeeded in generating multiple peptide-based

Table 1: Hydrolytic half-lives ($t_{1/2}$) of selected organofluorosilane building blocks.

Cpd	Structure	$t_{1/2}$ (h)	Reference
10	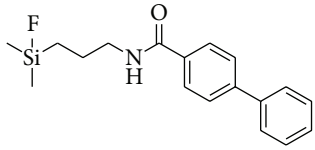	0.08[a]	[33]
19	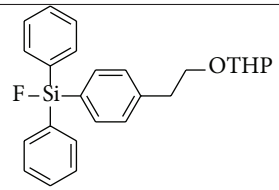	0.1[a]	[33]
20	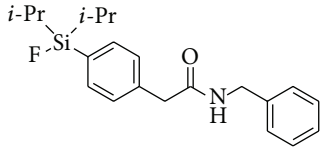	8[a]	[33]
11	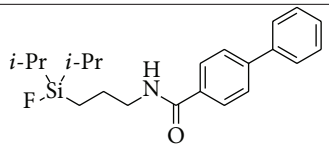	12[a]	[33]
21	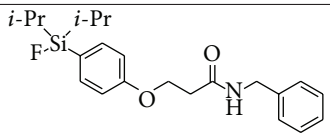	15[a]	[33]
22	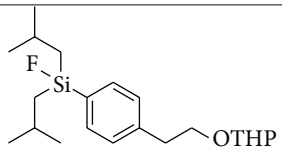	21[a]	[33]
23	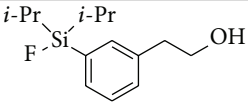	29[a]	[33]
24	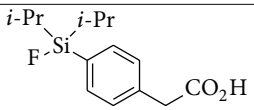	37[a]	[33]
25	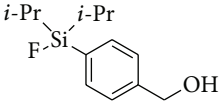	37[a]	[33]
26	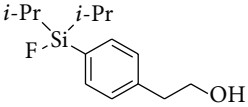	43[a]	[33]
27	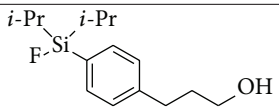	61[a]	[33]
28	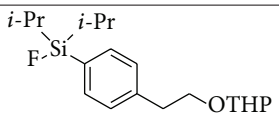	79[a]	[33]

Table 1: Continued.

Cpd	Structure	$t_{1/2}$ (h)	Reference
29	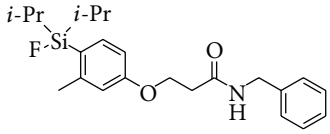	302[a]	[33]
30	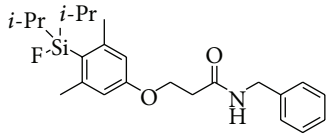	>300[a]	[33]
16	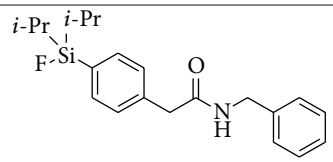	>300[a]	[33]
31	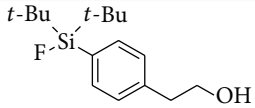	8[b]	[36]
32	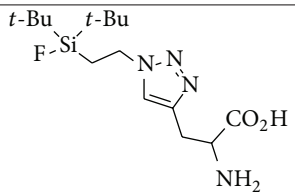	16[b]	[36]
33	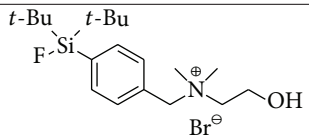	>> 2[c]	[32]

[a]Hydrolytic stability determination from nonradioactive compounds in MeCN/aqueous buffer (2 : 1; pH 7) at room temperature. [b]Hydrolytic stability determination from ^{18}F-labeled compounds in EtOH/aqueous buffer at room temperature. [c]95% intact after 2 h of incubation; hydrolytic stability determination from ^{18}F-labeled compounds at pH 7.4.

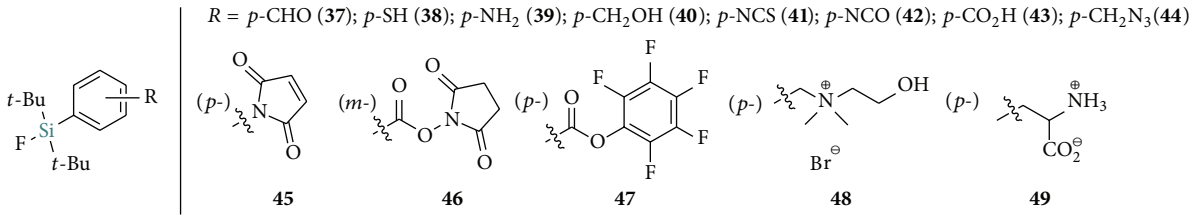

Figure 4: Structures of SiFA building blocks amenable to IE and peptide labeling.

PET probes for in vivo imaging [38–40] but it is inherently hampered by its technical complexity, harsh reaction conditions, and time-consuming HPLC purifications. Simplifying such procedures by means of mild and efficient radiolabeling approaches without HPLC purifications at one or all synthetic stages while maintaining sufficient SA represents an important challenge in ^{18}F-PET radiochemistry. The [^{18}F]SiFA method, as well as other promising emerging technologies such as the Al-^{18}F approach [14–19], is particularly well suited to address those classical limitations.

Figure 4 presents various synthesized SiFA building blocks bearing reactive groups for peptide conjugation (for proteins and small molecules *vide infra*) [6, 32, 41–45]. The coupling of those SiFAs to peptides prior to the IE labeling would in theory allow for a direct and mild ^{18}F-incorporation without subsequent HPLC purification. Indeed, this was early demonstrated by Schirrmacher et al. [5] with the direct radiosynthesis of [^{18}F]SiFA-derivatized Tyr^3-octreotate ([^{18}F]**50**, Scheme 6). Despite the unprecedented mild conditions encountered and the high ^{18}F-fluorination

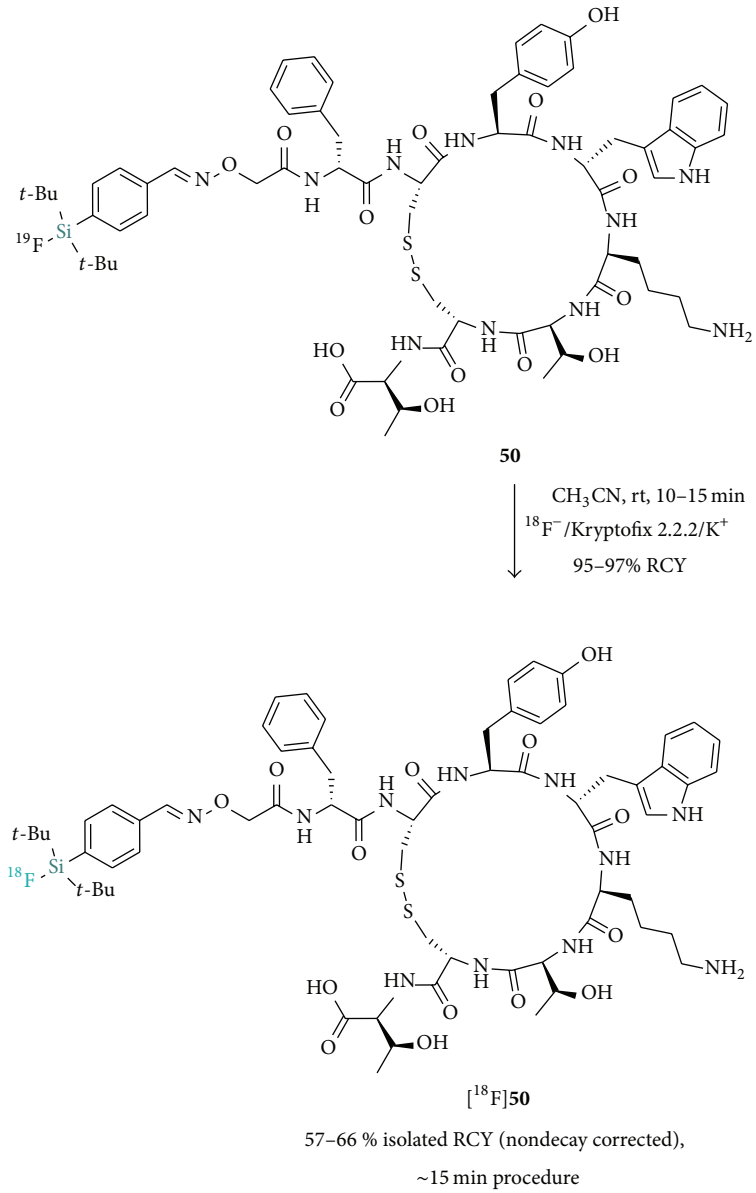

Scheme 6: Radiosynthesis of [^{18}F]SiFA-derivatized Tyr^3-octreotate ([^{18}F]**50**).

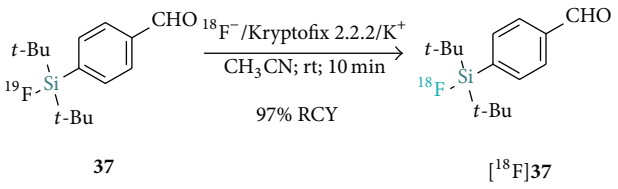

Scheme 7: Radiosynthesis of [^{18}F]-SiFA-*p*-CHO ([^{18}F]**37**) for the labeling of aminooxy derivatized peptides.

efficiency of 95–97% and 57–66% isolated RCYs (nondecay corrected), the approach suffered from low SAs (0.08–0.14 Ci μmol^{-1}).

Subsequently, a two-step procedure which consists of the near quantitative initial fluorination of the aldehyde [^{18}F]**37** (Scheme 7) in high SAs (>5000 Ci/mmol), followed by a rapid C-18 SPE purification and subsequent room temperature conjugation to *N*-terminal amino-oxy functionalized Tyr^3-octreotate, was reported [29] (Table 2 recapitulates selected examples of SiFA-peptide labeling). In the same study, the [^{18}F]**37** synthon was also efficiently applied to the labeling of a cyclic RGD (Arg-Gly-Asp) and a PEG-conjugated bombesin (BBN) analogue (*cyclo*(fK(AO-N)RGD and BZH3, resp.).

In parallel, important progress towards the direct fluorination of bioactive peptides from hydrosilanes and silanol precursors following the leaving group approach was made. The initial report by Mu et al. illustrates the methodology with the synthesis of two ^{18}F-labeled tetrapeptides. The reactions proceeded at 65–90°C with moderate incorporation of ^{18}F from either of the hydrosilane and the silanol (45% and 53%,

Table 2: Structure of selected [^{18}F]-silicon-based derivatives attached to different peptide ligands and their appended linkers and lipophilicity-reducing auxiliaries.

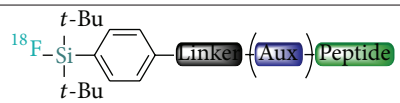

Entry		Labeled peptide	Labeling method[a]/ SA/purification method/RCY[b]	Reference
1	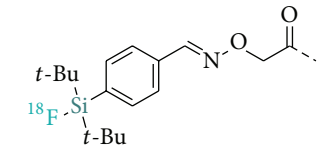	Octreotate analogues	Direct IE/0.08–0.14 Ci μmol^{-1}/C-18 SPE/55–65% eos	[5]
		cRGD	Prosthetic IE/6.1–18.4 Ci μmol^{-1}/HPLC/50–55% eos	[29]
			Prosthetic IE/6.1–18.4 Ci μmol^{-1}/HPLC/50–55% eos	[29]
2	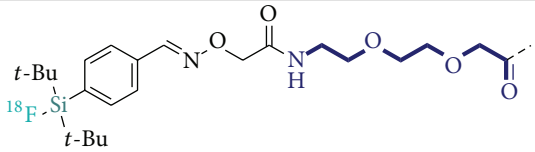	Bombesin analogues	Prosthetic IE/6.1–18.4 Ci μmol^{-1}/HPLC/50–55% eos	[29]
3	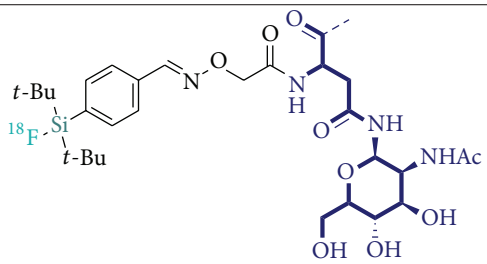	Octreotate analogues	Direct IE/0.78–1.5 Ci μmol^{-1} (18.4 Ci μmol^{-1} for prosthetic IE)/C-18 SPE/38 ± 4% eos	[47]
4	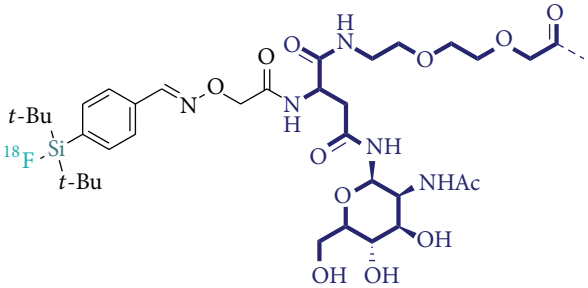	Octreotate analogues	Direct IE/0.78–1.5 Ci μmol^{-1} (18.4 Ci μmol^{-1} for prosthetic IE)/C-18 SPE/38 ± 4% eos	[47]
5	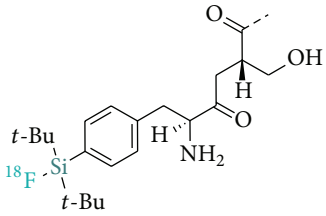	Octreotate analogues	Direct IE/1.30 Ci μmol^{-1}/C-18 SPE/34% eos	[41]
6	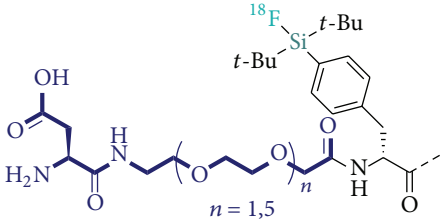	Octreotate analogues	Direct IE/1.30 Ci μmol^{-1}/C-18 SPE/70% eos (n = 1)	[41]

Table 2: Continued.

7	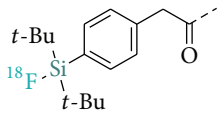	Bombesin analogues	Direct from silanol/ -/HPLC/34% incorporation Direct from hydrosilane/ -/HPLC/74% incorporation Direct from hydrosilane/1.68 Ci μmol^{-1}/HPLC/13.1 ± 3.3% dc eos	[9] [33] [9]
8	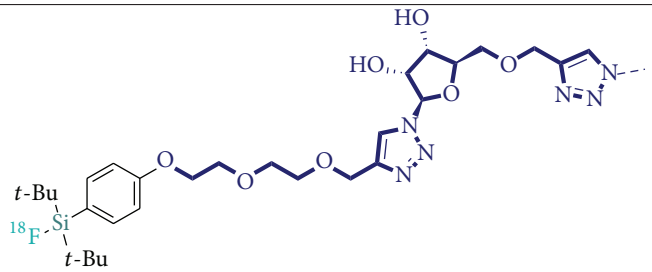	cRGD	Direct from hydrosilane/ 4.87 Ci μmol^{-1}/HPLC/17% ndc	[52]
9	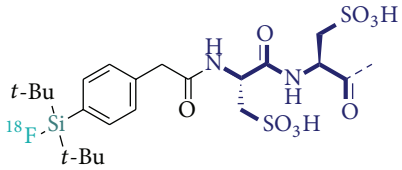	Bombesin analogues	Direct from hydrosilane/ 0.95 Ci μmol^{-1}/HPLC/1.8% dc eos	[36]
10	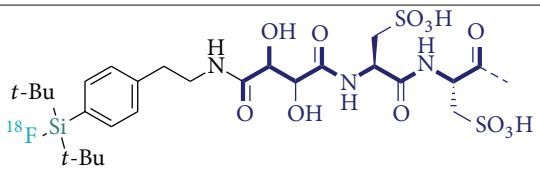	Bombesin analogues	Direct from hydrosilane/ 1.89 Ci μmol^{-1}/HPLC/1.1% dc eos	[36]

[a] Via isotopic exchange (IE) either direct or in two steps or via the leaving group approach from the specified precursor. [b] The RCYs are reported as isolated end of synthesis (eos) yields either decay correct (dc) or not (ndc); in the absence of available RCYs at eos, incorporation RCYs are reported.

resp.) [21]. The importance of the bulky tBu$_2$Ph-SiFA motif to guarantee hydrolytic stability was confirmed once more. Both an iPr$_2$Ph-SiFA bombesin analogue [33] and two alkyl-linked iPr$_2$-SiFA model tripeptides were shown to be unstable (pH 7.5, phosphate buffer) [46] (Figure 5). Following the leaving group approach, the development and first in vivo evaluation of a [^{18}F]SiFA labeled bombesin analogue in PC3 xenografted nude mice were subsequently reported [9, 33] (Table 2, Entry 7). The authors reported low uptake in gastrin-releasing peptide receptor (GRP) positive tumor bearing mice and high unspecific binding along with prominent hepatobiliary excretion, despite sufficient potency (IC_{50} = 22.9 nM) based on comparison with previously characterized successfully radiolabeled BBN analogues. The observation of gradually increasing but overall low bone uptake suggested that di-*tert*-butyl aryl [^{18}F]SiFA was sufficiently stable in vivo. Hence, the poor pharmacokinetic profile observed was reasonably ascribed to the overall high lipophilicity of the probe imparted by the SiFA moiety.

Wängler et al. reported the synthesis, HPLC-free purification, and in vivo evaluation of carbohydrate and carbohydrate/PEG derivatized [^{18}F]SiFA-octreotate probes for imaging sst2-expressing tumors (AR42J xenografts; Table 2; Entries 3 and 4). [47]. This study, based on the previously

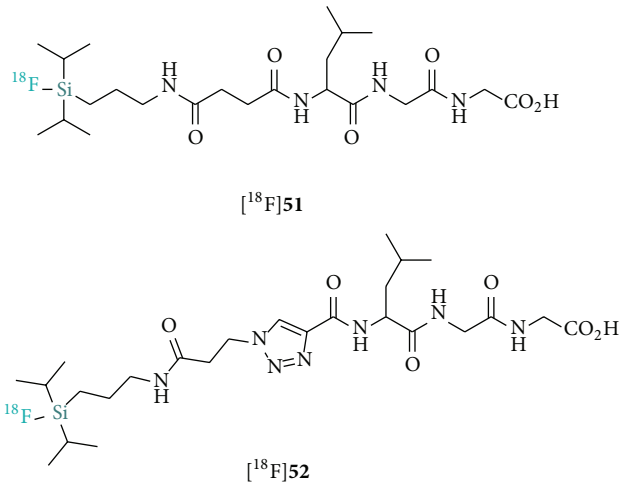

Figure 5: Hydrolytically unstable di-iPr-SiFAs tripeptides reported by Balentova et al.

successful use of hydrophilic linkers for enhanced tumor uptake and optimized excretion of PET/SPECT imaging peptides introduced by Schottelius and Antunes et al. [48–50], established the efficiency of peptide SiFA derivatives

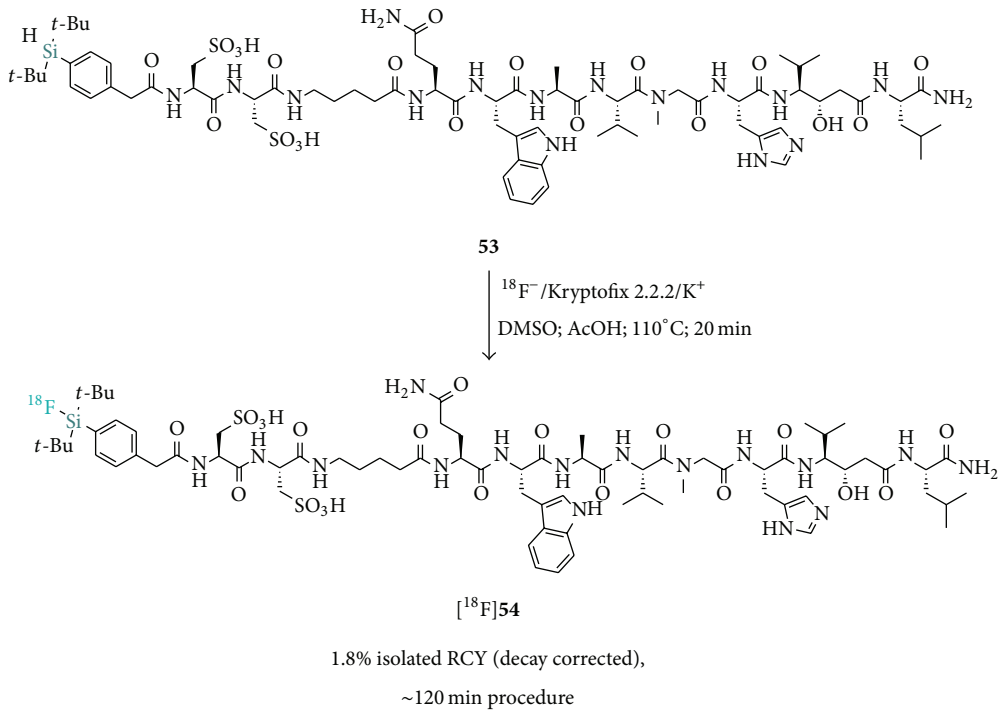

Scheme 8: Radiosynthesis of L-cysteic acid-containing SiFA bombesin analogue [^{18}F]**54**.

with lipophilicity-reducing auxiliaries as a potential strategy for optimized PET imaging. The in vivo investigation of the most promising PEG/glucose-linked derivative ([^{18}F]SiFA-Asn(AcNH-β-Glc)-PEG-Tyr^3-octrotate – IC_{50}(sst2) = 3.3 ± 0.3 nM; Table 2, Entry 4) showed enhanced tumor uptake (7.7% ID/g at 60 min p.i.) compared to the initial negligibly accumulating [^{18}F]-SiFA-Tyr^3-octreotate (entry 1). This positive, yet still nonoptimal result was attributed to the improved hydrophilicity of the probe (log P_{ow} = 0.96 versus 1.59 for [^{18}F]-SiFA-Tyr^3-octreotate) and encouraged the introduction of hydrophilic auxiliaries as a promising lipophilicity counterbalancing strategy for SiFA-peptide probe development. This approach has since been translated into a general procedure aiming at the modular cartridge-based radiosynthesis of various [^{18}F]SiFA peptides in conjunction with lipophilicity-reducing auxiliaries [51].

Two recent additional studies described further lipophilicity reducing auxiliaries for SiFA-peptides. Firstly, Amigues et al. introduced a PEG/ribose [^{18}F]-SiFA-RGD probe ([^{18}F]SiFA-RiboRGD; Table 2, Entry 8) as a silicon-based alternative with counterbalanced lipophilicity to the well-known [^{18}F]Galacto-RGD [52, 53]. [^{18}F]SiFA-RiboRGD was obtained from the corresponding hydrosilane in satisfactory yields and SA (Table 2) and the in vivo PET evaluation suggested that the tracer might be useful in the determination of $\alpha v\beta 3$ integrin expression as significant tumor uptake was reported.

Secondly, the group of Ametamey introduced another lipophilicity reducing strategy towards the development of optimized [^{18}F]SiFA bombesin analogues [36]. The synthesis of tartaric acid/L-cysteic acid-containing linked BBN derivatives allowed for a significant lipophilicity reduction (log $D_{7.4}$ = 0.3 ± 0.1 for [^{18}F]**54** versus 1.3 ± 0.1 for cysteic acid free peptide-entry 7, Table 2). The in vivo evaluation of the most potent derivative [^{18}F]**54**, which was labeled in low overall RCY of 1.8% from the hydrosilane **53**, demonstrated that the positive physicochemical alteration introduced by the hydrophilic auxiliary correlated with improved imaging properties (Scheme 8). Enhanced tumor accumulation and tumor-to-blood ratio were detected in PC-3 xenografted mice compared to the lipophilic [^{18}F]SiFA-BBN probe.

5. [^{18}F]SiFA Protein Labeling

The ^{18}F-labeling of large biomolecules, such as proteins, antibodies, and more recently affibodies, has traditionally been accomplished by ^{18}F-carbon prosthetic labeling agents such as [^{18}F]fluorobenzaldehyde ([^{18}F]FBA), *N*-(2-[4-([^{18}F]fluorobenzamido)ethyl]maleimide ([^{18}F]FBEM), and *N*-succinimidyl 4-[^{18}F]fluorobenzoate ([^{18}F]SFB) [54–57]. Notwithstanding successful conjugation of those prosthetic groups to various proteins, their conjugation normally requires multiple hours of technical manipulations from the initial $^{18}F^-$ drying to the delivery of the labeled proteins. SiFA-IE, which proceeds rapidly and efficiently under mild conditions, offers much simplified procedures towards ^{18}F-labeled proteins.

Initial attempts to radiolabel active esters such as *N*-succinimidyl 3-(di-*tert*-butyl[^{18}F]fluorosilyl)benzoate **46** ([^{18}F]SiFB) and the pentafluorophenyl ester **47** for protein labeling failed even under IE conditions due to the propensity

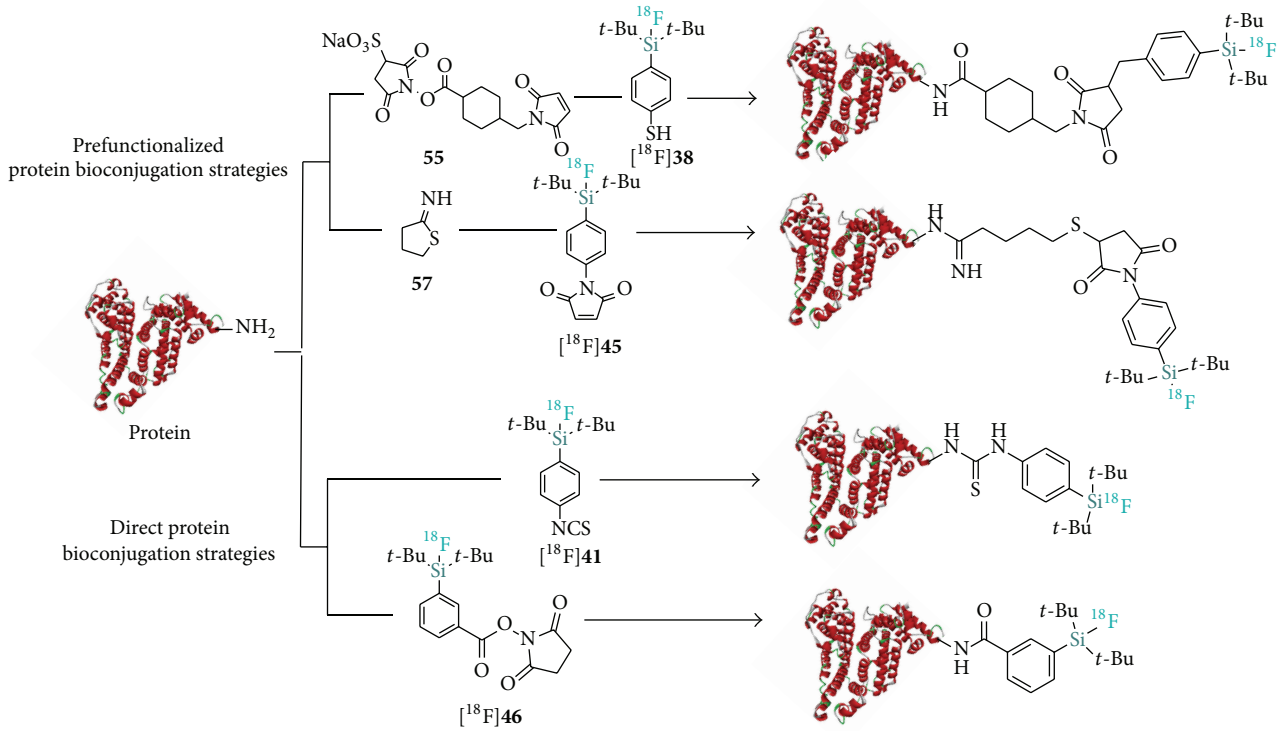

Scheme 9: Strategies towards the synthesis of [^{18}F]SiFA-labeled proteins by means of [^{18}F]SiFA prosthetic groups.

of those reactive moieties to hydrolyze under even slightly basic conditions. As an alternative approach, Iovkova et al. designed a prefunctionalization strategy involving protein derivatization with 2-iminithiolane (**57**) followed by the reaction with the SiFA maleimide [^{18}F]**45** for the labeling of rat serum albumin (RSA) used for blood pool PET imaging (Scheme 9) [45]. The derivatization strategy was also applied with success to RSA labeling with [^{18}F]SiFA-SH ([^{18}F]**38**) [6]. Protein functionalization with sulfo-SMCC (**55**) followed by treatment with [^{18}F]SiFA-SH obtained by IE allowed for the isolation of [^{18}F]SiFA-RSA in overall 12% RCY within 20–30 minutes. An important improvement towards simplified labeling was reported by Rosa-Neto et al. with the first introduction of a direct labeling agent, [^{18}F]SiFA-isothiocyanate ([^{18}F]**41**) which obviates preceding protein derivatization [44]. Remarkably, and despite the high reactivity of the isothiocyanate fragment, the IE proceeded nearly in quantitative yields (95% RCY; rt; 10 min) and allowed for the efficient direct synthesis of various ^{18}F-labeled model proteins (RSA, apotransferrin, and bovine IgG) in suitable SAs (2.7–4.5 Ci μmol^{-1}).

Subsequently, the decomposition of active esters such as [^{18}F]SiFB ([^{18}F]**46**) during radiolabeling due to the basicity of the reaction mixture (potassium oxalate/hydroxide) was resolved by addition of a suitable amount of oxalic acid in order to neutralize the base present during the labeling procedure [42]. This study showed the feasibility of the cartridge-based synthesis of [^{18}F]SiFB and demonstrated the applicability of this labeling synthon for protein labeling. This new SiFA based approach is technically much less demanding than the radiosynthesis of the well-known *N*-succinimidyl 4-[^{18}F]fluorobenzoate ([^{18}F]SFB), providing a simple access to ^{18}F-labeled proteins. This has led to the report of a standardized protocol for protein labeling via SiFB [58]. A straightforward labeling protocol has also been reported for protein labeling with [^{18}F]SiFA-SH ([^{18}F]**38**) [59].

The scope of SiFA-IE has recently been extended to the labeling of affibodies. Glaser et al. reported the efficient synthesis of a cysteine modified human epidermal growth factor receptor (HER2)-targeted affibody, [^{18}F]$Z_{HER2:2891}$-Cys-SiFA (Scheme 10) [60]. This study demonstrated the convenience and selectivity of the IE at a silicon-atom with the efficient aqueous radiolabeling of [^{19}F]-$Z_{HER2:2891}$-Cys-SiFA precursor from [^{18}F]F^-/[^{18}O]H_2O. Similar aqueous procedures had previously been described for the synthesis of a small SiFA-octreotate derivative (Scheme 7, [^{18}F]**50**) by Schirrmacher et al. [5]; however, direct aqueous labeling of large biomolecules such as affibodies (58 amino acids) is remarkable. Comparison with [^{18}F]benzaldehyde ([^{18}F]-FBA) and [^{18}F]Al-F/NOTA protocols conclusively demonstrated the efficiency of the SiFA-IE technique in terms of synthesis (RCYs, purity, and SA) despite an observed inferior in vivo profile, mainly attributed to hydrolysis leading to ^{18}F bone uptake.

6. Towards a Kit Formulation for SiFA-IE

Recently, a new drying method known as the "Munich method" has been introduced by Wessmann et al. which

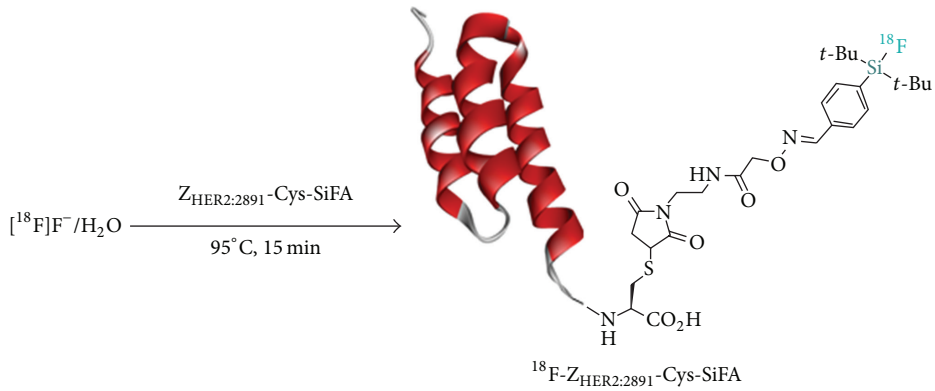

Scheme 10: Aqueous IE radiosynthesis of [^{18}F]-$Z_{HER2:2891}$-Cys-SiFA by Glaser et al.

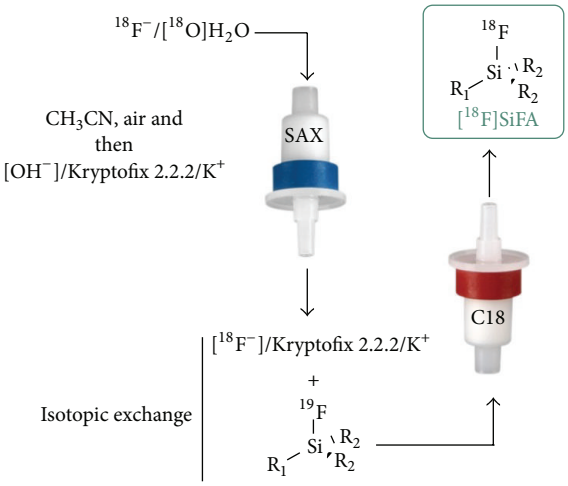

Figure 6: Combination of SiFA-IE strategy with the "Munich" ^{18}F drying method. The combination of the "Munich method" and the simple cartridge purification achievable by IE allows for a simple kit production procedure.

significantly simplified ^{18}F radiochemistry compared to the more classical and time-consuming azeotropic drying of $^{18}F^-$ [61]. The technique consists of the elution of dry $^{18}F^-$ from an anion exchange cartridge (SAX) with lyophilized Kryptofix 2.2.2./potassium hydroxide complex dissolved in anhydrous acetonitrile (Figure 6).

This procedure is fast (3–5 min) and fully devoid of azeotropic drying and is easily implemented into an automated setup. The recent implementation of the "Munich method" alongside the SiFA-IE labeling approach for peptide and protein labeling [43, 46, 58, 59] offers unique and unequalled simplicity, where, starting from commercially available [^{18}F]F^-/[^{18}O]H_2O, it is possible to deliver [^{18}F]SiFA radiopharmaceuticals using only room temperature transformations and facile cartridge-based manipulations. Following this approach, the ^{18}F-labeling of complex unprotected biomolecules becomes almost as easy as using a ^{99m}Tc-kit.

7. Small Molecules

It has previously been shown that, in the absence of suitable auxiliaries, the intrinsic lipophilicity introduced by the SiFA moiety often results in significant alteration of the overall physicochemical properties and in vivo biodistribution of the bioactive compound to which they are bound. This is especially true for ligands with low molecular weight. Nevertheless, certain groups have studied ^{18}F-radiolabeled silicon-based small ligands for PET imaging and, in some cases, obtained preliminary useful in vivo PET data.

An initial study by Bohn et al. and a follow-up investigation by Joyard et al. demonstrated the synthesis, radiolabeling, and in vivo evaluation of silicon-based analogues of [^{18}F]FMISO, an established tracer for detection of hypoxia [62, 63]. In spite of the well-known steric requirements of the silicon atom, the authors described a series of alkyl substituted [^{18}F]SiFA-FMISO analogues which resulted in insufficient hydrolytic stability both in vitro and in vivo (Table 3; Entries 1 and 2). Accordingly, the dimethyl [^{18}F]SiFA MISO compound ($t_{1/2} < 5$ min) only showed poor tumor uptake in mice while radioactivity accumulation occurred rapidly and significantly in bones due to the in vivo liberation of $^{18}F^-$. The more stable dinaphthyl derivative ($t_{1/2} = 125$ min) (Entry 4, Table 3) was retained in pulmonary capillaries due to its high lipophilicity (cLog P = 6.47). After evaluating other unstable derivatives, the authors described the synthesis and evaluation of a promising tBu$_2$Ph-based [^{18}F]SiFA tracer (Entry 7, Table 3) which was sufficiently stable for in vivo PET evaluations in rat. Upon injection, the tracer was shown to be heterogeneously distributed in healthy rats but unfortunately no evaluation in animals bearing a hypoxic tumor was reported.

Recently, Schulz et al. reported a protocol for the efficient radiolabeling of nucleosides and nucleotides derivatized with the SiFA building block. The labeled silylated thymidines [^{18}F]**58** and [^{18}F]**59** were obtained in high SA (10 Ci μmol^{-1}) from the corresponding hydrosilanes in 43% and 34% RCYs, respectively (Figure 7) [64]. Despite the potential application of those SiFA tracers as [^{18}F]FLT surrogates, no in vivo data is

Table 3: Structures of ^{18}F-silicon-based nitroimidazoles for PET hypoxia imaging.

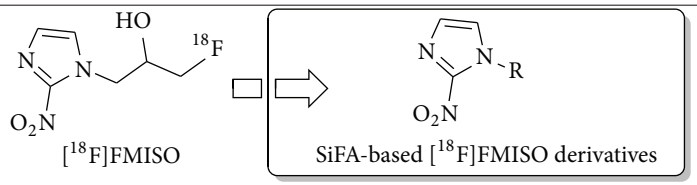

Entry	R[a]	Reference
1	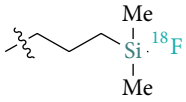	[62]
2	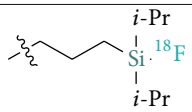	[62]
3	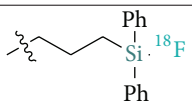	[62]
4	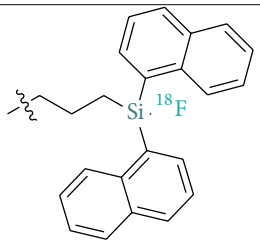	[62]
5	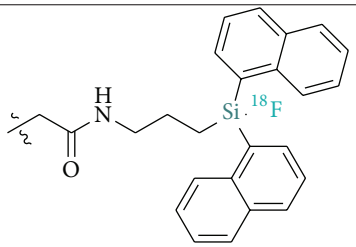	[63]
6	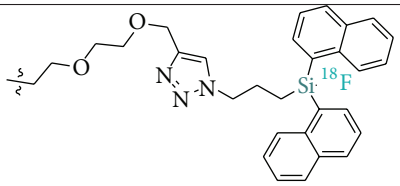	[63]
7	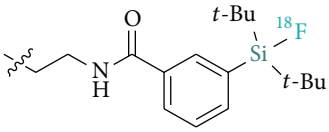	[63]

[a]Tracers were obtained via the SiFA leaving group approach from the corresponding silyl ethers.

currently available. The described procedure was also applied to the ^{18}F-radiolabeling of di- and oligonucleotide probes.

In a thorough study, silicon-based D_2-receptor ligands with structures analogous to [^{18}F]fallypride ([^{18}F]**60**) and [^{18}F]desmethoxyfallypride ([^{18}F]**61**) were reported (Figure 8) [65]. Derivatization with SiFA resulted in 44–650 times decreased affinities towards the D_2-receptor compared to fallypride (K_i = 0.0965 ± 0.0153 nM), yet remaining in the low nanomolar range. Upon optimization, the IE strategy delivered tracers [^{18}F]**62**, [^{18}F]**63**, and [^{18}F]**64** in 54–61% RCYs and all three tracers could be purified by just using SPE techniques. The measured SAs were in the range of 1.1–2.4 Ci μmol^{-1}. The most potent derivative, [^{18}F]**65** (K_i = 4.21 ± 0.41 nM), was labeled in only the modest RCY while stability issues prevented its purification following the solid-phase method. In vivo PET data were not reported.

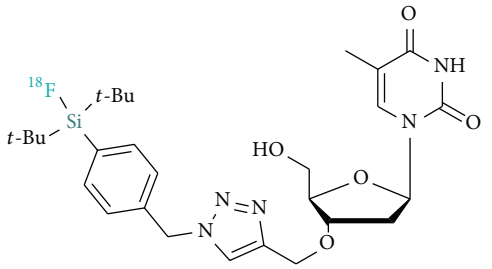

[^{18}F]**58**

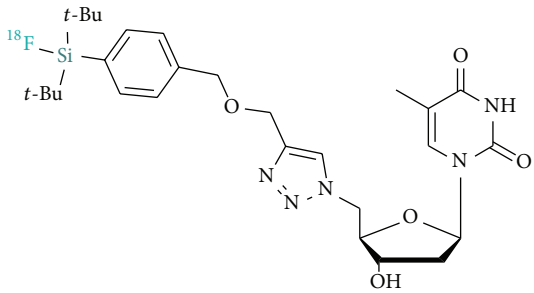

[^{18}F]**59**

Figure 7: Structures of ^{18}F-labeled thymidine probes.

The most recent contribution from Hazari et al. describes the design and evaluation of a highly potent and selective 5-HT$_{1A}$ homodimeric SiFA-dipropargyl glycerol derivatized radioligand aimed at PET imaging of dimeric serotonin receptors (Figure 9; [^{18}F]**65**) [66]. This multimeric approach is supported by the development of bivalent 5-HT ligands based on recent evidence suggesting that some 5-HT receptors exist as dimers/oligomers [67]. The tracer, [^{18}F]BMPPSiF, was obtained following the leaving group approach from the corresponding hydrosilane. The synthesis of the precursor was achieved via double azide-alkyne Huisgen cycloaddition with two azidoethyl (2-methoxyphenyl)piperazine fragments. Subsequent ^{18}F-radiofluorination occurred in 52 ± 10.5% RCY upon heating to yield [^{18}F]BMPPSiF with a SA of 13 Ci μmol^{-1}. Brain PET imaging in rats showed high uptake in 5-HT$_{1A}$ receptor rich regions. As expected, significant reduction of the uptake in the hippocampus was detected in serotonin-depleted rat models. Blocking studies did not reveal significant decrease in uptake. Notably, this report constitutes the first example of a SiFA-small ligand with positive PET imaging data. Interestingly, it also suggests that when applicable, [^{18}F]SiFA-based multimeric derivatization may help compensate the overall influence on physicochemical parameters of the SiFA moiety on small ligands.

8. SiFA: A Critical Assessment

From the very first appearance of SiFA compounds in 2006 and 2008 the groups of Ametamey and Schirrmacher/Wängler/Jurkschat have put extensive efforts into the structural optimization of the SiFA building blocks. The main drawback of this labeling technique irrespective of the actual labeling methodology (IE or leaving group approach) is the inherently extremely high lipophilicity hampering in vivo application in general. The compounds of the first generation when injected into animals were almost exclusively metabolized by the hepatobiliary system which lead to a high liver uptake and almost zero uptake in the target tissue. Both groups have approached this problem by introducing hydrophilic components into the SiFA tagged molecules to compensate for the high lipophilicity. However, this strategy is only useful for larger biomolecules such as peptides and proteins which tolerate an extensive structural modification. It could be convincingly demonstrated by Niedermoser et al. recently that highly hydrophilic SiFA derivatized somatostatin analogues can be labeled in a one-step reaction via IE in high RCYs and SAs of 1200–1700 Ci/mmol [68]. High IC$_{50}$ values of the SiFA-peptides in the low nanomolar range and a very high tumor uptake of >15% in a AR42J nude mice tumor model showed that the lipophilicity problem has been successfully solved, paving the way for a human clinical application in the near future. The most recently published paper by Lindner at al. demonstrated that SiFA tagged RGD peptides can serve as tumor imaging agents in a mouse U87MG tumor model if hydrophilic auxiliaries are added in combination with the SiFA labeling moiety [69]. A tumor uptake of 5.3% ID/g was observed, clearly delineating the tumor from other tissues. Unfortunately smaller molecules lend themselves less towards a SiFA labeling because of the difficulty of compensating for the SiFA lipophilicity. A small molecule such as a typical receptor ligand for brain imaging does not accept considerable structural modifications to adjust the SiFA lipophilicity without seriously compromising its binding properties to the target receptor. It is therefore unlikely that the SiFA labeling technique will grow into a staple for labeling molecules of small molecular weight. It is also true that all compounds reported so far have been only used in animal experiments. The SiFA methodology still has to prove its usefulness in a human clinical setting. This however requires extensive efforts and financial commitments from the academic research groups and it is hoped that the industry, which already showed interest in this labeling technique, will help transitioning this promising labeling technique to the clinic.

9. Conclusion

The SiFA methodology has grown over the years from a niche methodology to a broadly applied labeling strategy towards innovative ^{18}F-labeled radiopharmaceuticals for PET. SiFA radiolabeling procedures have been methodically studied and can be easily performed using either the SiFA leaving group approach or the SiFA-IE methodology. Moreover, those approaches are now well-established for a great variety of structurally distinct high affinity probes such as peptides, proteins, affibodies, and even small ligands. The practical simplicity and mild reaction conditions of the SiFA-IE strategy in particular represents a unique advantage in ^{18}F-labeling which, when applied in synergy with

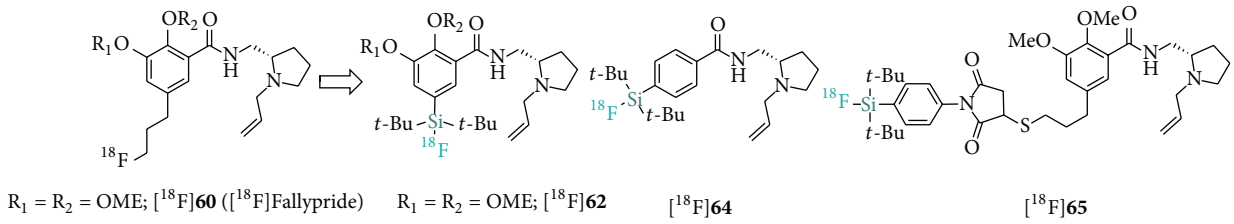

Figure 8: Structures of [^{18}F] SiFA D_2-receptor ligands.

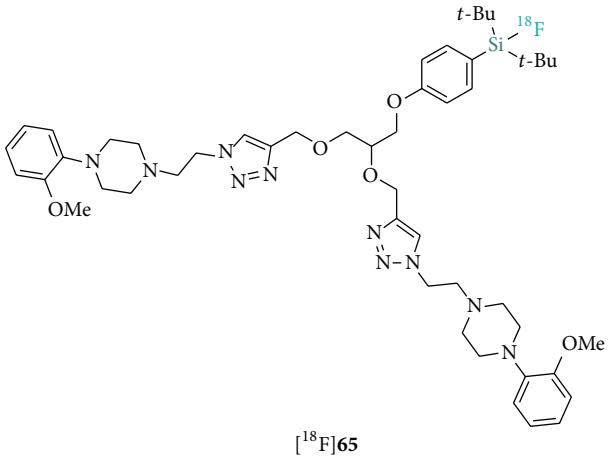

Figure 9: Structure of the dimeric 5-HT_{1A} radioligand [^{18}F] BMPP-SiF.

the recently developed Munich drying method, helps meeting the requirements for a true kit-like ^{18}F-labeling procedure.

Abbreviations

PET:	Positron emission tomography
SiFA:	Silicon-fluoride-acceptor
IE:	Isotopic exchange
HPLC:	High-performance liquid chromatography
D_2 receptor:	Dopamine receptor subtype D_2
RCY:	Radiochemical yield
SPECT:	Single-photon emission computed tomography
GMP:	Good Manufacturing Practice
Nca:	No-carrier-added
DFT:	Density functional theory
BDE:	Bond dissociation energy
SPE:	Solid phase extraction
NALG:	Nucleophile assisting leaving groups
S_N2:	Nucleophilic substitution bimolecular
BBN:	Bombesin
GRPR:	Gastrin-releasing peptide receptor
PEG:	Polyethylene glycol
SA:	Specific radioactivity
RSA:	Rat serum albumin
SAX:	Anion exchange cartridge
5-HT_{1A}:	Serotonin receptor.

Conflict of Interests

The authors declare that there is no conflict of interests regarding the publication of this paper.

References

[1] C. Yoshida, A. B. Tsuji, H. Sudo et al., "Development of positron emission tomography probe of ^{64}Cu-labeled anti-C-kit 12A8 Fab to measure protooncogene C-kit expression," *Nuclear Medicine and Biology*, vol. 38, no. 3, pp. 331–337, 2011.

[2] C. Wängler, B. Wängler, S. Lehner et al., "A universally applicable 68Ga-labeling technique for proteins," *Journal of Nuclear Medicine*, vol. 52, no. 4, pp. 586–591, 2011.

[3] P. Szymański, T. Fraczek, M. Markowicz, and E. Mikiciuk-Olasik, "Development of copper based drugs, radiopharmaceuticals and medical materials," *BioMetals*, vol. 25, no. 6, pp. 1089–1112, 2012.

[4] B. M. Zeglis, J. L. Houghton, M. J. Evans, N. Viola-Villegas, and J. S. Lewis, "Underscoring the influence of inorganic chemistry on nuclear imaging with radiometals," *Inorganic Chemistry*, vol. 53, no. 4, pp. 1880–1899, 2014.

[5] R. Schirrmacher, G. Bradtmöller, E. Schirrmacher et al., "18F-labeling of peptides by means of an organosilicon-based fluoride acceptor," *Angewandte Chemie International Edition*, vol. 45, no. 36, pp. 6047–6050, 2006.

[6] B. Wängler, G. Quandt, L. Iovkova et al., "Kit-like 18F-labeling of proteins: Synthesis of 4-(Di-tert-butyl[18F]fluorosuyl)benzenethiol (Si[18F]FA-SH) labeled rat serum albumin for blood pool imaging with PET," *Bioconjugate Chemistry*, vol. 20, no. 2, pp. 317–321, 2009.

[7] W. J. McBride, C. A. D'Souza, H. Karacay, R. M. Sharkey, and D. M. Goldenberg, "New lyophilized kit for rapid radiofluorination of peptides," *Bioconjugate Chemistry*, vol. 23, no. 3, pp. 538–547, 2012.

[8] E. Schirrmacher, B. Wängler, M. Cypryk et al., "ynthesis of p-(Di-tert-butyl[(18)f]fluorosilyl)benzaldehyde ([F-18]SiFA-A) with high specific activity by isotopic exchange: a convenient Labeling synthon for the F-18-labeling of n-amino-oxy derivatized peptides," *Bioconjugate Chemistry*, vol. 18, no. 6, pp. 2085–2089, 2007.

[9] A. Höhne, L. Mu, M. Honer et al., "Synthesis, ^{18}F-labeling, and *in vitro* and *in vivo* studies of bombesin peptides modified with

silicon-based building blocks," *Bioconjugate Chemistry*, vol. 19, no. 9, pp. 1871–1879, 2008.

[10] C. Wängler, A. Kostikov, J. Zhu, J. Chin, B. Wängler, and R. Schirrmacher, "Silicon-[18F]Fluorine radiochemistry: basics, application and challenges," *Applied Sciences*, vol. 2, pp. 227–302, 2012.

[11] R. Ting, M. J. Adam, T. J. Ruth, and D. M. Perrin, "Arylfluoroborates and alkylfluorosilicates as potential PET imaging agents: high-yielding aqueous biomolecular18F-labeling," *Journal of the American Chemical Society*, vol. 127, no. 38, pp. 13094–13095, 2005.

[12] R. Ting, C. Harwig, U. Auf Dem Keller et al., "Toward [18F]-labeled aryltrifluoroborate radiotracers: in vivo positron emission tomography imaging of stable aryltrifluoroborate clearance in mice," *Journal of the American Chemical Society*, vol. 130, no. 36, pp. 12045–12055, 2008.

[13] U. A. D. Keller, C. L. Bellac, Y. Li et al., "Novel matrix metalloproteinase inhibitor [18F]marimastat- aryltrifluoroborate as a probe for in vivo positron emission tomography imaging in cancer," *Cancer Research*, vol. 70, no. 19, pp. 7562–7569, 2010.

[14] L. Mu, P. A. Schubiger, and S. M. Ametamey, "[18F]fluorosilicon- and [18F]fluoroboron-based biomolecules for PET imaging," *Current Radiopharmaceuticals*, vol. 3, no. 3, pp. 224–242, 2010.

[15] W. J. McBride, R. M. Sharkey, H. Karacay et al., "A novel method of 18F radiolabeling for PET," *Journal of Nuclear Medicine*, vol. 50, no. 6, pp. 991–998, 2009.

[16] W. J. McBride, C. A. D'souza, R. M. Sharkey et al., "Improved 18F labeling of peptides with a fluoride-aluminum-chelate complex," *Bioconjugate Chemistry*, vol. 21, no. 7, pp. 1331–1340, 2010.

[17] P. Laverman, W. J. McBride, R. M. Sharkey et al., "A novel facile method of labeling octreotide with ^{18}F-fluorine," *Journal of Nuclear Medicine*, vol. 51, no. 3, pp. 454–461, 2010.

[18] W. J. McBride, R. M. Sharkey, and D. M. Goldenberg, "Radiofluorination using aluminum-fluoride (Al^{18}F)," *EJNMMI Research*, vol. 3, no. 1, pp. 1–11, 2013.

[19] G. E. Smith, H. L. Sladen, S. C. G. Biagini, and P. J. Blower, "Inorganic approaches for radiolabelling biomolecules with fluorine-18 for imaging with Positron Emission Tomography," *Dalton Transactions*, vol. 40, no. 23, pp. 6196–6205, 2011.

[20] U. Choudhry, K. E. Martin, S. Biagini, and P. J. Blower, "Alkoxysilane groups for instant labeling of biomolecules with ^{18}F," *Nuclear Medicine Communications*, vol. 27, no. 3, p. 27, 2006.

[21] L. Mu, A. Höhne, P. A. Schubiger et al., "Silicon-based building blocks for one-step ^{18}F-radiolabeling of peptides for PET imaging," *Angewandte Chemie International Edition*, vol. 47, no. 26, pp. 4922–4925, 2008.

[22] T. A. Gens, J. A. Wethington Jr., and A. R. Brosi, "The exchange of F-18 between metallic fluorides and silicon tetrafluoride," *Journal of Physical Chemistry*, vol. 62, no. 12, p. 1593, 1959.

[23] R. T. Poole and J. M. Winfield, "Radiotracers in fluorine chemistry. Part IV. Fluorine-18 exchange between labelled alkylfluorosilanes and fluorides, or fluoride methoxides, of tungsten(VI), molybdenum(VI), tellurium(VI), and iodine(V)," *Journal of the Chemical Society: Dalton Transactions*, vol. 12, no. 16, pp. 1557–1560, 1976.

[24] J. M. Winfield, "Preparation and use of 18-fluorine labelled inorganic compounds," *Journal of Fluorine Chemistry*, vol. 16, no. 1, pp. 1–17, 1980.

[25] B. W. Fry, G. M. Whitford, and D. H. Pashley, "A method for increasing the amount of 18F at the laboratory by recovery during transport from the reactor," *The International Journal Of Applied Radiation and Isotopes*, vol. 29, no. 2, pp. 123–125, 1978.

[26] M. S. Rosenthal, A. L. Bosch, R. J. Nickles, and S. J. Gatley, "Synthesis and some characteristics of no-carrier added [18F]fluorotrimethylsilane," *The International Journal of Applied Radiation and Isotopes*, vol. 36, no. 4, pp. 318–319, 1985.

[27] S. J. Gatley, "Rapid production and trapping of [F-18] fluorotrimethylsilane, and its use in nucleophilic F-18 labeling without an aqueous evaporation step," *Applied Radiation and Isotopes*, vol. 40, no. 6, pp. 541–544, 1989.

[28] G. K. Mulholland, "Recovery and purification of no-carrier-added [18F]fluoride with bistrimethylsilylsulfate (BTMSS)," *International Journal of Radiation Applications and Instrumentation*, vol. 42, no. 11, pp. 1003–1008, 1991.

[29] E. Schirrmacher, B. Wängler, M. Cypryk et al., "Synthesis of p-(Di-tert-butyl[18F]fluorosilyl)benzaldehyde ([18F]SiFA-A) with high specific activity by isotopic exchange: a convenient labeling synthon for the 18F-labeling of *N*-amino-oxy derivatized peptides," *Bioconjugate Chemistry*, vol. 18, no. 6, pp. 2085–2089, 2007.

[30] R. Damrauer, L. W. Burggraf, L. P. Davis, and M. S. Gordon, "Gas-phase and computational studies of pentacoordinate silicon," *Journal of the American Chemical Society*, vol. 110, no. 20, pp. 6601–6606, 1988.

[31] I. H. Krouse and P. G. Wenthold, "Formation and decomposition of hydroxysiliconates in the gas phase," *Organometallics*, vol. 23, no. 11, pp. 2573–2582, 2004.

[32] A. P. Kostikov, L. Iovkova, J. Chin et al., "N-(4-(di-tert-butyl[18F]fluorosilyl)benzyl)-2-hydroxy-N,N- dimethylethylammonium bromide ([^{18}F]SiFAN+Br-): a novel lead compound for the development of hydrophilic SiFA-based prosthetic groups for ^{18}F-labeling," *Journal of Fluorine Chemistry*, vol. 132, no. 1, pp. 27–34, 2011.

[33] A. Höhne, L. Yu, L. Mu et al., "Organofluorosilanes as model compounds for ^{18}F-labeled silicon-based PET tracers and their hydrolytic stability: experimental data and theoretical calculations (PET=Positron Emission Tomography)," *Chemistry*, vol. 15, no. 15, pp. 3736–3743, 2009.

[34] S. Lu, S. D. Lepore, Y. L. Song et al., "Nucleophile assisting leaving groups: a strategy for aliphatic 18F-fluorination," *Journal of Organic Chemistry*, vol. 74, no. 15, pp. 5290–5296, 2009.

[35] M. H. Al-Huniti, S. Lu, V. W. Pike, and S. D. Lepore, "Enhanced nucleophilic fluorination and radiofluorination of organosilanes appended with potassium-chelating leaving groups," *Journal of Fluorine Chemistry*, vol. 158, pp. 48–52, 2014.

[36] L. O. Dialer, S. V. Selivanova, C. J. Muller et al., "Studies toward the development of new silicon-containing building blocks for the direct ^{18}F-labeling of peptides," *Journal of Medicinal Chemistry*, vol. 56, no. 19, pp. 7552–7563, 2013.

[37] M. Fiorenza, A. Mordini, and A. Ricci, "The mechanism of solvolysis of β-ketosilanes," *Journal of Organometallic Chemistry*, vol. 280, no. 2, pp. 177–182, 1985.

[38] D. O. Kiesewetter, O. Jacobson, L. X. Lang, and X. Y. Chen, "Automated radiochemical synthesis of [^{18}F]FBEM: a thiol

reactive synthon for radiofluorination of peptides and proteins," *Applied Radiation and Isotopes*, vol. 69, no. 2, pp. 410–414, 2011.

[39] A. Speranza, G. Ortosecco, E. Castaldi, A. Nardelli, L. Pace, and M. Salvatore, "Fully automated synthesis procedure of 4-[18F]fluorobenzaldehyde by commercial synthesizer: amino-oxi peptide labelling prosthetic group," *Applied Radiation and Isotopes*, vol. 67, no. 9, pp. 1664–1669, 2009.

[40] D. Thonon, D. Goblet, E. Goukens et al., "Fully automated preparation and conjugation of N-succinimidyl 4-[(18)F]fluorobenzoate ([(18)F]SFB) with RGD peptide using a GE FASTlab synthesizer," *Molecular Imaging and Biology*, vol. 13, no. 6, pp. 1088–1095, 2011.

[41] L. Iovkova, D. Könning, B. Wängler et al., "SiFA-modified phenylalanine: a key compound for the efficient synthesis of18F-labelled peptides," *European Journal of Inorganic Chemistry*, no. 14, pp. 2238–2246, 2011.

[42] L. F. Tietze and K. Schmuck, "SiFA azide: a new building block for PET imaging using click chemistry," *Synlett*, no. 12, pp. 1697–1700, 2011.

[43] A. P. Kostikov, J. Chin, K. Orchowski et al., "Oxalic acid supported Si-18F-radiofluorination: one-step radiosynthesis of N-succinimidyl 3-(Di-tert-butyl[18F]fluorosilyl) benzoate ([18F]SiFB) for protein labeling," *Bioconjugate Chemistry*, vol. 23, no. 1, pp. 106–114, 2012.

[44] P. Rosa-Neto, B. Wängler, L. Iovkova et al., "[^{18}F]SiFA-isothiocyanate: a new highly effective radioactive labeling agent for lysine-containing proteins," *ChemBioChem*, vol. 10, no. 8, pp. 1321–1324, 2009.

[45] L. Iovkova, B. Wängler, E. Schirrmacher et al., "Para-functionalized aryl-di-tert-butylfluorosilanes as potential labeling synthons for18F radiopharmaceuticals," *Chemistry*, vol. 15, no. 9, pp. 2140–2147, 2009.

[46] E. Balentova, C. Collet, S. Lamandé-Langle et al., "Synthesis and hydrolytic stability of novel 3-[^{18}F] fluoroethoxybis(1-methylethyl)silyl]propanamine-based prosthetic groups," *Journal of Fluorine Chemistry*, vol. 132, no. 4, pp. 250–257, 2011.

[47] C. Wängler, B. Waser, A. Alke et al., "One-step 18F-labeling of carbohydrate-conjugated octreotate-derivatives containing a silicon-fluoride-acceptor (SiFA): in vitro and in vivo evaluation as tumor imaging agents for positron emission tomography (PET)," *Bioconjugate Chemistry*, vol. 21, no. 12, pp. 2289–2296, 2010.

[48] M. Schottelius, F. Rau, J. C. Reubi, M. Schwaiger, and H. Wester, "Modulation of pharmacokinetics of radioiodinated sugar-conjugated somatostatin analogues by variation of peptide net charge and carbohydration chemistry," *Bioconjugate Chemistry*, vol. 16, no. 2, pp. 429–437, 2005.

[49] M. Schottelius, H. J. Wester, J. C. Reubi, R. Senekowitsch-Schmidtke, and M. Schwaiger, "Improvement of pharmacokinetics of radioiodinated Tyr3-octreotide by conjugation with carbohydrates," *Bioconjugate Chemistry*, vol. 13, no. 5, pp. 1021–1030, 2002.

[50] P. Antunes, M. Ginj, M. A. Walter, J. H. Chen, J. C. Reubi, and H. R. Maecke, "Influence of different spacers on the biological profile of a DOTA-somatostatin analogue," *Bioconjugate Chemistry*, vol. 18, no. 1, pp. 84–92, 2007.

[51] C. Wängler, S. Niedermoser, J. Chin et al., "One-step ^{18}F-labeling of peptides for positron emission tomography imaging using the SiFA methodology," *Nature Protocols*, vol. 7, no. 11, pp. 1946–1955, 2012.

[52] E. Amigues, J. Schulz, M. Szlosek-Pinaud et al., "[18F]Si-RiboRGD: from design and synthesis to the imaging of $\alpha v\beta 3$ integrins in melanoma tumors," *ChemPlusChem*, vol. 77, no. 5, pp. 345–349, 2012.

[53] R. Haubner, B. Kuhnast, C. Mang et al., "[^{18}F]galacto-RGD: synthesis, radiolabeling , metabolic stability, and radiation dose estimates," *Bioconjugate Chemistry*, vol. 15, no. 1, pp. 61–69, 2004.

[54] G. Vaidyanathan and M. R. Zalutsky, "Labeling proteins with fluorine-18 using N-succinimidyl 4-[^{18}F]fluorobenzoate," *Nuclear Medicine and Biology*, vol. 19, no. 3, pp. 275–281, 1992.

[55] G. Vaidyanathan and M. R. Zalutsky, "Improved synthesis of N-succinimidyl 4-[^{18}F]fluorobenzoate and its application to the labeling of a monoclonal antibody fragment," *Bioconjugate Chemistry*, vol. 5, no. 4, pp. 352–356, 1994.

[56] F. Wuest, M. Berndt, R. Bergmann, J. van den Hoff, and J. Pietzsch, "Synthesis and application of [^{18}F]FDG-maleimidehexyloxime ([^{18}F]FDG-MHO): a [^{18}F]FDG-based prosthetic group for the chemoselective ^{18}F-labeling of peptides and proteins," *Bioconjugate Chemistry*, vol. 19, no. 6, pp. 1202–1210, 2008.

[57] Z. Miao, G. Ren, H. Liu, S. Qi, S. Wu, and Z. Cheng, "PET of EGFR expression with an 18F-labeled affibody molecule," *Journal of Nuclear Medicine*, vol. 53, no. 7, pp. 1110–1118, 2012.

[58] A. P. Kostikov, J. Chin, K. Orchowski et al., "Synthesis of [^{18}F]SiFB: a prosthetic group for direct protein radiolabeling for application in positron emission tomography," *Nature Protocols*, vol. 7, no. 11, pp. 1956–1963, 2012.

[59] B. Wängler, A. P. Kostikov, S. Niedermoser et al., "Protein labeling with the labeling precursor [^{18}F]SiFA-SH for positron emission tomography," *Nature Protocols*, vol. 7, no. 11, pp. 1964–1969, 2012.

[60] M. Glaser, P. Iveson, S. Hoppmann et al., "Three methods for 18F labeling of the HER2-binding affibody molecules $Z_{HER2:2891}$ including preclinical assessment," *Journal of Nuclear Medicine*, vol. 54, no. 11, pp. 1981–1988, 2013.

[61] S. H. Wessmann, G. Henriksen, and H.-J. Wester, "Cryptate mediated nucleophilic 18F-fluorination without azeotropic drying," *NuklearMedizin*, vol. 51, no. 1, pp. 1–8, 2012.

[62] P. Bohn, A. Deyine, R. Azzouz et al., "Design of silicon-based misonidazole analogues and 18F-radiolabelling," *Nuclear Medicine and Biology*, vol. 36, no. 8, pp. 895–905, 2009.

[63] Y. Joyard, R. Azzouz, L. Bischoff et al., "Synthesis of new 18F-radiolabeled silicon-based nitroimidazole compounds," *Bioorganic and Medicinal Chemistry*, vol. 21, no. 13, pp. 3680–3688, 2013.

[64] J. Schulz, D. Vimont, T. Bordenave et al., "Silicon-based chemistry: an original and efficient one-step approach to [18F]-Nucleosides and [18F]-Oligonucleotides for PET imaging," *Chemistry*, vol. 17, no. 11, pp. 3096–3100, 2011.

[65] L. Iovkova-Berends, C. Wängler, T. Zöller et al., "*t*-Bu_2SiF-derivatized D_2-receptor ligands: the first SiFA-containing small molecule radiotracers for target-specific PET-imaging," *Molecules*, vol. 16, no. 9, pp. 7458–7479, 2011.

[66] P. P. Hazari, J. Schulz, D. Vimont et al., "A new SiF-dipropargyl glycerol scaffold as a versatile prosthetic group to design dimeric radioligands: synthesis of the [^{18}F]BMPPSiF tracer to image serotonin receptors," *ChemMedChem*, vol. 8, pp. 1–14, 2013.

[67] M. J. Shashack, K. A. Cunningham, P. K. Seitz et al., "Synthesis and evaluation of dimeric derivatives of 5-HT 2A receptor (5-HT 2AR) antagonist M-100907," *ACS Chemical Neuroscience*, vol. 2, no. 11, pp. 640–644, 2011.

[68] S. Niedermoser, C. Wängler, J. Chin et al., "Chemical and biological evaluation of new hydrophilic [^{18}F] SiFA-derivatized somatostatin analogues," *Journal of Nuclear Medicine*, vol. 54, supplement 2, p. 60, 2013.

[69] S. K. Lindner, C. Michler, S. Leidner et al., "Synthesis, in vitro and in vivo evaluation of SiFA -tagged bombesin and RGD peptides as tumor imaging probes for positron emission tomography (PET)," *Bioconjugate Chemistry*, 2014.

Hindawi Publishing Corporation
BioMed Research International
Volume 2014, Article ID 380124, 10 pages
http://dx.doi.org/10.1155/2014/380124

Review Article

Radiosynthesis of [^{18}F]Trifluoroalkyl Groups: Scope and Limitations

V. T. Lien[1,2] and P. J. Riss[1,2]

[1] *Kjemisk Institutt, Universitetet I Oslo, Sem Sælands Vei 26, 0376 Oslo, Norway*
[2] *Norsk Medisinsk Syklotronsenter AS, Postboks 4950 Nydalen, 0424 Oslo, Norway*

Correspondence should be addressed to P. J. Riss; patrick.riss@kjemi.uio.no

Received 20 March 2014; Revised 21 April 2014; Accepted 6 May 2014; Published 10 July 2014

Academic Editor: Olaf Prante

The present paper is concerned with radiochemical methodology to furnish the trifluoromethyl motif labelled with ^{18}F. Literature spanning the last four decades is comprehensively reviewed and radiochemical yields and specific activities are discussed.

1. Introduction

Substantial interest has been given lately to the trifluoromethyl group in the context of radiotracer development for positron emission tomography (PET). PET imaging of radiotracer distribution in living systems provides noninvasive insights into biochemical transactions in vivo. PET relies on molecular probes labelled with positron emitting radionuclides that participate in the process of interest. Coincident detection of 511 keV photons originating from positron-electron annihilation allows for spatial localisation and quantification of the decaying radionuclide in tissue with some accuracy [1–4]. Application of PET in biomedical research, drug development, and clinical imaging creates an immanent need for radiotracers for a variety of biological targets.

The neutron-deficient fluorine isotope ^{18}F is the most frequently employed PET nuclide [5]. This is due to an expedient half-life of 109.7 min, which facilitates commercial distribution of ^{18}F-radiotracers and permits convenient handling of the tracer in multistep reactions and imaging studies [1–3]. Almost exclusive decay via the β^+ decay branch (97%), paired with a very low positron energy (638 keV), effectively limits the linear range of the emitted positron in water and makes up for the highest image resolution compared to most other PET nuclides. ^{18}F readily forms stable bonds to carbon atoms, which promotes the straightforward introduction of F atoms into most organic molecules. Using the ^{18}O(p,n)^{18}F nuclear reaction, batch production of 370 GBq [^{18}F]fluoride ion (10^3 human doses) is routinely achievable by irradiation of $H_2{}^{18}O$ liquid targets. High specific radioactivity (A_s; [A_s] = Bq/mol; >150 MBq/nmol) is a realistic expectation for radiotracers prepared from [^{18}F]fluoride ion. Likewise, high specific activity (>100 MBq/nmol) is inevitable to maintain genuine tracer conditions for PET-imaging of saturable biological systems [1, 4–7], particularly in small animals but even so in human subjects [8]. As such, high specific activity is a cornerstone of the tracer principle, first introduced by George de Hevesy [1, 6, 9]. In theory, PET may provide the means for noninvasive observation of chemical processes in tissues, exemplified here for receptor binding, as long as the injected amount of the radiotracer does not lead to significant receptor occupation (RO). Receptor occupation is closely linked to pharmacodynamic efficacy and a pharmacological effect can be omitted in cases when the RO is negligible. Figures for insignificant RO have been specified to <1%–5%; nevertheless, it has to be kept in mind that RO is a specific characteristic of a receptor-ligand system and thus may vary from target to target [6, 7, 9]. Hence, the specific activity of each individual radiotracer has to meet the requirements for noninvasive PET imaging. For these reasons, the A_s is the most important quality measure for a labelling reaction rather than chemical or radiochemical yield.

Evidently, an abundant motif such as the trifluoromethyl group and its presence in a large number of agrochemicals and biologically active drug molecules is of tremendous

Table 1: Survey of radiosynthetic approaches towards the radiosynthesis of [^{18}F]trifluoroalkyl groups.

Method	Year	Yield/%	As (reported value) comment	Reference
(1) ^{18}F-^{19}F exchange	1979	0.5–15	Low—carrier added	Ido et al. [10]
(2) Sb_2O_3 catalysed ^{18}F-Cl substitution	1986	20–50	Low—carrier added	Angelini et al. [11, 12]
(3) ^{18}F-^{19}F exchange	1990	85	Low—(0.00002–0.002 MBq/nmol) carrier added	Kilbourn and Subramanian [13]
(4) ^{18}F-^{19}F exchange	1993	78	Low—carrier added	Aigbirhio et al. [14]
(5) ^{18}F-^{19}F exchange	1994	15–99	Low—(0.2–16.6 MBq/nmol) [15] carrier added	Satter et al. [16]
(6) ^{18}F-Br substitution	1990	17–28	Low—(0.037 MBq/nmol) precursor separation	Kilbourn et al. [17]
(7) ^{18}F-Br substitution	1993	1–4	Low—(1.5–2.5 MBq/nmol) side reaction	Das and Mukherjee [15]
(8) ^{18}F-Br substitution	1995	45–60	Low—(0.040–0.800 MBq/nmol) side reactions	Johnstrom and Stone-Elander [18]
(9) ^{18}F-fluorodesulfurisation	2001	40	Low—(0.000002 MBq/nmol) carrier added	Josse et al. [19]
(10) ^{18}F-Br substitution	2007	10 ± 2	Low—(4.4 ± 1.5 MBq/nmol) side reactions	Prabhakaran et al. [20]
(11) ^{18}F-^{19}F exchange	2011	~60	Low—carrier added	Suehiro et al. [21]
(12) H^{18}F addition	2011	52–93	Moderate (86 MBq/nmol)—side reaction	Riss and Aigbirhio [22]
(13) ^{18}F-I substitution	2013	60 ± 15	Not given	Van der Born et al. [23]
(14) Nucleophilic trapping of difluorocarbene formed in situ and Cu(I) mediated trifluoromethylation with Cu-[^{18}F]CF_3	2013	5–87	Low—(0.1 MBq/nmol) side reactions	Huiban et al. [24]
(15) ^{18}F-I substitution, in situ formation of Cu-[^{18}F]CF_3	2014	12–93	Low—(0.15 MBq/nmol) side reactions	Ruehl et al. [25]
(16) ^{18}F-F_2 addition	2001	10–17	Low—carrier added	Dolbier et al. [26]
(17) ^{18}F-F_2 disproportionation	2003	22–28	Low—(0.015–0.020 MBq/nmol) carrier-added	Prakash et al. [27]
(18) ^{18}F-selectfluor bis-triflate	2013	9–18	Low—(3.3 MBq/nmol) carrier-added	Mizuta et al. [28]

interest for the PET community. Consequently, earliest attempts to access this group by nucleophilic and electrophilic radiofluorination protocols date back into the very beginnings of the field of PET chemistry (see Table 1 for an overview).

Classical organic chemistry has seen a surge in the development of novel trifluoromethylation strategies and protocols [29–35], owed to the high relevance of the trifluoromethyl motif [36, 37]. However, translation of these most useful and often robust and versatile protocols into radiochemistry is not without difficulties. Indeed, straightforward translation of known organic reactions under stoichiometric conditions into no-carrier-added nucleophilic radiosynthesis often precipitates in adverse findings. Polyfluorinated, organic moieties complicate nucleophilic radiofluorination using ^{18}F-fluoride ion. Under the common conditions used, there is an inherent vulnerability for isotopic dilution of the labelled product with its nonradioactive analogue. Inherently unproblematic exchange processes between carbon-bound ^{19}F and ^{19}F anions in the reaction mixture, which do not confound the final quality of a nonradioactive product, can devastate the specific activity of PET radiotracers [38].

2. Nucleophilic Radiosynthesis

Nucleophilic radiofluorination remained rarely a successful protocol prior to the advent of supramolecular chemistry and the development of potassium selective cryptands. The latter, when combined with mild organic potassium bases and aqueous solutions of $^{18}F^-$ proved to be key to improve the inherently low solubility and reactivity of fluoride ion in dipolar aprotic solvents [39, 40].

Earliest attempts of developing suitable methodology for the synthesis of the [^{18}F]CF_3 group involved transient incorporation of an ^{18}F label into trifluoromethylated scaffolds via ^{18}F-^{19}F isotopic exchange at high temperature as devised by Ido et al. [10]. Shortly thereafter, Lewis acid catalysed dechlorofluorination of chlorodifluoromethyl groups via a straightforward protocol using H^{18}F and Sb_2O_3 was utilised in the synthesis of ^{18}F-labelled trifluoromethyl arenes [11, 12]. Both of these procedures afforded the desired products in only moderate yields and low specific activity. Nevertheless, isotopic exchange protocols were soon found to be reliable protocols to achieve radiofluorination of di and trifluorinated carbon centres, somewhat tolerant to the presence

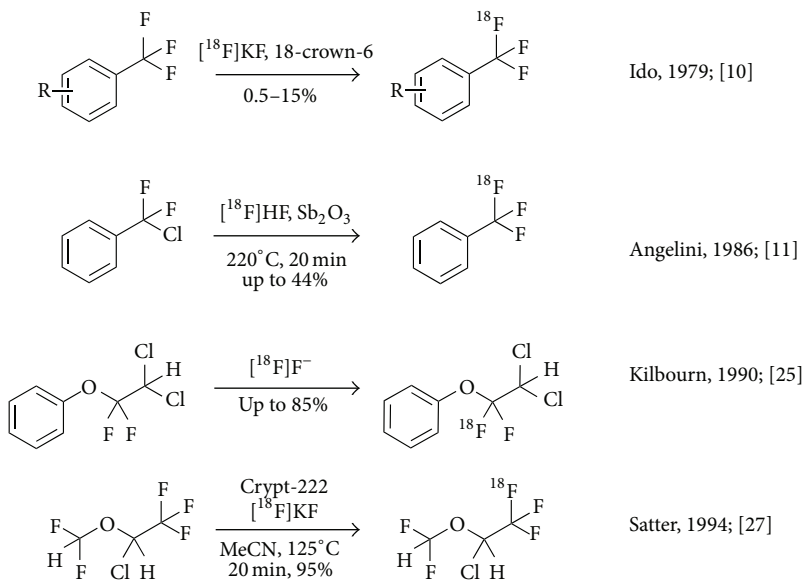

Figure 1: Nucleophilic radiosynthesis of ^{18}F-labelled trifluoroalkyl groups using isotopic exchange and antimony mediated ^{18}F-for-Cl substitution.

of water [13], albeit with strict limitation for the achievable specific activity, governed by the fact that only a fraction of the obtained carrier-added product will actually contain the radiolabel (see Figure 1).

However, low specific activity may not be an issue in PET studies targeting physical or metabolic processes in vivo, for example, in the case of the mechanisms of action of fast-acting aerosols for anaesthesia. Similarly, radiolabelling of chlorofluorocarbon (CFC) replacement agents such as 1,1,1,2-tetrafluoroethane (HFA 134a) for radiotracer studies does not require particularly high specific radioactivities. This fact was exploited by Satter et al. and Aigbirhio et al. who labelled the CFC replacement agent HFA 134a using an isotopic exchange reaction on the nonradioactive analogue [14, 16, 41, 42]. Satter et al. studied the isotopic exchange between ^{18}F and ^{19}F as a means for the synthesis of ten inhalation anaesthetics, including isoflurane and halothane, all of which possess a trifluoromethyl group. Labelling was achieved by heating the corresponding inhalants with potassium-4,7,13,16,21,24-hexaoxa-1,10-diazabicyclo[8.8.8]hexacosane (crypt-222) cryptate ^{18}F complex in dimethyl sulfoxide or acetonitrile in high yields.

Various reported products were subsequently studied in man, dog, and one compound; namely, [^{18}F]HFA-134a was studied in rat using PET (Figure 1) [42].

Kilbourn et al. then resorted to a classical ^{18}F-for-Br nucleophilic substitution procedure to obtain [^{18}F]trifluoromethyl arenes under no-carrier-added conditions in an elaborate multistep protocol. These researchers successfully established direct nucleophilic radiofluorination of a suitable difluorobenzylic bromide, which was subsequently employed as a building block in the radiosynthesis of an ^{18}F-labelled GABA transporter ligand. The [^{18}F]trifluoromethylated product was obtained in 17–28% radiochemical yield; decay corrected to the end of bombardment after a synthesis time of 150 minutes over 5 steps. In the original publication, the authors describe that the specific activity in this procedure is confounded by the presence of inseparable labelling precursor which is surmised to act as a biologically active pseudocarrier (Figure 2) [17].

Further insights into the nucleophilic radiofluorination of bromodifluoromethyl-precursors were obtained by Mukherjee and Das in 1993, when the team studied radiolabelling of the selective serotonin uptake inhibitor (S)-N-methyl-γ-[4-(trifluoromethyl)phenoxy]benzenepropanamine (fluoxetine) to obtain [^{18}F]fluoxetine as a potential radiotracer for serotonin transporter binding sites. Radiolabeling of α-bromo-α,α-difluoro-4-nitrotoluene with no-carrier-added [^{18}F]fluoride ion was described in low 2–4% yields and low specific activity of 2.59 MBq/nmol. A strong effect of the reaction temperature on the radiochemical yield and specific activity of the product were studied and a negative correlation between temperature and specific activity was observed. At higher temperatures, products were found to contain a larger amount of nonradioactive carrier, which had been formed in the reaction. Overall decay-corrected yields over 2-steps spanning a total radiosynthesis time of 150–180 min were 1-2%. The specific activity of the product was 1.48 MBq/nmol (Figure 2) [15, 43].

In parallel, Hammadi and Crouzel investigated radiosynthesis of [^{18}F]fluoxetine with [^{18}F]fluoride ion for PET imaging studies [44]. Radiosynthesis was achieved in a decay-corrected radiochemical yield of 9-10% and a specific radioactivity of 3.70–5.55 MBq/nmol within 150 min from the end of bombardment. A competing isotopic exchange reaction was demonstrated, which the authors suspected to reduce the specific activity of the final ^{18}F-labelled product.

Contrary to isotopic exchange reactions, wherein the factors limiting specific activity are evidently linked to the deliberate addition of nonradioactive carrier, the A_s limiting

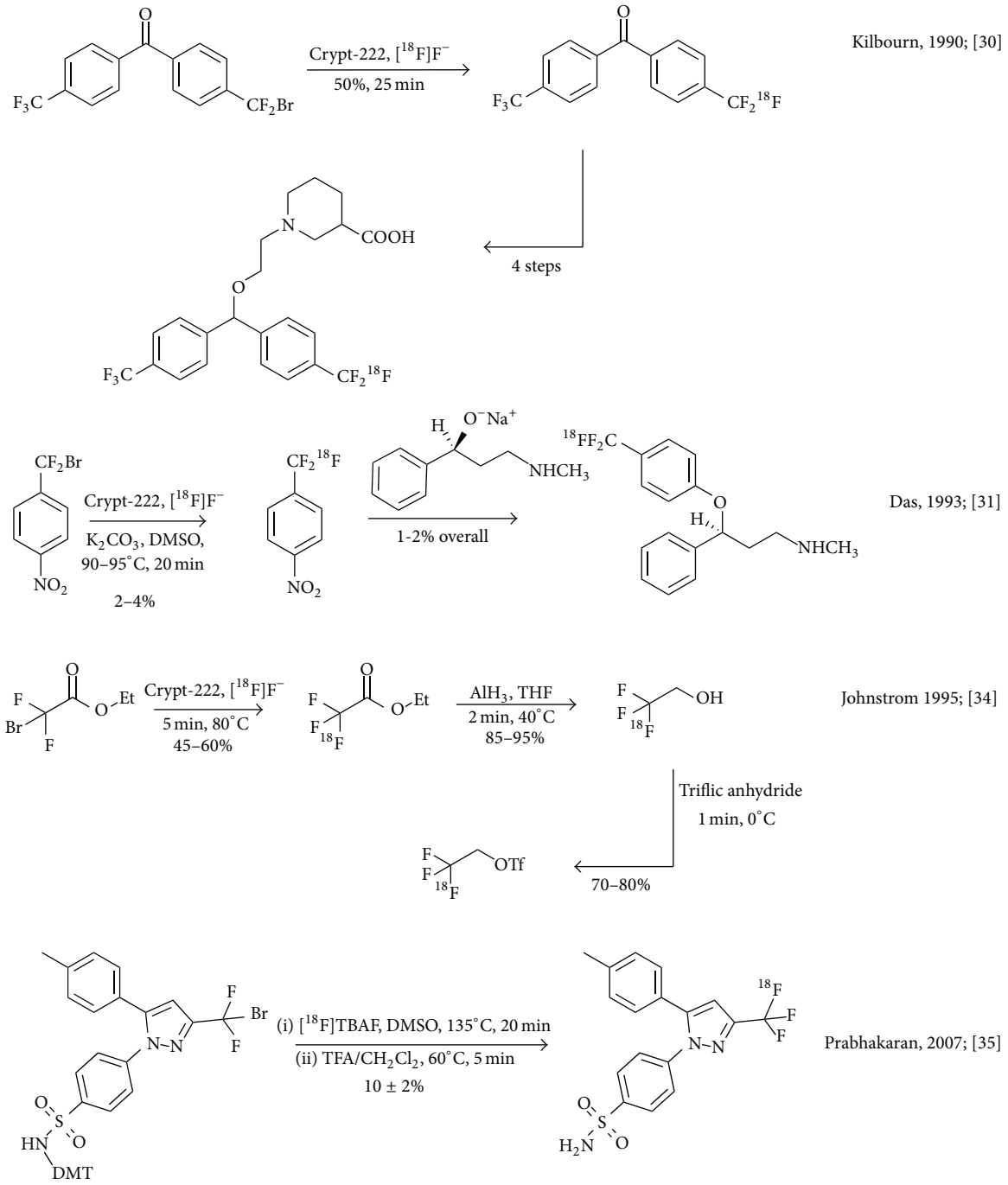

Figure 2: ^{18}F-for-Br nucleophilic substitution protocols yielding the $[^{18}F]CF_3$ motif.

factors in the studied nucleophilic substitution reaction are less apparent. Given that a temperature dependency of specific activity was observed by Das and Mukherjee, two principle mechanisms come to mind: (a) dilution through isotopic exchange with the precursor, which would effectively sacrifice ^{18}F to a labelled precursor molecule and yield a ^{19}F fluoride ion that could in itself react with the precursor and (b) degradation of a fluorinated component in the reaction mixture to afford a nonradioactive degradation product and free nonradioactive fluoride ion. However, we refrain from hypothesizing about nonvalidated theories within this paper.

Nevertheless, Johnström and Stone-Elander encountered what appeared to be an example of case (b) during attempts to synthesize the alkylating agent 2,2,2-[^{18}F]trifluoroethyl triflate via the nucleophilic reaction of $[^{18}F]F^-$ with ethyl bromodifluoroacetate [18]. These researchers were alerted by the observation of unlabeled ethyl trifluoroacetate produced from ethyl 2-bromo-2,2-difluoro-acetate which reduced the

specific activity of the product to only about 0.04 MBq/nmol [38]. Ethyl [^{18}F]trifluoroacetate was synthesized from [^{18}F]F$^-$ and ethyl bromodifluoroacetate in DMSO (45–60%, 5 min, 80°C) followed by distillation in a stream of nitrogen. Despite the use of no-carrier-added [^{18}F]F$^-$, the specific activity of the final product was found to be 0.037 MBq/nmol.

Attempts to mitigate the amount of ^{19}F released from the substrate during the reaction were only partially successful. Even under optimised conditions, the specific activity remained below 1 MBq/nmol, which is roughly two to three orders of magnitude below routinely achievable figures associated with direct nucleophilic substitution reactions with [^{18}F]fluoride ion on aliphatic or aromatic carbon centres (Figure 2).

Bromodifluoromethyl precursors were reconsidered in a more recent radiosynthesis of the selective COX-2 inhibitor 4-[5-(4-methylphenyl)-3-([^{18}F]trifluoromethyl)-1*H*-pyrazol-1-yl]benzenesulfonamide ([^{18}F]celecoxib). [^{18}F]celecoxib was obtained using [^{18}F]TBAF in DMSO at 135°C in 10 ± 2% yield with >99% radiochemical purity and a specific activity of about 4.4 ± 1.5 MBq/nmol (EOB). Although the CNS distribution of [^{18}F]celecoxib mirrored COX-2 expression in the primate brain, the radiotracer was found to be susceptible to defluorination in vivo in rodent and baboon PET studies [20].

A new approach to obtain the title motif of ^{18}F-labelled trifluorinated carbon centres was introduced by Josse et al. in 2001 and utilized in the synthesis of ^{18}F-labelled 2-(2-nitroimidazol-1-yl)-*N*-(3,3,3-trifluoropropyl)-acetamide ([^{18}F]EF3), a prospective PET radiotracer for tissue hypoxia. [^{18}F]EF3 was prepared in 3 steps from [^{18}F]fluoride ion via 3,3,3-[^{18}F]trifluoropropylamine. This ^{18}F-labelled building block was obtained in 40% overall chemical yield by oxidative ^{18}F-fluorodesulfurization of ethyl N-phthalimido-3-aminopropane dithioate, subsequent deprotection of the intermediate followed by coupling with 2,3,5,6-tetrafluorophenyl 2-(2-nitroimidazol-1-yl) acetate in 5% radiochemical yield within 90 min from cyclotron produced [^{18}F]fluoride ion [19]. Specific activity of the final product was limited due to the involvement of a stoichiometric fluoride source in the original desulfurization protocol. Later on the protocol was extended to accommodate a wider spectrum of substrates, namely, triethyl orthothioesters and dithioorthoesters (Figure 3) [45].

2-nitroimidazoles, such as [^{18}F]EF3, are used to detect hypoxia, based on the bioreductive metabolism of the nitroimidazole pharmacophore. This metabolism pathway leads to the formation of covalent bioconjugates between intracellular proteins and the imidazole core, which trap the radiotracer within the metabolizing cells. Even though the target compound was obtained in fairly low specific activity, this is not a concern in the study of hypoxia. Indeed, hypoxic tissues can accumulate considerable amounts of substance of nitroimidazoles via an oxygen-level dependent reductive mechanism [46].

Trifluoromisonidazole (1-(2-nitro-1*H*-imidazol-1-yl)-3-(2,2,2-trifluoroethoxy) propan-2-ol, TFMISO) has been considered as a nuclear magnetic resonance imaging (MRI) agent to visualize hypoxic tissues. TFMISO was successfully labelled with ^{18}F in an attempt to obtain a bimodal PET/MRI probe. In this report, ^{18}F-labeling was achieved via 2,2,2-[^{18}F]trifluoroethyl *p*-toluenesulfonate prepared by ^{18}F-^{19}F exchange. This reagent was used for *O*-^{18}F-trifluoroethylation of 3-chloropropane-1,2-diol sodium salt to obtain 1,2-epoxy-3-(2,2,2-[^{18}F]trifluoroethoxy)propane. [^{18}F]TFMISO was obtained in approximately 40% conversion by ring-opening of the epoxide with 2-nitroimidazole. The researchers "identified 2,2,2-[^{18}F]trifluoroethyl tosylate as an excellent [^{18}F]trifluoroethylating agent, which can convert efficiently an alcohol into the corresponding [^{18}F]trifluoroethyl ether" (Figure 3) [21]. Evidently, the isotopic exchange mechanism limited specific activity in congruence with the amount of added carrier.

The utility of an ^{18}F-labelled reagent that could be used as an [^{18}F]trifluoromethyl source for a wide variety of different reactions was recognised by Herscheid et al. who reported several nucleophilic approaches to obtain [^{18}F]trifluoromethyl iodide and [^{18}F]trifluoromethane, respectively, at the biannual symposium of the International Society of Radiopharmaceutical Sciences [47, 48]. This research ultimately resulted in a new strategy towards [^{18}F]trifluoromethyl-containing compounds via [^{18}F]trifluoromethane developed by van der Born et al. Gaseous [^{18}F]trifluoromethane was synthesised in solution at room temperature and trapped in a second reaction vessel. Two further applications of the reagent have been described; [^{18}F]trifluoromethane was subsequently used in a reaction with carbonyl compounds to obtain [^{18}F]trifluoromethyl carbinols in good yields. Unfortunately, the authors did not report a specific activity in their communication. The reagent was furthermore successfully employed in a preliminary study of Cu-mediated ^{18}F-trifluoromethylation; however, no details are available other than a conference abstract (Figure 3) [23, 49].

We devised a procedure for the radiosynthesis of aliphatic [^{18}F]trifluoromethyl groups involving the reaction of 1,1-difluorovinyl precursors with [^{18}F]fluoride ion, which results in the equivalent of direct nucleophilic addition of H[^{18}F]F. In theory, this protocol could make a large pool of trifluoroethylated compounds accessible for the straightforward development of PET radiotracers [22, 50, 51]. The protocol was optimised and applied to a set of substrates with moderate to good outcomes, showing that the method is widely applicable for the synthesis of novel radiotracers. Most notably, 2,2,2-[^{18}F]trifluoroethyl *p*-toluenesulfonate was obtained in high radiochemical yields of up to 93% and good specific activity of 86 MBq/nmol starting from a 5 GBq batch of ^{18}F. Nevertheless, the reaction requires meticulous control of the reaction conditions and the influence of competing elimination reactions has to be mitigated (Figure 4) [50].

Following the report of an indirect ^{18}F-trifluoromethylation reaction by Herscheid and coworkers, Huiban et al.

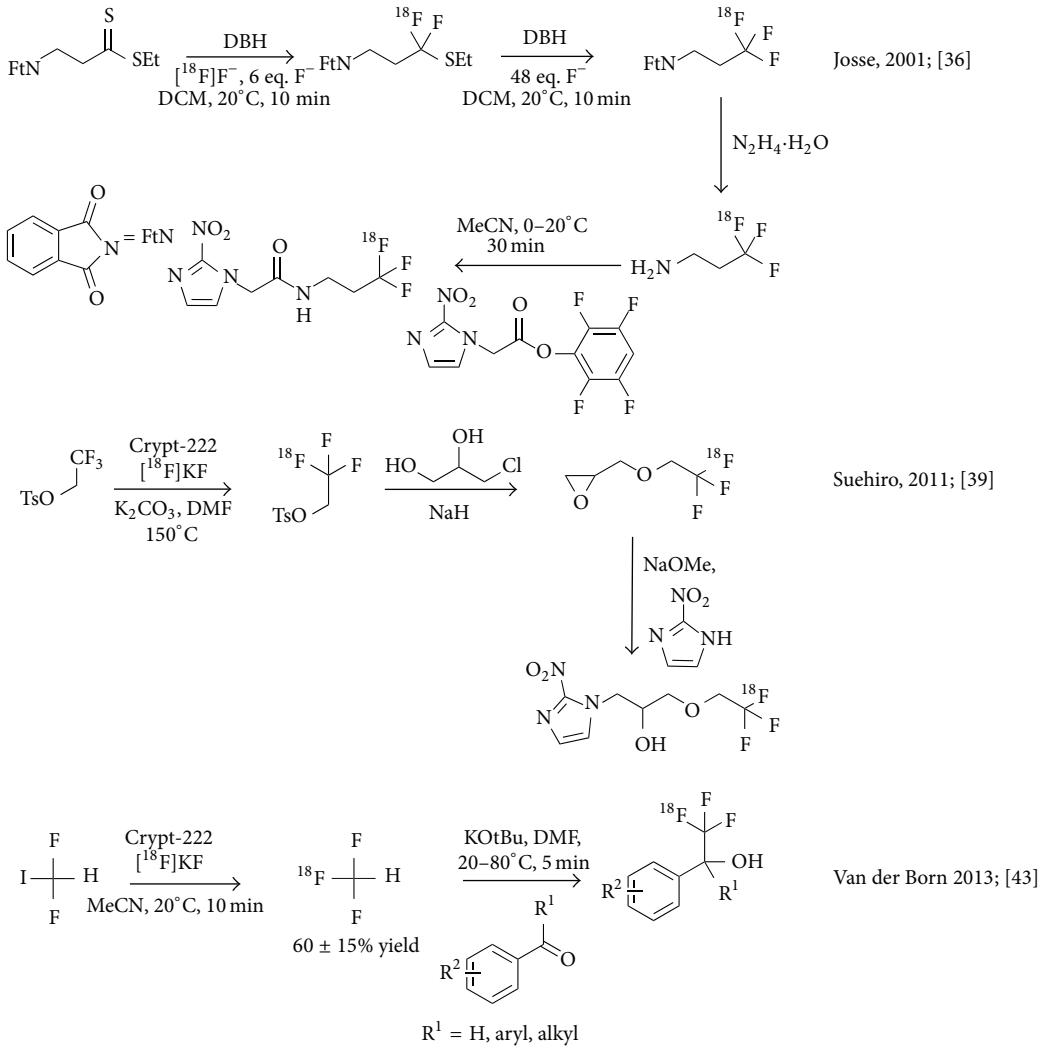

Figure 3: Carrier-added radiosynthesis of ^{18}F-labelled hypoxia imaging agents using ^{18}F-fluoro-desulfurisation and ^{18}F-for-^{19}F isotopic exchange and no-carrier-added nucleophilic radiosynthesis of [^{18}F]CHF_3.

extended a published protocol for direct trifluoromethylation by Su et al. and MacNeil and Burton to ^{18}F-radiochemistry [52, 53]. The reaction mechanism involves the formation of difluorocarbene from methyl chlorodifluoroacetate in the presence of a fluoride ion source and CuI. Under no-carrier-added conditions, trace amounts of [^{18}F]fluoride ion may only react with a small fraction of the intermediate carbene and form the trifluoromethylating reagent Cu-[^{18}F]CF_3, whereas the bulk of the carbene intermediate degrades to side products and ^{19}F fluoride ion. In consequence, the specific activity of the formed product is relatively low (0.1 MBq/nmol). Nevertheless, the method was found to tolerate a variety of substrates and may hence be of use for the study of nonsaturable biological systems (Figure 4) [24].

Seeking an efficient method for producing [^{18}F]trifluoromethyl arenes starting from [^{18}F]fluoride ion within our radiotracer development program, we have explored a route inspired by the use of [^{18}F]fluoroform as an intermediate by van der Born et al. We surmised that reactions involving [^{18}F]fluoroform require diligent control of the gaseous intermediate, including low temperature distillation and trapping of the product at −80°C in a secondary reaction vessel. These conditions and technical requirements are limiting factors with respect to the automated synthesis of high activity batches using automated synthesiser systems. In our eyes, widespread adoption of ^{18}F-trifluoromethylation reactions would strongly benefit from a straightforward nucleophilic one-pot method generally applicable to the latest generation of synthetic hardware. Such methodology would furthermore feature direct installation of nucleophilic fluorine-18 in the form of no-carrier-added [^{18}F]fluoride ion into candidate radiotracers to avoid losses of radioactivity, conserve specific radioactivity, and achieve rapid and simple radiosynthesis. Unfortunately, we were only partially successful; although we have shown that Cu(I) mediated ^{18}F-trifluoromethylation reactions are highly efficient in the presence of a simple combination of difluoroiodomethane, DIPEA, CuBr, $^{18}F^-$, and an iodo arene, we failed to overcome the known specific activity

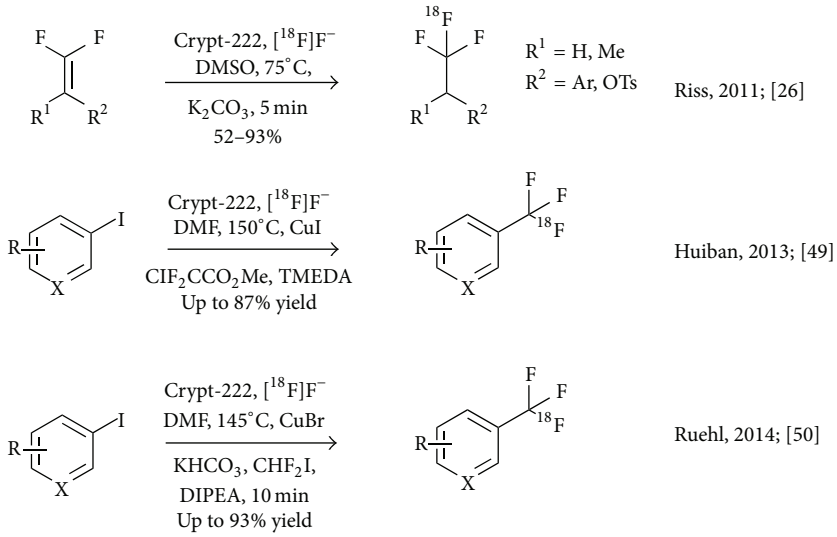

Figure 4: Recent reports on direct nucleophilic radiosynthesis of [^{18}F]trifluoroethyl and [^{18}F]trifluoromethyl groups.

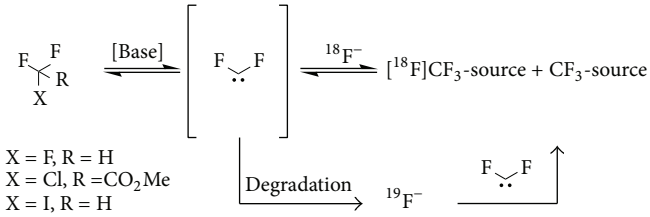

Figure 5: Base mediated α-elimination to yield difluoromethyl carbene and subsequent conversion into an ^{18}F-trifluoromethylating reagent.

limitations. Nevertheless, the resulting [^{18}F]trifluoromethyl arenes are obtained in sufficient yields of up to 93% in an operationally convenient protocol, suitable for straightforward automation (Figure 4) [25].

From a mechanistic point of view, the feasibility of the radiosynthesis of [^{18}F]trifluoromethylating agents such as [^{18}F]fluoroform or Cu-[^{18}F]CF_3 in high specific activity is questionable. In essence, the generation of the aforementioned labelling reagents would require a clean nucleophilic substitution of an appropriate leaving group, which is not likely to occur. Instead, the generic reaction mechanism involves an α-elimination in the presence of base to yield difluoromethyl carbene, which is subsequently scavenged by [^{18}F]fluoride ion in solution. The inherent low concentration of [^{18}F]fluoride ion, combined with the short half-life of difluorocarbene, which degrades to side products under liberation of two equivalents of ^{19}F in this pathway directly results in isotopic dilution, which confounds achieving a high specific activity. (Figure 5) [24, 25, 52–54].

Likewise, the intermediate organometallic reagents such as Cu-CF_3 are unstable in solution; again degradation occurs via a carbenoid pathway. In consequence, several research groups have resorted to the deliberate addition of a soluble source of fluoride ion under stoichiometric conditions to stabilise the equilibrium between the carbene intermediate and the desired reagent, thus adding further indirect proof of the mechanistic difficulties [34, 35].

3. Electrophilic Radiosynthesis

Electrophilic methodology has been employed in the synthesis of ^{18}F-labelled perfluoroalkyl moieties, for example, in the radiosynthesis and evaluation of the hypoxia imaging agent 2-(2-nitro-1[*H*]-imidazol-1-yl)-*N*-(2,2,3,3,3-[^{18}F]pentafluoropropyl)-acetamide ([^{18}F]EF-5) [26]. EF-5 is a compound belonging to the class of 2-nitroimidazoles. In this case, the requirements for specific activity are fairly forgiving and radiolabelling using electrophilic fluorine sources with low specific activity may be considered as a viable alternative to [^{18}F]fluoride ion. Consequently, stoichiometric reaction conditions are employed and the starting materials are consumed entirely over the course of the labelling reaction. Addition of [^{18}F]F_2 to perfluoroolefins appears to be the method of choice in this context and yields up to 17% of [^{18}F]EF-5 have been achieved using carrier-added, gaseous ^{18}F-fluorine (Figure 5). Subsequently, Kachur et al. described an improvement of the electrophilic addition of fluorine to a fluorinated double bond, which was achieved by the addition

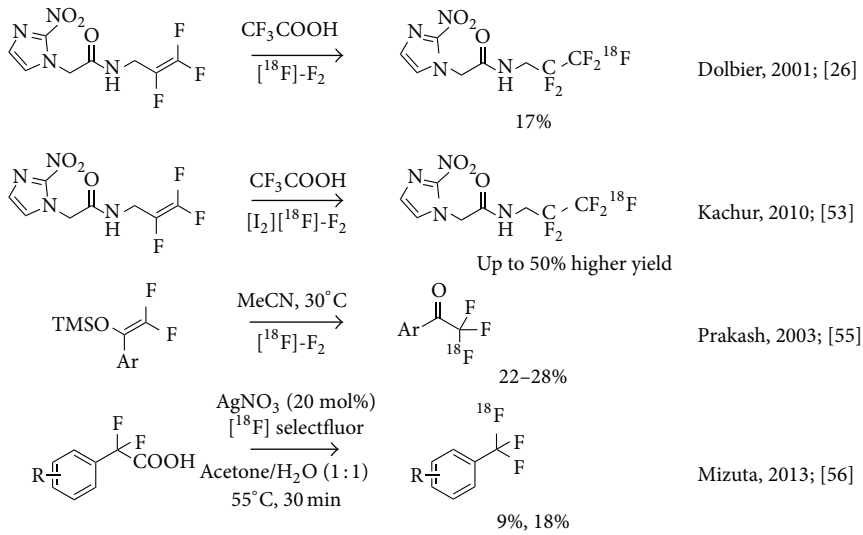

Figure 6: Electrophilic approaches for the radiosynthesis of the title function.

of catalytic amounts (0.5–1%) of boron trifluoride, bromine, or iodine, to the reaction mixture. Under these conditions the conversion of the labelling precursor to [^{18}F]EF-5 was improved by 50% [55].

More recently, a simplified procedure for radiosynthesis of [^{18}F]EF5 in trifluoroacetic acid (TFA) was devised. This new protocol allowed for straightforward automation of the production using a commercially available radiosynthesis module for routine synthesis of [^{18}F]EF-5 in sufficient amounts and purity for clinical PET studies. An evaluation of the radiotracer was conducted in HCT116 xenografts with small animal PET [56].

Another example of the use of low specific activity ^{18}F-F_2 under stoichiometric conditions for the synthesis of the CF_3-motif is the syntheses of several ^{18}F-labelled α-trifluoromethyl ketones reported by Prakash et al. [27]. Reactions of 2,2-difluoro-1-aryl-1-trimethylsiloxyethenes with [^{18}F]F_2 at low temperature were reported to afford ^{18}F-labelled α-trifluoromethyl ketones in moderate to good yields within 35–40 min from the end of bombardment. Decay-corrected, isolated yields (>99% radiochemical purity) were reported to fall between 22–28% for radiolabeled model compounds. Specific activities ranged from 0.015–0.020 MBq/nmol at the end of synthesis. This method may be of use for the radiochemical synthesis of biologically active ^{18}F-labelled α-trifluoromethyl ketones, however, with strict limitations since such low specific activities may confound tracer conditions for PET imaging of saturable biological processes (Figure 6).

Nevertheless, electrophilic fluorination may be the key approach to overcome the issues observed with nucleophilic fluorination attempts. This is owed to the availability of somewhat higher specific activity electrophilic labelling reagents derived from [^{18}F]fluoride ion in selected PET centres. A recent report on the reaction of readily available α,α-difluoro- and α-fluoroarylacetic acids with [^{18}F]selectfluor bis(triflate) makes accessible the corresponding [^{18}F]tri- and [^{18}F]difluoromethylarenes in two orders of magnitude higher specific activity compared to [^{18}F]F_2.

This straightforward silver(I) catalyzed decarboxylative fluorination reaction afforded a broad range of [^{18}F]trifluoromethyl arenes in moderate to good yields. These researchers reported a specific activity of about 3 MBq/nmol which is about twofold higher than the reported values for nucleophilic fluorination reactions (Figure 6) [28].

4. Conclusion

In conclusion, the trifluoromethyl motif has attracted a veritable interest from PET chemists as a relatively abundant fluorinated functional group, which has precipitated in a variety of novel labelling methods, some of which have been used to synthesise radiotracers for PET imaging studies. The major shortcoming of the available methodology is the low specific activity, which impedes PET imaging of saturable processes and may confound widespread application of these methods. Hence, continued effort may be warranted to overcome the limited scope of the available protocols and extend the knowledge base in PET chemistry with new methodology suitable for the radiosynthesis of ^{18}F-labelled trifluoromethyl groups in high specific activity.

Conflict of Interests

The authors declare that there is no conflict of interests regarding the publication of this paper.

References

[1] S. M. Ametamey, M. Honer, and P. A. Schubiger, "Molecular imaging with PET," *Chemical Reviews*, vol. 108, no. 5, pp. 1501–1516, 2008.

[2] P. W. Miller, N. J. Long, R. Vilar, and A. D. Gee, "Synthesis of ^{11}C, ^{18}F, ^{15}O, and ^{13}N radiolabels for positron emission tomography," *Angewandte Chemie—International Edition*, vol. 47, no. 47, pp. 8998–9033, 2008.

[3] L. Cai, S. Lu, and V. W. Pike, "Chemistry with [^{18}F]fluoride ion," *European Journal of Organic Chemistry*, no. 17, pp. 2853–2873, 2008.

[4] V. W. Pike, "PET radiotracers: crossing the blood-brain barrier and surviving metabolism," *Trends in Pharmacological Sciences*, vol. 30, no. 8, pp. 431–440, 2009.

[5] G.-J. Meyer, S. L. Waters, H. H. Coenen, A. Luxen, B. Maziere, and B. Langstrom, "PET radiopharmaceuticals in Europe: current use and data relevant for the formulation of summaries of product characteristics (SPCs)," *European Journal of Nuclear Medicine*, vol. 22, no. 12, pp. 1420–1432, 1995.

[6] S. P. Hume, R. N. Gunn, and T. Jones, "Pharmacological constraints associated with positron emission tomographic scanning of small laboratory animals," *European Journal of Nuclear Medicine*, vol. 25, no. 2, pp. 173–176, 1998.

[7] S. P. Hume and R. Myers, "Dedicated small animal scanners: a new tool for drug development?" *Current Pharmaceutical Design*, vol. 8, no. 16, pp. 1497–1511, 2002.

[8] K. Virdee, P. Cumming, D. Caprioli et al., "Applications of positron emission tomography in animal models of neurological and neuropsychiatric disorders," *Neuroscience and Biobehavioral Reviews*, vol. 36, no. 4, pp. 1188–1216, 2012.

[9] E. M. Jagoda, J. J. Vaquero, J. Seidel, M. V. Green, and W. C. Eckelman, "Experiment assessment of mass effects in the rat: implications for small animal PET imaging," *Nuclear Medicine and Biology*, vol. 31, no. 6, pp. 771–779, 2004.

[10] T. Ido, T. Irie, and Y. Kasida, "Isotope exchange with ^{18}F on superconjugate system," *Journal of Labelled Compounds and Radiopharmaceuticals*, vol. 16, no. 1, pp. 153–154, 1979.

[11] G. Angelini, M. Speranza, C.-Y. Shiue, and A. P. Wolf, "H^{18}F + Sb_2O_3: a new selective radiofluorinating agent," *Journal of the Chemical Society, Chemical Communications*, no. 12, pp. 924–925, 1986.

[12] G. Angelini, M. Speranza, A. P. Wolf, and C.-Y. Shiue, "Synthesis of N-(α,α,α-tri[^{18}F[fluoro-m-tolyl)piperazine. A potent serotonin agonist," *Journal of Labelled Compounds and Radiopharmaceuticals*, vol. 28, no. 12, pp. 1441–1448, 1990.

[13] M. R. Kilbourn and R. Subramanian, "Synthesis of fluorine-18 labeled 1,1-difluoro-2,2-dichloroethyl aryl ethers by ^{18}F-for-^{19}F exchange," *Journal of Labelled Compounds and Radiopharmaceuticals*, vol. 28, no. 12, pp. 1355–1361, 1990.

[14] F. I. Aigbirhio, V. W. Pike, S. L. Waters, J. Makepeace, and R. J. N. Tanner, "Efficient and selective labelling of the CFC alternative, 1,1,1,2-tetrafluoroethane, with ^{18}F in the 1-position," *Journal of the Chemical Society, Chemical Communications*, no. 13, pp. 1064–1065, 1993.

[15] M. K. Das and J. Mukherjee, "Radiosynthesis of [F-18]fluoxetine as a potential radiotracer for serotonin reuptake sites," *Applied Radiation and Isotopes*, vol. 44, no. 5, pp. 835–842, 1993.

[16] M. R. Satter, C. C. Martin, T. R. Oakes, B. Christian, and R. J. Nickles, "Synthesis of the fluorine-18 labeled inhalation anesthetics," *Applied Radiation and Isotopes*, vol. 45, no. 11, pp. 1093–1100, 1994.

[17] M. R. Kilbourn, M. R. Pavia, and V. E. Gregor, "Synthesis of fluorine-18 labeled GABA uptake inhibitors," *Applied Radiation and Isotopes*, vol. 41, no. 9, pp. 823–828, 1990.

[18] P. Johnstrom and S. Stone-Elander, "The ^{18}F-labelled alkylating agent 2,2,2-trifluoroethyl triflate: synthesis and specific activity," *Journal of Labelled Compounds and Radiopharmaceuticals*, vol. 36, no. 6, pp. 537–547, 1995.

[19] O. Josse, D. Labar, B. Georges, V. Grégoire, and J. Marchand-Brynaert, "Synthesis of [^{18}F]-labeled EF3 [2-(2-nitroimidazol-1-yl)-N-(3,3,3-trifluoropropyl)-acetamide], a marker for PET detection of hypoxia," *Bioorganic and Medicinal Chemistry*, vol. 9, no. 3, pp. 665–675, 2001.

[20] J. Prabhakaran, M. D. Underwood, R. V. Parsey et al., "Synthesis and in vivo evaluation of [^{18}F]-4-[5-(4-methylphenyl)-3-(trifluoromethyl)-1H-pyrazol-1-yl]benzenesulfonamide as a PET imaging probe for COX-2 expression," *Bioorganic and Medicinal Chemistry*, vol. 15, no. 4, pp. 1802–1807, 2007.

[21] M. Suehiro, G. Yang, G. Torchon et al., "Radiosynthesis of the tumor hypoxia marker [^{18}F]TFMISO via O-[^{18}F]trifluoroethylation reveals a striking difference between trifluoroethyl tosylate and iodide in regiochemical reactivity toward oxygen nucleophiles," *Bioorganic and Medicinal Chemistry*, vol. 19, no. 7, pp. 2287–2297, 2011.

[22] P. J. Riss and F. I. Aigbirhio, "A simple, rapid procedure for nucleophilic radiosynthesis of aliphatic [^{18}F]trifluoromethyl groups," *Chemical Communications*, vol. 47, no. 43, pp. 11873–11875, 2011.

[23] D. Van Der Born, J. D. M. Herscheid, R. V. A. Orru, and D. J. Vugts, "Efficient synthesis of [^{18}F]trifluoromethane and its application in the synthesis of PET tracers," *Chemical Communications*, vol. 49, no. 38, pp. 4018–4020, 2013.

[24] M. Huiban, M. Tredwell, S. Mizuta et al., "A broadly applicable [^{18}F]trifluoromethylation of aryl and heteroaryl iodides for PET imaging," *Nature Chemistry*, vol. 5, no. 11, pp. 941–944, 2013.

[25] T. Ruehl, W. Rafique, V. T. Lien, and P. Riss, "Cu(I)-mediated ^{18}F-trifluoromethylation of arenes," *Chemical Communications*, vol. 50, pp. 6056–6059, 2014.

[26] W. R. Dolbier Jr., A.-R. Li, C. J. Koch, C.-Y. Shiue, and A. V. Kachur, "[^{18}F]-EF5, a marker for PET detection of hypoxia: synthesis of precursor and a new fluorination procedure," *Applied Radiation and Isotopes*, vol. 54, no. 1, pp. 73–80, 2001.

[27] G. K. S. Prakash, M. M. Alauddin, J. Hu, P. S. Conti, and G. A. Olah, "Expedient synthesis of [^{18}F]-labeled α-trifluoromethyl ketones," *Journal of Labelled Compounds and Radiopharmaceuticals*, vol. 46, no. 11, pp. 1087–1092, 2003.

[28] S. Mizuta, I. S. R. Stenhagen, M. O'Duill et al., "Catalytic decarboxylative fluorination for the synthesis of Tri- and difluoromethyl arenes," *Organic Letters*, vol. 15, no. 11, pp. 2648–2651, 2013.

[29] D. A. Nagib and D. W. C. Macmillan, "Trifluoromethylation of arenes and heteroarenes by means of photoredox catalysis," *Nature*, vol. 480, no. 7376, pp. 224–228, 2011.

[30] A. Deb, S. Manna, A. Modak, T. Patra, S. Maity, and D. Maiti, "Oxidative trifluoromethylation of unactivated olefins: an efficient and practical synthesis of α-trifluoromethyl-substituted ketones," *Angewandte Chemie—International Edition*, vol. 52, no. 37, pp. 9747–9750, 2013.

[31] S. Mizuta, K. M. Engle, S. Verhoog et al., "Trifluoromethylation of allylsilanes under photoredox catalysis," *Organic Letters*, vol. 15, no. 6, pp. 1250–1253, 2013.

[32] T. Furuya, A. S. Kamlet, and T. Ritter, "Catalysis for fluorination and trifluoromethylation," *Nature*, vol. 473, no. 7348, pp. 470–477, 2011.

[33] S. Mizuta, S. Verhoog, K. M. Engle et al., "Catalytic hydrotrifluoromethylation of unactivated alkenes," *Journal of the American Chemical Society*, vol. 135, no. 7, pp. 2505–2508, 2013.

[34] A. Lishchynskyi, M. A. Novikov, E. Martin, E. C. Escudero-Adán, P. Novák, and V. V. Grushin, "Trifluoromethylation of aryl and heteroaryl halides with fluoroform-derived $CuCF_3$: scope, limitations, and mechanistic features," *Journal of Organic Chemistry*, vol. 78, no. 22, pp. 11126–11146, 2013.

[35] O. A. Tomashenko and V. V. Grushin, "Aromatic trifluoromethylation with metal complexes," *Chemical Reviews*, vol. 111, no. 8, pp. 4475–4521, 2011.

[36] H. L. Yale, "The trifluoromethyl group in medicinal chemistry," *Journal of Medicinal and Pharmaceutical Chemistry*, vol. 1, no. 2, pp. 121–133, 1959.

[37] P. Kirsch, *Modern Fluoroorganic Chemistry: Synthesis, Reactivity, Applications*, John Wiley & Sons, Weinheim, Germany, 2013.

[38] P. S. Johnstrom and S. Stone-Elander, "Strategies for reducing isotopic dilution in the synthesis of ^{18}F-labeled polyfluorinated ethyl groups," *Applied Radiation and Isotopes*, vol. 47, no. 4, pp. 401–407, 1996.

[39] K. Hamacher, H. H. Coenen, and G. Stocklin, "Efficient stereospecific synthesis of no-carrier-added 2-[^{18}F]-fluoro-2-deoxy-D-glucose using aminopolyether supported nucleophilic substitution," *Journal of Nuclear Medicine*, vol. 27, no. 2, pp. 235–238, 1986.

[40] T. Irie, K. Fukushi, T. Ido, T. Nozaki, and Y. Kasida, "^{18}F-Fluorination by crown ether-metal fluoride: (I) on labeling ^{18}F-21-fluoroprogesterone," *The International Journal Of Applied Radiation And Isotopes*, vol. 33, no. 12, pp. 1449–1452, 1982.

[41] R. J. Nickles, M. R. Satter, J. R. Votaw, J. J. Sunderland, and C. C. Martin, "The synthesis of ^{18}F-labeled potent anesthetics," *Journal of Labelled Compounds and Radiopharmaceuticals*, vol. 26, no. 1–12, pp. 448–449, 1989.

[42] J. R. Finch, W. R. Banks, D.-R. Hwang et al., "Synthesis and in vivo disposition studies of ^{18}F-labeled HFA-134a," *Applied Radiation and Isotopes*, vol. 46, no. 4, pp. 241–248, 1995.

[43] A. Hammadi and C. Crouzel, "Synthesis of [^{18}F]-(S)-fluoxetine: a selective serotonine uptake inhibitor," *Journal of Labelled Compounds and Radiopharmaceuticals*, vol. 33, no. 8, pp. 703–710, 1993.

[44] J. Mukherjee, M. K. Das, Z.-Y. Yang, and R. Lew, "Evaluation of the binding of the radiolabeled antidepressant drug, ^{18}F-fluoxetine in the rodent brain: an in vitro and in vivo study," *Nuclear Medicine and Biology*, vol. 25, no. 7, pp. 605–610, 1998.

[45] A. Cheguillaume, J. Gillart, D. Labar, V. Grégoire, and J. Marchand-Brynaert, "Perfluorinated markers for hypoxia detection: synthesis of sulfur-containing precursors and [^{18}F]-labelling," *Bioorganic and Medicinal Chemistry*, vol. 13, no. 4, pp. 1357–1367, 2005.

[46] C. J. Koch and S. M. Evans, "Non-invasive pet and spect imaging of tissue hypoxia using isotopically labeled 2-nitroimidazoles," *Advances in Experimental Medicine and Biology*, vol. 510, pp. 285–292, 2003.

[47] C. L. Koolen and J. D. M. Herscheid, "Approaches towards the radiosynthesis of [^{18}F]trifluoromethyl iodide," *Journal of Labelled Compounds and Radiopharmaceuticals*, vol. 44, supplement S1, pp. S993–S994, 2001.

[48] M. van der Mey and J. D. M. Herscheid, "[^{18}F]CF3H, a versatile synthon for the preparation of [^{18}F]trifluoromethylated radiopharmaceuticals," *Journal of Labelled Compounds and Radiopharmaceuticals*, vol. 50, supplemen S1, p. S3, 2007.

[49] D. van der Born, J. D. M. Herscheid, and D. J. Vugts, "Aromatic trifluoromethylation using [^{18}F]fluoroform," *Journal of Labelled Compounds and Radiopharmaceuticals*, vol. 56, supplement S1, p. S2, 2013.

[50] P. J. Riss, V. Ferrari, L. Brichard, P. Burke, R. Smith, and F. I. Aigbirhio, "Direct, nucleophilic radiosynthesis of [^{18}F]trifluoroalkyl tosylates: improved labelling procedures," *Organic and Biomolecular Chemistry*, vol. 10, no. 34, pp. 6980–6986, 2012.

[51] P. J. Riss, L. Brichard, V. Ferrari et al., "Radiosynthesis and characterization of astemizole derivatives as lead compounds toward PET imaging of τ-pathology," *Medicinal Chemistry Communications*, vol. 4, no. 5, pp. 852–855, 2013.

[52] D.-B. Su, J.-X. Duan, and Q.-Y. Chen, "A simple, novel method for the preparation of trifluoromethyl iodide and diiododifluoromethane," *Journal of the Chemical Society—Series Chemical Communications*, no. 11, pp. 807–808, 1992.

[53] J. G. MacNeil Jr. and D. J. Burton, "Generation of trifluoromethylcopper from chlorodifluoroacetate," *Journal of Fluorine Chemistry*, vol. 55, no. 2, pp. 225–227, 1991.

[54] W. Kirmse, *Carbene Chemistry*, vol. 1, Academic Press, New York, NY, USA, 2nd edition, 1971.

[55] A. V. Kachur, W. R. Dolbier Jr., W. Xu, and C. J. Koch, "Catalysis of fluorine addition to double bond: an improvement of method for synthesis of ^{18}F PET agents," *Applied Radiation and Isotopes*, vol. 68, no. 2, pp. 293–296, 2010.

[56] S. K. Chitneni, G. T. Bida, M. W. Dewhirst, and M. R. Zalutsky, "A simplified synthesis of the hypoxia imaging agent 2-(2-Nitro-1H-imidazol-1-yl)-N-(2,2,3,3,3-[^{18}F]pentafluoropropyl)-acetamide ([^{18}F]EF5)," *Nuclear Medicine and Biology*, vol. 39, no. 7, pp. 1012–1018, 2012.

Hindawi Publishing Corporation
BioMed Research International
Volume 2014, Article ID 812973, 15 pages
http://dx.doi.org/10.1155/2014/812973

Review Article

^{18}F-Labelled Intermediates for Radiosynthesis by Modular Build-Up Reactions: Newer Developments

Johannes Ermert

Institut für Neurowissenschaften und Medizin, INM-5: Nuklearchemie, Forschungszentrum Jülich, 52425 Jülich, Germany

Correspondence should be addressed to Johannes Ermert; j.ermert@fz-juelich.de

Received 27 March 2014; Accepted 12 May 2014; Published 23 June 2014

Academic Editor: Patrick Riss

This brief review gives an overview of newer developments in ^{18}F-chemistry with the focus on small ^{18}F-labelled molecules as intermediates for modular build-up syntheses. The short half-life (<2 h) of the radionuclide requires efficient syntheses of these intermediates considering that multistep syntheses are often time consuming and characterized by a loss of yield in each reaction step. Recent examples of improved synthesis of ^{18}F-labelled intermediates show new possibilities for no-carrier-added ring-fluorinated arenes, novel intermediates for tri[^{18}F]fluoromethylation reactions, and ^{18}F-fluorovinylation methods.

1. Introduction

The positron emitter fluorine-18 is a commonly used radionuclide in molecular imaging with positron emission tomography (PET) due to its advantageous nuclear properties. Thus, it finds wide application as noninvasive, quantitative, and versatile modality in medical diagnosis, research, and drug development [1]. Fluorine-18 has a short half-life of 109.7 min which only allows time-limited syntheses and study protocols. The methods for introducing this short-lived radionuclide into organic molecules thus require fast chemistry, and it is desirable to introduce the ^{18}F-label during the last possible synthetic step.

A further aspect is the stoichiometry of ^{18}F-chemistry that differs from "cold" fluorinations. The radionuclide is produced in low (nano- to picomolar) amounts and its concentration in reaction mixtures is several orders of magnitude lower than the precursor concentration. Furthermore, the syntheses of the radiotracers have to be performed in closed, lead-shielded hot cells, which necessitates an easily applicable and remote-controlled process. Thus, besides the development of more efficient and flexible ^{18}F-labelling methods new technological approaches have been examined, especially in the field of microfluidic chemistry [2–10]. The development of a reliable ^{18}F-labelling technique together with an automatic synthesis module is a major prerequisite of routine production of ^{18}F-labelled PET radiopharmaceuticals [11–13].

Methods for the introduction of [^{18}F]fluorine into organic molecules can be divided into two groups, namely, direct and indirect. The direct method entails introduction of [^{18}F]fluorine without changing the carbon skeleton structure of the molecule. However, in many cases this necessitates the protection of functional groups or requires other transformations like reduction or oxidation of functional groups after introduction of radiofluorine [14].

The indirect method involves build-up syntheses, that is, changing the carbon skeleton structure and starting from small molecules which themselves can be easily ^{18}F-fluorinated by nucleophilic substitution. Such small ^{18}F-labelled alkyl [15] or aryl [16] groups bear typically reactive functional groups for further transformation reactions. Those intermediates are used to synthesize more complex biological molecules which cannot be labelled with fluorine-18 due to mechanistic reasons or are not stable enough to tolerate direct ^{18}F-fluorination conditions.

In the case of ^{18}F-labelling of macromolecules like peptides, proteins, and antibodies, these small ^{18}F-labelled intermediates are commonly called "prosthetic groups." In the last decade progress has been made regarding the ^{18}F-labelling of macromolecules [17, 18]. Besides the use of prosthetic groups

several alternative methods have also been introduced, capable of using even mild and aqueous conditions, for example, chelated aluminum [19–21], boron- [22], and/or silicon-based [^{18}F]fluoride acceptor groups [23–26]. The latter methods were also used for the synthesis of small molecules [27].

This review focuses on new developments regarding the use of small ^{18}F-labelled intermediates for build-up syntheses of biologically active compounds. The ^{18}F-labelling of macromolecules and the click chemistry approach are not considered. Those special topics of ^{18}F-labelling can be found in other contributions to this issue [28–30].

2. ^{18}F-Fluorinating Agents

As starting material for all chemical syntheses either aqueous [^{18}F]fluoride or gaseous [^{18}F]F_2 is used, both of which are generally produced at a cyclotron via the ^{18}O(p,n)^{18}F nuclear reaction [31]. The nucleophilic [^{18}F]fluoride ion is available in no-carrier-added (n.c.a.) form which allows the synthesis of radiotracers with high specific activity. In contrast, in-target produced [^{18}F]F_2 is available only in carrier-added (c.a.) form which leads to radiotracers with low specific activity.

Historically, for important radiopharmaceuticals like 2-[^{18}F]fluoro-2-deoxy-D-glucose ([^{18}F]FDG) and 6-[^{18}F] fluoro-L-dopa only electrophilic ^{18}F-fluorination was available. Today this method is rarely used because of the need of carrier for [^{18}F]F_2 production. Thus, the use of electrophilic ^{18}F-fluorination is limited to nontoxic compounds as well as to those that can be applied with a low specific activity. Also, since [^{18}F]F_2 is very reactive and ^{18}F-labelled side products are formed, less reactive electrophilic ^{18}F-agents were developed [32]. More recently, the synthesis of N-[^{18}F]fluorobenzenesulfonimide (NFSi) was described, which is a highly stable, reactive and selective electrophilic ^{18}F-labelling agent and allows the synthesis of ^{18}F-labelled allylic fluorides and α-fluorinated ketones from allylsilanes and silyl enol ethers, respectively [33].

An alternative method using a "posttarget" synthesis of [^{18}F]F_2 leads to moderate specific activity of up to 24.7 GBq/μmol, starting from n.c.a. [^{18}F]fluoride [34]. It was recently revisited for the radiosynthesis of [^{18}F]selectfluor bis(triflate), the ^{18}F-labelled form of (1-chloromethyl-4-fluorodiazonia-bicyclo[2.2.2]-octane bis-(tetra-fluoroborate)), an easy to handle and stable electrophilic fluorinating reagent (cf. Figure 1) [35]. This reagent could successfully be used for the silver(I)-mediated ^{18}F-fluorination of electron-rich arylstannane models and intermediates, as well as for the preparation of 6-[^{18}F]fluoro-L-DOPA [36], albeit all with limited specific activity of 3.7 ± 0.9 GBq/μmol.

3. Aliphatic Intermediates

Aliphatic ^{18}F-fluorination is certainly the most prominent method for ^{18}F-labelling [32], and important PET-radiotracers for clinical use are aliphatically ^{18}F-labelled compounds which fulfill these requirements, for example,

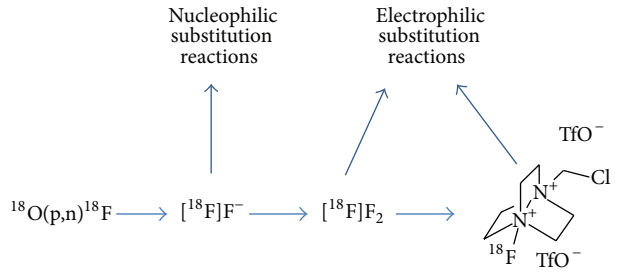

Figure 1: Nuclear reactions to produce fluorine-18 and the ^{18}F-fluorinating agents [^{18}F]fluoride, [^{18}F]fluorine gas, and [^{18}F]selectfluor bis(triflate).

[^{18}F]FDG, 3′-deoxy-3′-[^{18}F]fluorothymidine ([^{18}F]FLT), [^{18}F]fluoro(m)ethylcholine, and O-2-[^{18}F]fluoroethyl-L-tyrosine ([^{18}F]FET) (cf. Figure 2) [15, 37, 38]. [^{18}F]Fluoro(m)-ethylcholine is an example for ^{18}F-labelled endogenous compounds, whereas [^{18}F]FDG and [^{18}F]FLT are ^{18}F-labelled deoxy derivatives of the corresponding endogenous substances. In all cases a proton is replaced by a fluorine atom without changing the carbon skeleton of the original compound. In contrast, [^{18}F]FET is an example of an endogenous ^{18}F-labelled compound where the introduction of the radionuclide is performed by an ^{18}F-fluoroalkylation reaction. Here, the ^{18}F-label is introduced into the molecule by addition of further C-atoms which means that the skeleton of the molecule is significantly changed. Other examples of this kind of reaction are the ^{18}F-fluoroacylation and ^{18}F-fluoroamidation reactions which are widely used for labelling of macromolecules [39], most often in aqueous solution.

3.1. Intermediates for Nucleophilic Substitution and Other Coupling Reactions. The synthesis of intermediates for ^{18}F-fluoroalkylation is characterized by a two- or three-step procedure (cf. Figure 3) [40]. First, [^{18}F]fluoride is introduced into a molecule using precursors containing a good leaving group. The ^{18}F-labelled precursor is then isolated and purified before coupling with a further molecule.

In the first step the [^{18}F]fluoride has to be separated from the target water and activated for a nucleophilic substitution reaction. The standard conditions of these basic methods are described in several reviews [11, 32, 41]. A simplification of this approach was achieved by water removal on a strong anion-exchange resin [42] or by use of strong organic bases as additives replacing the inorganic bases or salts classically used in the resin eluent [43–46]. Instead of trapping on anion-exchange resins n.c.a. [^{18}F]fluoride can also be separated by electrochemical methods which are useful to minimize the reaction volume especially for the use in microfluidic systems [47–51]. The use of mixtures of nonpolar tert-alcohols with acetonitrile as a reaction medium enhanced the reactivity of cesium[^{18}F]fluoride or tetrabutylammonium [^{18}F]fluoride and reduced the formation of typical by-products compared

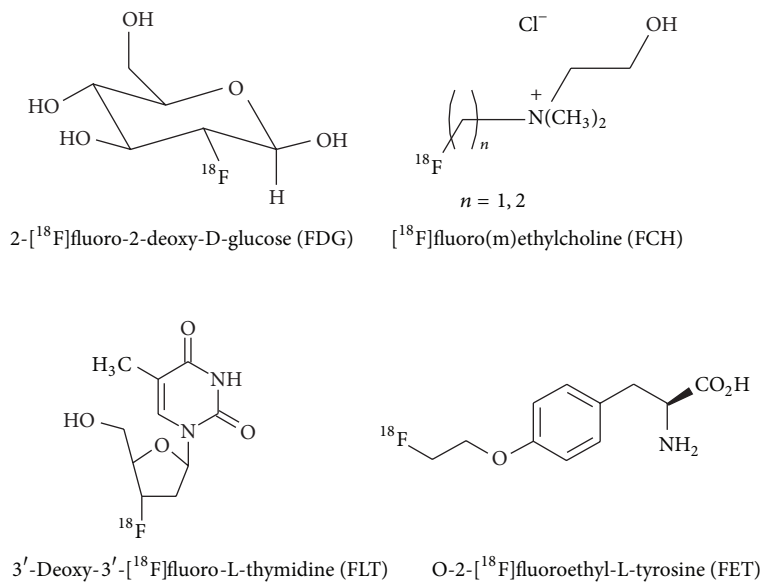

Figure 2: Important ^{18}F-labelled radiotracers in clinical use.

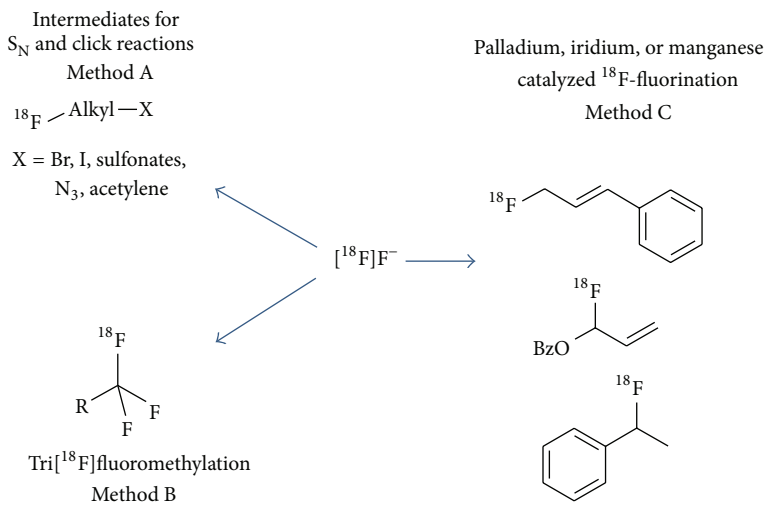

Figure 3: Pathways for aliphatic ^{18}F-labelling intermediates starting from n.c.a. [^{18}F]fluoride.

to those conventionally obtained only with dipolar aprotic solvents [52, 53].

Bromine and iodine and several sulfonate derivatives serve generally as leaving groups for a nucleophilic aliphatic radiofluorination [15, 40, 54, 55]. Alternatively, in the case of preparation of O-[^{18}F]fluoromethylated aliphatic and aromatic ethers, the 1,2,3-triazolium triflate group serves as a very good nucleofuge for displacement by the [^{18}F]fluoride ion [56].

The purification of ^{18}F-fluorinating agents is performed by HPLC, solid phase extraction (SPE), or distillation. The main challenge is the complete separation of the ^{18}F-labelled intermediate from the precursor which also would act as reaction partner in the following coupling step. This leads to unwanted side reactions which could lower the radiochemical yield (RCY) or necessitate a higher concentration of the precursor for the subsequent coupling reaction. A purification of the ^{18}F-fluorinating agent via HPLC (or GC) is very effective and is often used [57–59], but it is more inconvenient for automatization [60, 61]. The use of SPE [62–64] or a distillation process for purification is principally easier to automate [40]. For instance, 1-bromo-3-(nitrobenzene-4-sulfonyloxy)-propane as starting precursor will be retained in the reaction vessel during the distillation process of 1-bromo-3-[^{18}F]fluoropropane, due to its very high boiling point, thus eliminating the risk of formation of pseudocarrier [65]. In a few cases the direct coupling of the ^{18}F-labelled intermediate was performed without former separation and purification [66].

Another possibility for simplified workup is the use of fluorous solid phase extraction (FSPE). A nucleophilic ^{18}F-fluorination of fluorous-tagged precursors can easily be

purified by FSPE regardless of the affinity of the untagged substrate for the stationary phase. FSPE-purified labelled compounds can then be used in subsequent reactions or more easily purified by HPLC before administration [67, 68]. A similar approach was performed using molecular imprinted polymers [69].

Coupling reactions of the ^{18}F-fluorination agent with the desired target molecule are performed either by the use of a further leaving group, by the click chemistry approach [70], by Staudinger ligation [71–73], or by Pd(0) mediated reactions [74].

A series of arylsulfonates were prepared as nucleophile assisting leaving groups (NALG) in which the metal chelating unit is attached to the aryl ring by an ether linker. Under microwave irradiation and without the assistance of a cryptand, such as Kryptofix 2.2.2, primary substrates with selected NALGs led to a 2-3-fold improvement in radiofluorination yields over traditional leaving groups [75].

3.2. Tri[^{18}F]fluoromethyl Group. The CF_3 group has an electronegativity similar to that of oxygen [76] and is characterized by a large hydrophobic parameter as measured by the relative partition coefficient [77]. The trifluoromethyl group is an important pharmacophore present in many biologically active pharmaceutical and agrochemical drugs. The increased lipophilicity and a superior metabolic stability compared to that of the trifluoromethyl analogues often account for an improved activity profile [78]. Thus, radiolabelled trifluoromethyl groups are of potential interest to facilitate drug discovery. Earlier attempts to synthesize an ^{18}F-labelled trifluoromethyl group were also characterized by low RCY and low specific activity due to decomposition of the target material [79–81].

The recently published developments can be divided in aliphatic and aromatic tri[^{18}F]fluoromethylation reactions (cf. Figure 3, method B).

A novel, one-step method for nucleophilic radiosynthesis of aliphatic tri[^{18}F]fluoromethyl groups using the n.c.a. [^{18}F]fluoride ion under relatively mild conditions was developed by incorporation of the radiolabel by an equivalent nucleophilic addition of H[^{18}F]F to the 1-tosyl-2,2-difluorovinyl group (cf. Figure 4). The tosylate function then serves as leaving group in a subsequent coupling step [82, 83]. The specific activity of the tri[^{18}F]fluoromethylether was determined to be 86 MBq/nmol. The need of a double bond to achieve the addition of the [^{18}F]fluoride limits this reaction to aliphatic tri[^{18}F]fluoromethylations.

Aromatic tri[^{18}F]fluoromethyl groups were formerly synthesized using hardly accessible aromatic-CF_2Br groups [84]. Two new approaches were published quite recently (cf. Figure 5). Both methods start with an aliphatic precursor which is first labelled with fluorine-18 and then coupled to the benzene ring. In a two-step procedure tri[^{18}F]fluoromethane ([^{18}F]fluoroform) available from difluoroiodomethane and [^{18}F]fluoride [85] is coupled in a copper(I) mediated reaction to aromatic halides using potassium tert-butoxide as base.

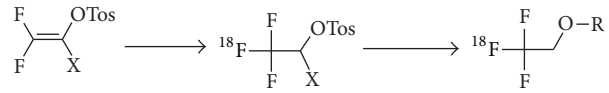

Figure 4: New aliphatic tri[^{18}F]fluoromethylation.

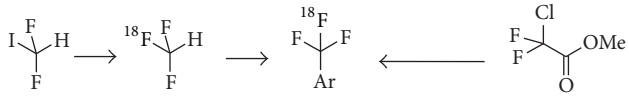

Figure 5: Aromatic tri[^{18}F]fluoromethylation reactions.

The RCY was determined up to 65% with a specific activity of up to 50 GBq/μmol [86]. This method has recently been improved performing a one-pot synthesis in the presence of copper(I)bromide, N,N-diisopropyl-N-ethylamine, and the corresponding iodoarene without separation of the [^{18}F]fluoroform intermediate [87]. The RCYs of the desired tri[^{18}F]fluoroarenes were determined with up to 90%, but no information on the specific activities was given.

An alternative method is used in a one-pot process. The trifluoromethylation agent [^{18}F]CF_3Cu, generated *in situ* from methyl chlorodifluoroacetate, CuI, TMEDA, and [^{18}F]fluoride, is coupled to (hetero)aryl iodides in RCYs ranging from 17 to 87% [88]. A drawback of this procedure is still the relative low specific activity of 0.1 GBq/μmol exemplified so far only for 4-tri[^{18}F]fluoromethyl nitrobenzene. However, the method enables an efficient tri-[^{18}F]fluoromethylation of complex molecules like [^{18}F]fluoxetine. N-Boc protected [^{18}F]fluoxetine was readily prepared in 37% RCY. The subsequent N-Boc deprotection delivered [^{18}F]fluoxetine with 95% yield. A more detailed review on the scope and limitations of the radiosynthesis of tri[^{18}F]fluoromethyl groups is provided as part of this special issue [89].

3.3. Palladium, Managnese and Iridium Catalyzed ^{18}F-Fluorovinylation. Transition metal catalyzed allylic substitution is a powerful method for carbon–carbon and carbon–heteroatom bond formation (cf. Figure 3 above, method C). These reactions encompass a wide variety of heteroatoms (N, O, and S) as nucleophiles [90]. In the field of ^{18}F-chemistry a palladium catalyzed allylic fluorination reaction was developed and transferred to n.c.a. conditions yielding ^{18}F-labelled cinnamyl fluoride starting from [^{18}F]TBAF, cinnamyl methyl carbonate, [Pd $(dba)_2$], and triphenylphosphine in anhydrous acetonitrile [91].

Further, a rapid allylic fluorination method utilizing trichloroacetimidates in conjunction with an iridium catalyst has been developed. The reaction is performed at room temperature without the need of inert gas atmosphere and relies on the $Et_3N{\cdot}3HF$ reagent to provide branched allylic fluorides with complete regioselectivity. This high-yielding reaction can be carried out on a multigram scale and shows considerable functional group tolerance. The use of Kryptofix 2.2.2/K_2CO_3 allowed an incorporation of fluorine-18 within 10 min [92]. The RCY of allylic [^{18}F]fluoride was determined

to be 38%. A specific activity for the aforementioned reactions, however, was not reported.

A new method enables the facile n.c.a. ^{18}F-labelling of aliphatic C–H bonds in benzylic position using manganese salen catalysts with RCY ranging from 20% to 72% within 10 min without the need for preactivation of the labelling precursor [93].

4. Aromatic and Heteroaromatic Intermediates

4.1. ^{18}F-Labelled Aromatic and Heteroaromatic Intermediates by Classic Approaches. Historically, the use of the Balz-Schiemann or Wallach reaction was the first attempt to synthesize ^{18}F-labelled aromatic rings starting from [^{18}F]fluoride (cf. Figure 6, method A) [94, 95]. However, the thermal decomposition of the corresponding aryl diazonium salts and of the aryl triazenes is characterized by low RCY, a low specific radioactivity, and extensive byproduct formation [95]. The use of tetrachloroborate or 2,4,6-triisopropylbenzenesulfonate as counterions led to improvements of the Balz-Schiemann reaction which enables the synthesis of [^{18}F]fluoroarenes in 39% RCY at the n.c.a. level, exemplified for 4-[^{18}F]fluorotoluene [96]. In a recently published study these nucleophilic ^{18}F-labelling methods were reinvestigated using polymer bound aryl diazonium salts and aryl triazenes [97]. The solid phase supported dediazofluorination using arenediazonium cations, ionically bound to a sulfonate functionalised ion exchange resin, was, however, not suitable for nucleophilic ^{18}F-labelling of aromatic compounds, whereas the solid supported triazene yielded the ^{18}F-labelled product in a reasonable RCY of 16%.

Most successful for the introduction of fluorine-18 into aromatic rings is the conventional aromatic nucleophilic substitution (S_NAr) reaction using the [^{18}F]fluoride anion to displace a suitable leaving group from an electron deficient benzene ring. As leaving groups serve halides, the nitro and the trimethylammonium function. The activation of the aromatic ring is usually achieved by suitable functional groups with a–M effect like the carbonyl, carboxyl, cyano, and nitro group [32]. These highly activating groups especially enable the efficient introduction of [^{18}F]fluoride into aromatic rings to label small ^{18}F-intermediates for build-up syntheses. The activating functionality is then converted by reduction, oxidation, or hydrolysis to nucleophilic groups for subsequent coupling reactions. The n.c.a. intermediates 4-[^{18}F]fluoroaniline, 4-[^{18}F]fluorobenzylamine [98, 99], 4-[^{18}F]fluorobenzoic acid, or 4-[^{18}F]fluorophenol (see Section 3.3), which are not directly achievable by a ^{18}F-fluorination reaction, are obtained by these strategies (cf. Figure 7) [16, 100]. 4-[^{18}F]Fluorobenzaldehyde is also used in multicomponent reactions to yield ^{18}F-radiotracers with the label positioned on an aryl moiety, not susceptible to direct nucleophilic fluorination [101].

The azocarbonyl unit is a new group for activation of the arene ring by an S_NAr mechanism. The aromatic core of phenylazocarboxylic esters is highly activated towards nucleophilic aromatic ^{18}F-substitution (cf. Figure 8) [102]. This kind of compounds was converted in a radical arylation reaction into biaryl compounds or in substitutions at its carbonyl unit to produce azocarboxamides. Because of the high reactivity of the aryl radical, side products like [^{18}F]fluorobenzene and 4-[^{18}F]fluorophenol were also formed.

The conventional nucleophilic aromatic substitution reaction can principally be used for the n.c.a. ^{18}F-labelling of aromatic rings in complex molecules [14]. However, the direct introduction of [^{18}F]fluoride is often hampered by a lack of activation and further functional groups, especially those which have acidic protons. In the case of free amino, hydroxyl, or carboxylic acid functions the use of protecting groups is indispensable which have to be removed at the end of synthesis. Generally, the direct ^{18}F-labelling of complex molecules enables the establishment of one-pot syntheses which is advantageous of being better introduced in a remote controlled synthesizer. In a multistep synthesis the intermediates have often to be purified (e.g., [103]) which hampers the installation in a synthesis module. Thus, one-pot syntheses are normally preferable over the build-up synthesis using several reactor vessels. There are exceptions to this rule, for example, when the build-up synthesis gives substantially higher RCYs [104].

In contrast to benzene, some heteroarenes like pyridine efficiently support the S_NAr reaction and can directly be used to prepare ^{18}F-labelled heteroarenes in the 2- or 4-position [105–107]. Because of its straightforward feasibility, this method was even applied for radiofluorination of complex structures containing an azabenzoxazole [108], a 1,3-thiazole [109], a fluoropurine [110], a pyridine [111–118], a quinolinol [119], or a pyrimidine moiety [120].

4.2. New Developments on Radiofluorination of Arenes. In general, the examination of new methods for ^{18}F-labelling of arene rings focuses on the late stage introduction of [^{18}F]fluorine into complex organic molecules without the need of any transformation reaction afterwards. This principally simplifies the establishment of ^{18}F-labelling methods in fully automated, remotely controlled synthesis units. However, these new methods are also useful for the synthesis of small intermediates for build-up synthesis. The novel methods of two prominent ones, [^{18}F]fluorophenol and [^{18}F]fluoro-halobenzene, are separately described (see Sections 4.3 and 4.4).

4.2.1. Iodonium Salts (See Figure 6, Method D, and Figure 9). The classical approach of n.c.a. nucleophilic aromatic ^{18}F-substitution reactions is limited to activated arene rings. The use of diaryliodonium salts enables the introduction of n.c.a. [^{18}F]fluoride into aromatic rings without further activation of strong electron withdrawing groups, which was first demonstrated in 1995 [121]. The reaction via an S_NAr mechanism leads to n.c.a. [^{18}F]fluoroarenes and the corresponding iodoarenes. The nucleophilic attack on the diaryliodonium salt occurs preferably at the more electron-deficient ring and a steric influence of substituents, especially

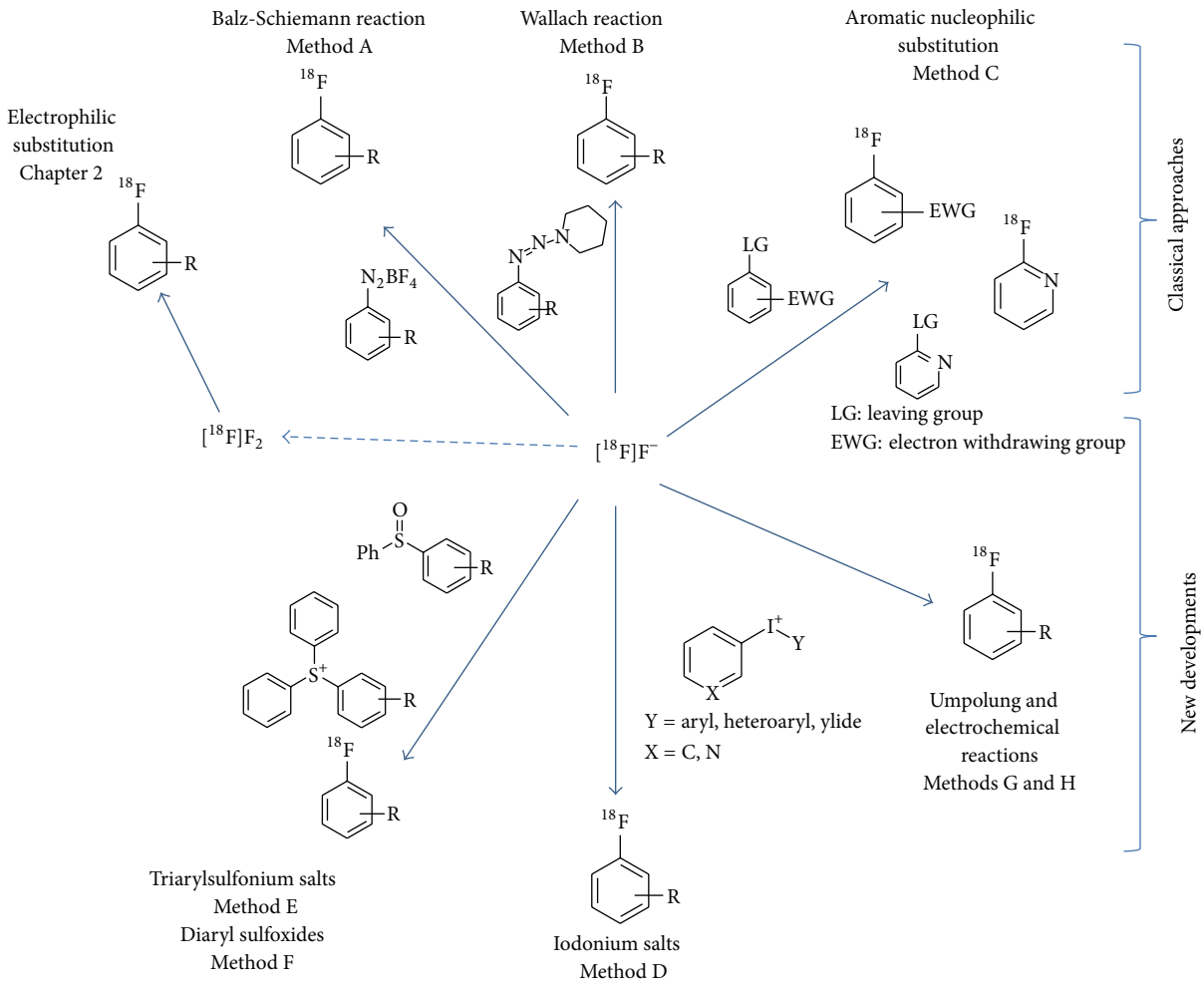

Figure 6: Pathways for aromatic ^{18}F-labelling.

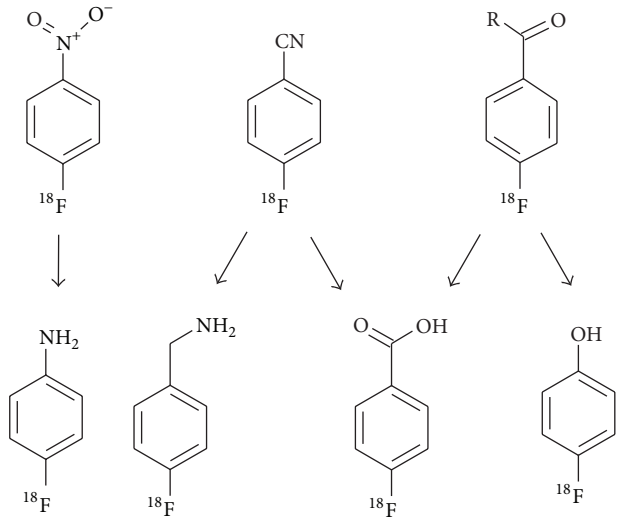

Figure 7: ^{18}F-labelled aromatic small molecules available by S_NAr reactions used as intermediates and further important ^{18}F-intermediates derived therefrom.

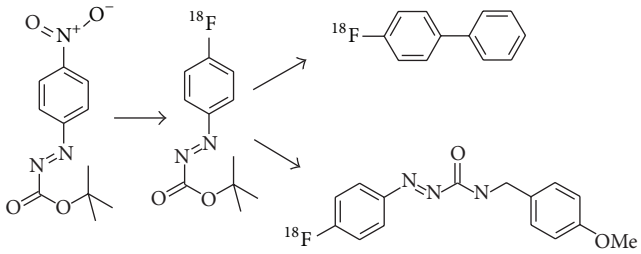

Figure 8: Radical arylation and substitution reactions of a ^{18}F-labelled phenylazocarboxylic ester [102].

of ortho-substituted, could be observed [95]. Further studies have recently been performed to examine the possibilities and limitations of this reaction, with a focus on the synthesis of ortho- and meta-substituted arenes and the use of microreactors [122–124].

An interesting aspect here is that the reaction of diaryliodonium salts with [^{18}F]fluoride is feasible in the presence of water, however, depending on the substituents present

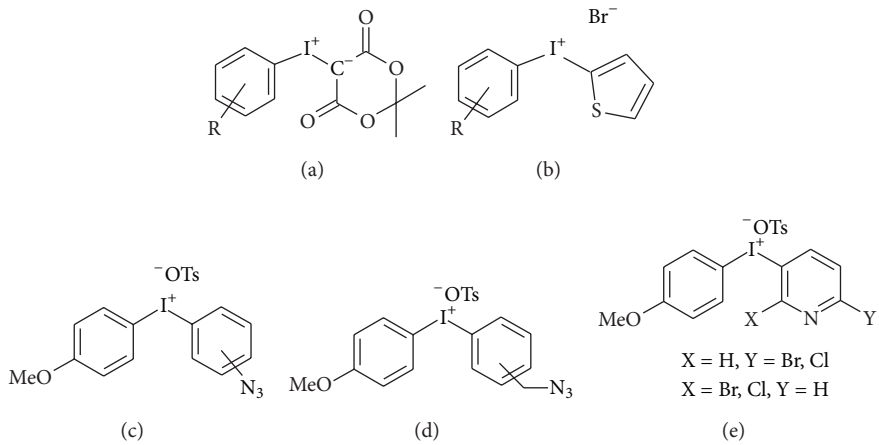

Figure 9: Structures of several iodonium salts for ^{18}F-labelling: (a) iodonium ylide, (b) aryl(thienyl) iodonium salt, (c) [(azidomethyl)phenyl](4′-methoxyphenyl) iodonium tosylate, (d) [(azido)phenyl](4′-methoxyphenyl) iodonium tosylates, and (e) halopyridinyl-(4′-methoxyphenyl)iodonium tosylate.

on the arene ring. Iodonium salts bearing a para- or ortho-electron-withdrawing group (e.g., p-CN) reacted rapidly (~ 3 min) to give the expected major [^{18}F]fluoroarene product in useful, albeit moderate radiochemical yields even when the solvent had a water content of up to 28%. Iodonium salts bearing electron-withdrawing groups in metaposition (e.g., m-NO_2) or an electron-donating substituent (p-OMe) gave low radiochemical yields under the same conditions. The finding that [^{18}F]fluoroarenes, that having an ortho-alkyl substituent or an ortho- or a para-electron withdrawing group, can be synthesized without the need to remove irradiated water or to add a cryptand, could be attractive in some radiotracer production settings, particularly as this method saves time, avoids any need for automated drying of cyclotron-produced [^{18}F]fluoride, and also avoids substantial loss of radioactivity through adsorption onto hardware surfaces [125].

In order to control the attack of the [^{18}F]fluoride ion on the diaryliodonium salts it is important that one arene ring be more electron-rich than the ring to be labelled with fluorine-18. Here, the use of symmetrically substituted diaryliodonium salts [126] or the use of aryl(heteroaryl) iodonium salts [127] is an alternative to direct the ^{18}F-labelling to the desired ring. More recently, the use of aryiodonium ylides became of interest for this purpose. The electron-rich status of the ylides, made, for example, from dimedone (5,5-dimethylcyclohexane-1,3-dione), even enables the synthesis of electron-rich arenes in high RCY [128]. This type of precursor has recently been demonstrated to be even suitable for complex molecules [129].

Some special intermediates like azide-containing diaryliodonium salts bearing an azidomethyl group on one aryl ring and with a 4-methoxy group on the second one enable the synthesis of click-labelling synthons up to 50 % RCY, even in the presence of a high fraction of water in the reaction solvent [130].

Halopyridinyl-(4′-methoxyphenyl)iodonium tosylates were used to rapidly produce [^{18}F]fluorohalopyridines and in useful RCYs, including the otherwise difficult to access 3-[^{18}F]fluorohaloisomers [131].

4.2.2. Sulfur Activated Systems (See Figure 6 and Methods E and F). Another newer method for the ^{18}F-labelling of non-activated aromatic compounds makes use of triarylsulfonium salts. The method is applicable to a wide range of substituted aryl systems including amides [132].

A new radiosynthetic method for producing n.c.a. [^{18}F]fluoroarenes is based on the reactions of diaryl sulfoxides bearing electron-withdrawing paragroups with the [^{18}F]fluoride ion. These reactions are relatively mild, rapid, and efficient. However, this reaction is limited to aromatic rings bearing an electron withdrawing function like the nitro, cyano, or trifluoromethyl group [133].

4.2.3. Umpolungs Reactions (See Figure 6 and Methods G and H). New concepts to synthesize ^{18}F-labelled aromatic rings try to achieve fluoride-derived electrophilic n.c.a. fluorination reagents by fluoride umpolung [134, 135]. A preliminary realization of this concept was achieved by using a n.c.a. [^{18}F]fluoride capture by a Pd(IV) complex to form an electrophilic ^{18}F-fluorination reagent followed by a subsequent n.c.a. ^{18}F-fluorination of palladium aryl complexes [136, 137]. Another kind of palladium catalyzed fluoride activation enables the synthesis of ^{18}F-labelled 1-[^{18}F]fluoronaphthalene in 33% RCY but only in the presence of fluoride carrier [138]. Another advanced method for a transition metal catalyzed late-stage radiofluorination relies on a one-step oxidative ^{18}F-fluorination using a nickel aryl complex and a strong oxidation agent [139].

[^{18}F]Fluoride can also be introduced into organic molecules by electrochemical oxidative fluorination via an aryl cation that undergoes rearomatization by loss of a proton. Oxidation of benzene in an electrolysis cell, using $Et_3N{\cdot}3HF$ and $Et_3N{\cdot}HCl$ in acetonitrile as the electrolyte, gave c.a. [^{18}F]fluorobenzene in 17% RCY [140] and

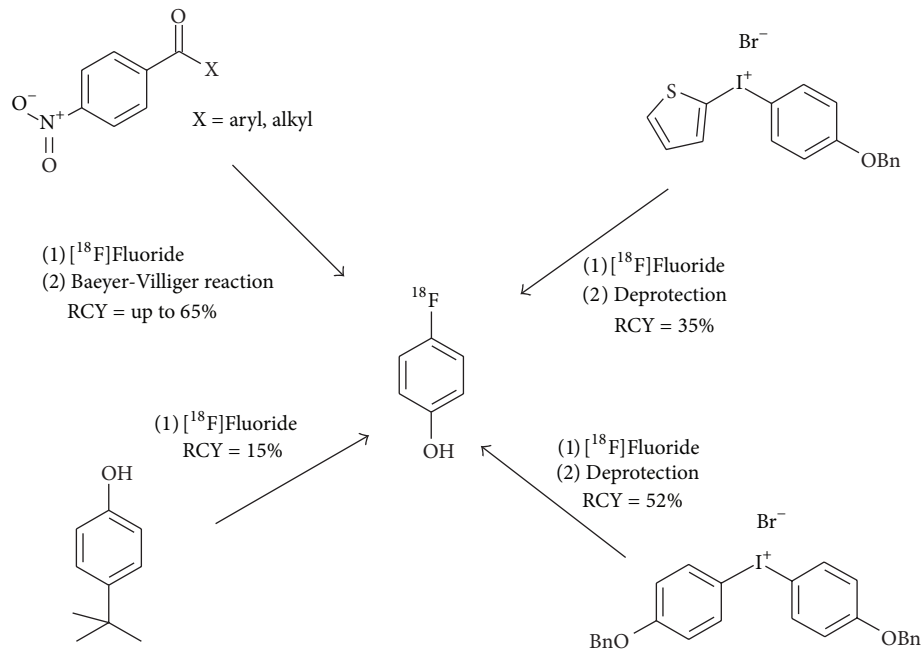

Figure 10: Methods for the synthesis of n.c.a. 4-[^{18}F]fluorophenol.

[^{18}F]fluorophenylalanine in 10.5% RCY with a specific activity of 1.2 GBq/mmol [141].

However, the aim of all these methods is the late stage ^{18}F-fluorination of electron-neutral and electron-rich aromatic compounds to simplify the synthesis of radiotracers. Regarding the palladium and nickel reactions, the precursor synthesis is often complex, has to be carefully handled under inert atmosphere, and needs high synthetic experience. This method is far from ideal, given the many reagents and demanding reaction conditions necessary, which hamper to fulfill a "good manufacturing practice" (GMP) pharmaceutical production [142, 143]. Thus, although principally applicable, their limitation and complexity do not warrant usefulness for the syntheses of build-up intermediates, as there are more efficient methods available for those molecules.

4.3. N.c.a. 4-[^{18}F]Fluorophenol. 4-[^{18}F]Fluorophenol is a versatile structural unit for the synthesis of more complex radiopharmaceuticals bearing a 4-[^{18}F]fluorophenoxy moiety. Former syntheses of n.c.a. 4-[^{18}F]fluorophenol were made either by a modified Balz-Schiemann reaction or by hydrolysis of a 4-[^{18}F]fluorobenzene diazonium salt with radiochemical yields of only 10–15% and 15–33% within 35 and 60 min, respectively [144]. These methods required either the preparation of an anhydrous tetrachloroborate or a two-step synthesis from [^{18}F]fluoroaniline and were not established for radiotracer production.

A more reliable preparation of n.c.a. 2- and 4-[^{18}F]fluorophenol was achieved using the Baeyer-Villiger reaction on ^{18}F-labelled benzaldehyde, acetophenone, or benzophenone derivatives. Total radiochemical yields of about 25% were received using *m*-chloroperbenzoic acid as oxidant in the presence of trifluoroacetic acid [145]. The Baeyer-Villiger reaction of ^{18}F-labelled benzophenone derivatives containing further electron withdrawing groups yielded up to 65% of 4-[^{18}F]fluorophenol within 60 min with a high radiochemical purity. However, a considerable disadvantage of this method is the somewhat cumbersome work-up of the aqueous reaction mixture in order to isolate the product for its further use [146]. The formation of ^{18}F-labelled 4-phenol derivatives by Baeyer-Villiger oxidation was, for example, applied to the direct ^{18}F-fluorination of 6-[^{18}F]fluoro-L-dopa [147].

A novel radiochemical transformation by an oxidative ^{18}F-fluorination of tert-butylphenols uses the concept of an aryl umpolung (cf. Figure 10) and is also applicable to other O-unprotected phenols. The reaction is performed at room temperature by applying a one-pot protocol and can also be performed in a commercially available microfluidic device [148].

Furthermore, aryl(thienyl) iodonium salts [149] and bis(4-benzyloxyphenyl) iodonium salts [150] have successfully been employed for the preparation of [^{18}F]fluorophenol in a two-step procedure. Compared with the Baeyer Villiger method using benzophenone derivatives, this pathway saves 20 to 45 min of preparation time and delivers [^{18}F]fluorophenol in an organic solution. So these methods are more useful for subsequent coupling reactions under anhydrous conditions. In contrast to the aryl umpolung reaction, the iodonium strategy, however, necessitates a deprotection step after the ^{18}F-exchange.

4.4. N.c.a. 4-[^{18}F]Fluorohalobenzene. Recently, the synthesis of 4-[^{18}F]fluorohalobenzenes has comprehensively been described [151]; here a few further aspects are added.

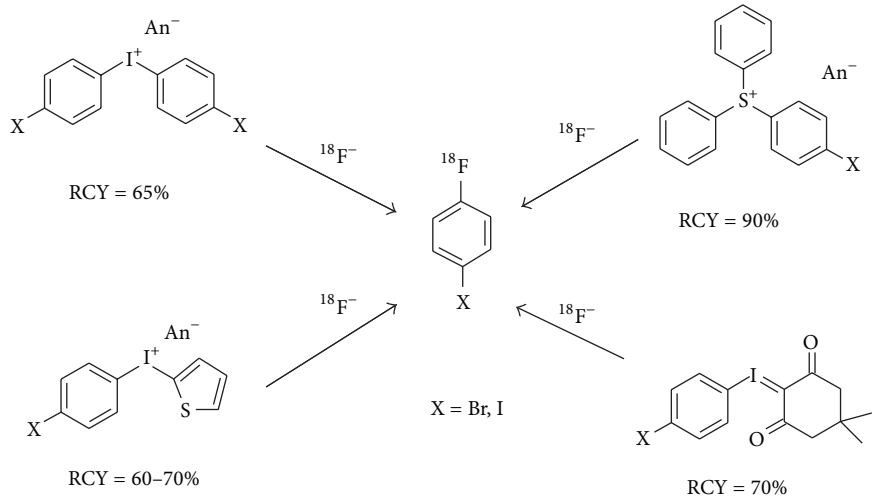

Figure 11: Most efficient one-step approaches for the n.c.a synthesis of [^{18}F]fluoro-halobenzenes.

1-Bromo-4-[^{18}F]fluorobenzene or 4-[^{18}F]fluoro-1-iodobenzene serves as intermediates for C–C coupling reactions using Grignard-, lithium- [152], or palladium-mediated reactions [151, 153]. In Figure 11 the most efficient routes for the synthesis of n.c.a. 4-[^{18}F]fluorohalobenzenes are illustrated. The use of symmetrically substituted diaryliodonium salts enables an efficient one-step synthesis of n.c.a. 1-bromo-4-[^{18}F]fluorobenzene [154] as well as n.c.a. 4-[^{18}F]fluoro-1-iodobenzene [155]. For the latter, the precursor synthesis is more challenging and has recently been improved [156]. The precursor syntheses of iodophenylthienyliodonium bromide and 4-iodophenyliodonium-(5-[2,2-dimethyl-1,3-dioxane-4,6-dione]) ylide [157] are easier to perform and the latter gave up to 70% RCY of 4-[^{18}F]fluoro-1-iodobenzene [158]. The most efficient method for the one-step synthesis of 4-[^{18}F]fluoro-1-iodobenzene is, however, the use of triarylsulfonium salts [132, 159] which leads to 90% RCY. A challenge, when using iodonium salts as precursor for the synthesis of 4-[^{18}F]fluorohalobenzenes, is the formation of other nonradioactive halobenzene derivatives which are normally not separated from the ^{18}F-labelled product and thus could hamper the final product separation.

5. Conclusion

The lack of universally useful methods for direct n.c.a. radiofluorination of complex molecules causes the wide use of ^{18}F-labelled intermediates for the build-up synthesis of radiotracers. Nevertheless, multistep build-up syntheses of ^{18}F-labelled radiotracers are confronted with several fundamental challenges, which often hamper a remotely controlled, large scale production by this type of reactions. Time consuming separation steps and the use of moisture or even air sensitive reagents complicate the automation of these build-up syntheses. Their application is therefore limited to specialized laboratories with the suitable equipment and experienced staff. The use of build-up reactions then often enables the only way to achieve the synthesis of new radiotracers. Once proven that a radiotracer has the potential to be a useful radiopharmaceutical for molecular imaging, most often ways can be found to establish its routine production via an alternative, simpler synthetic concept and/or by optimisation. Here, the novel developments in umpolung reactions or the improvements in iodonium chemistry in ^{18}F-labelling of arenes are promising methods, which might also be effective for the late-stage ^{18}F-fluorination of complex precursors. However, their suitability for daily routine GMP-production of radiopharmaceuticals remains to be elucidated.

Conflict of Interests

The author declares that there is no conflict of interests regarding the publication of this paper.

Acknowledgment

The author wishes to thank Professor Heinz H. Coenen for his critical discussions and helpful suggestions.

References

[1] S. M. Ametamey, M. Honer, and P. A. Schubiger, "Molecular imaging with PET," *Chemical Reviews*, vol. 108, no. 5, pp. 1501–1516, 2008.

[2] S. Y. Lu and V. W. Pike, "Micro-reactors for PET tracer labeling," in *PET Chemistry: the Driving Force in Molecular Imaging*, P. A. Schubiger, L. Lehmann, and M. Friebe, Eds., vol. 62 of *Ernst Schering Research Foundation Workshop*, pp. 271–287, Springer , Berlin, Germany, 2007.

[3] G. Pascali, P. Watts, and P. A. Salvadori, "Microfluidics in radiopharmaceutical chemistry," *Nuclear Medicine and Biology*, vol. 40, no. 6, pp. 776–787, 2013.

[4] S. H. Liang, T. L. Collier, B. H. Rotstein et al., "Rapid microfluidic flow hydrogenation for reduction or deprotection of ^{18}F-labeled compounds," *Chemical Communications*, vol. 49, pp. 8755–8757, 2013.

[5] A. Lebedev, R. Miraghaie, K. Kotta et al., "Batch-reactor microfluidic device: first human use of a microfluidically produced PET radiotracer," *Lab on a Chip: Miniaturisation for Chemistry and Biology*, vol. 13, no. 1, pp. 136–145, 2013.

[6] K. Dahl, M. Schou, and C. Halldin, "Radiofluorination and reductive amination using a microfluidic device," *Journal of Labelled Compounds and Radiopharmaceuticals*, vol. 55, no. 13, pp. 455–459, 2012.

[7] V. Bouvet, M. Wuest, P.-H. Tam, M. Wang, and F. Wuest, "Microfluidic technology: an economical and versatile approach for the synthesis of O-(2-[^{18}F]fluoroethyl)-l-tyrosine ([^{18}F]FET)," *Bioorganic and Medicinal Chemistry Letters*, vol. 22, no. 6, pp. 2291–2295, 2012.

[8] V. R. Bouvet, M. Wuest, L. I. Wiebe, and F. Wuest, "Synthesis of hypoxia imaging agent 1-(5-deoxy-5-fluoro-α-d-arabinofuranosyl)-2-nitroimidazole using microfluidic technology," *Nuclear Medicine and Biology*, vol. 38, no. 2, pp. 235–245, 2011.

[9] C. Rensch, A. Jackson, S. Lindner et al., "Microfluidics: a groundbreaking technology for PET tracer production?" *Molecules*, vol. 18, no. 7, pp. 7930–7956, 2013.

[10] B. Y. Yang, J. M. Jeong, Y.-S. Lee, D. S. Lee, J.-K. Chung, and M. C. Lee, "Facile calculation of specific rate constants and activation energies of ^{18}F-fluorination reaction using combined processes of coat-capture-elution and microfluidics," *Tetrahedron*, vol. 67, no. 13, pp. 2427–2433, 2011.

[11] L. Cai, S. Lu, and V. W. Pike, "Chemistry with [^{18}F]fluoride ion," *European Journal of Organic Chemistry*, no. 17, pp. 2853–2873, 2008.

[12] W. Wadsak, L.-K. Mien, D. E. Ettlinger et al., " ^{18}F fluoroethylations: different strategies for the rapid translation of ^{11}C-methylated radiotracers," *Nuclear Medicine and Biology*, vol. 34, no. 8, pp. 1019–1028, 2007.

[13] B. Amaraesekera, P. D. Marchis, K. P. Bobinski et al., "High-pressure, compact, modular radiosynthesizer for production of positron emitting biomarkers," *Applied Radiation and Isotopes*, vol. 78, pp. 88–101, 2013.

[14] J. Ermert and H. H. Coenen, "Nucleophilic ^{18}F-fluorination of complex molecules in activated carbocyclic aromatic position," *Current Radiopharmaceuticals*, vol. 3, no. 2, pp. 109–126, 2010.

[15] D. Roeda and F. Dollé, "Aliphatic nucleophilic radiofluorination," *Current Radiopharmaceuticals*, vol. 3, no. 2, pp. 81–108, 2010.

[16] J. Ermert and H. H. Coenen, "No-carrier-added [^{18}F]fluorobenzene derivatives as intermediates for built-up radiosyntheses," *Current Radiopharmaceuticals*, vol. 3, no. 2, pp. 127–160, 2010.

[17] B. Kuhnast and F. Dollé, "The challenge of labeling macromolecules with fluorine-18: three decades of research," *Current Radiopharmaceuticals*, vol. 3, no. 3, pp. 174–201, 2010.

[18] T. A. D. Smith, "Fluoride labelling of macromolecules in aqueous conditions: silicon and boroaryl-based [^{18}F]fluorine acceptors, [^{18}F]FDG conjugation and Al^{18}F chelation," *Journal of Labelled Compounds and Radiopharmaceuticals*, vol. 55, no. 8, pp. 281–288, 2012.

[19] W. J. McBride, R. M. Sharkey, H. Karacay et al., "A novel method of ^{18}F radiolabeling for PET," *Journal of Nuclear Medicine*, vol. 50, no. 6, pp. 991–998, 2009.

[20] P. Laverman, W. J. McBride, R. M. Sharkey et al., "A novel facile method of labeling octreotide with ^{18}F-fluorine," *Journal of Nuclear Medicine*, vol. 51, no. 3, pp. 454–461, 2010.

[21] W. J. McBride, C. A. D'Souza, H. Karacay, R. M. Sharkey, and D. M. Goldenberg, "New lyophilized kit for rapid radiofluorination of peptides," *Bioconjugate Chemistry*, vol. 23, no. 3, pp. 538–547, 2012.

[22] Z. Liu, Y. Li, J. Lozada et al., "Stoichiometric leverage: rapid ^{18}F-aryltrifluoroborate radiosynthesis at high specific activity for click conjugation," *Angewandte Chemie: International Edition*, vol. 52, no. 8, pp. 2303–2307, 2013.

[23] R. Schirrmacher, G. Bradtmöller, E. Schirrmacher et al., " ^{18}F-labeling of peptides by means of an organosilicon-based fluoride acceptor," *Angewandte Chemie: International Edition*, vol. 45, no. 36, pp. 6047–6050, 2006.

[24] L. Mu, P. A. Schubiger, and S. M. Ametamey, "[^{18}F]fluorosilicon- and [^{18}F]fluoroboron-based biomolecules for PET imaging," *Current Radiopharmaceuticals*, vol. 3, no. 3, pp. 224–242, 2010.

[25] L. O. Dialer, S. V. Selivanova, C. J. Müller et al., "Studies toward the development of new silicon-containing building blocks for the direct ^{18}F-labeling of peptides," *Journal of Medicinal Chemistry*, vol. 56, pp. 7552–7563, 2013.

[26] B. Wängler, A. P. Kostikov, S. Niedermoser et al., "Protein labeling with the labeling precursor [^{18}F]SiFA-SH for positron emission tomography," *Nature Protocols*, vol. 7, no. 11, pp. 1964–1969, 2012.

[27] Y. Joyard, R. Azzouz, L. Bischoff et al., "Synthesis of new ^{18}F-radiolabeled silicon-based nitroimidazole compounds," *Bioorganic and Medicinal Chemistry*, vol. 21, no. 13, pp. 3680–3688, 2013.

[28] K. Kettenbach, H. Schieferstein, and T. Ross, " ^{18}F-Labeling using click cycloadditions," *BioMed Research International*, vol. 2014, Article ID 361329, 16 pages, 2014.

[29] S. Maschauer and O. Prante, "Sweetening pharmaceutical radiochemistry by fluoroglycosylation: a short review," *BioMed Research International*, vol. 2014, Article ID 214748, 16 pages, 2014.

[30] V. Bernard-Gauthier, C. Wängler, E. Schirrmacher et al., " ^{18}F-Labeled silicon-based fluoride acceptors-opportunities for novel positron emitting radiopharmaceuticals," *BioMed Research International*. In press.

[31] S. M. Qaim, J. C. Clark, C. Crouzel et al., "PET radionuclide production," in *Radiopharmaceuticals for Positron Emission Tomography: Methodological Aspects*, G. Stöcklin and V. W. Pike, Eds., pp. 15–26, Kluwer Academic Publishers, Dordrecht, The Netherlands, 1993.

[32] H. H. Coenen, "Fluorine-18 labeling methods: features and possibilities of basic reactions," in *PET Chemistry: The Driving Force in Molecular Imaging*, P. A. Schubiger, L. Lehmann, and M. Friebe, Eds., vol. 62 of *Ernst Schering Research Foundation Workshop*, pp. 15–50, Springer, Berlin, Germany, 2007.

[33] H. Teare, E. G. Robins, E. Årstad, S. K. Luthra, and V. Gouverneur, "Synthesis and reactivity of [^{18}F]-N-fluorobenzenesulfonimide," *Chemical Communications*, no. 23, pp. 2330–2332, 2007.

[34] J. Bergman, P. Johnström, M. Haaparanta, O. Solin, T. Duelfer, and S. Stone-Elander, "Radiolabelling of 2-oxoquazepam with electrophilic ^{18}F prepared from [^{18}F]fluoride," *Applied Radiation and Isotopes*, vol. 46, no. 10, pp. 1027–1034, 1995.

[35] H. Teare, E. G. Robins, A. Kirjavainen et al., "Radiosynthesis and evaluation of [^{18}F]Selectfluor bis(triflate)," *Angewandte Chemie: International Edition*, vol. 49, no. 38, pp. 6821–6824, 2010.

[36] I. S. R. Stenhagen, A. K. Kirjavainen, S. J. Forsback et al., "Fluorination of an arylboronic ester using [^{18}F]selectfluor bis(triflate): application to 6-[^{18}F]fluoro-l-DOPA," *Chemical Communications*, vol. 49, no. 14, pp. 1386–1388, 2013.

[37] H.-J. Wester, "Nuclear imaging probes: from bench to bedside," *Clinical Cancer Research*, vol. 13, no. 12, pp. 3470–3481, 2007.

[38] H. H. Coenen, P. H. Elsinga, R. Iwata et al., "Fluorine-18 radiopharmaceuticals beyond [^{18}F]FDG for use in oncology and neurosciences," *Nuclear Medicine and Biology*, vol. 37, no. 7, pp. 727–740, 2010.

[39] H. J. Wester and M. Schottelius, "Fluorine-18 labeling of peptides and proteins," in *PET Chemistry: the Driving Force in Molecular Imaging*, A. P. Schubiger, L. Lehmann, and M. Friebe, Eds., vol. 62 of *Ernst Schering Research Foundation Workshop*, pp. 79–111, 2007.

[40] M.-R. Zhang and K. Suzuki, "[^{18}F]Fluoroalkyl agents: synthesis, reactivity and application for development of PET ligands in molecular imaging," *Current Topics in Medicinal Chemistry*, vol. 7, no. 18, pp. 1817–1828, 2007.

[41] O. Jacobson and X. Chen, "PET designated flouride-18 production and chemistry," *Current Topics in Medicinal Chemistry*, vol. 10, no. 11, pp. 1048–1059, 2010.

[42] S. H. Wessmann, G. Henriksen, and H.-J. Wester, "Cryptate mediated nucleophilic ^{18}F-fluorination without azeotropic drying," *NuklearMedizin*, vol. 51, no. 1, pp. 1–8, 2012.

[43] C. F. Lemaire, J. J. Aerts, S. Voccia et al., "Fast production of highly reactive no-carrier-added [^{18}F] fluoride for the labeling of radiopharmaceuticals," *Angewandte Chemie: International Edition*, vol. 49, no. 18, pp. 3161–3164, 2010.

[44] J. Aerts, S. Voccia, C. Lemaire et al., "Fast production of highly concentrated reactive [^{18}F] fluoride for aliphatic and aromatic nucleophilic radiolabelling," *Tetrahedron Letters*, vol. 51, no. 1, pp. 64–66, 2010.

[45] B. Mathiessen, A. T. I. Jensen, and F. Zhuravlev, "Homogeneous nucleophilic radiofluorination and fluorination with phosphazene hydrofluorides," *Chemistry*, vol. 17, no. 28, pp. 7796–7805, 2011.

[46] B. Mathiessen and F. Zhuravlev, "Automated solid-phase radiofluorination using polymer-supported phosphazenes," *Molecules*, vol. 18, pp. 10531–10547, 2013.

[47] K. Hamacher, T. Hirschfelder, and H. H. Coenen, "Electrochemical cell for separation of [^{18}F]fluoride from irradiated ^{18}O-water and subsequent no carrier added nucleophilic fluorination," *Applied Radiation and Isotopes*, vol. 56, no. 3, pp. 519–523, 2002.

[48] G. Reischl, W. Ehrlichmann, and H.-J. Machulla, "Electrochemical transfer of [^{18}F] fluoride from [^{18}O]water into organic solvents ready for labeling reactions," *Journal of Radioanalytical and Nuclear Chemistry*, vol. 254, no. 1, pp. 29–31, 2002.

[49] H. Saiki, R. Iwata, H. Nakanishi et al., "Electrochemical concentration of no-carrier-added [^{18}F]fluoride from [^{18}O]water in a disposable microfluidic cell for radiosynthesis of ^{18}F-labeled radiopharmaceuticals," *Applied Radiation and Isotopes*, vol. 68, no. 9, pp. 1703–1708, 2010.

[50] R. Wong, R. Iwata, H. Saiki, S. Furumoto, Y. Ishikawa, and E. Ozeki, "Reactivity of electrochemically concentrated anhydrous [^{18}F]fluoride for microfluidic radiosynthesis of ^{18}F-labeled compounds," *Applied Radiation and Isotopes*, vol. 70, no. 1, pp. 193–199, 2012.

[51] S. Sadeghi, V. Liang, S. Cheung et al., "Reusable electrochemical cell for rapid separation of [^{18}F]fluoride from [^{18}O]water for flow-through synthesis of ^{18}F-labeled tracers," *Applied Radiation and Isotopes*, vol. 75, pp. 85–94, 2013.

[52] W. K. Dong, H.-J. Jeong, T. L. Seok, M.-H. Sohn, J. A. Katzenellenbogen, and Y. C. Dae, "Facile nucleophilic fluorination reactions using tert-alcohols as a reaction medium: significantly enhanced reactivity of alkali metal fluorides and improved selectivity," *Journal of Organic Chemistry*, vol. 73, no. 3, pp. 957–962, 2008.

[53] K. Sachin, H.-J. Jeong, S. T. Lim, M.-H. Sohn, D. Y. Chi, and D. W. Kim, "An efficient synthesis of ([^{18}F]fluoropropyl)quinoline-5,8-diones by rapid radiofluorination-oxidative demethylation," *Tetrahedron*, vol. 67, no. 10, pp. 1763–1767, 2011.

[54] T. Priem, C. Bouteiller, D. Camporese, A. Romieu, and P.-Y. Renard, "Synthesis and reactivity of a bis-sultone cross-linker for peptide conjugation and [^{18}F]-radiolabelling via unusual "double click" approach," *Organic and Biomolecular Chemistry*, vol. 10, no. 5, pp. 1068–1078, 2012.

[55] R. Löser, R. Bergmann, M. Frizler et al., "Synthesis and radiopharmacological characterisation of a fluorine-18-labelled azadipeptide nitrile as a potential PET tracer for invivo imaging of cysteine cathepsins," *ChemMedChem*, vol. 8, no. 8, pp. 1330–1344, 2013.

[56] C. Park, B. S. Lee, and D. Y. Chi, "High efficiency synthesis of F-18 fluoromethyl ethers: an attractive alternative for C-11 methyl groups in positron emission tomography radiopharmaceuticals," *Organic Letters*, vol. 15, pp. 4346–4349, 2013.

[57] N. Jarkas, R. J. Voll, and M. M. Goodman, "Synthesis of a phenolic precursor and its efficient O-[^{18}F]fluoroethylation with purified no-carrier-added [^{18}F]2-fluoroethyl brosylate as the labeling agent," *Journal of Labelled Compounds and Radiopharmaceuticals*, vol. 56, pp. 539–543, 2013.

[58] V. J. Majo, M. S. Milak, J. Prabhakaran et al., "Synthesis and in vivo evaluation of [^{18}F]2-(4-(4-(2-(2-fluoroethoxy)phenyl) piperazin-1-yl)butyl)-4-methyl-1,2,4-triazine-3,5(2H,4H)-dione ([^{18}F]FECUMI-101) as an imaging probe for 5-HT1A receptor agonist in nonhuman primates," *Bioorganic and Medicinal Chemistry*, vol. 21, no. 17, pp. 5598–5604, 2013.

[59] F. Caillé, T. J. Morley, A. A. S. Tavares et al., "Synthesis and biological evaluation of positron emission tomography radiotracers targeting serotonin 4 receptors in brain: [^{18}F]MNI-698 and [^{18}F]MNI-699," *Bioorganic and Medicinal Chemistry Letters*, vol. 23, pp. 6243–6247, 2013.

[60] M.-R. Zhang, A. Tsuchiyama, T. Haradahira, Y. Yoshida, K. Furutsuka, and K. Suzuki, "Development of an automated system for synthesizing ^{18}F-labeled compounds using [^{18}F]fluoroethyl bromide as a synthetic precursor," *Applied Radiation and Isotopes*, vol. 57, no. 3, pp. 335–342, 2002.

[61] P. J. Riss, S. Hoehnemann, M. Piel, and F. Roesch, "Two-step radiosynthesis of [^{18}F]FE-β-CIT and [^{18}F]PR04.MZ," *Journal of Labelled Compounds and Radiopharmaceuticals*, vol. 56, no. 7, pp. 356–359, 2013.

[62] M. E. Rodnick, A. F. Brooks, B. G. Hockley, B. D. Henderson, and P. J. H. Scott, "A fully-automated one-pot synthesis of [^{18}F]fluoromethylcholine with reduced dimethylaminoethanol contamination via [^{18}F]fluoromethyl tosylate," *Applied Radiation and Isotopes*, vol. 78, pp. 26–32, 2013.

[63] D. Franck, T. Kniess, J. Steinbach et al., "Investigations into the synthesis, radiofluorination and conjugation of a new [^{18}F]fluorocyclobutyl prosthetic group and its in vitro stability using a tyrosine model system," *Bioorganic and Medicinal Chemistry*, vol. 21, no. 3, pp. 643–652, 2013.

[64] T. Sun, G. Tang, H. Tian et al., "Radiosynthesis of 1-[^{18}F]fluoroethyl-L-tryptophan as a novel potential amino acid PET tracer," *Applied Radiation and Isotopes*, vol. 70, no. 4, pp. 676–680, 2012.

[65] R. P. Klok, P. J. Klein, J. D. M. Herscheid, and A. D. Windhorst, "Synthesis of N-(3-[^{18}F]fluoropropyl)-2β-carbomethoxy-3β-(4-iodophenyl)nortropane ([^{18}F]FP-β-CIT)," *Journal of Labelled Compounds and Radiopharmaceuticals*, vol. 49, no. 2, pp. 77–89, 2006.

[66] E. M. F. Billaud, L. Rbah-Vidal, A. Vidal et al., "Synthesis, radiofluorination, and in vivo evaluation of novel fluorinated and iodinated radiotracers for PET imaging and targeted radionuclide therapy of melanoma," *Journal of Medicinal Chemistry*, vol. 56, pp. 8455–8467, 2013.

[67] R. Bejot, T. Fowler, L. Carroll et al., "Fluorous synthesis of ^{18}F radiotracers with the [^{18}F]fluoride ion: nucleophilic fluorination as the detagging process," *Angewandte Chemie: International Edition*, vol. 48, no. 3, pp. 586–589, 2009.

[68] R. Bejot, J. Goggi, S. S. Moonshi, and E. G. Robins, "A practical synthesis of [^{18}F]FtRGD: an angiogenesis biomarker for PET," *Journal of Labelled Compounds and Radiopharmaceuticals*, vol. 56, no. 2, pp. 42–49, 2013.

[69] G. E. Smith, S. Bayoudh, C. Perollier et al., "Rapid purification of fluorine-18 containing synthons using molecularly imprinted polymer cartridges," *Journal of Labelled Compounds and Radiopharmaceuticals*, vol. 56, article S119, 2013.

[70] M. Pretze, D. Pietzsch, and C. Mamat, "Recent trends in bioorthogonal click-radiolabeling reactions using fluorine-18," *Molecules*, vol. 18, no. 7, pp. 8618–8665, 2013.

[71] M. Pretze, F. Wuest, T. Peppel, M. Köckerling, and C. Mamat, "The traceless Staudinger ligation with fluorine-18: a novel and versatile labeling technique for the synthesis of PET-radiotracers," *Tetrahedron Letters*, vol. 51, no. 49, pp. 6410–6414, 2010.

[72] L. Carroll, S. Boldon, R. Bejot, J. E. Moore, J. Declerck, and V. Gouverneur, "The traceless Staudinger ligation for indirect ^{18}F-radiolabelling," *Organic and Biomolecular Chemistry*, vol. 9, no. 1, pp. 136–140, 2011.

[73] C. Mamat, M. Franke, T. Peppel, M. Köckerling, and J. Steinbach, "Synthesis, structure determination, and (radio-)fluorination of novel functionalized phosphanes suitable for the traceless Staudinger ligation," *Tetrahedron*, vol. 67, no. 25, pp. 4521–4529, 2011.

[74] H. Doi, M. Goto, and M. Suzuki, "Pd_0-mediated rapid C-[^{18}F]fluoromethylation by the cross-coupling reaction of a [^{18}F]fluoromethyl halide with an arylboronic acid ester: novel method for the synthesis of a ^{18}F-labeled molecular probe for positron emission tomography," *Bulletin of the Chemical Society of Japan*, vol. 85, no. 11, pp. 1233–1238, 2012.

[75] S. Lu, S. D. Lepore, Y. L. Song et al., "Nucleophile assisting leaving groups: a strategy for aliphatic ^{18}F-fluorination," *Journal of Organic Chemistry*, vol. 74, no. 15, pp. 5290–5296, 2009.

[76] J. E. Huheey, "The electronegativity of groups," *Journal of Physical Chemistry*, vol. 69, no. 10, pp. 3284–3291, 1965.

[77] M. A. McClinton and D. A. McClinton, "Trifluoromethylations and related reactions in organic chemistry," *Tetrahedron*, vol. 48, no. 32, pp. 6555–6666, 1992.

[78] J.-A. Ma and D. Cahard, "Asymmetric fluorination, trifluoromethylation, and perfluoroalkylation reactions," *Chemical Reviews*, vol. 104, no. 12, pp. 6119–6146, 2004.

[79] J. Prabhakaran, M. D. Underwood, R. V. Parsey et al., "Synthesis and in vivo evaluation of [^{18}F]-4-[5-(4-methylphenyl)-3-(trifluoromethyl)-1H-pyrazol-1-yl]benzenesulfonamide as a PET imaging probe for COX-2 expression," *Bioorganic and Medicinal Chemistry*, vol. 15, no. 4, pp. 1802–1807, 2007.

[80] V. J. Majo, V. Arango, N. R. Simpson et al., "Synthesis and in vitro evaluation of [^{18}F]BMS-754807: a potential PET ligand for IGF-1R," *Bioorganic and Medicinal Chemistry Letters*, vol. 23, no. 14, pp. 4191–4194, 2013.

[81] M. C. Lasne, C. Perrio, J. Rouden et al., "Chemistry of beta-emitting compounds based on fluorine-18+," *Topics in Current Chemistry*, vol. 222, pp. 201–258, 2002.

[82] P. J. Riss and F. I. Aigbirhio, "A simple, rapid procedure for nucleophilic radiosynthesis of aliphatic [^{18}F]trifluoromethyl groups," *Chemical Communications*, vol. 47, no. 43, pp. 11873–11875, 2011.

[83] P. J. Riss, V. Ferrari, L. Brichard, P. Burke, R. Smith, and F. I. Aigbirhio, "Direct, nucleophilic radiosynthesis of [^{18}F]trifluoroalkyl tosylates: improved labelling procedures," *Organic and Biomolecular Chemistry*, vol. 10, no. 34, pp. 6980–6986, 2012.

[84] A. Hammadi and C. Crouzel, "Synthesis of [^{18}F]-(S)-fluoxetine: a selective serotonine uptake inhibitor," *Journal of Labelled Compounds and Radiopharmaceuticals*, vol. 33, no. 8, pp. 703–710, 1993.

[85] D. Van Der Born, J. D. M. Herscheid, R. V. A. Orru, and D. J. Vugts, "Efficient synthesis of [^{18}F]trifluoromethane and its application in the synthesis of PET tracers," *Chemical Communications*, vol. 49, no. 38, pp. 4018–4020, 2013.

[86] D. van der Born, J. D. M. Herscheid, and D. J. Vugts, "Aromatic trifluoromethylation using [^{18}F]fluoroform," *Journal of Labelled Compounds and Radiopharmaceuticals*, vol. 56, article S2, 2013.

[87] T. Rühl, W. Rafique, V. T. Lien et al., "Cu(i)-mediated ^{18}F-trifluoromethylation of arenes: rapid synthesis of ^{18}F-labeled trifluoromethylarenes," *Chemical Communications*, vol. 50, pp. 6056–6059, 2014.

[88] M. Huiban, M. Tredwell, S. Mizuta et al., "A broadly applicable [^{18}F]trifluoro-methylation of aryl and heteroaryl iodides for PET imaging," *Nature Chemistry*, vol. 5, pp. 941–944, 2013.

[89] V. T. Lien and P. Riss, "Radiosynthesis of [^{18}F]trifluoralkylgroups: scope and limitations," *BioMed Research International*. In press.

[90] B. Sundararaju, M. Achard, and C. Bruneau, "Transition metal catalyzed nucleophilic allylic substitution: activation of allylic alcohols via p-allylic species," *Chemical Society Reviews*, vol. 41, pp. 4467–4483, 2012.

[91] C. Hollingworth, A. Hazari, M. N. Hopkinson et al., "Palladium-catalyzed allylic fluorination," *Angewandte Chemie: International Edition*, vol. 50, no. 11, pp. 2613–2617, 2011.

[92] J. J. Topczewski, T. J. Tewson, and H. M. Nguyen, "Iridium-catalyzed allylic fluorination of trichloroacetimidates," *Journal of the American Chemical Society*, vol. 133, no. 48, pp. 19318–19321, 2011.

[93] X. Huang, W. Liu, H. Ren et al., "Late stage benzylic C-Hf with [^{18}F]fluoride for PET imaging," *Journal of the American Chemical Society*, vol. 136, no. 19, pp. 6842–6845, 2014.

[94] A. J. Palmer, J. C. Clark, and R. W. Goulding, "The preparation of fluorine 18 labelled radiopharmaceuticals," *International Journal of Applied Radiation and Isotopes*, vol. 28, no. 1-2, pp. 53–65, 1977.

[95] H. H. Coenen and J. Ermert, "Direct nucleophilic ^{18}F-fluorination of electron rich arenes: present limits of no-carrier-added reactions," *Current Radiopharmaceuticals*, vol. 3, no. 3, pp. 163–173, 2010.

[96] A. Knöchel and O. Zwernemann, "Development of a no-carrier-added method for ^{18}F-labelling of aromatic compounds by fluorodediazonation," *Journal of Labelled Compounds and Radiopharmaceuticals*, vol. 38, no. 4, pp. 325–336, 1996.

[97] P. J. Riss, S. Kuschel, and F. I. Aigbirhio, "No carrier-added nucleophilic aromatic radiofluorination using solid phase supported arenediazonium sulfonates and 1-(aryldiazenyl)piperazines," *Tetrahedron Letters*, vol. 53, no. 14, pp. 1717–1719, 2012.

[98] I. Koslowsky, J. Mercer, and F. Wuest, "Synthesis and application of 4-[^{18}F]fluorobenzylamine: a versatile building block for the preparation of PET radiotracers," *Organic and Biomolecular Chemistry*, vol. 8, no. 20, pp. 4730–4735, 2010.

[99] J. Way and F. Wuest, "Fully automated synthesis of 4-[^{18}F]fluorobenzylamine based on borohydride/$NiCl_2$ reduction," *Nuclear Medicine and Biology*, vol. 40, no. 3, pp. 430–436, 2013.

[100] F. Wuest, "Fluorine-18 labeling of small molecules: the use of ^{18}F-labeled aryl fluorides derived from no-carrier-added [^{18}F]fluoride as labeling precursors," in *PET Chemistry: The Driving Force in Molecular Imaging*, vol. 64 of *Ernst Schering Research Foundation workshop*, pp. 51–78, 2007.

[101] L. Li, M. N. Hopkinson, R. L. Yona, R. Bejot, A. D. Gee, and V. Gouverneur, "Convergent ^{18}F radiosynthesis: a new dimension for radiolabelling," *Chemical Science*, vol. 2, no. 1, pp. 123–131, 2011.

[102] S. K. Fehler, S. Maschauer, S. B. Höfling et al., "Fast and efficient ^{18}F-labeling by [^{18}F] fluorophenylazocarboxylic esters," *Chemistry*, vol. 20, pp. 370–375, 2014.

[103] U. Mühlhausen, J. Ermert, and H. H. Coenen, "Synthesis, labelling and first evaluation of [^{18}F]R91150 as a serotonin 5-HT_{2A} receptor antagonist for PET," *Journal of Labelled Compounds and Radiopharmaceuticals*, vol. 52, no. 1, pp. 13–22, 2009.

[104] F. Kügler, J. Ermert, and H. H. Coenen, "Labeling of benzodioxin piperazines with fluorine-18 as prospective radioligands for selective imaging of dopamine D4 receptors," *Journal of Labelled Compounds and Radiopharmaceuticals*, vol. 56, pp. 609–618, 2013.

[105] F. Dollé, "[^{18}F]Fluoropyridines: from conventional radiotracers to the labeling of macromolecules such as proteins and oligonucleotides," in *PET Chemistry: The Driving Force in Molecular Imaging*, P. A. Schubiger, L. Lehmann, and M. Friebe, Eds., vol. 62, pp. 113–157, 2007.

[106] N. Malik, C. Solbach, W. Voelter, and H.-J. MacHulla, "Nucleophilic aromatic substitution by [^{18}F]fluoride at substituted 2-nitropyridines," *Journal of Radioanalytical and Nuclear Chemistry*, vol. 283, no. 3, pp. 757–764, 2010.

[107] N. Malik, W. Voelter, H.-J. MacHulla, and C. Solbach, "Radiofluorination of 2-fluoropyridines by isotopic exchange with [^{18}F]fluoride," *Journal of Radioanalytical and Nuclear Chemistry*, vol. 287, no. 1, pp. 287–292, 2011.

[108] E. D. Hostetler, S. Sanabria-Bohórquez, H. Fan, Z. Zeng et al., "[^{18}F]Fluoroazabenzoxazoles as potential amyloid plaque PET tracers: synthesis and in vivo evaluation in rhesus monkey," *Nuclear Medicine and Biology*, vol. 38, pp. 1193–1203, 2011.

[109] F. G. Siméon, M. T. Wendahl, and V. W. Pike, "The [^{18}F]2-fluoro-1,3-thiazolyl moiety: an easily-accessible structural motif for prospective molecular imaging radiotracers," *Tetrahedron Letters*, vol. 51, no. 46, pp. 6034–6036, 2010.

[110] P. Marchand, C. Lorilleux, G. Gilbert et al., "Efficient radiosynthesis of 2-[^{18}F]fluoroadenosine: a new route to 2-[^{18}F]fluoropurine nucleosides," *ACS Medicinal Chemistry Letters*, vol. 1, no. 6, pp. 240–243, 2010.

[111] F. Kügler, W. Sihver, J. Ermert et al., "Evaluation of ^{18}F-labeled benzodioxine piperazine-based dopamine D 4 receptor ligands: lipophilicity as a determinate of nonspecific binding," *Journal of Medicinal Chemistry*, vol. 54, no. 24, pp. 8343–8352, 2011.

[112] L. Rbah-Vidal, A. Vidal, S. Besse et al., "Early detection and longitudinal monitoring of experimental primary and disseminated melanoma using [^{18}F]ICF01006, a highly promising melanoma PET tracer," *European Journal of Nuclear Medicine and Molecular Imaging*, vol. 39, no. 9, pp. 1449–1461, 2012.

[113] S. Fischer, A. Hiller, R. Smits et al., "Radiosynthesis of racemic and enantiomerically pure (-)-[^{18}F]flubatine-A promising PET radiotracer for neuroimaging of α4B2 nicotinic acetylcholine receptors," *Applied Radiation and Isotopes*, vol. 74, pp. 128–136, 2013.

[114] J. Liu, L. Zhu, K. Plössl, B. P. Lieberman, and H. F. Kung, "Synthesis and evaluation of novel N-fluoropyridyl derivatives of tropane as potential PET imaging agents for the dopamine transporter," *Bioorganic and Medicinal Chemistry Letters*, vol. 21, no. 10, pp. 2962–2965, 2011.

[115] B.-M. Swahn, J. Sandell, D. Pyring et al., "Synthesis and evaluation of pyridylbenzofuran, pyridylbenzothiazole and pyridylbenzoxazole derivatives as^{18}F-PET imaging agents for β-amyloid plaques," *Bioorganic and Medicinal Chemistry Letters*, vol. 22, no. 13, pp. 4332–4337, 2012.

[116] A. Damont, R. Boisgard, B. Kuhnast et al., "Synthesis of 6-[^{18}F]fluoro-PBR28, a novel radiotracer for imaging the TSPO 18 kDa with PET," *Bioorganic and Medicinal Chemistry Letters*, vol. 21, no. 16, pp. 4819–4822, 2011.

[117] T. G. Hamill, W. Eng, A. Jennings et al., "The synthesis and preclinical evaluation in rhesus monkey of [^{18}F]MK-6577 and [11C]CMPyPB glycine transporter 1 positron emission tomography radiotracers," *Synapse*, vol. 65, no. 4, pp. 261–270, 2011.

[118] E. D. Hostetler, W. Eng, A. D. Joshi et al., "Synthesis, characterization, and monkey PET studies of [^{18}F]MK-1312, a PET tracer for quantification of mGluR1 receptor occupancy by MK-5435," *Synapse*, vol. 65, no. 2, pp. 125–135, 2011.

[119] N. Vasdev, P. Cao, E. M. Van Oosten et al., "Synthesis and PET imaging studies of [^{18}F]2-fluoroquinolin-8-ol ([^{18}F]CABS13) in transgenic mouse models of Alzheimer's disease," *MedChemComm*, vol. 3, no. 10, pp. 1228–1230, 2012.

[120] O. Tietz, S. K. Sharma, J. Kaur et al., "Synthesis of three ^{18}F-labelled cyclooxygenase-2 (COX-2) inhibitors based on a pyrimidine scaffold," *Organic and Biomolecular Chemistry*, vol. 11, pp. 8052–8064, 2013.

[121] V. W. Pike and F. I. Aigbirhio, "Reactions of cyclotron-produced [^{18}F]fluoride with diaryliodonium salts: a novel single-step route to no-carrier-added [^{18}F]fluoroarenes," *Journal of the Chemical Society, Chemical Communications*, no. 21, pp. 2215–2216, 1995.

[122] J.-H. Chun and V. W. Pike, "Single-step syntheses of no-carrier-added functionalized [^{18}F]fluoroarenes as labeling synthons from diaryliodonium salts," *Organic and Biomolecular Chemistry*, vol. 11, no. 37, pp. 6300–6306, 2013.

[123] J.-H. Chun, S. Lu, and V. W. Pike, "Rapid and efficient radiosyntheses of meta-substituted [^{18}F]fluoroarenes from [^{18}F]fluoride ion and diaryliodonium tosylates within a microreactor," *European Journal of Organic Chemistry*, no. 23, pp. 4439–4447, 2011.

[124] J.-H. Chun, S. Lu, Y.-S. Lee, and V. W. Pike, "Fast and high-yield microreactor syntheses of ortho -substituted [^{18}F]Fluoroarenes from reactions of [^{18}F]Fluoride ion with diaryliodonium salts," *Journal of Organic Chemistry*, vol. 75, no. 10, pp. 3332–3338, 2010.

[125] J.-H. Chun, S. Telu, S. Lu, and V. W. Pike, "Radiofluorination of diaryliodonium tosylates under aqueous-organic and cryptand-free conditions," *Organic and Biomolecular Chemistry*, vol. 11, no. 31, pp. 5094–5099, 2013.

[126] J. Ermert, C. Hocke, T. Ludwig, R. Gail, and H. H. Coenen, "Comparison of pathways to the versatile synthon of no-carrier-added 1-bromo-4-[^{18}F]fluorobenzene," *Journal of Labelled Compounds and Radiopharmaceuticals*, vol. 47, no. 7, pp. 429–441, 2004.

[127] T. L. Ross, J. Ermert, C. Hocke, and H. H. Coenen, "Nucleophilic ^{18}F-fluorination of heteroaromatic iodonium salts with no-carrier-added [^{18}F]fluoride," *Journal of the American Chemical Society*, vol. 129, no. 25, pp. 8018–8025, 2007.

[128] N. Satyamurthy and J. R. Barrio, "Preparing F-18 labeled aryl derivative, useful for preparation of F-18 labeled biomarkers, comprises replacing iodonium ylide group of benzene derivative containing iodonium ylide group with no-carrier-added F-18 fluoride ion," Patent WO2010117435-A2, 2010.

[129] J. Cardinale, J. Ermert, S. Humpert et al., "Iodonium ylides for one-step, no-carrier-added radiofluorination of electron rich arenes, exemplified with 4-(([^{18}F]fluoro-phenoxy)-phenylmethyl)piperidine NET and SERT ligands," *RSC Advances*, vol. 4, pp. 17293–17299, 2014.

[130] J.-H. Chun and V. W. Pike, "Single-step radiosynthesis of "^{18}F-labeled click synthons" from azide-functionalized diaryliodonium salts," *European Journal of Organic Chemistry*, no. 24, pp. 4541–4547, 2012.

[131] J.-H. Chun and V. W. Pike, "Selective syntheses of no-carrier-added 2- and 3-[^{18}F] fluorohalopyridines through the radiofluorination of halopyridinyl(4′-methoxyphenyl)iodonium tosylates," *Chemical Communications*, vol. 48, no. 79, pp. 9921–9923, 2012.

[132] L. Mu, C. R. Fischer, J. P. Holland et al., " ^{18}F-radiolabeling of aromatic compounds using triarylsulfonium salts," *European Journal of Organic Chemistry*, no. 5, pp. 889–892, 2012.

[133] J.-H. Chun, C. L. Morse, F. T. Chin, and V. W. Pike, "No-carrier-added [^{18}F]fluoroarenes from the radiofluorination of diaryl sulfoxides," *Chemical Communications*, vol. 49, no. 21, pp. 2151–2153, 2013.

[134] M. Tredwell and V. Gouverneur, " ^{18}F labeling of arenes," *Angewandte Chemie: International Edition*, vol. 51, no. 46, pp. 11426–11437, 2012.

[135] V. Gouverneur, "Radiochemistry: flipping fluoride's reactivity," *Nature Chemistry*, vol. 4, no. 3, pp. 152–154, 2012.

[136] E. Lee, A. S. Kamlet, D. C. Powers et al., "A fluoride-derived electrophilic late-stage fluorination reagent for PET imaging," *Science*, vol. 334, no. 6056, pp. 639–642, 2011.

[137] J. R. Brandt, E. Lee, G. B. Boursalian et al., "Mechanism of electrophilic fluorination with Pd(IV): fluoride capture and subsequent oxidative fluoride transfer," *Chemical Science*, vol. 5, pp. 169–179, 2014.

[138] J. Cardinale, J. Ermert, F. Kügler, A. Helfer, M. R. Brandt, and H. H. Coenen, "Carrier-effect on palladium-catalyzed, nucleophilic ^{18}F-fluorination of aryl triflates," *Journal of Labelled Compounds and Radiopharmaceuticals*, vol. 55, no. 12, pp. 450–453, 2012.

[139] E. Lee, J. M. Hooker, and T. Ritter, "Nickel-mediated oxidative fluorination for PET with aqueous [^{18}F] fluoride," *Journal of the American Chemical Society*, vol. 134, no. 42, pp. 17456–17458, 2012.

[140] G. Reischl, G. J. Kienzle, and H.-J. Machulla, "Electrochemical radiofluorination. Part 2. Anodic monofluorination of substituted benzenes using [^{18}F]fluoride," *Applied Radiation and Isotopes*, vol. 58, no. 6, pp. 679–683, 2003.

[141] G. J. Kienzle, G. Reischl, and H.-J. Machulla, "Electrochemical radiofluorination. 3. Direct labeling of phenylalanine derivatives with [^{18}F]fluoride after anodic oxidation," *Journal of Labelled Compounds and Radiopharmaceuticals*, vol. 48, no. 4, pp. 259–273, 2005.

[142] B. Långström and P. Hartvig, "GMP: three letters with many interpretations: protection of patients or killing the clinical and research applications of PET?" *European Journal of Nuclear Medicine and Molecular Imaging*, vol. 35, no. 4, pp. 693–694, 2008.

[143] P. H. Elsinga, "Present and future of PET-radiopharmaceuticals," *Nuclear Medicine Review*, vol. 15, pp. C13–C16, 2012.

[144] L. Barre, L. Barbier, and M. C. Lasne, "Investigation of possible routes to no-carrier-added 4-[^{18}F]fluorophenol," *Journal of Labelled Compounds and Radiopharmaceuticals*, vol. 35, pp. 167–168, 1994.

[145] I. Ekaeva, L. Barre, M.-C. Lasne, and F. Gourand, "2- and 4-[^{18}F]Fluorophenols from Baeyer-Villiger Oxidation of [^{18}F]Fluorophenylketones and [^{18}F]Fluorobenzaldehydes," *Applied Radiation and Isotopes*, vol. 46, no. 8, pp. 777–782, 1995.

[146] T. Ludwig, J. Ermert, and H. H. Coenen, "4-[^{18}F]fluoroarylalkylethers via an improved synthesis of n.c.a. 4-[^{18}F]fluorophenol," *Nuclear Medicine and Biology*, vol. 29, no. 2, pp. 255–262, 2002.

[147] F. M. Wagner, J. Ermert, and H. H. Coenen, "Three-step, "one-pot" radiosynthesis of 6-fluoro-3,4-dihydroxy-l-phenylalanine by isotopic exchange," *Journal of Nuclear Medicine*, vol. 50, no. 10, pp. 1724–1729, 2009.

[148] Z. Gao, Y. H. Lim, M. Tredwell et al., "Metal-free oxidative fluorination of phenols with [^{18}F]fluoride," *Angewandte Chemie: International Edition*, vol. 51, no. 27, pp. 6733–6737, 2012.

[149] T. L. Ross, J. Ermert, and H. H. Coenen, "Synthesis of no-carrier-added 4-[^{18}F]fluorophenol from 4-benzyloxyphenyl-(2-thienyl)iodonium bromide," *Molecules*, vol. 16, no. 9, pp. 7621–7626, 2011.

[150] A. Helfer, J. Castillo Meleán, J. Ermert et al., "Bis(4-benzyloxyphenyl)iodonium salts as effective precursors for the no-carrier-added radiosynthesis of 4-[^{18}F]fluorophenol," *Applied Radiation and Isotopes*, vol. 82, pp. 264–267, 2013.

[151] J. Way, V. Bouvet, and F. Wuest, "Synthesis of 4-[^{18}F]fluorohalobenzenes and Palladium-mediated Cross-coupling Reactions for the Synthesis of F-18-labeled Radiotracers," *Current Organic Chemistry*, vol. 17, pp. 2138–2152, 2013.

[152] J. Ermert, T. Ludwig, R. Gail, and H. H. Coenen, "[^{18}F]Fluorophenyl organometallics as intermediates of no-carrier-added ^{18}F-fluoroarylation reactions," *Journal of Organometallic Chemistry*, vol. 692, no. 19, pp. 4084–4092, 2007.

[153] Z. Gao, V. Gouverneur, and B. G. Davis, "Enhanced aqueous Suzuki-Miyaura coupling allows site-specific polypeptide ^{18}F-labeling," *Journal of the American Chemical Society*, vol. 135, pp. 13612–13615, 2013.

[154] J. Ermert, C. Hocke, T. Ludwig, R. Gail, and H. H. Coenen, "Comparison of pathways to the versatile synthon of no-carrier-added 1-bromo-4-[^{18}F]fluorobenzene," *Journal of Labelled Compounds and Radiopharmaceuticals*, vol. 47, no. 7, pp. 429–441, 2004.

[155] F. R. Wüst and T. Kniess, "Synthesis of 4-[^{18}F]fluoroiodobenzene and its application in Sonogashira cross-coupling reactions," *Journal of Labelled Compounds and Radiopharmaceuticals*, vol. 46, no. 8, pp. 699–713, 2003.

[156] J. Cardinale, J. Ermert, and H. H. Coenen, "Convenient preparation of (4-iodophenyl)aryliodonium salts," *Tetrahedron*, vol. 68, no. 22, pp. 4112–4116, 2012.

[157] J. Cardinale and J. Ermert, "Simplified synthesis of aryliodonium ylides by a one-pot procedure," *Tetrahedron Letters*, vol. 54, no. 16, pp. 2067–2069, 2013.

[158] F. Kügler, J. Cardinale, P. Kaufholz et al., "Efficient radiosyntheses of ^{18}F-fluorinated aromatic amines using innovative iodonium precursors," *Journal of Nuclear Medicine, Meeting Abstract*, vol. 53, abstract 185, 2012.

[159] J. D. Way and F. Wuest, "Automated radiosynthesis of no-carrier-added 4-[^{18}F]fluoroiodobenzene: a versatile building block in ^{18}F radiochemistry," *Journal of Labelled Compounds and Radiopharmaceuticals*, vol. 57, pp. 104–109, 2014.

Hindawi Publishing Corporation
BioMed Research International
Volume 2014, Article ID 871609, 17 pages
http://dx.doi.org/10.1155/2014/871609

Review Article

PET Radiopharmaceuticals for Imaging Integrin Expression: Tracers in Clinical Studies and Recent Developments

Roland Haubner,[1] Simone Maschauer,[2] and Olaf Prante[2]

[1] *Department of Nuclear Medicine, Innsbruck Medical University, Anichstraße 35, 6020 Innsbruck, Austria*
[2] *Molecular Imaging and Radiochemistry, Department of Nuclear Medicine, Friedrich-Alexander University, Schwabachanlage 6, 91054 Erlangen, Germany*

Correspondence should be addressed to Roland Haubner; roland.haubner@i-med.ac.at

Received 25 March 2014; Accepted 29 April 2014; Published 11 June 2014

Academic Editor: Patrick Riss

Noninvasive determination of integrin expression has become an interesting approach in nuclear medicine. Since the discovery of the first ^{18}F-labeled cyclic RGD peptide as radiotracer for imaging integrin $\alpha_v\beta_3$ expression in vivo, there have been carried out enormous efforts to develop RGD peptides for PET imaging. Moreover, in recent years, additional integrins, including $\alpha_5\beta_1$ and $\alpha_v\beta_6$, came into the focus of pharmaceutical radiochemistry. This review will discuss the tracers already evaluated in clinical trials and summarize the preliminary outcome. It will also give an overview on recent developments to further optimize the first-generation compounds such as [^{18}F]Galacto-RGD. This includes recently developed ^{18}F-labeling strategies and also new approaches in ^{68}Ga-complex chemistry. Furthermore, the approaches to develop radiopharmaceuticals targeting integrin $\alpha_5\beta_1$ and $\alpha_v\beta_6$ will be summarized and discussed.

1. Introduction

Integrins are heterodimeric glycoproteins consisting of an α- and β-subunit. There are 24 different combinations of the eight β-units and the eighteen α-units known. The integrins mediate cell-cell and cell-matrix interactions and transduce signals across the plasma membrane via insight-out and outside-in signaling [1]. Some of the integrins play an important role during migration of endothelial as well as tumor cells during tumor-induced angiogenesis and tumor metastasis. Angiogenesis, the formation of new blood vessels out of the preexisting vasculature, is a critical step in the development and dissemination of many human tumors. A variety of therapeutic strategies in oncology are focused on the inhibition of tumor-induced angiogenesis [2–4]. This includes approaches to inhibit VEGF, MMP, or integrin interactions. Concerning the integrins, most attention has been paid to the role of integrin $\alpha_v\beta_3$ and $\alpha_v\beta_5$ as they are prominent on proliferating vascular endothelial cells [5].

Thus, one of the most prominent target structures used for the development of radiopharmaceuticals for imaging angiogenesis is the integrin $\alpha_v\beta_3$ [6]. It has been shown that this integrin is involved in endothelial cell/matrix interaction during tumor-induced formation of new vessels as well as in mediation of tumor cell migration during invasion and extravasation [7]. A series of studies using a variety of different radiopharmaceuticals have already demonstrated that noninvasive determination of $\alpha_v\beta_3$ expression is feasible (for review, see [6, 8]).

In contrast to the data found in a variety of inhibition studies, which suggest a critical role for $\alpha_v\beta_3$ in angiogenesis, genetic studies indicate that the integrin $\alpha_v\beta_3$ is not required for angiogenesis [5]. An explanation for this discrepancy could be findings that animals lacking $\alpha_v\beta_3$ develop compensatory changes in VEGF signaling, which permit angiogenesis to occur during embryogenesis [9]. Anyway, genetic ablation of the integrin $\alpha_5\beta_1$, the major fibronectin-binding integrin, leads to severe vascular abnormalities [10] indicating that this integrin may play an even more important role as the integrin $\alpha_v\beta_3$ in neovascularization. Additionally, this integrin is upregulated in tumor blood vessels and plays a role in tumor angiogenesis and tumor growth [11, 12].

Thus, recently this integrin became another target structure in the development of radiopharmaceuticals for imaging angiogenesis.

A third class of tracer developed for the noninvasive determination of integrin expression focus on the integrin $\alpha_v\beta_6$. This integrin is unique in that it is exclusively expressed on epithelial cells [13]. It is highly upregulated during development of lung, skin, and kidney epithelia but its expression is low in healthy adult epithelia [14]. Elevated expression in adults is found only during wound healing [15]. It is found to regulate epithelial remodeling during development and tissue repair. Thus, it became an interesting target in tracer development because integrin $\alpha_v\beta_6$ is also found to be highly expressed on a variety of tumors including carcinoma of the breast, lung, colon, stomach, and oral and skin squamous cell carcinoma [13] and is associated with a more aggressive disease outcome [16].

There are already a variety of reviews dealing with the development of tracer targeting the integrins $\alpha_v\beta_3/\alpha_v\beta_5$ [6, 8, 25–27]. On the one hand, this review will focus on compounds which are already in clinical studies and, on the other hand, highlight most recent aspects of the preclinical development of tracer targeting these integrins. Moreover, it will summarize the developments concerning radiopharmaceuticals targeting the integrins, $\alpha_5\beta_1$ and $\alpha_v\beta_6$, which came most recently in the focus for PET tracer development (Table 1).

2. Tracer Targeting Integrin $\alpha_v\beta_3/\alpha_v\beta_5$

2.1. Tracers Already in Clinical Studies

2.1.1. [^{18}F]Galacto-RGD. The first target structure used for the development of radiopharmaceuticals was the integrin $\alpha_v\beta_3$ [46]. Among the great variety of compounds introduced meanwhile, only a small set entered clinical studies. The first compound studied in patients was [^{18}F]Galacto-RGD. This compound was developed based on an optimization strategy introducing sugar moieties to improve the pharmacokinetics [28, 47]. Initial clinical studies showed that the tracer was well tolerated with no severe side effects [48–50]. The effective dose calculated from an i.v. injection of [^{18}F]Galacto-RGD was found to be approximately 0.02 mSv/MBq [50], being in the range of a routine [^{18}F]FDG-PET scan [51]. The tracer was rapidly cleared predominately via kidneys, resulting in good tumor/background ratios. The highest background uptake was found in kidneys, liver, spleen, and intestine. Tumor uptake showed high variability and standard uptake values (SUV) ranged from 1.2 to 10. An additional study including 19 patients compared [^{18}F]Galacto-RGD uptake in the lesions with immunohistochemical staining after tumor resection using angiogenesis markers (Figure 1) [17, 49].

A good correlation between tracer uptake and $\alpha_v\beta_3$ expression as well as microvessel density was found. In further investigations, the detection rate of a variety of different malignant lesions was studied including sarcoma, melanoma, renal cell cancer, squamous cell carcinoma of the head and neck, breast cancer, and glioblastoma multiforme [52–54]. In general, detection of the primary tumor was high (80%–100%) with a lower detection rate for lymph nodes and distant metastases. It has to be mentioned that the different studies also revealed that chronic inflammatory lesions like villonodular synovitis can also show significant uptake of [^{18}F]Galacto-RGD [17], raising the same problem as with [^{18}F]FDG that the tracer does not clearly differentiate between benign and malignant lesions. All the clinical as well as the preclinical data (which are not discussed here) have demonstrated that specific imaging of integrin $\alpha_v\beta_3$ expression is feasible using [^{18}F]Galacto-RGD and PET; however, it has to be kept in mind that this receptor is not only expressed on endothelial cells during neovascularization but can also be present on the tumor cells themselves. Static PET imaging cannot distinguish the origin of the signal; thus, solely assessing angiogenesis is only possible if the tumor cells do not express the receptor.

Integrin $\alpha_v\beta_3$ is also expressed by macrophages and angiogenic endothelial cells in atherosclerotic lesions [55, 56]. Based on this, Beer et al. studied the potential of [^{18}F]Galacto-RGD as a probe for imaging plaque inflammation and plaque vulnerability [57]. The pilot study including 10 patients with high-grade carotid artery stenosis scheduled for carotid endarterectomy revealed specific tracer accumulation in atherosclerotic carotid plagues and correlation of the tracer uptake with $\alpha_v\beta_3$ expression analyzed by immunohistochemical staining of the surgical specimen. Based on the promising initial results it was concluded that larger prospective studies have to be carried out to fully evaluate the potential of molecular imaging of integrin $\alpha_v\beta_3$ expression for the assessment of plaque inflammation in patients.

2.1.2. [^{18}F]Fluciclatide. Another integrin $\alpha_v\beta_3/\alpha_v\beta_5$ targeting PET radiopharmaceutical, which has already been studied in patients, is [^{18}F]Fluciclatide. Similar to [^{18}F]Galacto-RGD, this peptide derivative includes the RGD sequence as binding motif, but in contrast to the backbone cyclization found in [^{18}F]Galacto-RGD this compound is cyclized via a thioether and a disulfide bridge. As a pharmacokinetic modifier, polyethylene glycol (PEG), instead of the sugar moiety and for radiolabeling an aminooxy function, was introduced. The labeling with ^{18}F was carried out using 4-[^{18}F]fluorobenzaldehyde. This approach using the chemoselective oxime formation for labeling clearly reduced the synthesis time of this radiotracer compared to [^{18}F]Galacto-RGD and made the clinical routine production more feasible. In contrast to Galacto-RGD, which belongs to the family of tracer based on the cyclic pentapeptide c(RGDfV), Fluciclatide shows higher binding affinity for integrin $\alpha_v\beta_5$ than for integrin $\alpha_v\beta_3$ [18].

In a study including 7 breast cancer patients it could be shown that all lesions found by CT could also be detected by [^{18}F]Fluciclatide PET (Figure 2). In analogy to [^{18}F]Galacto-RGD, a great variance in tracer uptake in the lesions was found with SUVs ranging from 2.0 to 40.0 [18]. Interestingly, metastases in the liver have been identified as regions of deficit uptake, because of the high background activity in

Table 1: Summary of the most important RGD peptide tracers discussed.

Compound name	Used peptide sequence	"Labeling species"	Total prod. time	Labeling yield/spec act	Reference
$\alpha_v\beta_3/\alpha_v\beta_5$ targeting					
[^{18}F]Galacto-RGD	**c(RGDfK)** Lysine-NH_2 SAA[1] modified	**nitrophenyl-2-[^{18}F]fluoropropionate** via amide formation	200 min	29 ± 5% (dc[7]) 40–100 GBq/μmol	[28]
[^{18}F]Fluciclatide	**-^{*1}CH$_2$-CO-KC^{*2}RGDC^{*2}FC^{*1}-** ^{*1}Thioether bridge ^{*2}Disulfide bridge C-terminal PEG modified Lysine-NH_2 PEGylated and aminooxy derivatized	**p-[^{18}F] fluorobenzaldehyde** via oxime formation	75 min	40 ± 12% (dc) 173 ± 52 GBq/μmol	[29]
[^{18}F]RGD-K5	**c(RGDfK)** Lysine-NH_2 SAA modified SAA N_3-functionalyzed	**5-[^{18}F]fluoro-1-pentyne** via "click chemistry"	75 min	35% (dc) 100–200 GBq/μmol	[30]
[^{18}F]FPTA-RGD2	**Dimeric c(RGDyK)** Lysine-NH_2 used for dimerization Bridged via glutamic acid Derivatized with 5-azidopentanoic acid	**[^{18}F]fluoro-PEG3-alkyne** via "click chemistry"	110 min	54% (dc) 100–200 GBq/μmol	[31]
[^{18}F]Mlt-RGD	**c(RGDfPra)**[4]	**6′-deoxy-6′-[^{18}F]fluoro-β-maltosyl azide** via "click chemistry"	75 min	24% (ndc) 50–200 GBq/μmol	[32]
c(fK([^{18}F]SiFA-AO-N) RGD)	**c(RGDfK)** Lysine-NH_2 aminooxy acetic acid derivatized	**p-(di-tert-butyl-[^{18}F]fluorosilyl)-benzaldehyde**[5] via oxime formation	40 min	50–55% (ns[8]) 225–680 GBq/μmol	[33]
RGD-[^{18}F]ArBF$_3^-$	**c(RGDfK)** Lysine-NH_2 1-succinyl-4-(2-Trifluoroboryl-1,3,5-trifluorobenzoyl)-piperazine derivatized	**[^{18}F]fluoride** isotopic exchange	35 min	65% (dc) 518 GBq/μmol	[21]
[^{18}F]Alfatide	**Dimeric c(RGDyK)** Lysine-NH_2 used for dimerisation Bridged via glutamic acid PEG linker and NOTA for complexation	**[^{18}F]aluminum fluoride species** via complexation	20 min	42% (dc) 37 GBq/μmol	[19]
[^{68}Ga]NOTA-RGD	**c(RGDyK)** Lysine-NH_2 SCN-Bz-NOTA conjugated	**^{68}Ga** via complexation	10 min[2]	89% (ns) 18 GBq/μmol	[34]
[^{68}Ga]DOTA-RGD	**c(RGDfK)** Lysine-NH_2 DOTA conjugated	**^{68}Ga** via complexation	7 min[2]	>95% (ns) —	[35]
[^{68}Ga]NODAGA-RGD	**c(RGDfK)** Lysine-NH_2 NODAGA conjugated	**^{68}Ga** via complexation	5 min[2]	>96% (ns) 10–20 GBq/μmol	[36]
[^{68}Ga]TRAP(RGD)$_3$	**Trimeric c(RGDfK)** Lysine-NH_2 TRAP conjugated Chelator PEG modified Monomers linked via chelator	**^{68}Ga** via complexation	5 min[2]	— 0.8–1 TBq/μmol	[20]

Table 1: Continued.

Compound name	Used peptide sequence	"Labeling species"	Total prod. time	Labeling yield/spec act	Reference
[^{68}Ga]NOPO-RGD	**c(RGDfK)** Lysine-NH_2 NOPO conjugated	**^{68}Ga** via complexation	15 min	94% (dc) 1.4 TBq/μmol	[37]
[^{68}Ga-(RGD-1)]$^+$	**c(RGDyK)** Lysine-NH_2 H_2dedpa conjugated	**^{68}Ga** via complexation	10 min[2]	97% (ns) 34 GBq/μmol	[38]
[^{68}Ga-(RGD-2)]$^+$	**Dimeric c(RGDyK)** Lysine-NH_2 H_2dedpa conjugated monomers linked via chelator	**^{68}Ga** via complexation	10 min[2]	99% (ns) 25 GBq/μmol	[38]
$\alpha_5\beta_1$ targeting					
[^{68}Ga]$\alpha_5\beta_1$-ANT	**Nonpeptide RGD mimetic** Conjugated via linker with NODAGA	**^{68}Ga** via complexation	—	—	[22]
[^{18}F]FProp-CRRETAWAC-OH	**H-*CRRETAWAC*-OH** *Disulfide bridge	**nitrophenyl-2-[^{18}F]fluoropropionate** via amide formation	200 min	—	[39]
$\alpha_v\beta_6$ targeting					
[^{18}F]FBA-A20FMDV2	**NAVPNLRGDLQVLAQKVART** (derived from foot-and-mouth disease virus)	**solid-phase p-[^{18}F]fluorobenzoyl labeling** via amide formation	130 min	3.6% (dc) 37 GBq/μmol	[23]
[^{18}F]FBA-$(PEG_{28})_2$-A20FMDV2	**NAVPNLRGDLQVLAQKVART** PEG linker	**solid-phase p-[^{18}F]fluorobenzoyl labeling** via amide formation	—	—	[40]
[^{18}F]FBA-C_6-ADIBON$_3$-PEG$_7$-A20FMDV2	**NAVPNLRGDLQVLAQKVART** N-terminal azido-PEG derivatized	**[^{18}F]FBA-C_6-ABIO** (^{18}F-labelled cyclooctyne derivative) Cu-free strain-promoted "click chemistry"	45 min	12% (dc) 70 GBq/μmol	[41]
[^{111}In]DTPA-A20FMDV2	**NK(biotinyl)VPNLRGDLQVLAQKVART** N-terminal DTPA conjugated 2nd amino acid replaced by biotinyl-lysine	**^{111}In** via complexation	—	—	[42]
[^{64}Cu]CB-TE1A1P-PEG$_{28}$-A20FMDV2	**NAVPNLRGDLQVLAQKVART** N-terminal tetraazabicyclo[6.6.2.]hexadecane derivative conjugated	**^{64}Cu** via complexation	15 min[2]	>98% (ns) 22 GBq/μmol	[43]
[^{64}Cu]DOTA-$S_0$2	**RSLARTDLDHLRGR** (sequence engrafted into loop 1 of a acyclized cystine knot scaffold) Loop 2 serine-rich N-terminal DOTA conjugation	**^{64}Cu** via complexation	—	80% (ns) 18.5 GBq/μmol	[44]

Table 1: Continued.

Compound name	Used peptide sequence	"Labeling species"	Total prod. time	Labeling yield/spec act	Reference
^{18}F-fluorobenzoate-$R_0$1	**ILNMRTDLGTLLFR** (sequence engrafted into loop 1 of a acyclized cystine knot scaffold) Loop 2 arginine-rich	**succinimidyl-p-[^{18}F]fluorobenzoate** via amide formation at N-terminus	45 min[2]	7% (dc) —	[24]
[^{99m}Tc]SAAC-$S_0$2	**RSLARTDLDHLRGR** (sequence engrafted into loop 1 of a acyclized cystine knot scaffold) Loop 2 serine-rich N-terminal SAAC[6] modified	**[^{99m}Tc$(H_2O)_3(CO)_3]^-$** Tc-tricarbonyl method	60 min[2]	40% (ns) 15 GBq/μmol	[45]

[1]SAA: galactose based sugar amino acid.
[2]Synthesis time only (overall production time depends on several parameters, e.g., type of automated system, labeling technique, and postprocessing).
[3]TRAP: 1,4,7-triazacyclononane-1,4,7-tris(2-carboxyethyl)methylenephosphinic acid.
[4]Pra: propargyl glycine.
[5]Precursor is produced via isotopic exchange.
[6]SAAC: single amino acid chelate.
[7]dc: decay corrected.
[8]ns: not specified.

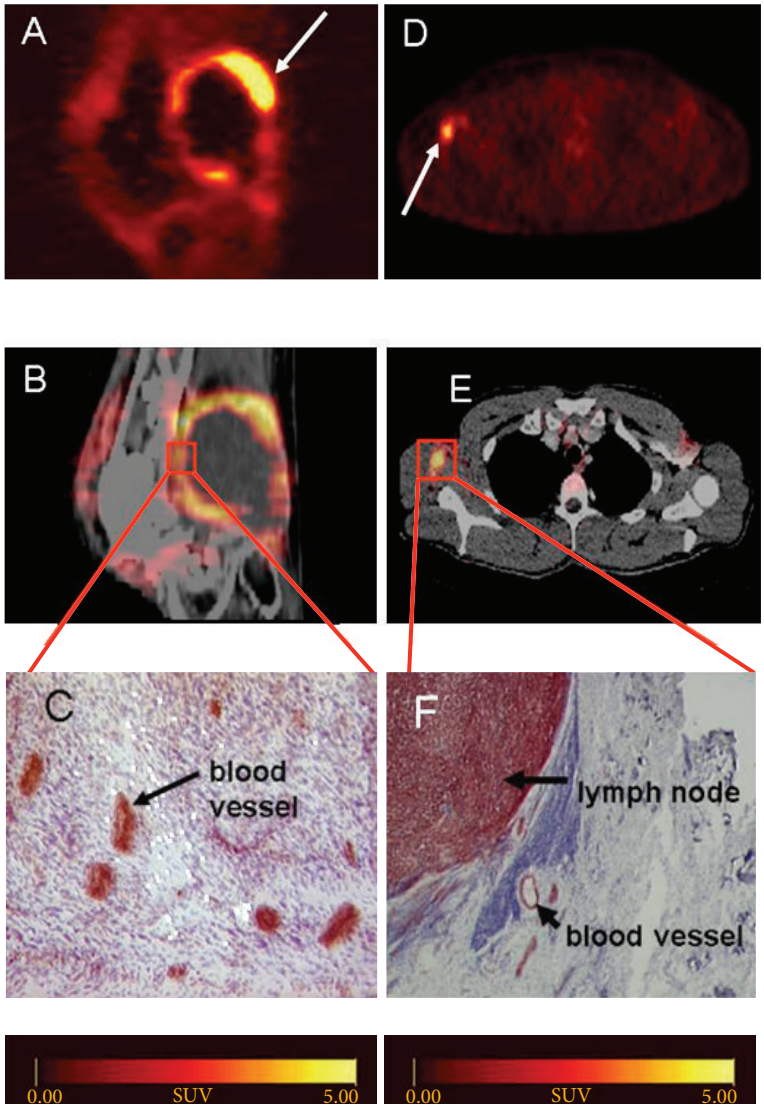

Figure 1: [^{18}F]Galacto-RGD PET: (A–C) patient with a soft tissue sarcoma dorsal of the right knee joint. (A) Sagittal section acquired 170 min p.i. (B) PET/CT image fusion. (C) Immunohistochemistry of a peripheral tumor section using the anti-$\alpha_v\beta_3$ monoclonal antibody LM609 demonstrates intense staining predominantly of tumor vasculature. (D–F) Patient with malignant melanoma and a lymph node metastasis in the right axilla. (D) Axial section acquired 140 min p.i. (E) PET/Ct image fusion. (F) Immunohistochemistry of the lymph node demonstrates intense staining predominantly of tumor cells and also blood vessels (with permission from Haubner et al. [17]).

normal liver tissue. Stability studies in vivo showed 74% intact tracer after 60 min in blood. Biodistribution and dosimetry studies in 8 healthy volunteers showed predominately renal excretion with the highest uptake in liver, combined walls of the intestine, and kidneys [58]. The compound was well tolerated with no drug-related adverse events reported. The mean effective dose was 0.026 mSv/MBq comparable to [^{18}F]Galacto-RGD. An advantage of [^{18}F]Fluciclatide compared with [^{18}F]Galacto-RGD is the easier availability. However, further clinical studies are needed to demonstrate the potential of this compound for imaging integrin $\alpha_v\beta_3/\alpha_v\beta_5$ expression. Anyway, preclinical studies in mice already showed that monitoring of tumor response to an antiangiogenic sunitinib therapy using [^{18}F]Fluciclatide-PET is feasible [59].

2.1.3. [^{18}F]RGD-K5. RGD-K5 is a closely related derivative to Galacto-RGD. The used cyclic pentapeptide c(RGDfK) and the sugar amino acid are identical for both compounds. The difference is found in the conjugation of 2-azidoacetic acid to the amino function of the sugar amino acid of RGD-K5 allowing labeling via "click chemistry" using 5-[^{18}F]fluoro-1-pentyne. Similar to the labeling strategy using oxime formation for labeling, the click chemistry approach also reduced the overall synthesis time compared with [^{18}F]Galacto-RGD, thereby increasing the availability of [^{18}F]RGD-K5 [30].

Initial preclinical studies showed high affinity for integrin $\alpha_v\beta_3$ and predominantly renal elimination and high plasma stability in mice [60, 61]. This was confirmed by biodistribution and radiation dosimetry studies in monkeys

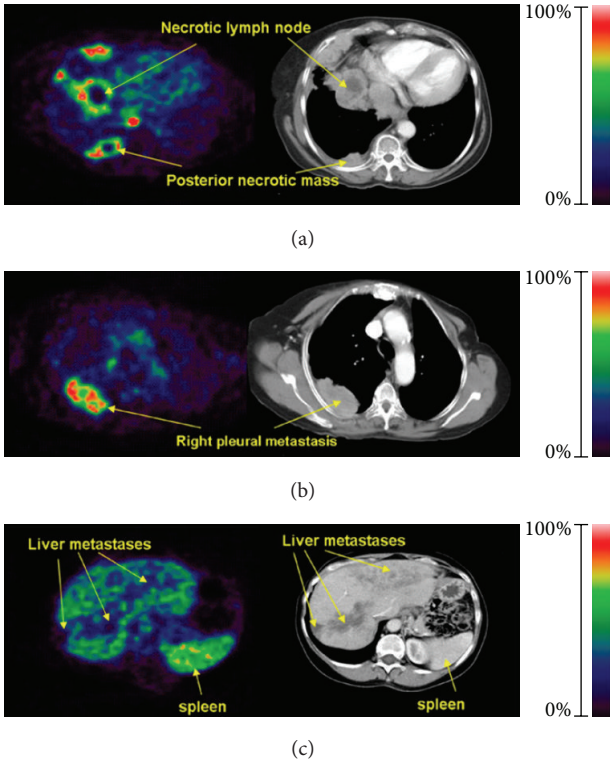

Figure 2: [^{18}F]Fluciclatide PET: (a) patient with lung and pleural metastases. (b) Intralesion heterogeneity of uptake within pleural metastasis in PET image, which was not demonstrated as necrosis on corresponding CT section. (c) Liver metastases imaged as hypointense lesions because of high background signal (high uptake in spleen is possibly due to blood pooling) (with permission from Kenny et al. [18]).

and four healthy volunteers [62]. Organs with the highest activity concentration were bladder, kidneys, gallbladder, and liver. It was found that the plasma clearance half-life was approximately 12 min and that approximately 44% of the injected activity had been excreted in the urine by end of the study (~2.5 h). No clinical significant effects on vital signs had been found during the follow-up until 24 h after tracer injection. Depending on the bladder-voiding model the mean effective dose calculated was between 0.015 and 0.031 mSv/MBq and thus in the range of the other RGD tracers already in clinical studies. In an initial study with 12 breast cancer patients, [^{18}F]RGD-K5 PET was compared with [^{18}F]FDG-PET [63]. Out of 157 lesions detected using [^{18}F]FDG, 122 lesions could be visualized by [^{18}F]RGD-K5. In most lesions, [^{18}F]FDG uptake was higher as found for [^{18}F]RGD-K5 with no correlation between the uptake of the two compounds, confirming the results already found with other RGD tracers.

2.1.4. [^{68}Ga]NOTA-RGD. [^{68}Ga]NOTA-RGD is the first ^{68}Ga-labeled $\alpha_v\beta_3$ integrin-targeting compound for which initial clinical data are available. Due to the increasing availability of corresponding ^{68}Ge/^{68}Ga generators, this PET isotope becomes an interesting alternative to ^{18}F especially for radiolabeling of peptides (see also below). NOTA-RGD is produced by conjugating SCN-Bz-NOTA to the amino function of the lysine in the cyclic pentapeptide c(RGDyK) [34]. The chelator forms very stable complexes with ^{68}Ga, allowing labeling in short reaction times even at room temperature. The compound showed high affinity for the integrin $\alpha_v\beta_3$ in in vivo binding assays and rapid predominantly renal excretion with good tumor-to-background ratios in murine tumor models [34].

A biodistribution and radiation dosimetry study with 10 patients with lung cancer or lymphoma confirmed the excretion route with the highest activity found in kidneys and urinary bladder [64]. Comparably high radioactivity was also found in the liver. The effective dose was between 0.021 and 0.025 mSv/MBq depending on the calculation model and the voiding interval. Although tumor patients were included in this study, no information concerning tumor uptake was found. Anyway, in a preliminary study with six patients with liver metastases of a colorectal carcinoma in three out of the six patients increased [^{68}Ga]NOTA-RGD uptake in the liver lesions could be detected [65]. Moreover, the patients who showed [^{68}Ga]NOTA-RGD uptake revealed partial response after an antiangiogenic therapy with FOLFOX and bevacizumab, whereas the other half showed stable or progressive disease.

2.1.5. [^{18}F]Alfatide. Attempts optimizing the strategies in labeling peptides with ^{18}F led to the introduction of ^{18}F-aluminum fluoride [66]. This compound behaves similarly to radiometals concerning formation of complexes with, for example, NOTA derivatives introducing the advantage of using much faster and easier labeling protocols than those needed for ^{18}F-labeling using prosthetic group strategies. The first compound of this class of tracer studied in patients is the ^{18}F-labeled dimeric RGD-peptide [^{18}F]AlF-NOTA-PRGD2 ([^{18}F]Alfatide) [67]. It includes, besides the two cyclic RGD peptides c(RGDyK) bridged via a lysine, a PEG moiety as pharmacokinetic modifier and a Bz-NOTA moiety for complexation of "[^{18}F]AlF." In a pilot study including nine patients with lung cancer, [^{18}F]Alfatide allowed identification of all tumors with SUVs of 2.9 ± 0.1 indicating a lower variance in tumor uptake as found by most other studies using RGD-derivatives in patients [19]. Major uptake was found in kidneys and bladder indicating renal excretion. Liver, spleen, and intestine showed comparable uptake as found in the tumor (Figure 3). Kinetic modeling based on dynamic PET scans suggested specific binding of the tracer. Moreover, immunohistochemical staining confirmed $\alpha_v\beta_3$ expression on both the tumor cells and the neovasculature of the squamous carcinoma patients.

2.2. Recent Tracer Developments for Imaging Integrin $\alpha_v\beta_3$/$\alpha_v\beta_5$ Expression. Since the first radiotracer for imaging integrin $\alpha_v\beta_3$ has been introduced in 1999 [46], a great variety of different derivatives have been described and a selection of optimization strategies have been introduced including optimization of the pharmacokinetics (e.g., glycosylation

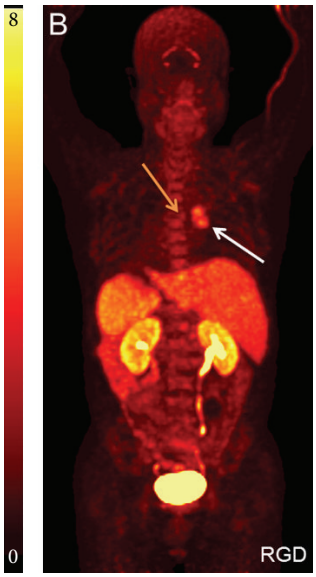

Figure 3: [^{18}F]Alfatide PET: maximum intensity projection imaging of a patient with primary squamous carcinoma (white arrow) and lymph node metastasis (yellow arrow) (with permission from Wan et al. [19]).

and PEGylation), the binding affinity (multimerization), and the labeling strategies. There are already a range of reviews dealing with the different aspects (e.g., [6, 8]). Here, we focus on the most recent approaches in introducing new or optimized labeling strategies.

2.2.1. ^{68}Ga-Labeled Derivatives. Preclinical as well as clinical data demonstrated successful noninvasive determination of integrin $\alpha_v\beta_3$ expression with [^{18}F]Galacto-RGD PET (see [17, 49, 50, 52] and above). The major drawback of this compound is the complex and time consuming labeling strategy using [^{18}F]fluoropropionic acid as prosthetic group. One strategy to overcome this problem is based on the introduction of ^{68}Ga. Due to the increasing amount of commercially available ^{68}Ga/^{68}Ge generators [68], this isotope becomes an interesting alternative to ^{18}F, especially when peptide labeling is considered. Direct labeling of peptides modified with the corresponding chelator systems with ^{68}Ga avoids the time consuming preparation of prosthetic groups usually needed for labeling peptides with ^{18}F.

First approaches to introduce ^{68}Ga-labeled RGD peptides are focused on the use of DOTA-conjugated RGD peptides. [^{68}Ga]DOTA-RGD showed high affinity for the integrin $\alpha_v\beta_3$ in in vitro binding studies and receptor selective tracer accumulation in a murine tumor model [35]. However, high protein bound activity was also found compared to the ^{111}In-labeled analog. The high plasma protein binding leads to increased activity concentration in blood and to inferior imaging properties compared with [^{18}F]Galacto-RGD. Although DOTA is successfully used in DOTA-TOC and derivatives for binding of ^{68}Ga, it is known that the cyclododecane ring of DOTA does not have the optimal size for complexing gallium [69]. A more favorable chelating system is the NOTA system, which contains a nine-membered ring more suitable for binding ^{68}Ga. This system was initially introduced with NOTA-RGD [34] and NODAGA-RGD [36, 70]. The later showed significantly reduced binding to plasma proteins compared to [^{68}Ga]DOTA-RGD resulting in equal imaging properties in a murine tumor model as found for [^{18}F]Galacto-RGD. Moreover, due to the high complex binding constant labeling of NODAGA-RGD can be carried out at room temperature with low amounts of peptide in high radiochemical yield and purity. Based on these positive results initial clinical studies are most recently started.

The last few years, alternative chelating systems have been introduced for ^{68}Ga-labeling of RGD peptides. This include RGD peptides conjugated to H_2dedpa derivatives [38] and TRAP(RGD)$_3$ [20]. Based on the H_2dedpa scaffold a monomeric and a dimeric tracer have been introduced (H_2-RGD-1 and H_2-RGD-2). Both compounds showed rapid ^{68}Ga-labeling at room temperature in high radiochemical yield. The complexes were stable if challenged with transferrin and showed IC_{50} values determined using a competitive cell binding assay of approximately 2.4 μM for the monomeric H_2-RGD-1 and approximately 0.2 μM for the dimeric H_2-RGD-2. Anyway, in biodistribution as well as small animal PET studies high activity concentration was found in blood even 2 hours after injection making these compounds uncompetitive with the already introduced ^{68}Ga-labeled derivatives. Although no log P values are described, it is assumed that the aromatic components of the chelating systems increase the lipophilicity which might be the reason for this finding.

The TRAP chelator uses the similar nine-membered ring system as found in NOTA but possesses phosphinic acid groups instead of the carboxylic acid groups. This modification results in two advantages: (a) due to the high binding affinity of the chelator for gallium it allows labeling with very low amounts of TRAP-modified peptides and (b) due to the additional functionality of the phosphinic acid it allows direct conjugation of up to three targeting peptides per chelating system, making it an advantage system for introducing the multimerization approach. Based on these results, the trimeric TRAP(RGD)$_3$ was introduced [20]. This compound demonstrated rapid labeling using low peptide amounts, resulting in specific activities of up to 1 TBq/μmol, very high binding affinity for the integrin $\alpha_v\beta_3$ in a competitive cell binding assay, and good tumor/background ratios in a murine tumor model. Anyway, direct comparison of the biodistribution data in the murine M21/M21-L tumor model with [^{68}Ga]NODAGA-RGD 90 min after injection showed comparable values for both compounds indicating that, despite better performance in vitro, the in vivo effect is negligible (Figure 4). Most recently, [^{68}Ga]NOPO-RGD was introduced [37]. This chelator belongs to the "TRAP family" with the known advantages of fast complexation kinetics, high stability, and extremely high resulting specific activity. Major difference is found in the fact that only one phosphinic acid group is functionalized for conjugation to peptides. Thus, multimeric compounds cannot be produced. But the

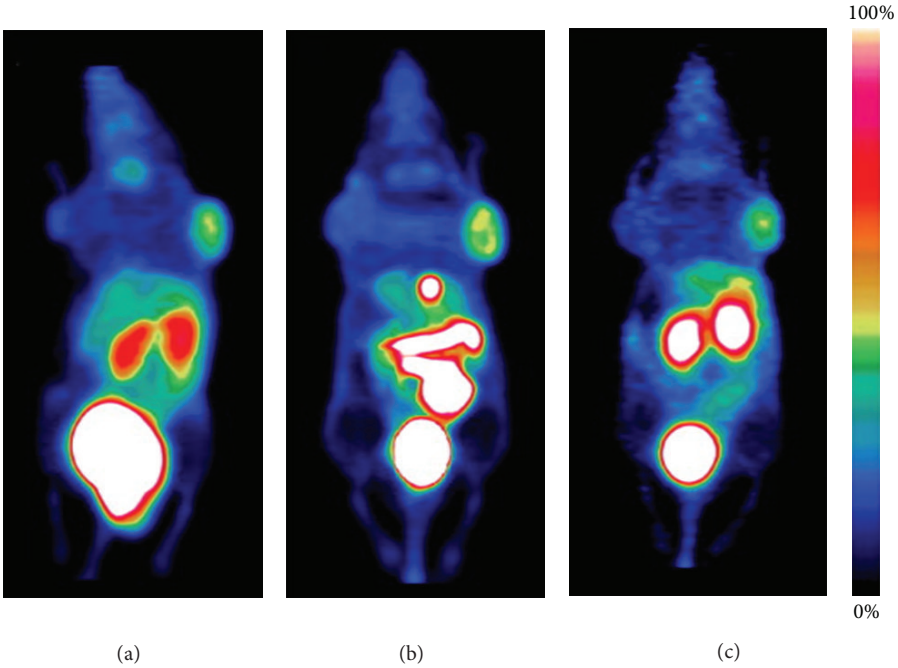

Figure 4: [^{68}Ga]TRAP(RGD)$_3$: comparison of maximum intensity projections of microPET scans of the same M21/M21L human melanoma xenografted mouse (a) [^{68}Ga]TRAP(RGD)$_3$, (b) [^{18}F]Galacto-RGD, (c) [^{68}Ga]NODAGA-RGD (scaling adapted to show equal intensities in M21 tumors and background. Scale indicates percentage of the maximum displayed signal level) (with permission from Notni et al. [20]).

additional hydroxymethyl groups increase the polarity of any conjugated peptide and may improve renal elimination.

2.2.2. RGD Peptides Labeled with ^{18}F via Click Chemistry Approaches. After the Cu(I)-catalyzed azide-alkyne 1,3-cycloaddition (CuAAC) reaction (better known as the most prominent example of "click chemistry") was introduced for radiolabeling with ^{99m}Tc in 2006 [71], this technique was also applied for ^{18}F-labeling of RGD peptides. The apparent advantages of the CuAAC reaction are mainly reflected by their high yield under mild conditions, its chemoselectivity, and the formation of 1,2,3-triazole with similar polarity and size as found in an amide bond [72]. Most importantly, for peptide labeling, there are no interferences with common functionalities found in amino acid side chains. These aspects make click chemistry based approaches an interesting alternative to common prosthetic group techniques for labeling peptides with ^{18}F, as highlighted by the reviews of Kettenbach et al. [73] and Maschauer and Prante [74] within this special issue. In general, there are two possible approaches for the CuAAC reaction: either a ^{18}F-labeled organoazide or a ^{18}F-labeled alkyne is used as prosthetic group.

In a preliminary study, a dimeric RGD peptide was modified with an azide and as prosthetic group a ^{18}F-fluoro-PEG-alkyne derivative was used [31]. The product could be achieved in good radiochemical yield. Anyway, this procedure includes two HPLC separation steps, rendering it unfavorable compared to other prosthetic group labeling techniques. Glaser et al. compared the ^{18}F-labeling of RGD peptides via oxime formation, click labeling, and S-alkylation [29]. The prosthetic groups include [^{18}F]fluorobenzaldehyde, 2-[^{18}F]fluoroethylazide, and [^{18}F]fluoropropanethiol. It was concluded that the click labeling resulted in comparable yields as found for the fluorobenzaldehyde approach without the need for purification of the prosthetic group. However, 2-[^{18}F]fluoroethylazide seems to be too small to be separated from the labeled RGD peptide. For the synthesis of [^{18}F]RGD-K5, [^{18}F]fluoropentyne was used as prosthetic group. With an optimized protocol for radiosynthesis the peptide could be labeled within 70 min with 35% radiochemical yield (EOB) [30]. Due to the good preclinical performance, this compound is already studied in patients (see also above).

Introduction of sugar derivatives as pharmacokinetic modifier has successfully been introduced with [^{18}F]Galacto-RGD [47] and was later also used with [^{18}F]RGD-K5 [30]. Maschauer et al. combined the click labeling approach with the introduction of sugar derivatives allowing labeling as well as pharmacokinetic optimization in one step [32, 75, 76]. Four different sugar azides have been used as prosthetic groups, including glucose, galactose, maltose, and cellobiose derivatives, which were conjugated via propargylglycine to the modified RGD peptide. The overall synthesis time was in the range of 70–75 min with decay-uncorrected radiochemical yields between 16% and 24%. A favorable performance was found for [^{18}F]Mlt-RGD, revealing comparable tumor-to-background ratios as found for [^{18}F]Galacto-RGD with the advantage of a more rapid and simplified radiosynthesis [32].

2.2.3. ^{18}F/^{19}F Isotopic Exchange and ^{18}F-Fluoride Aluminum Complexes for Labeling RGD Peptides. Despite a great variety of studies focused on the optimization of ^{18}F-labeling of

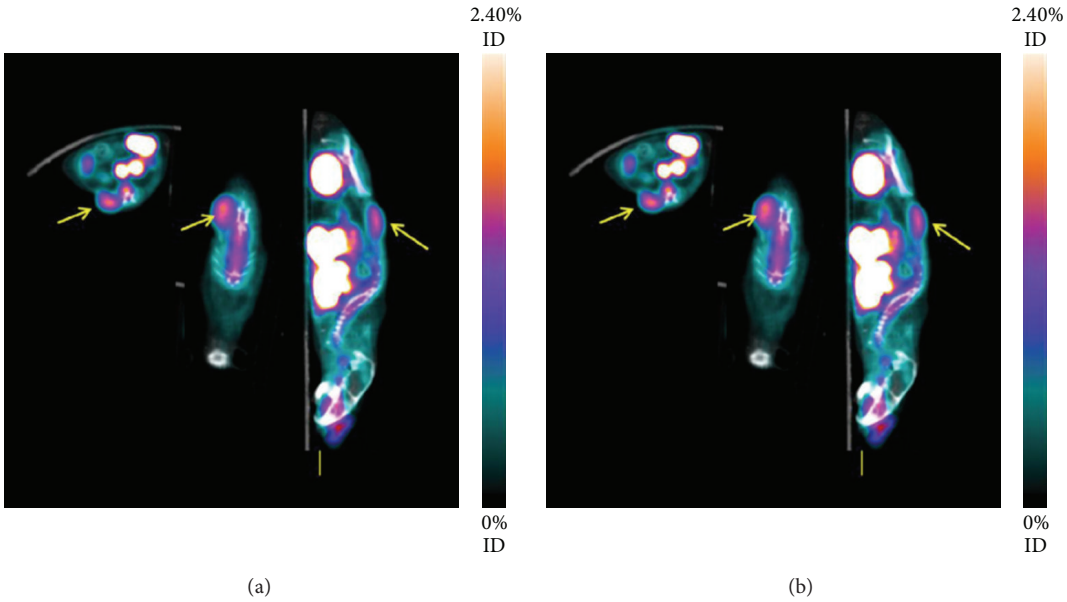

Figure 5: RGD-[^{18}F]ArBF$_3^-$: PET/CT images of (a) an unblocked and (b) a blocked mouse. Arrow marks the tumor in three perspectives (with permission from Liu et al. [21]).

RGD peptides including some approaches with improved labeling conditions compared to [^{18}F]Galacto-RGD, none of the newly introduced prosthetic group approaches can compete with the simple and rapid labeling strategies based on ^{68}Ga. Thus, alternative ^{18}F-labeling approaches have been studied for labeling RGD peptides including isotopic exchange strategies using silicon fluoride acceptors (SiFA) [33] or arylfluoroborates [21] as well as complexation of an ^{18}F-aluminum fluoride species (AlF) [77].

The SiFA method is based on ^{18}F-labeling of p-(di-tert-butylfluorosilyl) benzaldehyde. It has been shown that this labeling precursor allows isotopic exchange in almost quantitative yields, resulting in unexpected high specific activities [33], which are even higher as specific activities found for peptides labeled via conventional n.c.a. ^{18}F-labeling techniques, without HPLC purification. Conjugation of the prosthetic group was carried out via oxime formation using an aminooxy modified cyclic RGD peptide. Altogether, this results in cyclo (fK([^{18}F]SiFA-AO-N)RGD) in high radiochemical yield within approximately one hour. In vitro and in vivo evaluation of the compound still remains to be elucidated to demonstrate the imaging properties of this RGD derivative. However, a highly lipophilic precursor is needed for this labeling technique, which might negatively influence the pharmacokinetics of the radiolabeled peptides. Another strategy using radiolabeling by isotopic exchange is based on boron derivatives. It was shown that kit-like ^{18}F-labeling resulting in an [^{18}F]aryl trifluoroborate-containing RGD peptide is feasible in high specific activity in reaction times below one hour [21]. Initial small animal PET data showed high activity concentration in bladder indicating predominantly renal elimination (Figure 5). However, despite high specific activity tracer accumulation in a murine U87MG glioblastoma model was comparably low; thus, further studies are needed to finally access the quality of this kind of tracer for imaging integrin $\alpha_v\beta_3$ expression.

Recently, a technique to produce the ^{18}F-aluminum fluoride species $(Al^{18}F)^{2+}$ has been introduced [66] and has shown that this compound forms stable complexes with the NOTA ligand conjugated to peptides. After optimization [78], this technique allows labeling of peptides in a one-step synthesis without HPLC purification in analogy to radiometal labeling with, for example, ^{68}Ga or ^{64}Cu. Based on these developments, [^{18}F]Alf-NOTA-RGD$_2$ has been introduced [77]. In this case, labeling including HPLC could be carried out in 40 min. In a cell binding study, the compound showed comparable IC$_{50}$ values as found for the dimeric lead structure and high tumor uptake and rapid elimination from the body in a murine tumor model. Comparison of [^{18}F]AlF-NOTA-PRGD$_2$, which differs in an additional PEG linker from the initial compound, with a dimer labeled with ^{18}F via fluoropropionic acid as prosthetic group and a dimer labeled with ^{68}Ga using small animal PET showed comparable pharmacokinetics and quantitative parameters for all three compounds [79]. Based on this data, the so-called [^{18}F]Alfatide is already studied in initial clinical trials (see also above). Subsequently, the influence on different linker was studied and the labeling protocol was optimized [80]. The replacement of the HPLC separation by C-18 cartridge purification allowed production of the compound with good radiochemical yield and high radiochemical purity within 30 min. The compounds were stable in mouse serum up to 120 min and the highest binding affinity using a cell binding assay as well was found for NOTA-E[PEG$_4$-c(RGDfK)]$_2$. However, in vivo studies using a murine glioblastoma model could not confirm the in vitro findings. The biodistribution

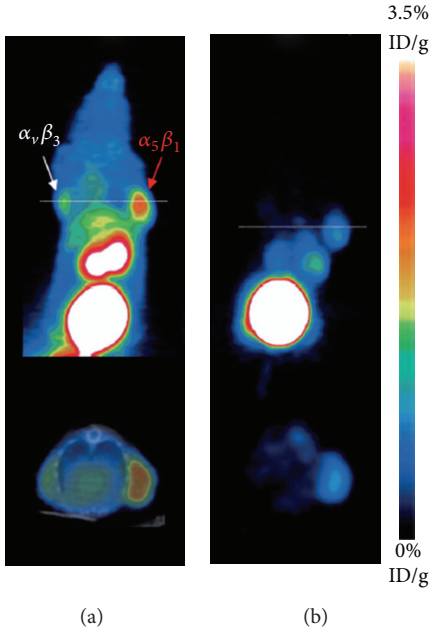

Figure 6: [^{68}Ga]$\alpha_5\beta_1$-ANT: maximum intensity projection images (MIP) of microPET scans. Upper row: mice bearing RKO ($\alpha_5\beta_1$-positive) and M21 ($\alpha_v\beta_3$-positive)tumor xenografts on right and left shoulder, respectively, (white arrow: M21; red arrow: RKO). Lower row: axial slices corresponding to the white line in upper row MIP images. (a) Injection of [^{68}Ga]$\alpha_5\beta_1$-ANT. (b) Blocking experiment (with permission from Neubauer et al. [22]).

data demonstrated comparable tumor uptake for NOTA-E[c(RGDfK)]$_2$ and NOTA-E[PEG$_4$-c(RGDfK)]$_2$ but slightly better tumor-to-background ratios are found for the latter.

3. Tracer Targeting Integrins $\alpha_5\beta_1$ and $\alpha_v\beta_6$

As already mentioned, most work on the development of tracer for imaging integrins is dedicated to the development of compounds targeting the integrins $\alpha_v\beta_3$ and $\alpha_v\beta_5$. Recently, additional integrins came into the focus of interest. These include the integrins $\alpha_5\beta_1$ and $\alpha_v\beta_6$.

3.1. Integrin $\alpha_5\beta_1$. Heckmann et al. [81] developed based on tyrosine and azaglycine scaffolds nonpeptide antagonists of the integrin $\alpha_5\beta_1$. Comprehensive structure activity relationship studies including docking experiments with a homology model resulted in azaglycine derivatives with low nanomolar affinity for $\alpha_5\beta_1$ and up to 10^4-fold higher selectivity when compared with $\alpha_v\beta_3$. The superior properties of the azaglycine derivatives compared with the tyrosine scaffold based compounds may result from enhanced rigidity of the first. Based on this data, one of the most promising azaglycine derivatives was modified by conjugation of NODAGA to the alkoxy benzoic acid moiety of the $\alpha_5\beta_1$ antagonist [22]. A competitive solid phase integrin binding assay demonstrated that this modification had no influence on binding affinity and selectivity to integrin $\alpha_5\beta_1$. A murine tumor model of mice bearing an $\alpha_5\beta_1$-positive human colon carcinoma (RKO) on the one flank and an $\alpha_v\beta_3$-positive human melanoma (M21) on the other flank confirmed receptor specific uptake and allows visualization of the $\alpha_5\beta_1$-positive tumor only (Figure 6).

A common approach to search for biological active peptides is based on phage display libraries. Screening a CX7C library including a random heptapeptide sequence flanked by two cysteine for high affinity integrin $\alpha_5\beta_1$ binder resulted in the peptide H-Cys*-Arg-Arg-Glu-Thr-Ala-Trp-Ala-Cys*-OH (H-C*RRETAWAC*-OH) [82]. This peptide was used as lead structure for the development of a ^{18}F-labeled derivative for noninvasive imaging of integrin $\alpha_5\beta_1$ expression (more detailed information will be found in this special issue under Haubner et al. "*H-CRRETAWAC-OH, a lead structure for the development of radiotracer targeting integrin* $\alpha_5\beta_1$*?*" [39]). Briefly, for labeling, 2-[^{18}F]fluoropropionic acid was used as prosthetic group. With an isolated receptor binding assay it was demonstrated that modification of the lead structure reduced binding to integrin $\alpha_5\beta_1$ by a factor of 10. Comparison of the binding affinity for $\alpha_5\beta_1$, $\alpha_v\beta_3$, and $\alpha_{IIb}\beta_3$ revealed that selectivity was not affected. Despite high affinity for the integrin and stability in human serum in vivo, biodistribution data of [^{18}F]FProp-C*RRETAWAC*-OH using a murine tumor model were disappointing. In fact, the highest tracer accumulation was found for the tumor, but similar high radioactivity concentration was found in blood. Additionally, activity concentration in the organs remains almost constant over the observation period of 120 min leading to tumor-to-background ratios between 1 and 2, making this compound not suitable for imaging integrin $\alpha_5\beta_1$ expression.

3.2. Integrin $\alpha_v\beta_6$. The most prominent lead structure for the development of radiotracer for imaging integrin

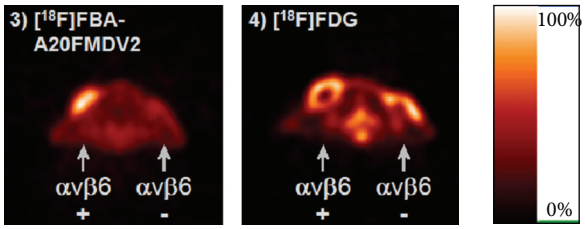

Figure 7: [^{18}F]FBA-A20FMDV2: (3) representative transaxial microPET 45–60 min after injection. The positive ($\alpha_v\beta_6$-expressing DX3puroβ6) tumors were located near the left shoulder and the negative (control DX3puro) tumors near the right shoulder. For comparison, (4) depicts a [^{18}F]FDG scan of the animal shown in (3), obtained within 5 d. (with permission form Hausner et al. [23]).

$\alpha_v\beta_6$ is the 20-amino acid peptide A20FMDV2 (sequence: NAVPNL**RGDLQVL**AQKVART). The sequence is derived from the GH loop of an envelope protein of the foot-and-mouth diseases virus (FMDV) [83] which mediates FMDV infection via binding to the integrin $\alpha_v\beta_6$ [84, 85]. The central binding region includes the RGD sequence followed by an LXXL motif, where X specifies variable amino acids. Phage display libraries indicate that the DLXXL sequence is responsible for the high $\alpha_v\beta_6$ specificity [86].

This peptide was initially labeled with a [^{18}F]fluorobenzoyl group via a solid-phase labeling strategy [23]. In a competitive binding ELISA including integrin $\alpha_v\beta_6$, $\alpha_v\beta_3$, $\alpha_v\beta_5$, and $\alpha_5\beta_1$ it was demonstrated that the N-terminal modification has no influence on binding affinity and selectivity. Evaluation of the tracer using a murine tumor model including $\alpha_v\beta_6$-positive (DX3puro) and $\alpha_v\beta_6$-negative (DX3puroβ6) xenografts demonstrated receptor selective uptake of [^{18}F]FBA-A20FMDV2 (Figure 7) [23]. However, uptake and retention in the tumor were comparably low, which might be due to the low metabolic stability of the compound. To improve the stability and the pharmacokinetic behavior, polyethylene glycol (PEG) moieties have been introduced. This resulted in [^{18}F]FBA-PEG$_{28}$-A20FMDV2 and [^{18}F]FBA-(PEG$_{28}$)$_2$-A20FMDV2 [40]. HPLC analysis of mouse urine samples showed increased stability of the PEGylated compounds with only one major metabolite detected. Also tumor retention could be significantly improved with almost constant uptake up to 4 h after injection. However, also retention in other organs has been increased. In particular, the introduction of a second PEG$_{28}$ unit was not beneficial due to the resulting high uptake and retention in the kidneys. Most recently, Hausner et al. [41] evaluated the copper-free, strain-promoted click chemistry for ^{18}F-labeling of A20FMDV2. This modified click chemistry approach should eliminate the need for potentially toxic copper catalysts. The radiotracer was readily prepared with high radiochemical purity, but the required cyclooctyne derivative introduces a very lipophilic moiety which negatively influences the pharmacokinetic of the resulting [^{18}F]FBA-C$_6$-ADIBON$_3$-PEG$_7$-A20FMDV2. Thus, despite receptor specific binding and good metabolic stability, the tumor uptake was low and the radioactivity concentration in urine as well as gall bladder was very high, indicating both renal and hepatobiliary elimination making this compound not suitable for imaging integrin $\alpha_v\beta_6$ expression.

Additional approaches are based on the introduction of chelating systems for labeling with ^{111}In-indium or ^{64}Cu-copper. For ^{111}In-labeling, DTPA was conjugated to the N-terminal end of the peptide [42]. DTPA conjugation has no effect on peptide binding affinity and receptor specificity. Serum stability was comparable as found for [^{18}F]FBA-A20FMDV2 with several metabolites found after 4 h incubation. Despite comparable low stability, tumor uptake was higher as found for the ^{18}F-labeled derivative. If this could be ascribed to the different tumor models used or to a better performance of the [^{111}In]DTPA-A20FMDV2, it has to be figured out by direct comparison in the same animal model. Extremely high radioactivity concentration was found in kidneys at 1 hour after injection. Other organs with comparable uptake as found in the tumor are lower gastrointestinal tract, gall bladder, and stomach. This seems to be due to expression of the integrin $\alpha_v\beta_6$ in these organs, which were examined by immunohistochemical staining of the corresponding paraffin-embedded murine tissue and confirmed by blocking studies. High-resolution SPECT of mice demonstrate clear visualization of $\alpha_v\beta_6$-expressing tumors but also indicate high activity concentration in kidneys and bladder. [^{111}In]DTPA-A20FMDV2 was also used to study imaging of $\alpha_v\beta_6$ integrin for molecular stratification of idiopathic pulmonary fibrosis [87]. It could be demonstrated that levels of [^{111}In]DTPA-A20FMDV2 in the lung correlated positively with hydroxyproline, $\alpha_v\beta_6$ protein, and itgb6 messenger RNA levels indicating that this technique might be feasible to be used for stratifying therapy for patients with pulmonary fibrosis.

A study by Hu et al. [43] was designed to determine the best candidate out of four chelating systems to label PEG$_{28}$-A20FMDV2 with ^{64}Cu. This include a triazacyclononane derivative (NOTA), a tetraazacyclododecane derivative (DOTA), a tetraazabicyclo[6.6.2] hexadecane derivative (CB-TE1A1P), and a hexaazabicyclo[6.6.6]icosane derivative (BaBaSar). Independent of the chelating system, all compounds could be labeled under mild conditions in good radiochemical purity and specific activity. None of the chelating systems influenced the selectivity for the integrin $\alpha_v\beta_6$ in a cell binding assay. The lowest binding and internalization were found for [^{64}Cu]NOTA-PEG$_{28}$-A20FMDV2. Stability studies in mouse serum after 24 hours incubation revealed the highest amount of intact tracer for [^{64}Cu]CB-TE1A1P-PEG$_{28}$-A20FMDV2 (<45%) and the lowest for [^{64}Cu]BaBaSar-PEG$_{28}$-A20FMDV2 (14%). Initial biodistribution data did not present the best candidate. Although high positive-to-negative tumor uptake ratios were found for [^{64}Cu]CB-TE1A1P-PEG$_{28}$-A20FMDV2 and for [^{64}Cu]BaBaSar-PEG$_{28}$-A20FMDV2, there was significant higher kidney uptake as found for the other two tracers. Another unpredicted finding was that blocking resulted only for three compounds in a reduced uptake in the receptor-positive tumor. For [^{64}Cu]NOTA-PEG$_{28}$-A20FMDV2, an unexplained increase of tumor uptake was found. Altogether, this study demonstrated that ^{64}Cu-labeling of A20FMDV2 derivatives is

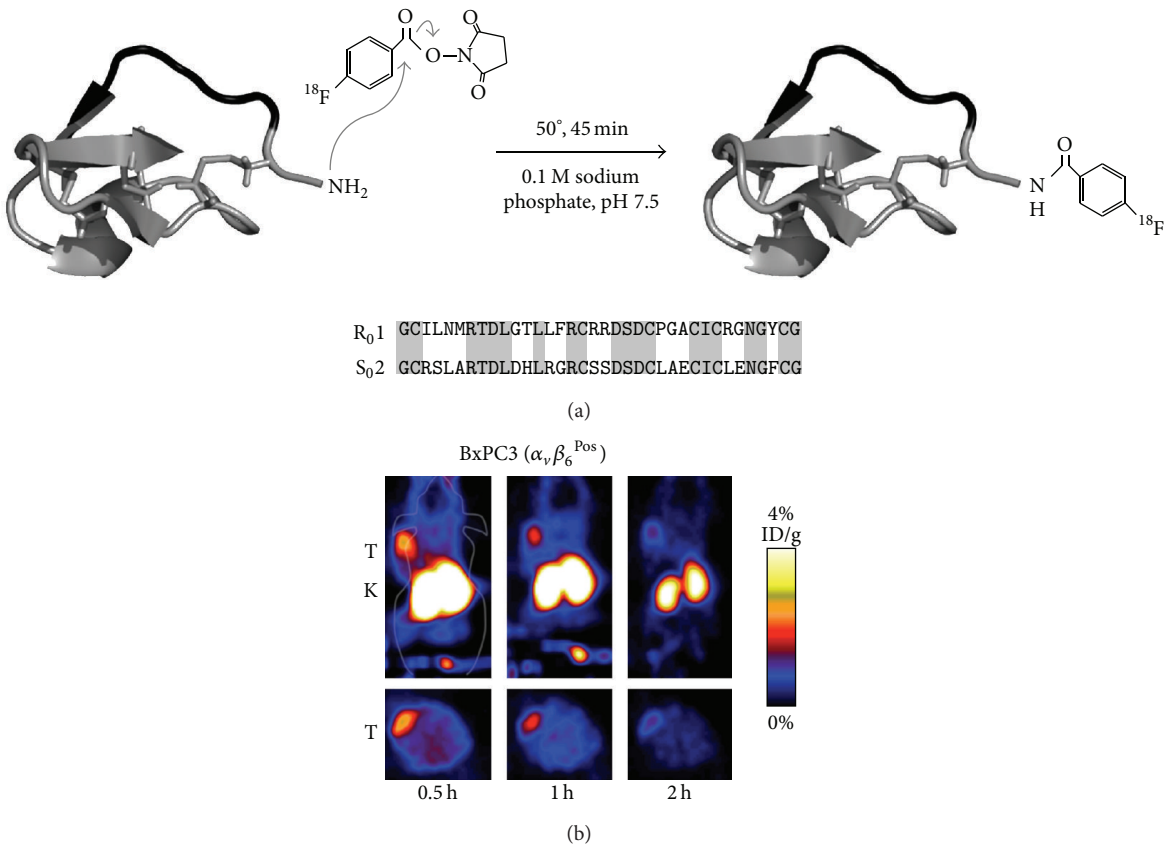

Figure 8: Cystine knot based tracer: (a) $R_0 1$ and $S_0 2$ are cystine knot peptides that contain 3 disulfide bonds, an active binding loop (black), and a sole primary amine at N terminus used for labeling via ^{18}F-SFB. Peptide sequences are presented with conserved residues highlighted. (b) ^{18}F-fluorobenzoate-$R_0 1$ small-animal PET imaging of BxPC3 pancreatic adenocarcinoma (integrin $\alpha_v\beta_6$-positive) bearing nude mice (five-minute static scans were acquired at 0.5, 1, and 2 h p.i.; decay-corrected coronal and transverse slices are presented; tumor (T) and kidneys (K) are marked on images) (with permission from Hackel et al. [24]).

possible but much more detailed experiments that may be also including alternative chelating systems are necessary before a final decision about the best performer can be made.

To develop a more stable and effective agent for imaging integrin $\alpha_v\beta_6$ cysteine knot peptides were engineered which demonstrated nanomolar affinity for this integrin [44]. Four DOTA-derivatized compounds were labeled with ^{64}Cu and metabolic stability was studied in mouse serum. Two derivatives ([^{64}Cu]DOTA-$S_0 2$ and [^{64}Cu]DOTA-$E_0 2$) showed high stability with more than 95% intact tracer after 24 hours incubation. In vivo biodistribution as well as small animal PET demonstrated receptor specific tumor uptake for all compounds tested but also extremely high activity concentration in kidneys for [^{64}Cu]DOTA-$R_0 2$, [^{64}Cu]DOTA-$E_0 2$, and [^{64}Cu]DOTA-$R_0 1$. In a further study $R_0 1$ and $S_0 2$, were labeled via N-succinimidyl-4-^{18}F-fluorobenzoate (Figure 8) [24]. In particular, ^{18}F-fluorobenzoate-$S_0 2$ showed high serum stability. Despite lower stability in the in vitro assay, tumor uptake was superior for ^{18}F-fluorobenzoate-$R_0 1$. For both compounds, a clear reduction in kidney uptake was found when compared with the ^{64}Cu-labeled analogs. Anyway, with 16% ID/g at 1 h p.i. it remains high especially for ^{18}F-fluorobenzoate-$R_0 1$. However, the results from coinjection studies remained inexplicable. For ^{18}F-fluorobenzoate-$R_0 1$, at least a slight reduction in tumor uptake was found, but no reduction was observed for ^{18}F-fluorobenzoate-$S_0 2$. Most recently, $S_0 2$ was modified with a single amino acid chelator (SAAC) and labeled with ^{99m}Tc $(CO)_3$ [45]. Similar to the other cysteine knot derivatives, [^{99m}Tc]SAAC-$S_0 2$ showed high metabolic stability and integrin $\alpha_v\beta_6$ specific uptake but biodistribution studies revealed, with exception of tumor-to-muscle ratio, that most of the tumor-to-organ ratios are approximately one or even clearly below one. Very high activity concentration is again found for the kidneys, independent of the use of the serine-rich derivative, which should avoid high kidney uptake.

4. Summary and Conclusion

Approximately 15 years ago, the first radiolabeled RGD peptides were introduced to image integrin $\alpha_v\beta_3$. Starting from the initially iodinated derivatives, a great variety of different compounds labeled with almost the whole set of available isotopes used in nuclear medicine tracer techniques have been described, but only a small set yet entered clinical trials. The first and most intensively studied one is [^{18}F]Galacto-RGD which showed receptor selective tracer accumulation in

the tumor with rapid predominantly renal elimination resulting in good tumor-to-background ratios and low radiation burden for the patient. The drawback of this compound is the complex time-consuming radiosynthesis. Thus, one major goal of the subsequently developed compounds was to optimize the radiolabeling strategy. One approach was focused on alternative ^{18}F-labeling strategies including oxime formation, click chemistry, isotopic exchange labeling, and introduction of aluminum fluoride species. Another approach to develop new PET tracer was focused on the introduction of ^{68}Ga as an alternative to ^{18}F for PET imaging. Based on each of the described labeling strategies, at least one candidate RGD peptide has entered clinical studies, with the exception of the isotopic exchange labeling strategy. All approaches produce the radiopharmaceutical in shorter production times as described for [^{18}F]Galacto-RGD, with most significant reductions found for the ^{68}Ga-labeling approach followed by the aluminum fluoride approach. All tracers have in common that they allow receptor specific imaging of integrin $\alpha_v\beta_3$ (and $\alpha_v\beta_5$) expression, show rapid predominately renal excretion with low radiation burden, and are well tolerated. For most radiopharmaceuticals, a great variance in tracer uptake in the lesions is found. One exception is the dimeric tracer [^{18}F]Alfatide. The initial study with nine patients resulted in very low variance in the SUV. However, a clinical study directly comparing different RGD tracers is lacking; thus, a final conclusion which compound performs best is not possible, yet. However, as there are already a variety of clinical studies using radiolabeled RGD peptides demonstrating their feasibility for imaging $\alpha_v\beta_3$, it is now of utmost importance to study how patients can benefit from this PET imaging approach. Therefore, further studies have to demonstrate whether corresponding antiangiogenic therapies can be controlled using this imaging technique. Most recently, alternative applications are also studied including assessment of plaque inflammation. However, again more comprehensive studies are needed allowing a final conclusion. In parallel to the radiopharmaceuticals already in clinical studies, a set of new compounds and strategies are evaluated. Among this set of candidates, several may enter clinical trials soon, including [^{68}Ga]NODAGA-RGD and [^{68}Ga]TRAP(RGD)$_3$.

In addition to the integrins $\alpha_v\beta_3/\alpha_v\beta_5$ the integrins $\alpha_5\beta_1$ and $\alpha_v\beta_6$ recently came into the focus of interest. Integrin $\alpha_5\beta_1$ might even be more important in the angiogenic process as the integrin $\alpha_v\beta_3$; thus, initial tracer either based on nonpeptidic scaffolds or on results from screening phage display libraries has been developed. The performance of the latter was not sufficient to be used for imaging integrin $\alpha_5\beta_1$ whereas the nonpeptide derivatives seem to be promising and are the basis for further studies. Integrin $\alpha_v\beta_6$ does not seem to be involved in angiogenesis but was found to be highly expressed on a variety of tumors. Moreover, expression seems to correlate with pure outcome; thus, this integrin was also used as target structure for the development of radiopharmaceuticals. In the present days, two lead structures are studied. One is based on the sequence of a loop of an envelope protein of the foot-and-mouth diseases virus and the other is based on cystine knots. Both classes of compounds were radiolabeled with different isotopes, including ^{18}F and ^{64}Cu, and revealed receptor-specific binding in vitro and in vivo. However, on the one hand, some of the tracers lack metabolic stability and, on the other hand, tracer excretion is not optimal, leading to high activity in a variety of organs including the kidneys as the dose-limiting organ. Thus, although initial data demonstrate that $\alpha_v\beta_6$-specific imaging is feasible, further optimizations are needed to find suitable compounds for noninvasive imaging of this receptor in patients.

Conflict of Interests

The authors declare that there is no conflict of interests regarding the publication of this paper.

References

[1] C. Margadant, H. N. Monsuur, J. C. Norman, and A. Sonnenberg, "Mechanisms of integrin activation and trafficking," *Current Opinion in Cell Biology*, vol. 23, no. 5, pp. 607–614, 2011.

[2] J. Welti, S. Loges, S. Dimmeler, and P. Carmeliet, "Recent molecular discoveries in angiogenesis and antiangiogenic therapies in cancer," *The Journal of Clinical Investigation*, vol. 123, no. 8, pp. 3190–3200, 2013.

[3] M. Petrillo, G. Scambia, and G. Ferrandina, "Novel targets for VEGF-independent anti-angiogenic drugs," *Expert Opinion on Investigational Drugs*, vol. 21, no. 4, pp. 451–472, 2012.

[4] K. Seystahl and M. Weller, "Is there a world beyond bevacizumab in targeting angiogenesis in glioblastoma?" *Expert Opinion on Investigational Drugs*, vol. 21, no. 5, pp. 605–617, 2012.

[5] B. Garmy-Susini and J. A. Varner, "Roles of integrins in tumor angiogenesis and lymphangiogenesis," *Lymphatic Research and Biology*, vol. 6, no. 3-4, pp. 155–163, 2008.

[6] R. Haubner, A. J. Beer, H. Wang, and X. Chen, "Positron emission tomography tracers for imaging angiogenesis," *European Journal of Nuclear Medicine and Molecular Imaging*, vol. 37, supplement 1, pp. S86–S103, 2010.

[7] P. C. Brooks, R. A. Clark, and D. A. Cheresh, "Requirement of vascular integrin alpha v beta 3 for angiogenesis," *Science*, vol. 264, no. 5158, pp. 569–571, 1994.

[8] F. C. Gaertner, H. Kessler, H. J. Wester, M. Schwaiger, and A. J. Beer, "Radiolabelled RGD peptides for imaging and therapy," *European Journal of Nuclear Medicine and Molecular Imaging*, vol. 39, supplement 1, pp. 126–138, 2012.

[9] G. H. Mahabeleshwar, W. Feng, D. R. Phillips, and T. V. Byzova, "Integrin signaling is critical for pathological angiogenesis," *The Journal of Experimental Medicine*, vol. 203, no. 11, pp. 2495–2507, 2006.

[10] K. L. Goh, J. T. Yang, and R. O. Hynes, "Mesodermal defects and cranial neural crest apoptosis in α5 integrin-null embryos," *Development*, vol. 124, no. 21, pp. 4309–4319, 1997.

[11] S. Kim, K. Bell, S. A. Mousa, and J. A. Varner, "Regulation of angiogenesis *in vivo* by ligation of integrin $\alpha_5\beta_1$ with the central cell-binding domain of fibronectin," *The American Journal of Pathology*, vol. 156, no. 4, pp. 1345–1362, 2000.

[12] N. J. Boudreau and J. A. Varner, "The homeobox transcription factor hox D3 promotes integrin $\alpha_5\beta_1$ expression and function during angiogenesis," *The Journal of Biological Chemistry*, vol. 279, no. 6, pp. 4862–4868, 2004.

[13] A. Bandyopadhyay and S. Raghavan, "Defining the role of integrin $\alpha_v\beta_6$ in cancer," *Current Drug Targets*, vol. 10, no. 7, pp. 645–652, 2009.

[14] J. M. Breuss, J. Gallo, H. M. DeLisser et al., "Expression of the β_6 integrin subunit in development, neoplasia and tissue repair suggests a role in epithelial remodeling," *Journal of Cell Science*, vol. 108, no. 6, pp. 2241–2251, 1995.

[15] R. A. Clark, G. S. Ashcroft, M.-J. Spencer, H. Larjava, and M. W. Ferguson, "Re-epithelialization of normal human excisional wounds is associated with a switch from $\alpha_v\beta_5$ to $\alpha_v\beta_6$ integrins," *British Journal of Dermatology*, vol. 135, no. 1, pp. 46–51, 1996.

[16] R. C. Bates, "Colorectal cancer progression: integrin $\alpha_v\beta_6$ and the epithelial-mesenchymal transition (EMT)," *Cell Cycle*, vol. 4, no. 10, pp. 1350–1352, 2005.

[17] R. Haubner, W. A. Weber, A. J. Beer et al., "Noninvasive visualization of the activated $\alpha_v\beta_3$ integrin in cancer patients by positron emission tomography and [^{18}F]Galacto-RGD," *PLoS Medicine*, vol. 2, no. 3, article e70, 2005.

[18] L. M. Kenny, R. C. Coombes, I. Oulie et al., "Phase I trial of the positron-emitting Arg-Gly-Asp (RGD) peptide radioligand ^{18}F-AH111585 in breast cancer patients," *The Journal of Nuclear Medicine*, vol. 49, no. 6, pp. 879–886, 2008.

[19] W. Wan, N. Guo, D. Pan et al., "First experience of ^{18}F-alfatide in lung cancer patients using a new lyophilized kit for rapid radiofluorination," *The Journal of Nuclear Medicine*, vol. 54, no. 5, pp. 691–698, 2013.

[20] J. Notni, K. Pohle, and H.-J. Wester, "Be spoilt for choice with radiolabelled RGD peptides: preclinical evaluation of ^{68}Ga-TRAP(RGD)$_3$," *Nuclear Medicine and Biology*, vol. 40, no. 1, pp. 33–41, 2013.

[21] Z. Liu, Y. Li, J. Lozada et al., "Kit-like ^{18}F-labeling of RGD-^{19}F-Arytrifluroborate in high yield and at extraordinarily high specific activity with preliminary *in vivo* tumor imaging," *Nuclear Medicine and Biology*, vol. 40, no. 6, pp. 841–849, 2013.

[22] S. Neubauer, F. Rechenmacher, A. J. Beer et al., "Selective imaging of the angiogenic relevant integrins $\alpha_5\beta_1$ and $\alpha_v\beta_3$," *Angewandte Chemie*, vol. 52, no. 44, pp. 11656–11659, 2013.

[23] S. H. Hausner, D. DiCara, J. Marik, J. F. Marshall, and J. L. Sutcliffe, "Use of a peptide derived from foot-and-mouth disease virus for the noninvasive imaging of human cancer: generation and evaluation of 4-[^{18}F]fluorobenzoyl A20FMDV2 for *in vivo* imaging of integrin $\alpha_v\beta_6$ expression with positron emission tomography," *Cancer Research*, vol. 67, no. 16, pp. 7833–7840, 2007.

[24] B. J. Hackel, R. H. Kimura, Z. Miao et al., "^{18}F-fluorobenzoate-labeled cystine knot peptides for PET imaging of integrin $\alpha_v\beta_6$," *The Journal of Nuclear Medicine*, vol. 54, no. 7, pp. 1101–1105, 2013.

[25] L. Auzzas, F. Zanardi, L. Battistini et al., "Targeting $\alpha_v\beta_3$ integrin: design and applications of mono- and multifunctional RGD-based peptides and semipeptides," *Current Medicinal Chemistry*, vol. 17, no. 13, pp. 1255–1299, 2010.

[26] H. Cai and P. S. Conti, "RGD-based PET tracers for imaging receptor integrin $\alpha_v\beta_3$ expression," *Journal of Labelled Compounds and Radiopharmaceuticals*, vol. 56, no. 5, pp. 264–279, 2013.

[27] M. Schottelius, B. Laufer, H. Kessler, and H.-J. Wester, "Ligands for mapping $\alpha_v\beta_3$-integrin expression *in vivo*," *Accounts of Chemical Research*, vol. 42, no. 7, pp. 969–980, 2009.

[28] R. Haubner, B. Kuhnast, C. Mang et al., "[^{18}F]Galacto-RGD: synthesis, radiolabeling, metabolic stability, and radiation dose estimates," *Bioconjugate Chemistry*, vol. 15, no. 1, pp. 61–69, 2004.

[29] M. Glaser, M. Solbakken, D. R. Turton et al., "Methods for ^{18}F-labeling of RGD peptides: comparison of aminooxy [^{18}F]fluorobenzaldehyde condensation with "click labeling" using 2-[^{18}F]fluoroethylazide, and *S*-alkylation with [^{18}F] fluoropropanethiol," *Amino Acids*, vol. 37, no. 4, pp. 717–724, 2009.

[30] L. Mirfeizi, J. Walsh, H. Kolb et al., "Synthesis of [^{18}F]RGD-K5 by catalyzed [3 + 2] cycloaddition for imaging integrin $\alpha_v\beta_3$ expression *in vivo*," *Nuclear Medicine and Biology*, vol. 40, no. 5, pp. 710–716, 2013.

[31] Z.-B. Li, Z. Wu, K. Chen, F. T. Chin, and X. Chen, "Click chemistry for ^{18}F-labeling of RGD peptides and microPET imaging of tumor integrin $\alpha_v\beta_3$ expression," *Bioconjugate Chemistry*, vol. 18, no. 6, pp. 1987–1994, 2007.

[32] S. Maschauer, R. Haubner, T. Kuwert, and O. Prante, "^{18}F-Glyco-RGD peptides for PET imaging of integrin expression: efficient radiosynthesis by click chemistry and modulation of biodistribution by glycosylation," *Molecular Pharmaceutics*, vol. 11, no. 2, pp. 505–515, 2014.

[33] E. Schirrmacher, B. Wängler, M. Cypryk et al., "Synthesis of *p*-(Di-*tert*-butyl[^{18}F]fluorosilyl)benzaldehyde ([^{18}F]SiFA-A) with high specific activity by isotopic exchange: a convenient labeling synthon for the ^{18}F-labeling of N-amino-oxy derivatized peptides," *Bioconjugate Chemistry*, vol. 18, no. 6, pp. 2085–2089, 2007.

[34] J. M. Jeong, M. K. Hong, Y. S. Chang et al., "Preparation of a promising angiogenesis PET imaging agent: ^{68}Ga-labeled c(RGDyK)-isothiocyanatobenzyl-1,4,7-triazacyclononane-1, 4,7-triacetic acid and feasibility studies in mice," *The Journal of Nuclear Medicine*, vol. 49, no. 5, pp. 830–836, 2008.

[35] C. Decristoforo, I. H. Gonzalez, J. Carlsen et al., "^{68}Ga- and ^{111}In-labelled DOTA-RGD peptides for imaging of $\alpha_v\beta_3$ integrin expression," *European Journal of Nuclear Medicine and Molecular Imaging*, vol. 35, no. 8, pp. 1507–1515, 2008.

[36] P. A. Knetsch, M. Petrik, C. M. Griessinger et al., "[^{68}Ga]NODAGA-RGD for imaging $\alpha_v\beta_3$ integrin expression," *European Journal of Nuclear Medicine and Molecular Imaging*, vol. 38, no. 7, pp. 1303–1312, 2011.

[37] J. Šimeček, J. Notni, T. G. Kapp, H. Kessler, and H.-J. Wester, "Benefits of NOPO as chelator in Gallium-68 peptides, exemplified by preclinical characterization of ^{68}Ga-NOPO-c(RGDfK)," *Molecular Pharmaceutics*, vol. 11, no. 5, pp. 1687–1695, 2014.

[38] E. Boros, C. L. Ferreira, D. T. Yapp et al., "RGD conjugates of the H_2dedpa scaffold: synthesis, labeling and imaging with ^{68}Ga," *Nuclear Medicine and Biology*, vol. 39, no. 6, pp. 785–794, 2012.

[39] R. Haubner, S. Maschauer, J. Einsiedel et al., "H-CRRETAWAC-OH, a lead structure for the development of tracer targeting integrin $\alpha_5\beta_1$?" *BioMed Research International*. In press.

[40] S. H. Hausner, C. K. Abbey, R. J. Bold et al., "Targeted *in vivo* imaging of integrin $\alpha_v\beta_6$ with an improved radiotracer and its relevance in a pancreatic tumor model," *Cancer Research*, vol. 69, no. 14, pp. 5843–5850, 2009.

[41] S. H. Hausner, R. D. Carpenter, N. Bauer, and J. L. Sutcliffe, "Evaluation of an integrin $\alpha_v\beta_6$-specific peptide labeled with [^{18}F]fluorine by copper-free, strain-promoted click chemistry," *Nuclear Medicine and Biology*, vol. 40, no. 2, pp. 233–239, 2013.

[42] A. Saha, D. Ellison, G. J. Thomas et al., "High-resolution *in vivo* imaging of breast cancer by targeting the pro-invasive integrin $\alpha_v\beta_6$," *The Journal of Pathology*, vol. 222, no. 1, pp. 52–63, 2010.

[43] L. Y. Hu, N. Bauer, L. M. Knight et al., "Characterization and evaluation of ^{64}Cu-labeled A20FMDV2 conjugates for imaging the integrin $\alpha_v\beta_6$," *Molecular Imaging and Biology*, 2014.

[44] R. H. Kimura, R. Teed, B. J. Hackel et al., "Pharmacokinetically stabilized cystine knot peptides that bind $\alpha_v\beta_6$ integrin with single-digit nanomolar affinities for detection of pancreatic cancer," *Clinical Cancer Research*, vol. 18, no. 3, pp. 839–849, 2012.

[45] X. Zhu, J. Li, Y. Hong et al., "^{99m}Tc-labeled cystine knot peptide targeting integrin $\alpha_v\beta_6$ for tumor SPECT imaging," *Molecular Pharmaceutics*, vol. 11, no. 4, pp. 1208–1217, 2014.

[46] R. Haubner, H.-J. Wester, U. Reuning et al., "Radiolabeled $\alpha_v\beta_3$ integrin antagonists: a new class of tracers for tumor targeting," *The Journal of Nuclear Medicine*, vol. 40, no. 6, pp. 1061–1071, 1999.

[47] R. Haubner, H.-J. Wester, W. A. Weber et al., "Noninvasive imaging of $\alpha_v\beta_3$ integrin expression using ^{18}F-labeled RGD-containing glycopeptide and positron emission tomography," *Cancer Research*, vol. 61, no. 5, pp. 1781–1785, 2001.

[48] A. J. Beer, R. Haubner, M. Goebel et al., "Biodistribution and pharmacokinetics of the $\alpha_v\beta_3$-selective tracer ^{18}F-Galacto-RGD in cancer patients," *The Journal of Nuclear Medicine*, vol. 46, no. 8, pp. 1333–1341, 2005.

[49] A. J. Beer, R. Haubner, M. Sarbia et al., "Positron emission tomography using [^{18}F]Galacto-RGD identifies the level of integrin $\alpha_v\beta_3$ expression in man," *Clinical Cancer Research*, vol. 12, no. 13, pp. 3942–3949, 2006.

[50] A. J. Beer, R. Haubner, I. Wolf et al., "PET-based human dosimetry of ^{18}F-Galacto-RGD, a new radiotracer for imaging $\alpha_v\beta_3$ expression," *The Journal of Nuclear Medicine*, vol. 47, no. 5, pp. 763–769, 2006.

[51] ICRP, "Radiation dose to patients from radiopharmaceuticals. Addendum 3 to ICRP Publication 53. ICRP Publication 106. Approved by the Commission in October 2007," *Annals of the ICRP*, vol. 38, no. 1-2, pp. 7–33, 2008.

[52] A. J. Beer, A.-L. Grosu, J. Carlsen et al., "[^{18}F]Galacto-RGD positron emission tomography for imaging of $\alpha_v\beta_3$ expression on the neovasculature in patients with squamous cell carcinoma of the head and neck," *Clinical Cancer Research*, vol. 13, no. 22, pp. 6610–6616, 2007.

[53] O. Schnell, B. Krebs, J. Carlsen et al., "Imaging of integrin $\alpha_v\beta_3$ expression in patients with malignant glioma by [^{18}F] Galacto-RGD positron emission tomography," *Neuro-Oncology*, vol. 11, no. 6, pp. 861–870, 2009.

[54] A. J. Beer, S. Lorenzen, S. Metz et al., "Comparison of integrin $\alpha_v\beta_3$ expression and glucose metabolism in primary and metastatic lesions in cancer patients: a PET study using ^{18}F-galacto-RGD and 18F-FDG," *The Journal of Nuclear Medicine*, vol. 49, no. 1, pp. 22–29, 2008.

[55] M. Hoshiga, C. E. Alpers, L. L. Smith, C. M. Giachelli, and S. M. Schwartz, "$\alpha_v\beta_3$ integrin expression in normal and atherosclerotic artery," *Circulation Research*, vol. 77, no. 6, pp. 1129–1135, 1995.

[56] A. S. Antonov, F. D. Kolodgie, D. H. Munn, and R. G. Gerrity, "Regulation of macrophage foam cell formation by $\alpha_v\beta_3$ integrin: potential role in human atherosclerosis," *The American Journal of Pathology*, vol. 165, no. 1, pp. 247–258, 2004.

[57] A. J. Beer, J. Pelisek, P. Heider et al., "PET/CT imaging of integrin $\alpha_v\beta_3$ expression in human carotid atherosclerosis," *JACC: Cardiovascular Imaging*, vol. 7, no. 2, pp. 178–187, 2014.

[58] B. J. McParland, M. P. Miller, T. J. Spinks et al., "The biodistribution and radiation dosimetry of the Arg-Gly-Asp peptide ^{18}F-AH111585 in healthy volunteers," *The Journal of Nuclear Medicine*, vol. 49, no. 10, pp. 1664–1667, 2008.

[59] M. R. Battle, J. L. Goggi, L. Allen, J. Barnett, and M. S. Morrison, "Monitoring tumor response to antiangiogenic sunitinib therapy with ^{18}F-fluciclatide, an ^{18}F-labeled $\alpha_v\beta_3$-integrin and $\alpha_v\beta_5$-integrin imaging agent," *The Journal of Nuclear Medicine*, vol. 52, no. 3, pp. 424–430, 2011.

[60] H. C. Kolb, K. Chen, J. C. Walsh et al., "Synthesis and imaging of an ^{18}F-labelled RGD peptide for detecting $\alpha_v\beta_3$ integrin expression," *Journal of Labelled Compounds and Radiopharmaceuticals*, vol. 52, supplement 1, pp. S67–S73, 2009.

[61] H. Kolb, J. Walsh, Q. Liang et al., "^{18}F-RGD-K5: a cyclic triazole-bearing RGD peptide for imaging integrin $\alpha_v\beta_3$ expression *in vivo*," *The Journal of Nuclear Medicine*, vol. 50, supplement 2, p. 329, 2009.

[62] M. Doss, H. C. Kolb, J. J. Zhang et al., "Biodistribution and radiation dosimetry of the integrin marker ^{18}F-RGD-K5 determined from whole-body PET/CT in monkeys and humans," *The Journal of Nuclear Medicine*, vol. 53, no. 5, pp. 787–795, 2012.

[63] H. J. Cho, J. D. Lee, J. Y. Park et al., "First in human evaluation of a newly developed integrin binding PET tracer, ^{18}F-RGD-K5 in patients with breast cancer: comparison with ^{18}F-FDG uptake pattern and microvessel density," *The Journal of Nuclear Medicine*, vol. 50, supplement 2, p. 1910, 2009.

[64] J. H. Kim, J. S. Lee, K. W. Kang et al., "Whole-body distribution and radiation dosimetry of ^{68}Ga-NOTA-RGD, a positron emission tomography agent for angiogenesis imaging," *Cancer Biotherapy & Radiopharmaceuticals*, vol. 27, no. 1, pp. 65–71, 2012.

[65] S. Fanti, M. Farsad, and L. Mansi, *PET-CT Beyond FDG: A Quick Guide to Image Interpretation*, Springer, Berlin, Germany, 2010.

[66] W. J. McBride, R. M. Sharkey, H. Karacay et al., "A novel method of ^{18}F radiolabeling for PET," *The Journal of Nuclear Medicine*, vol. 50, no. 6, pp. 991–998, 2009.

[67] L. Lang, W. Li, N. Guo et al., "Comparison study of [^{18}F]FAl-NOTA-PRGD2, [^{18}F] FPPRGD2, and [^{68}Ga]Ga-NOTA-PRGD2 for PET imaging of U87MG tumors in mice," *Bioconjugate Chemistry*, vol. 22, no. 12, pp. 2415–2422, 2011.

[68] C. Decristoforo, "Gallium-68—a new opportunity for PET available from a long shelflife generator automation and applications," *Current Radiopharmaceuticals*, vol. 5, no. 3, pp. 212–220, 2012.

[69] E. T. Clarke and A. E. Martell, "Stabilities of trivalent metal ion complexes of the tetraacetate derivatives of 12-, 13- and 14-membered tetraazamacrocycles," *Inorganica Chimica Acta*, vol. 190, no. 1, pp. 37–46, 1991.

[70] R. A. Dumont, F. Deininger, R. Haubner, H. R. Maecke, W. A. Weber, and M. Fani, "Novel ^{64}Cu- and ^{68}Ga-labeled RGD conjugates show improved PET imaging of $\alpha_v\beta_3$ integrin expression and facile radiosynthesis," *The Journal of Nuclear Medicine*, vol. 52, no. 8, pp. 1276–1284, 2011.

[71] T. L. Mindt, H. Struthers, L. Brans et al., ""Click to chelate": synthesis and installation of metal chelates into biomolecules in a single step," *Journal of the American Chemical Society*, vol. 128, no. 47, pp. 15096–15097, 2006.

[72] V. D. Bock, H. Hiemstra, and J. H. van Maarseveen, "Cu^{I}-catalyzed alkyne-azide "click" cycloadditions from a mechanistic and synthetic perspective," *European Journal of Organic Chemistry*, vol. 2006, no. 1, pp. 51–68, 2006.

[73] K. Kettenbach, H. Schieferstein, and T. Ross, "^{18}F-labeling using click cycloadditions," *BioMed Research International*. In press.

[74] S. Maschauer and O. Prante, "Sweetening pharmaceutical radiochemistry by ^{18}F-fluoroglycosylation: a short review," *BioMed Research International*. In press.

[75] S. Maschauer and O. Prante, "A series of 2-*O*-trifluoromethylsulfonyl-D-mannopyranosides as precursors for concomitant ^{18}F-labeling and glycosylation by click chemistry," *Carbohydrate Research*, vol. 344, no. 6, pp. 753–761, 2009.

[76] S. Maschauer, J. Einsiedel, R. Haubner et al., "Labeling and glycosylate of peptides using click chemistry: a general approach to ^{18}F-glycopeptides as effective imaging probes for positron emission tomography," *Angewandte Chemie*, vol. 49, no. 5, pp. 976–979, 2010.

[77] S. Liu, H. Liu, H. Jiang, Y. Xu, H. Zhang, and Z. Cheng, "One-step radiosynthesis of ^{18}F-AlF-NOTA-RGD2 for tumor angiogenesis PET imaging," *European Journal of Nuclear Medicine and Molecular Imaging*, vol. 38, no. 9, pp. 1732–1741, 2011.

[78] W. J. McBride, C. A. D'souza, R. M. Sharkey et al., "Improved ^{18}F labeling of peptides with a fluoride-aluminum- chelate complex," *Bioconjugate Chemistry*, vol. 21, no. 7, pp. 1331–1340, 2010.

[79] N. Guo, L. Lang, W. Li et al., "Quantitative analysis and comparison study of [^{18}F]AlF-NOTA-PRGD2, [^{18}F]FPPRGD2 and [^{68}Ga]Ga-NOTA-PRGD2 using a reference tissue model," *PLoS ONE*, vol. 7, no. 5, Article ID e37506, 2012.

[80] N. Guo, L. Lang, H. Gao et al., "Quantitative analysis and parametric imaging of ^{18}F-labeled monomeric and dimeric RGD peptides using compartment model," *Molecular Imaging and Biology*, vol. 14, no. 6, pp. 743–752, 2012.

[81] D. Heckmann, A. Meyer, B. Laufer, G. Zahn, R. Stragies, and H. Kessler, "Rational design of highly active and selective ligands for the $\alpha_5\beta_1$ integrin receptor," *ChemBioChem*, vol. 9, no. 9, pp. 1397–1407, 2008.

[82] E. Koivunen, B. Wang, and E. Ruoslahti, "Isolation of a highly specific ligand for the $\alpha_5\beta_1$ integrin from a phage display library," *The Journal of Cell Biology*, vol. 124, no. 3, pp. 373–380, 1994.

[83] D. Logan, R. Abu-Ghazaleh, W. Blakemore et al., "Structure of a major immunogenic site on foot-and-mouth disease virus," *Nature*, vol. 362, no. 6420, pp. 566–568, 1993.

[84] T. Jackson, D. Sheppard, M. Denyer, W. Blakemore, and A. M. Q. King, "The epithelial integrin $\alpha_v\beta_6$ is a receptor for foot-and-mouth disease virus," *Journal of Virology*, vol. 74, no. 11, pp. 4949–4956, 2000.

[85] A. Burman, S. Clark, N. G. A. Abrescia, E. E. Fry, D. I. Stuart, and T. Jackson, "Specificity of the VP1 GH loop of foot-and-mouth disease virus for α_v integrins," *Journal of Virology*, vol. 80, no. 19, pp. 9798–9810, 2006.

[86] S. Kraft, B. Diefenbach, R. Mehta, A. Jonczyk, G. A. Luckenbach, and S. L. Goodman, "Definition of an unexpected ligand recognition motif for $\alpha_v\beta_6$ integrin," *The Journal of Biological Chemistry*, vol. 274, no. 4, pp. 1979–1985, 1999.

[87] A. E. John, J. C. Luckett, A. L. Tatler et al., "Preclinical SPECT/CT imaging of $\alpha_v\beta_6$ integrins for molecular stratification of idiopathic pulmonary fibrosis," *The Journal of Nuclear Medicine*, vol. 54, no. 12, pp. 2146–2152, 2013.

Hindawi Publishing Corporation
BioMed Research International
Volume 2014, Article ID 214748, 16 pages
http://dx.doi.org/10.1155/2014/214748

Review Article

Sweetening Pharmaceutical Radiochemistry by ^{18}F-Fluoroglycosylation: A Short Review

Simone Maschauer and Olaf Prante

Molecular Imaging and Radiochemistry, Department of Nuclear Medicine, Friedrich Alexander University, Schwabachanlage 6, 91054 Erlangen, Germany

Correspondence should be addressed to Olaf Prante; olaf.prante@uk-erlangen.de

Received 19 March 2014; Accepted 15 April 2014; Published 1 June 2014

Academic Editor: Roland Haubner

At the time when the highly efficient [^{18}F]FDG synthesis was discovered by the use of the effective precursor 1,3,4,6-tetra-*O*-acetyl-2-*O*-trifluoromethanesulfonyl-β-D-mannopyranose (mannose triflate) for nucleophilic ^{18}F-substitution, the field of PET in nuclear medicine experienced a long-term boom. Thirty years later, various strategies for chemoselective ^{18}F-labeling of biomolecules have been developed, trying to keep up with the emerging field of radiopharmaceutical sciences. Among the new radiochemical strategies, chemoselective ^{18}F-fluoroglycosylation methods aim at the sweetening of pharmaceutical radiochemistry by providing a powerful and highly valuable tool for the design of ^{18}F-glycoconjugates with suitable *in vivo* properties for PET imaging studies. This paper provides a short review (reflecting the literature not older than 8 years) on the different ^{18}F-fluoroglycosylation reactions that have been applied to the development of various ^{18}F-glycoconjugate tracers, including not only peptides, but also nonpeptidic tracers and high-molecular-weight proteins.

1. Introduction

In 1984, thirty years ago, the synthesis of 1,3,4,6-tetra-*O*-acetyl-2-*O*-trifluoromethanesulfonyl-β-D-mannopyranose (mannose triflate) was published by Hamacher in *Carbohydrate Research* [1]. Meanwhile, the mannosyl precursor is commercially available and its daily routine application for the highly reliable and efficient radiosynthesis of 2-deoxy-2-[^{18}F]fluoroglucose ([^{18}F]FDG, [2]) has been the major driving force in the emerging field of positron emission tomography (PET) within nuclear medicine. [^{18}F]FDG represents by far the most frequently used radiopharmaceutical worldwide for PET imaging studies in oncology and neurology [3, 4].

Among the positron emitters, F-18 represents a superior PET radionuclide with outstanding physical characteristics ($E_{\max}(\beta^+) = 635$ keV, $t_{1/2} = 109.7$ min) allowing for multistep radiochemical syntheses. In recent years, various strategies for chemoselective ^{18}F-labeling reactions have been successfully developed, facilitating the accessibility of new PET radiopharmaceuticals [5–7]. The variety of new ^{18}F-labeling strategies is the focus of review articles as part of this special issue, provided by Bernard-Gauthier et al. [8], Kettenbach et al. [9], and Ermert [10].

In some cases it is desirable not only to use chemoselective and mild labeling methods, but also to have the opportunity to influence the biodistribution and tracer uptake characteristics simultaneously. Noteworthy, the glycosylation of biomolecules, such as peptides or proteins, has been frequently shown to improve the *in vivo* kinetics and stability in blood and to accelerate the clearance of such glycoconjugates *in vivo* [11–13]. Moreover, it has been shown by numerous examples that glycosylation of peptides with subsequent radiolabeling opens the way to radiotracers with improved *in vivo* properties [12–16]. Not surprisingly, Sharpless' concept of "click chemistry" introduced over 10 years ago [17] has been quickly adapted to carbohydrate chemistry in the field of glycoscience, facilitating the synthesis of new glycoconjugates derived from proteins, lipids and nucleic acids, new glycomaterials, such as glycosurfaces, glycodendrimers,

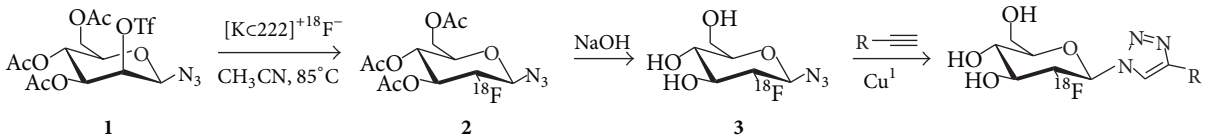

Scheme 1: General reaction scheme for [^{18}F]fluoroglycosylation via CuAAC using 2-deoxy-2-[^{18}F]fluoroglucopyranosyl azide **3**, starting from the β-mannosyl azide **1**.

and glycopolymers, and a wide variety of glycoconjugates in medicinal chemistry as putative chemotherapeuticals [18].

Therefore, our group envisaged the appropriate idea to develop a click chemistry-based ^{18}F-fluoroglycosylation method to provide a general approach to the radiosynthesis of ^{18}F-labeled glycoconjugates as effective imaging agents for PET [19, 20].

In 2009, we reported the synthesis of a series of "clickable" mannosides and showed their potential as ^{18}F-labeling precursors [20], which has been the starting point of a number of publications by others reporting on various ^{18}F-glycoconjugates as new PET tracers.

This paper provides a short review (reflecting the literature not older than 8 years) on the different ^{18}F-fluoroglycosylation reactions that have been applied to the development of various ^{18}F-glycoconjugate tracers for PET, including not only peptides but also nonpeptidic tracers and high-molecular-weight proteins. An overview of the radiotracers obtained by ^{18}F-fluoroglycosylation is given in Tables 1, 2 and 3.

2. ^{18}F-Fluoroglycosylation via Copper-Catalyzed Azide-Alkyne Cycloaddition (CuAAC)

In 2001, the Sharpless group introduced the term "click chemistry" to define the most efficient chemical reactions [17]. Click chemistry-based reactions are easy to perform, high-yielding, highly chemoselective, and orthogonal reactions that proceed without the formation of by-products under multiple reaction conditions. The copper-catalyzed azide-alkyne cycloaddition (CuAAC), introduced in 2002 [48, 49], is one of the most widely used click chemistry reactions, due to its high yield and easy accessibility of the azide and terminal alkyne reactants. Its successful adaption to ^{18}F-radiosynthetic methods in order to take advantage of its high selectivity, reliability, and speed under aqueous mild Cu^{I}-promoted reaction conditions has now been amply documented [50, 51].

The synthesis of the ^{18}F-fluoroglycosylating agent 3,4,6-tri-*O*-acetyl-2-deoxy-2-[^{18}F]fluoroglucopyranosyl azide (**3**) was achieved by the ^{18}F-labeling of the precursor 3,4,6-tri-*O*-acetyl-2-*O*-trifluoromethanesulfonyl-β-D-mannopyranosyl azide (**1**) in high radiochemical yields (RCY) as described by Maschauer and Prante (Scheme 1) [20]. Very similar to the well-known [^{18}F]FDG synthesis, the yield of this radiochemical reaction relies mainly on the chemical purity of the labeling precursor. In the case of mannosyl azide **1**, the synthesis was achieved by comprehensive carbohydrate chemistry via the pentafluoropropionyl protected β-mannosyl bromide and the purification of **1** was achieved by recrystallization in ethanol. The radiolabeling reaction according to Scheme 1 could be performed under standard reaction condition (Kryptofix 222, K_2CO_3) or with a slight modification using a mixture of K_2CO_3/KH_2PO_4 so that the solution is less basic and therefore the degradation of the mannosyl precursor **1** during the labeling reaction is significantly reduced, resulting in a more accurate HPLC separation of **2** without the interference of by-products. The CuAAC could also be performed with high RCY by omitting the HPLC separation. However, the presence of precursor azide **1** in the CuAAC reaction required the high alkyne concentration of 33 mM, making it inefficient for most rare peptides.

The applicability of the prosthetic group **3** for CuAAC was first verified with alkyne-bearing amino acids [20]. In ongoing studies the methodology was transferred to the radiosynthesis of an ^{18}F-fluoroglycosylated RGD peptide (**4**) and a neurotensin peptoid (**5**) [19]. The optimized CuAAC was carried out in PBS/ethanol (10 : 1, v/v) at 60°C with only 0.2 mM alkyne-peptide in the presence of $CuSO_4$ (4 mM) and sodium ascorbate (12 mM). After 15–20 min the reaction was complete and the ^{18}F-glycopeptides were isolated by HPLC in overall (non-decay-corrected) yields of 17–20% in a total synthesis time of only 70–75 min (starting form [^{18}F]fluoride) with specific activities of 55–210 GBq/μmol.

Furthermore, this ^{18}F-fluoroglycosylation approach was adopted in the radiosynthesis of ^{18}F-glycoproteins [21]. The first reaction step (^{18}F-labeling of the precursor **1**, Scheme 1) was performed under standard reaction conditions and yielded 3,4,6-tri-*O*-acetyl-2-deoxy-2-[^{18}F]fluoroglucopyranosyl azide **2** after HPLC separation in surprisingly low yields of only 1.3–4.7% after 80–100 min. After deacetylation the solution was neutralized by passing it through a cation exchange resin and the CuAAC was performed with an alkyne-bearing protein (6 μM) in the presence of copper(I) bromide and a tris-triazolyl amine ligand (triethyl 2, 2′, 2″-[nitrilotris(methylene-1*H*-1,2,3-triazole-4,1-diyl)]triacetate, TTMA) in sodium phosphate buffer (pH 8.2)/acetonitrile (6 : 1, v/v). After 45 minutes at room temperature the RCY of **6** was 4.1%. The observed low RCY is clearly due to the extremely low amount of the alkyne-bearing protein that was not available in higher amounts since it was a mutated protein that was produced in bacteria using site-directed mutagenesis of the protein gene.

Table 1: ^{18}F-Fluoroglycosylated imaging probes and ^{19}F-fluoroglycosyl derivatives (*) synthesized via CuAAC.

Structure	Target	Reference
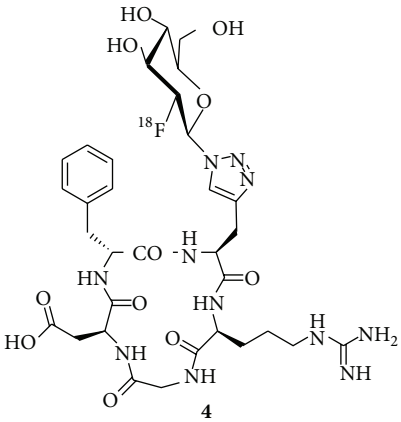 **4**	Integrin $\alpha_v\beta_3$	[19]
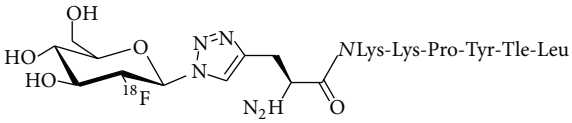 **5**	Neurotensin receptor NTS-1	[19]
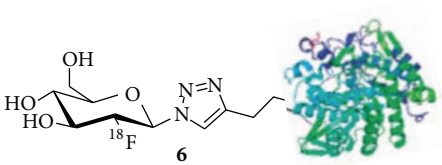 **6**	None	[21]
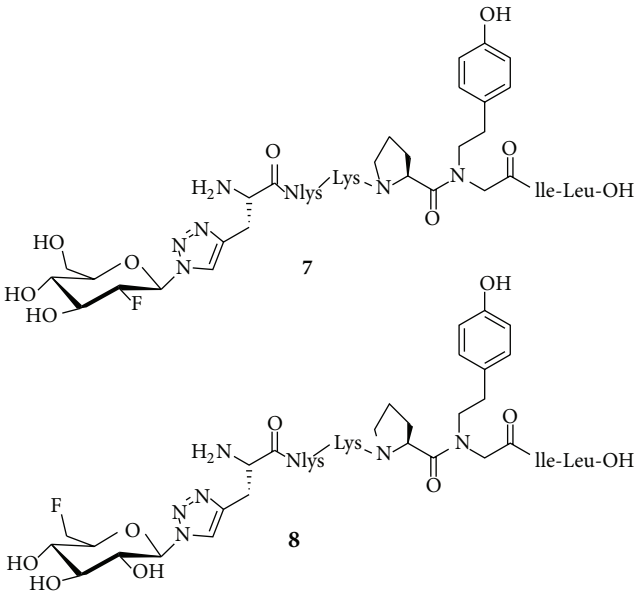 **7** **8**	Neurotensin receptor NTS-2*	[22]
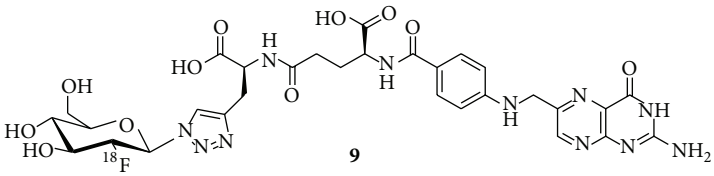 **9**	Folate receptor	[23]

Table 1: Continued.

Structure	Target	Reference
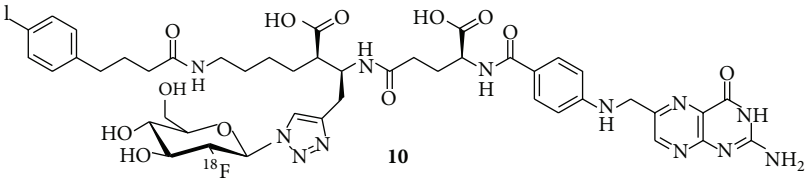 **10**	Folate receptor	[24]
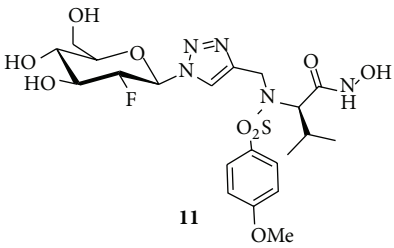 **11**	Matrix metalloproteinases MMP-2, MMP-8, MMP-9, and MMP-13*	[25]
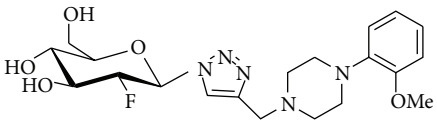 **12** 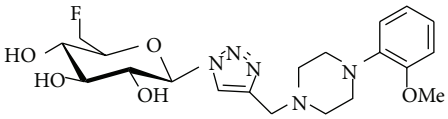 **13**	Dopamine receptor D4*	[26]
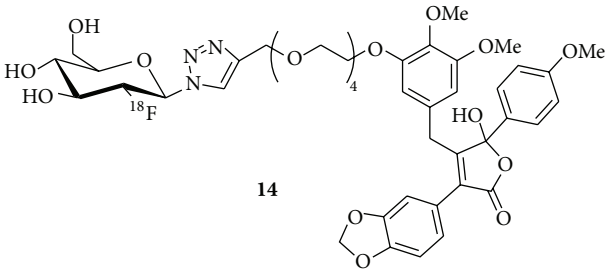 **14**	Endothelin receptor ET_AR	[27]
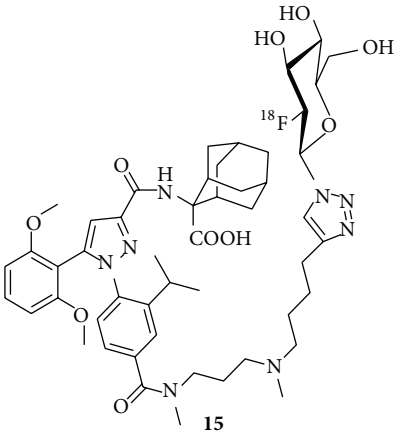 **15**	Neurotensin receptor NTS-1	[28]

Table 1: Continued.

Structure	Target	Reference
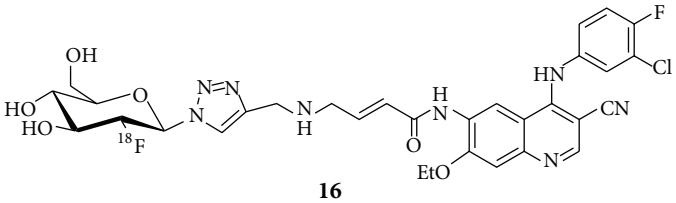 **16**	Epidermal growth factor receptor EGFR	[29]
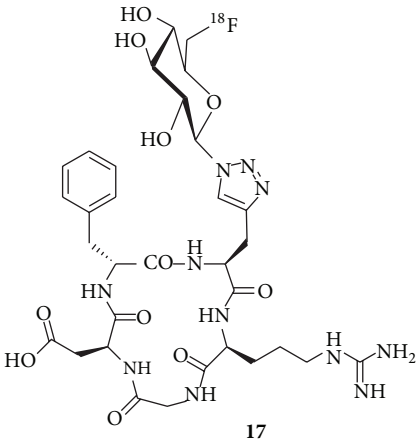 **17** 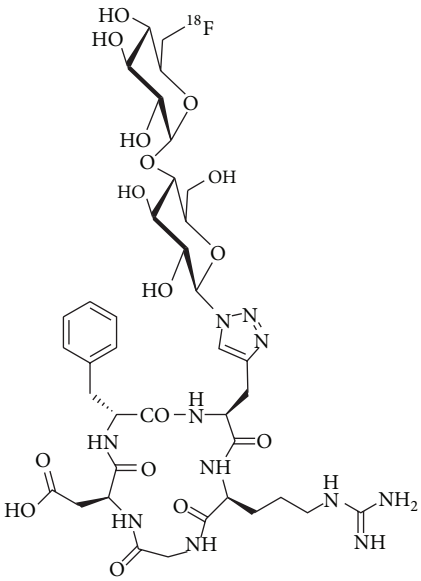 **18**	Integrin $\alpha_v\beta_3$	[30]

* Only the ^{19}F-compounds were synthesized.

In an approach toward the synthesis of selective PET ligands for the neurotensin receptor subtype-2 (NTS2), Held et al. synthesized a series of NT(8-13) peptide-peptoid hybrids with *N*-homo-Tyr instead of Tyr^{11} and variations of the original Arg^{8}-Arg^{9} leading to peptides with very high NTS2 affinity and selectivity over NTS1 [22]. The sequence *N*lys-Lys-Pro-*N*-homo-Tyr-Ile-Leu-OH was further derivatized at the *N*-terminus with propargylglycine making it suitable for CuAAC with 2-deoxy-2-fluoroglucopyranosyl azide and 6-deoxy-6-fluoroglucopyranosyl azide. Surprisingly, both analogues **7** and **8** showed a dramatic loss of NTS2 affinity compared to the nonglycosylated compound (110–290 nM versus 4 nM), rendering this approach for the development of NTS2-selective PET ligands unfavorable.

The ^{18}F-glycosylation via CuAAC was also transferred to the radiosyntheses of a couple of nonpeptidic compounds [23–29]. For the radiosynthesis of an ^{18}F-fluoroglycosylated folate derivative by Fischer et al., the intermediate 3,4,6-tri-*O*-acetyl-2-deoxy-2-[^{18}F]fluoroglucopyranosyl azide **2** was separated by solid phase extraction, excluding the HPLC purification [23]. After hydrolysis, the CuAAC with folate alkyne was performed in aqueous ethanol (38%) in the presence of $Cu(OAc)_2$ (1.2 mM) and sodium ascorbate (2.4 mM). After 15 min at 50°C the conversion was complete and the ^{18}F-labeled product was obtained after HPLC isolation in overall RCY of up to 25%, with a specific activity of 90 ± 38 GBq/μmol. Unfortunately, the authors did not provide any information on the amount of folate alkyne needed for the CuAAC reaction. The stability of [^{18}F]FDG-folate **9** was analyzed in human serum and murine liver microsomes and did not reveal any defluorination or radioactive degradation products within 120 and 60 min, respectively, at 37°C. Analyses of plasma, urine, and liver tissue at 30 min postinjection (p.i.) in mice confirmed high tracer stability *in vivo*. In addition, biodistribution and small-animal PET studies were performed in nude mice bearing folate receptor- (FR-) expressing KB-tumors. High specific uptake and retention were found in the KB tumor and in all organs with known FR expression (i.e., kidneys and the salivary glands) from 30 to 90 min p.i. The blood clearance was fast, resulting in tumor-to-blood ratios of 36 ± 15 at 90 min p.i. Although the $\log D_{7.4}$ value of −4.2 indicated high hydrophilicity of the compound, a high nonspecific accumulation in liver and gall bladder was observed, possibly due to a carrier-mediated uptake of the folic acid derivative **9** into the hepatocytes.

Table 2: ^{18}F-Fluoroglycosylated imaging probes and ^{19}F-fluoroglycosyl derivatives (*) synthesized via oxime formation.

Structure	Target	Reference
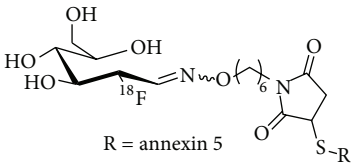 R = annexin 5 **23**	Apoptosis	[31]
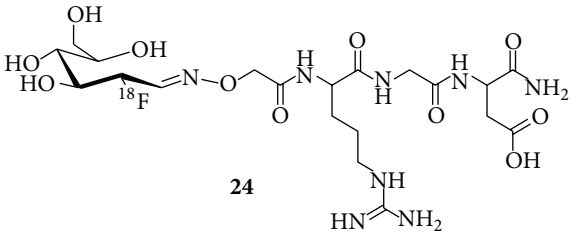 **24**	Integrin $\alpha_v\beta_3$	[32]
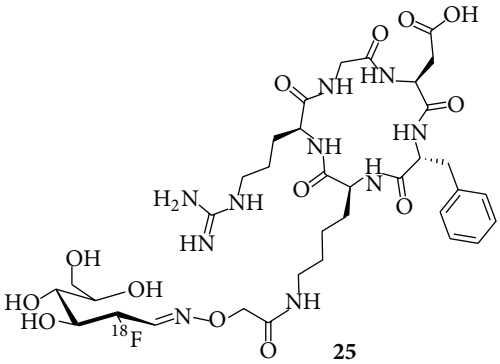 **25**	Integrin $\alpha_v\beta_3$	[33]
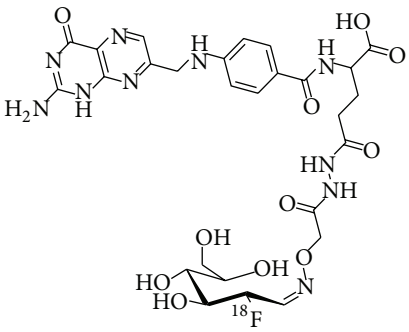 **26** 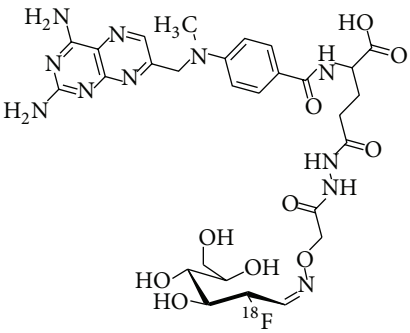 **27**	Folate receptor	[34]
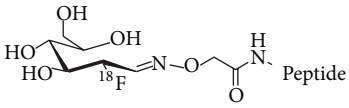 Peptide = NT (8–13); Glu – NT (8–13), NT (8–13) **28**; Glu – NT (8–13), Glu – NT (8–13), Glu – NT (8–13), NT (8–13)	Neurotensin receptor NTS-1	[35]

Table 2: Continued.

Structure	Target	Reference
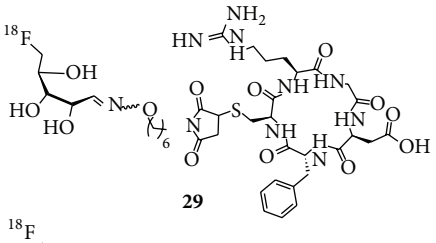 **29** 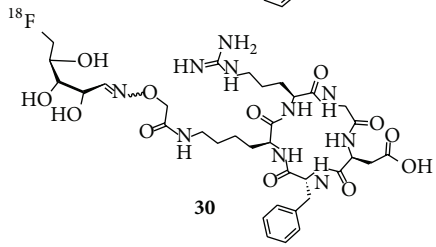 **30**	Integrin $\alpha_v\beta_3$	[36]
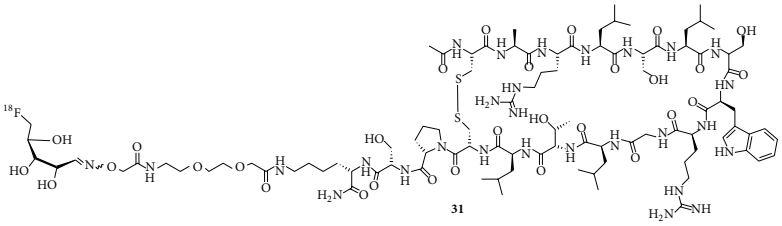 **31**	Vascular adhesion protein 1 (VAP-1)	[37]
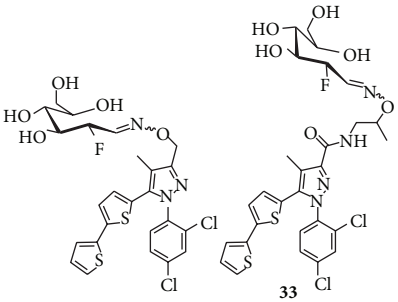 **32** **33** 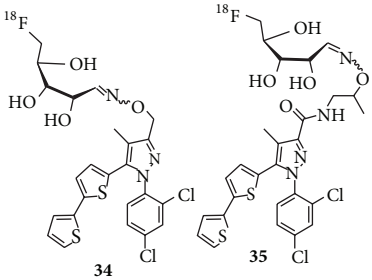 **34** **35**	Cannabinoid receptors CB1 and CB2*	[38]

*Only the ^{19}F compounds were synthesized.

Recently, an improved ^{18}F-fluoroglycosylated folate conjugate with an albumin binding entity has been reported by the same group [24]. This study aimed at the enhancement of the blood circulation time of the tracer by an albumin-binding moiety and hence improvement of the tumor-to-kidney ratio of the radiotracer uptake. The conjugate was radiolabelled via CuAAC using 2-deoxy-2-[^{18}F]fluoroglucopyranosyl azide **3** and the alkyne-functionalized folate precursor (2.2 mM) in the presence of $Cu(OAc)_2$ (1 mM) and sodium ascorbate (3 mM) in water/DMF (60 : 40) at 50°C for 15 min in a RCY of 15%. The HPLC separated product **10** was obtained in an overall RCY of only 1-2% after a total synthesis time of 3 h in specific activities of 20 to 50 GBq/μmol. Biodistribution and PET studies on KB tumor-bearing nude mice **10** revealed a slow blood clearance with uptake values of 2.2% ID/g at 4 h p.i., substantially high tumor uptake values

Table 3: ^{18}F-Glycoconjugates synthesized by miscellaneous ^{18}F-fluoroglycosylation.

Structure	Conjugation	Target	Reference
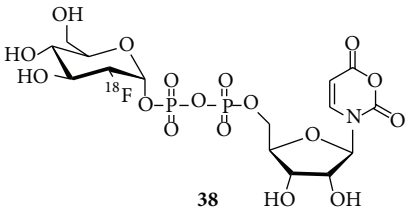 **38**	Enzymatic glycosylation	Glycosyltransferases	[39, 40]
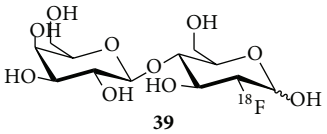 **39**	Enzymatic glycosylation	β-Galactosidase/LacZ gene	[41]
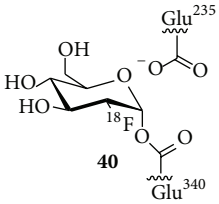 **40**	Enzymatic glycosylation	GCase	[42]
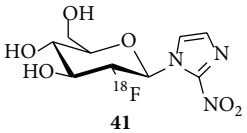 **41**	Lewis acid promoted N-glycosylation	Hypoxia	[43]
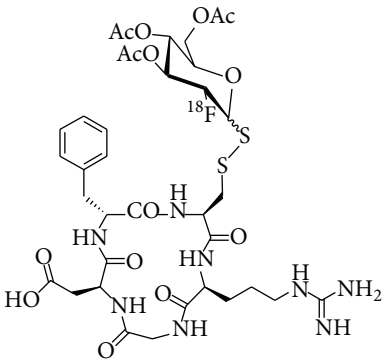 **42**	Thiol-selective S-glycosylation	Integrin $\alpha_v\beta_3$	[44]
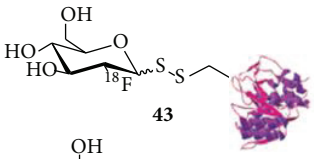 **43** 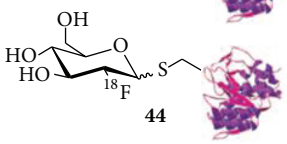 **44**	Thionation + site selective conjugation	Cys-containing proteins	[45]
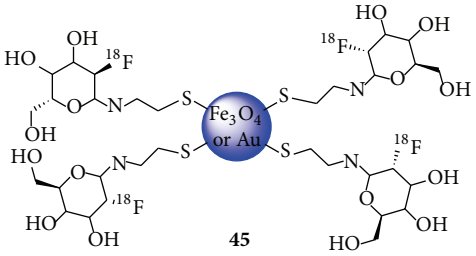 **45**		Breast cancer cells	[46, 47]

of 11–15% ID/g at 1–4 h p.i., and improved tumor-to-kidney ratios of about 1. Similar to the previously published folate **9** this albumin-binding tracer (**10**) also showed very high nonspecific uptake in the gall bladder.

A series of inhibitors for the matrix metalloproteinases (MMPs) MMP-2, MMP-8 MMP-9, and MMP-13 as tools for the visualization of activated MMPs with PET were developed by Hugenberg et al. [25]. Therefore, the hydroxamate-based lead structures CGS 27023A and CGS 25966 were triazole-substituted resulting in several mini-PEG-derivatized and glycosylated ligands. From all compounds the inhibition potencies were determined and $\log D_{7.4}$ values were calculated. The fluoroglycosylated compound displayed a $\log D_{7.4}$ of 0.58 and subnanomolar inhibition potencies (0.2–0.6 nM) for the various MMPs, rendering the corresponding ^{18}F-glycoconjugate a potential PET tracer candidate. However, the fluoroethyl-1,2,3-triazole derivative had a calculated $\log D_{7.4}$ of 1.53 and revealed outstanding inhibition potencies of 0.006–0.13 nM (for MMP-2, -8, -9, and -13), so this compound was chosen for radiolabeling and further studies.

An example where fluoroglycosylation leads to a complete loss of affinity was reported by Banerjee et al. [26]. In their search for subtype selective dopamine D4 receptor radioligands, a series of *N*-aryl piperazinyl methyl triazoles bearing fluorine-substituted appendages was synthesized and the target compounds were investigated for dopamine and serotonin receptor binding. With the aim of biasing the hydrophilicity and optimizing the D4 receptor affinity and selectivity, a concise series of triazoles containing fluoroalkyl, fluoroalkoxy, fluoroalkoxyphenyl, and deoxyfluoroglucosyl substituents was studied. The glycosylated compounds **12** and **13** had low calculated $\log P$ values of about 0, but affinities for the D4 receptor of 500 nM and 340 nM, respectively, which are 100 and 66 times lower when compared to the fluoropropoxyphenyl compound (5.1 nM) which had the highest affinity for D4 in this series.

The ^{18}F-fluoroglycosylation by CuAAC was also used for the radiosynthesis of an ET_A receptor (ET_AR) ligand [27]. Therefore the fluoroglycosyl moiety was introduced into the lead compound PD156707 as a hydrophilic building block. For the radiosynthesis of the glycoconjugate (**14**), the appropriate alkyne (0.6 mM) was allowed to react with ^{18}F-glucosyl azide **3** in saline/ethanol (3 : 2, v/v) in the presence of sodium ascorbate (12 mM) and $CuSO_4$ (4 mM), providing **14** in high non-decay-corrected yields (20–25%, 70 min) and a specific activity of 41–138 GBq/μmol. The triazolyl conjugated fluoroglucosyl derivative had high selectivity for ET_AR (4.5 nM) over ET_BR (1.2 μM). The high metabolic stability of the glycoconjugate was demonstrated by HPLC analysis of extracts from mouse blood and gall bladder collected at 60 min p.i. Biodistribution studies on K1 tumor-bearing nude mice revealed **14** to have fast blood clearance, low uptake in the kidneys and liver, but a very high uptake in the bile and intestines. This indicates that despite glycosylation the tracer is predominantly excreted via hepatobiliary clearance, a finding in accordance with previously studied ^{18}F-derivatives of PD 156707.

The radiosynthesis of a diarylpyrazole glycoconjugate, derived from the potent NTS1 antagonist SR142948A, was also successfully performed by the click ^{18}F-fluoroglycosylation using the CuAAC reaction [28]. This nonpeptidic NTS1 ligand was achieved by allowing **3** to react with the alkyne-bearing diarylpyrazole precursor (0.3 mM) in saline/tetrahydrofuran (3 : 4, v/v) for 10 min at 60°C. The ^{18}F-fluoroglycosylation proceeded in a total synthesis time of 70 min, and the ^{18}F-glycoconjugate (**15**) was obtained in a non-decay-corrected yield of 20 ± 3% and a specific activity of 35–74 GBq/μmol. The $\log D_{7.4}$ was determined to be −0.24. The glycoconjugate **15** displayed excellent affinity toward NTS1 (K_i = 1 nM) and substantial stability *in vivo*. Biodistribution and PET studies in nude mice bearing NTS1-expressing HT29 tumors demonstrated excellent tumor retention with an uptake of 0.84% ID/g at 10 min p.i. and 0.74% ID/g at 60 min p.i. and fast clearance from blood and all other organs resulting in a tumor-to-blood ratio rapidly increasing from 0.3 to 4.4 from 10 to 60 min p.i.

In a study reported by Pisaneschi et al. 2-deoxy-2-[^{18}F]fluoroglucopyranosyl azide **3** was used for the radiosynthesis of a new ^{18}F-fluoroglycosylated cyanoquinoline for PET imaging of epidermal growth factor receptor (EGFR) [29]. In this study **3** was not isolated by HPLC, but only separated via SPE. Subsequently, the CuAAC was performed with the alkyne precursor (3 mM) in a mixture of PBS/acetonitrile (96 : 4, v/v) in the presence of $CuSO_4$ (10 mM), sodium ascorbate (66 mM), and bathophenanthroline disulfonic acid disodium salt (BPDS) (6.7 mM), as an additive to stabilize Cu(I) oxidation state, at room temperature for 5 min in the RCY of about 50%. The final ^{18}F-labeled glycoconjugate **16** was isolated by semipreparative HPLC and obtained in 9% non-decay-corrected yield (starting from [^{18}F]fluoride) after a total synthesis time of 90 min with a specific activity of 7.3 GBq/μmol. **16** was tested *in vitro* in a cellular uptake experiment using A431 cells, harbouring high EGFR expression, in comparison with low EGFR-expressing MCF7 cells, demonstrating selective uptake in EGFR-positive cells.

Very recently, the reliability and robustness of the above described ^{18}F-fluoroglycosylation strategy prompted us to extend the series of ^{18}F-fluoroglycosyl azides by introducing 6-deoxy-6-[^{18}F]fluoroglucopyranosyl azide and 6′-deoxy-6′-[^{18}F]fluoromaltosyl azide (Scheme 2) [30]. Both compounds were synthesized from their corresponding peracetylated 6-tosylate precursors **19** and **21** in high RCY of 84% and 61%, respectively. The acetylated intermediates were isolated by HPLC and subsequently hydrolyzed with NaOH (60 mM) to give the "clickable" glycosyl azides **20** and **22**. The CuAAC was performed with alkyne-bearing RGD-peptide c(RGDfPra) (0.3 mM) in saline/ethanol in the presence of $CuSO_4$ (4 mM), sodium ascorbate (10 mM) at 60°C for 15–20 min. The RCY of this step was about 80% for both [^{18}F]fluoroglycosyl derivatives **17** and **18** with specific activities of 50–200 GBq/μmol; the overall yield was 16–24% (non-decay-corrected, starting from [^{18}F]fluoride) within a total synthesis time of 70–75 min. Both ^{18}F-glycopeptides **17** and **18** (abbreviated by [^{18}F]6Glc-RGD and [^{18}F]Mlt-RGD, [30]) were studied *in vivo*

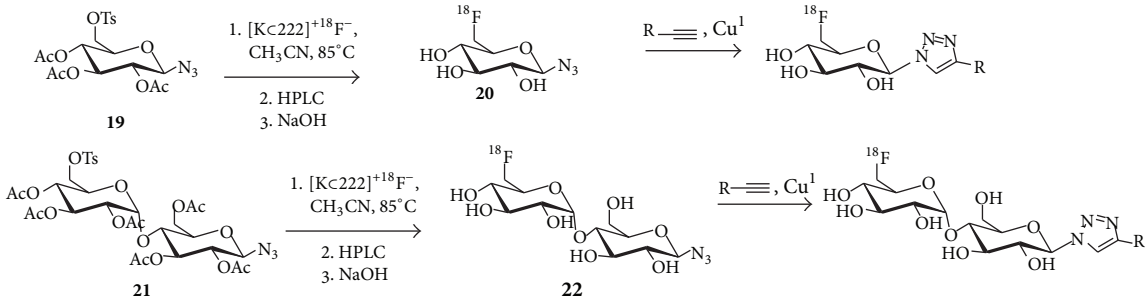

Scheme 2: General reaction scheme for ^{18}F-fluoroglycosylation via CuAAC using 6-deoxy-6-[^{18}F]fluoroglucopyranosyl azide **20** and 6′-deoxy-6′-[^{18}F]fluoromaltosyl azide **22**; a recent example for the alkyne is cyclic peptide c(RGDfPra), as reported by Maschauer et al. [30].

using U87MG tumor-bearing nude mice and compared to the previously published 2-deoxy-2-[^{18}F]fluoroglucopyranosyl RGD derivative **4** ([^{18}F]2Glc-RGD, [19]). It was observed that [^{18}F]6Glc-RGD (**17**) and [^{18}F]Mlt-RGD (**18**) showed significantly decreased liver and kidney uptake relative to [^{18}F]2Glc-RGD (**4**). More importantly, [^{18}F]Mlt-RGD (**18**) revealed substantial tumor uptake and high retention in the U87MG tumors comparable to that of [^{18}F]galacto-RGD [14, 52], resulting in tumor-to-kidney ratios comparable with some dimeric RGD peptides [53, 54]. Its favorable biodistribution together with excellent clearance properties *in vivo* makes [^{18}F]Mlt-RGD (**18**) a viable alternative PET tracer for imaging integrin expression.

3. ^{18}F-Fluoroglycosylation via Oxime Formation

The principle advantages of oxime formation by click reaction between an aminooxy- and a carbonyl functionality for ^{18}F-fluoroglycosylation are its high chemoselectivity, the use of unprotected aminooxy precursors, and the fact that coupling with the carbonyl component can be performed in aqueous media (pH 4–7). The formed oxime occurs in E- and Z-form in solution, both being stable under physiological conditions. The resulting E/Z isomeric ratio of an oxime depends on the size of substitutes at the C=N double bond. However, as the two isomers equilibrate very quickly in solution, the E- and Z-forms are usually not isolated from each other, but collectively considered as one compound.

[^{18}F]FDG can be used for a fluoroglycosylation reaction by oxime formation, because in aqueous solutions it undergoes mutarotation; that is, [^{18}F]FDG isomerizes between the α- and β-anomer through the intermediate acyclic aldehyde (Scheme 3). The mutarotation equilibrium is sometimes described to be favored at high temperatures (80–120°C) and to be more efficient at acidic pH (1.5–2.5) [32, 33, 35]. This is a drawback when using large peptides which can undergo degradation under such high temperatures and acidic conditions. The use of 5-[^{18}F]fluoro-5-deoxyribose ([^{18}F]FDR) (Scheme 4) could compensate for these limitations because the location of the fluorine at C-5 of the 5-membered ring might facilitate the formation of the acyclic form of [^{18}F]FDR making it possible to perform the oxime formation at room temperature at pH 6.0 with high yields [37].

An approach to use [^{18}F]FDG not for direct radiolabeling but for the preparation of a maleimidehexyloxime prosthetic group ([^{18}F]FDG-MHO) for the chemoselective ^{18}F-labeling of thiol-containing peptides and proteins was reported in 2008 by Wuest et al. [31]. [^{18}F]FDG-MHO was prepared by conjugation of [^{18}F]FDG with aminooxymaleimide hydrochloride (40 mM) in saline/ethanol (1 : 5) at 100°C for 15 min. After HPLC isolation, [^{18}F]FDG-MHO was obtained in 42% RCY (based upon [^{18}F]FDG) in a synthesis time of 45 min. The conjugation with the 36 kDa, single thiol group-containing protein annexin-V was performed in tris-buffer (pH 7.4)/ethanol (1 : 5, v/v) at room temperature for 30 min. Using only low amount of the protein (22 μM), [^{18}F]FDG-MHO-anxA5 (**23**) was obtained after size-exclusion chromatography in RCY of 43–58% (based upon [^{18}F]FDG-MHO) within 60 min and in specific activities of 2–4 GBq/μmol.

The first studies using [^{18}F]FDG as prosthetic group for the direct labeling of aminooxy-functionalized peptides were published in 2009 from two different groups [32, 33]. The group of Gambhir reported the synthesis of an ^{18}F-labeled linear RGD peptide ([^{18}F]FDG-RGD, **24**) and a cyclic RGD peptide ([^{18}F]FDG-cyclo(RGDyK)) as the first examples for the use of [^{18}F]FDG in the oxime formation with aminooxy-peptides [32]. They prepared [^{18}F]FDG-RGD (**24**) and [^{18}F]FDG-cyclo(RGDyK) within 60–70 min in 27.5% and 41% overall RCY (based on [^{18}F]FDG), respectively. [^{18}F]FDG was allowed to react with aminooxy-functionalised RGD (48 mM) or aminooxy-functionalised c(RGDyK) (24 mM) in TFA (0.4%) in saline or TFA (0.4%)/ethanol (16%) in saline at 100°C for 30 or 45 min, respectively. They found that under these experimental conditions maximum RCY was obtained at pH values of 1.5–2.5. When the reaction was performed at pH 4 in ammonium acetate buffer, no significant products were produced. Both ^{18}F-labeled glycopeptides were isolated by radio-HPLC and used for small-animal PET studies with U87MG-xenografted nude mice. At 120 min p.i. the uptake of **24** in the U87MG tumor was quite low (0.3% ID/g), whereas the uptake in heart was very high (3.7% ID/g). [^{18}F]FDG-cyclo(RGDyK) showed

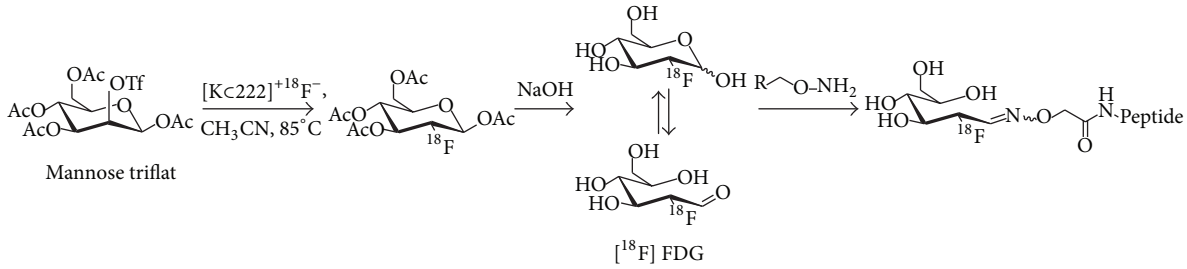

Scheme 3: General reaction scheme for ^{18}F-fluoroglycosylation via oxime formation using [^{18}F]FDG.

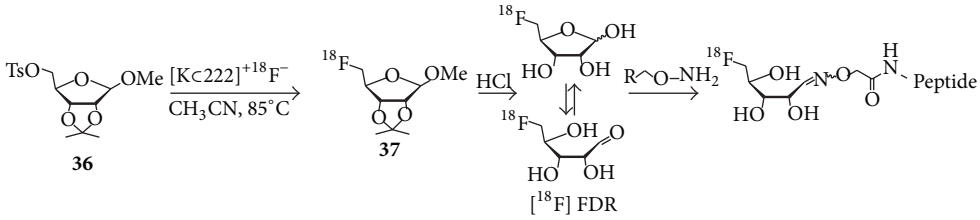

Scheme 4: General reaction scheme for ^{18}F-fluoroglycosylation via oxime formation using [^{18}F]FDR.

increasing uptake in the kidneys (4.7–12% ID/g) and in the tumor (0.6–1.5% ID/g) over time (30–120 min) with tumor-to-blood ratios of only 3 after 120 min. Unfortunately, the authors did not provide any information on the specific activity of the ^{18}F-labeled glycopeptides.

Simultaneously, the use of [^{18}F]FDG in oxime formation with peptide derivatives was published by Hultsch et al. [33]. They found that the use of clinical grade [^{18}F]FDG containing about 200 μg/mL glucose did not allow the radiosynthesis of [^{18}F]FDG-RGD (**25**) in sufficient yield. The use of a small volume of [^{18}F]FDG (37 MBq) corresponding to a molar ratio of peptide to D-glucose in the reaction mixture of approximately 40 and a concentration of the aminooxy-functionalized peptide of 35–50 mM leads to a high RCY of 73% for the oxime formation of **25**; however, this procedure is restricted to maximal yields of only 37 MBq. When using a 10 times larger volume of [^{18}F]FDG (370 MBq) corresponding to a peptide-to-glucose ratio of 4 and a peptide concentration of 4-5 mM, almost no RCY was obtained. Instead, the nearly exclusive formation of the nonradioactive D-glucose-RGD oxime conjugate was observed. Therefore, n.c.a. [^{18}F]FDG was produced by separation of the clinical grade [^{18}F]FDG from excess glucose by radio-HPLC. Following this strategy, the conjugation of n.c.a. [^{18}F]FDG with Boc-protected aminooxyacetyl-conjugated c(RGDfK) (5 mM) was performed in DMSO/HCl (3 mM) (1 : 9, pH 2.5) at 130°C for 20 min, successfully leading to the oxime-coupled **25** in RCY of 56–93%. Noteworthy, the Boc-protective group was removed thermolytically during the radiolabeling reaction. Finally, the ^{18}F-labeled RGD glycopeptide **25** was studied in M21 tumor-bearing nude mice at 120 min p.i. Compared to **24** [32], this [^{18}F]FDG-RGD (**25**) also showed a relatively high accumulation in the heart (0.9% ID/g) and a high uptake in the tumor (2.2% ID/g) with an excellent tumor-to-blood-ratio of 18.

Al Jammaz et al. used [^{18}F]FDG as a building block for the radiosynthesis of folate and methotrexate carbohydrazide conjugates **26** and **27** [34]. The respective aminooxy-functionalized precursors (9 mM) were used in DMSO/1% acetic acid/methanol (1 : 1, v/v, pH ~4.5) at 60°C for 10–15 min. After workup using solid phase extraction (SPE) the product conjugates **26** and **27** were obtained in overall RCY of greater than 80% (based on starting [^{18}F]FDG), with total syntheses times of approximately 20 min and in specific activities of greater than 9 GBq/μmol. The ^{18}F-fluoroglycosylation resulted in folate (**26**) and methotrexate carbohydrazide (**27**) conjugates with log P values of −1.5 and −1.6, respectively. Both glycoconjugates were stable in human serum *in vitro* at 37°C for at least 4 hours. Binding affinities to folate receptor-positive KB cells revealed binding characteristics which were superior to binding affinities obtained for the same compounds labeled with radiofluorinated benzene and pyridine prosthetic groups and are comparable to that of native folic acid (K_d (**26**) = 1.8 nM and K_d (**27**) = 4.7 nM). In *in vivo* studies using KB tumor-bearing nude mice **26** showed a favorable biodistribution profile with low uptake in intestine, liver, and kidney, rapid clearance from the blood, and high specific uptake in the tumor, resulting in tumor-to-blood and tumor-to-muscle ratios of 11.07 and 9.22, respectively.

[^{18}F]FDG has also been used for the ^{18}F-fluoroglycosylation of multimeric peptides applying the oxime formation strategy [35]. In this study, monomeric, dimeric, and tetrameric neurotensin (8-13) was aminooxy-functionalized and coupled to [^{18}F]FDG in methanol/water (2 : 1, v/v).

After 30 min at 80°C the RCY was 63% or 80% when using 3 mM or 7.5 mM peptide, respectively. A decreased RCY of 15% and 88% was achieved when using 1.4 mM or 4 mM of the dimeric neurotensin (8-13) derivative. With the tetrameric derivative only low RCY of 5–8% were achieved, probably due to the very low concentration of the aminooxy-functionalized peptide (0.7–2 mM). The monomeric labeling product could be separated from [^{18}F]FDG by radio-HPLC; however, the authors did not give any information on the specific activity of the final ^{18}F-labeled glycopeptide.

In the endeavor to improve the oxime conjugation step, 5-[^{18}F]fluoro-5-deoxyribose ([^{18}F]FDR) has been considered as an alternative prosthetic group (Scheme 4) [36, 37, 55, 56]. The idea is that, in comparison to [^{18}F]FDG, the 5-membered ring sugar [^{18}F]FDR with the fluorine at C-5 instead of C-6 favors the ring opening of the sugar to the aldehydic form and therefore promotes the oxime ligation with aminooxy-functionalized peptides even under mild reaction conditions, such as ambient temperature and less acidic pH of 4.6.

[^{18}F]FDR has been synthesized starting from methyl 2,3-*O*-isopropylidene-5-*O*-(*p*-toluenesulfonyl)-β-D-ribofuranoside (**36**, Scheme 4) using standard kryptate-based ^{18}F-labeling conditions. After HPLC isolation, which turned out to be essential for separation of free ribose from the ^{18}F-labeled product, the resulting methyl 2,3-*O*-isopropylidene-5-deoxy-5-[^{18}F]fluororibofuranoside (**37**, Scheme 4) is hydrolyzed with aqueous HCl and purified by solid phase extraction. The average RCY for [^{18}F]FDR is about 35% and the radiosynthesis takes 85 min [37, 55]. This ribose-free sugar was used for the conjugation of the two aminooxy-functionalized RGD peptides c(RGDfK) and c(RGDfC) [36], which were conjugated at room temperature in sodium acetate buffer at pH 4.6. With a peptide concentration of 10 mM the achieved RCY were 65–92% after 15 min. The radiolabeled products **29** and **30** were purified by radio-HPLC; however, the specific activity of the final ^{18}F-glycopeptide was not reported. Cell binding experiments were performed, revealing specific binding of **29** and **30** to $\alpha_v\beta_3$-expressing PC3 cells.

Moreover, the ^{18}F-fluoroglycosylation by the use of [^{18}F]FDR was also demonstrated using sialic acid-binding Ig-like lectin 9 (siglec-9) [37]. Siglec-9 is peptide targeting vascular adhesion protein 1 (VAP-1) which is a unique target in inflammatory processes. Performing the oxime formation reaction with [^{18}F]FDR in sodium acetate buffer (pH 4.6, 90 mM) at room temperature, the peptide concentration required for an adequate RCY was 15 mM, which was not applicable in the case of a 2 kDa peptide. Applying an anilinium buffer (pH 4.6) instead, the required peptide concentration could be reduced to 0.3 mM and the conversion at room temperature was 50–60% after 10 min. The ^{18}F-labeled glycopeptide [^{18}F]FDR-Siglec-9 (**31**) was isolated by HPLC and was prepared in a total synthesis time of 120 minutes in an overall RCY of about 27% (referred to [^{18}F]fluoride at EOB) with specific activities of 36–43 GBq/μmol. Finally, Li et al. showed that **31** was suitable for the visualization of the inflammation focus in rats with turpentine oil induced inflammation.

Another approach using [^{18}F]FDG and [^{18}F]FDR for oxime formation with target molecules aimed at the synthesis of cannabinoid ligands for PET imaging of the cannabinoid receptors 1 (CB1) and 2 (CB2) [38]. Therefore, hydroxylamine-functionalized Rimonabant-type pyrazoles were conjugated to [^{19}F]FDG and [^{19}F]FDR and affinities for the CB1 and CB2 receptors were determined. In this study, FDR proved to be superior to FDG conjugation, as the conjugation occurred under milder conditions and at higher reaction rate (room temperature, 20 min versus 100°C, 30 min). Compared to NESS125A, which was used as lead structure, the resulting fluoroglycosylated ligands **32**–**35** showed only weak affinities to CB1 (540–720 nM) and CB2 (310–1400 nM) and low subtype-selectivity (CB2 : CB1 = 0.7–2). Thus, the ^{18}F-radiosyntheses of these compounds were not performed by the authors.

4. Miscellaneous ^{18}F-Fluoroglycosylation Reactions

The first study dealing with the idea of using [^{18}F]FDG as ^{18}F-fluoroglycosylating agent was reported by Prante et al. in 1999 [39] aiming at a highly selective and mild ^{18}F-labeling method of biomolecules by enzymatic ^{18}F-fluoroglycosylation. The authors succeeded in the radiosynthesis of UDP-2-deoxy-2-[^{18}F]fluoro-α-D-glucopyranose (UDP-[^{18}F]FDG, **38**) as a substrate for glycosyltransferases. The radiosynthesis started from 1,3,4,6-tetra-*O*-acetyl-2-deoxy-2-[^{18}F]fluoroglucopyranose as an easily available intermediate in the [^{18}F]FDG synthesis, which was converted to [^{18}F]FDG-1-phosphate by MacDonald phosphorylation and further allowed to react by enzymatic activation to obtain UDP-[^{18}F]FDG (**38**) in a RCY of 20% (based on [^{18}F]fluoride) after a total synthesis time of 110 min [40]. UDP-[^{18}F]FDG (**38**) was obtained in aqueous medium in the void volume of a solid phase cartridge for further glycosyltransferase-mediated reactions.

Bormans and Verbruggen used an enzymatic approach with an *in situ* glycosyl transfer reaction for the synthesis of 2′-[^{18}F]fluorodeoxylactose (**39**) [41]. They applied an enzymatic method starting from [^{18}F]FDG in a mixture of $MnSO_4$, α-lactalbumin, galactosyltransferase, and UDP-galactose in HEPES buffer (pH 7.5) at 37°C for 3 h, providing 2′-[^{18}F]fluorodeoxylactose after HPLC isolation in a RCY of 3.4%. To evaluate its usefulness for *in vivo* visualization of LacZ gene expression biodistribution studies were performed in normal mice and in Rosa-26 mice that express bacterial LacZ in most of their tissues. **39** was cleared by urinary excretion and was not retained in any particular organ, neither in normal nor in Rosa-26 mice, suggesting that **39** is not able to cross the cell membrane.

Phenix et al. used an analogue of [^{18}F]FDG in an enzymatic approach for tagging acid β-glucocerebrosidase (GCase), a recombinant enzyme formulated in Cerezyme which is used to treat Gaucher disease [42]. In this innovative method 2,4-dinitrophenyl-2-deoxy-[^{18}F]-2-fluoro-β-D-glucopyranoside (β-DNP-[^{18}F]FDG) is formed from [^{18}F]FDG and 1-fluoro-2,4-dinitrobenzene in aqueous

$NaHCO_3$/ethanol (1 : 1, v/v) in a one-step reaction at 37°C yielding the ^{18}F-labeled product in 85% RCY after 10 min. β-DNP-[^{18}F]FDG was isolated by HPLC and the enzymatic approach was evaluated with the test-enzyme β-glucosidase from *Agrobacterium* sp. as well as with the therapeutically relevant enzyme GCase. ^{18}F-labeling of glucosidase from *Agrobacterium* sp. proceeded within a few minutes in high RCY, whereas ^{18}F-labeling of GCase was hampered by the much higher K_i value. ^{18}F-labeled GCase (**40**) was obtained in a total synthesis time of about 2.5 h in a specific activity of ~2 GBq/μmol and was used to monitor the biodistribution of GCase in mice. The highest uptake was observed in macrophage-rich organs, such as the liver and spleen, as well as in the gall bladder, kidneys, intestines, heart, and femur, indicating elimination of **40** through renal and hepatobiliary routes. Almost no radioactivity was detected in the brain indicating high stability of ^{18}F-Glc-GCase (**40**) as enzymatic turnover or proteolytic degradation would result in free [^{18}F]FDG which would show high uptake in the brain. The biodistribution and PET imaging studies on animals revealed that ^{18}F-labeled GCase (**40**) is a powerful tool for monitoring the enzyme distribution and tissue half-life *in vivo* by PET with an immediate clinical application to Gaucher disease. The authors conclude that the ^{18}F-labeling method, starting from [^{18}F]FDG, could be adapted to alternative enzymes, opening the path for application to a variety of enzyme replacement therapies.

In one of the earlier studies on ^{18}F-fluoroglycosylation reactions, the radiosynthesis of a new carbohydrate-conjugated 2-nitroimidazole derivative starting from peracetylated [^{18}F]FDG as potential agent for tracking hypoxic tissues was reported by Patt et al. [43]. Peracetylated [^{18}F]FDG was isolated by semipreparative HPLC and then allowed to react with 2-nitroimidazole (88 mM) in the presence of $Hg(CN)_2$ and $SnCl_4$ in acetonitrile at 70°C for 60 min to give the ^{18}F-labeled product in high RCY of 80%. After a second HPLC isolation and Zemplén deacetylation [57] with sodium methylate in methanol the glucose derivative **41** was subjected to cell uptake experiments *in vitro* and biodistribution studies in tumor-bearing rats. However, the uptake of the ^{18}F-glucosylated nitroimidazole **41** in cells under normoxic conditions was very low (0.1-0.2%) and the *in vivo* data did not indicate significant tumor uptake, rendering this radiotracer unsuitable for the detection of hypoxic tissues *in vivo* by PET.

A thiol-reactive ^{18}F-glucosyl derivative for the site-specific ^{18}F-fluoroglycosylation of peptides was developed by Prante et al. [44], applying the chemoselective thiol substitution reaction of mixed thiols. Aiming at the synthesis of ^{18}F-labeled glycosyl thiosulfonates as a "mixed thiol" analog, peracetylated [^{18}F]FDG was isolated by HPLC and converted to the corresponding bromide [58, 59] and subsequently allowed to react to the 1-phenylthiosulfonate using sodium phenylthiosulfonate (NaPTS) and tetrabutylammonium bromide in acetonitrile/DMF (4 : 1, v/v). Ac_3[^{18}F]FGlc-PTS was obtained in a RCY of 33% in a synthesis time of 90 min (related to [^{18}F]fluoride) which was further used for the chemoselective ^{18}F-fluoroglycosylation of thiols, that is, the model peptide CAKAY and the thiol-bearing cyclo-RGD peptide c(RGDfC). The ^{18}F-fluoroglycosylation proceeded chemoselectively with 1 mM peptide in tris-buffer (pH 7.7)/acetonitrile (4 : 1, v/v) at room temperature and in high RCY of >90% after 15 min. The total radiosynthesis, including the preparation of the ^{18}F-fluoroglycosylating reagent Ac_3-[^{18}F]FGlc-PTS, peptide ligation, and final HPLC purification, provided a non-decay-corrected yield of 13% after 130 min. The stability of the ^{18}F-fluoroglycosylated RGD peptide **42** was verified in human serum *in vitro* showing no cleavage of the carbohydrate moiety for at least 90 min.

Transferring this method to the ^{18}F-fluoroglycosylation of proteins, an approach for site-specific conjugation of thiol-functionalized [^{18}F]fluorosugars to cysteine (Cys) or dehydroalanine (Dha, directly accessible from Cys) tagged proteins was reported by the Davis group [45]. Direct thionation of [^{18}F]FDG was achieved using Lawesson's reagent in 1,4-dioxane at 100°C during 45 min, resulting in the formation of 2-deoxy-2-[^{18}F]fluoro-1-thio-glucopyranose in 98% RCY. In a one-pot procedure 2-deoxy-2-[^{18}F]fluoro-1-thio-glucopyranose was directly used for mixed disulfide formation with a Cys-bearing protein (3 μM) or conjugate addition to a Dha-bearing protein (0.85 μM) in sodium phosphate buffer (pH 8.0) at room temperature or 37°C. The RCY for the site-specific labeling procedure were between 40 and 60% after 15 min. Starting from [^{18}F]FDG, SS- and S-linked 2-[^{18}F]fluoroglycoproteins **43** and **44** were synthesized in overall RCY of 55–60% after a total synthesis time of 90 min. The suitability of such ^{18}F-fluoroglycosylated proteins for the application as PET imaging agents still has to be shown.

In an attempt to synthesize a PET-MR hybrid imaging agent [^{18}F]FDG was conjugated to magnetic iron oxide nanoparticles (MNPs) [46]. The labeling precursor 3,4,6-tri-O-acetyl-2-*O*-trifluoromethanesulfonyl-(*N*-(2-mercaptoethyl))mannopyranosylamine was synthesized by reductive amination from the precursor 1,3,4,6-tetra-*O*-acetyl-2-*O*-trifluoromethanesulfonyl-β-D-mannopyranose (mannose triflate) with 2-aminoethanethiol. The ^{18}F-fluorination was performed using standard labeling conditions in DMF at 90°C for 20 min. SPE purified 2-deoxy-2-[^{18}F]fluoro-(*N*-(2-mercaptoethyl))-β-D-glucopyranosylamine was added to a $FeCl_3$ solution (25 mM), followed by $NaBH_4$ (1 M) at 60°C until pH 9 was reached. Black MNPs were formed in 2 h, which were separated from the mixture by a magnet. A similar attempt was performed by the same group for the radiosynthesis of [^{18}F]FDG conjugated gold nanoparticles **45** that were further conjugated to an anti-metadherin antibody for targeting breast cancer cells [47].

5. Conclusion

There are several methodologies to introduce an ^{18}F-fluoroglycosyl residue into a biomolecule. Besides enzymatic or thiol-selective reactions the most frequently used ones are the ^{18}F-fluoroglycosylation via CuAAC and via oxime formation. One drawback of the CuAAC supported glycosylation is

the fact that the labeling precursor 3,4,6-tri-*O*-acetyl-2-*O*-trifluoromethanesulfonyl-β-D-mannopyranosyl azide (**1**) is not commercially available and that its synthesis is challenging. This was circumvented by the development of the new and very easy to synthesize precursor 2,3,4-tri-*O*-acetyl-6-*O*-tosyl-glucopyranosyl azide **19** which has the additional advantage that, at least in the case of glycosylated RGD peptides [30], the resulting 6-deoxy-6-[^{18}F]fluoroglucosyl conjugates have favorable bioproperties compared to the 2-deoxy-2-[^{18}F]fluoroglucosyl derivatives.

The major advantage of the ^{18}F-fluoroglycosylation via oxime formation is the fact that widely available [^{18}F]FDG can be used; the limitations are the difficulties associated with the synthesis and stability of biomolecules containing aminooxy moieties and the harsh reaction conditions (high temperature, low pH) that are required for sufficient RCY. The use of [^{18}F]FDR needs much milder reaction conditions, but then the advantage of easy accessible [^{18}F]FDG is forfeited.

In conclusion, several examples published in the last few years have shown that ^{18}F-fluoroglycosylation is a powerful and highly valuable tool for the radiosynthesis of ^{18}F-glycoconjugates with suitable *in vivo* properties for PET imaging studies.

Conflict of Interests

The authors declare that there is no conflict of interests regarding the publication of this paper.

Acknowledgment

This work was supported by the Deutsche Forschungsgemeinschaft (DFG, Grants MA 4295/1-2).

References

[1] K. Hamacher, "Phase-transfer catalysed synthesis of 4-*S*-β-D-glucopyranosyl-4-thio-D-glucopyranose (thiocellobiose) and 2-*S*-β-D-glucopyranosyl-2-thio-D-glucopyranose (thiosophorose)," *Carbohydrate Research*, vol. 128, no. 2, pp. 291–295, 1984.

[2] K. Hamacher, H. H. Coenen, and G. Stöcklin, "Efficient stereospecific synthesis of no-carrier-added 2-[^{18}F]-fluoro-2-deoxy-D-glucose using aminopolyether supported nucleophilic substitution," *Journal of Nuclear Medicine*, vol. 27, no. 2, pp. 235–238, 1986.

[3] T. F. Massoud and S. S. Gambhir, "Molecular imaging in living subjects: seeing fundamental biological processes in a new light," *Genes & Development*, vol. 17, no. 5, pp. 545–580, 2003.

[4] S. M. Ametamey, M. Honer, and P. A. Schubiger, "Molecular imaging with PET," *Chemical Reviews*, vol. 108, no. 5, pp. 1501–1516, 2008.

[5] R. Schirrmacher, C. Wängler, and E. Schirrmacher, "Recent developments and trends in ^{18}F-radiochemistry: syntheses and applications," *Mini-Reviews in Organic Chemistry*, vol. 4, no. 4, pp. 317–329, 2007.

[6] H. H. Coenen, "Fluorine-18 labeling methods: features and possibilities of basic reactions," in *PET Chemistry*, vol. 64 of *Ernst Schering Research Foundation Workshop*, pp. 15–50, Springer, Berlin, Germany, 2007.

[7] C. Wängler, R. Schirrmacher, P. Bartenstein, and B. Wängler, "Click-chemistry reactions in radiopharmaceutical chemistry: fast & easy introduction of radiolabels into biomolecules for in vivo imaging," *Current Medicinal Chemistry*, vol. 17, no. 11, pp. 1092–1116, 2010.

[8] V. Bernard-Gauthier, C. Wängler, E. Schirrmacher et al., "^{18}F-labeled silicon-based fluoride acceptors-opportunities for novel positron emitting radiopharmaceuticals," *Biomed Research International*. In press.

[9] K. Kettenbach, H. Schieferstein, and T. Ross, "^{18}F-labeling using click cycloadditions," *Biomed Research International*. In press.

[10] J. Ermert, "^{18}F-labelled prosthetic groups and intermediates for build-up syntheses," *Biomed Research International*. In press.

[11] R. D. Egleton and T. P. Davis, "Development of neuropeptide drugs that cross the blood-brain barrier," *NeuroRx*, vol. 2, no. 1, pp. 44–53, 2005.

[12] R. Haubner, B. Kuhnast, C. Mang et al., "[^{18}F]-Galacto-RGD: synthesis, radiolabeling, metabolic stability, and radiation dose estimates," *Bioconjugate Chemistry*, vol. 15, no. 1, pp. 61–69, 2004.

[13] M. Schottelius, F. Rau, J. C. Reubi, M. Schwaiger, and H.-J. Wester, "Modulation of pharmacokinetics of radioiodinated sugar-conjugated somatostatin analogues by variation of peptide net charge and carbohydration chemistry," *Bioconjugate Chemistry*, vol. 16, no. 2, pp. 429–437, 2005.

[14] R. Haubner, H. J. Wester, W. A. Weber et al., "Noninvasive imaging of $\alpha_v\beta_3$ integrin expression using ^{18}F-labeled RGD-containing glycopeptide and positron emission tomography," *Cancer Research*, vol. 61, no. 5, pp. 1781–1785, 2001.

[15] M. Schottelius, H.-J. Wester, J. C. Reubi, R. Senekowitsch-Schmidtke, and M. Schwaiger, "Improvement of pharmacokinetics of radioiodinated Tyr^3-octreotide by conjugation with carbohydrates," *Bioconjugate Chemistry*, vol. 13, no. 5, pp. 1021–1030, 2002.

[16] H. J. Wester, M. Schottelius, K. Scheidhauer et al., "PET imaging of somatostatin receptors: design, synthesis and preclinical evaluation of a novel ^{18}F-labelled, carbohydrated analogue of octreotide," *European Journal of Nuclear Medicine and Molecular Imaging*, vol. 30, no. 1, pp. 117–122, 2003.

[17] H. C. Kolb, M. G. Finn, and K. B. Sharpless, "Click chemistry: diverse chemical function from a few good reactions," *Angewandte Chemie International Edition*, vol. 40, no. 11, pp. 2004–2021, 2001.

[18] Z. J. Witczak and R. Bielski, *Click Chemistry in Glycoscience: New Developments and Strategies*, John Wiley & Sons, New York, NY, USA, 2013.

[19] S. Maschauer, J. Einsiedel, R. Haubner et al., "Labeling and glycosylate of peptides using click chemistry: a general approach to ^{18}F-glycopeptides as effective imaging probes for positron emission tomography," *Angewandte Chemie—International Edition*, vol. 49, no. 5, pp. 976–979, 2010.

[20] S. Maschauer and O. Prante, "A series of 2-O-trifluoromethylsulfonyl-D-mannopyranosides as precursors for concomitant ^{18}F-labeling and glycosylation by click chemistry," *Carbohydrate Research*, vol. 344, no. 6, pp. 753–761, 2009.

[21] O. Boutureira, F. D'Hooge, M. Fernández-González et al., "Fluoroglycoproteins: ready chemical site-selective incorporation of fluorosugars into proteins," *Chemical Communications*, vol. 46, no. 43, pp. 8142–8144, 2010.

[22] C. Held, M. Plomer, H. Hübner, J. Meltretter, M. Pischetsrieder, and P. Gmeiner, "Development of a metabolically stable neurotensin receptor 2 (NTS2) ligand," *Chemmedchem*, vol. 8, no. 1, pp. 75–81, 2013.

[23] C. R. Fischer, C. Müller, J. Reber et al., "[^{18}F]-fluoro-deoxy-glucose folate: a novel PET radiotracer with improved in vivo properties for folate receptor targeting," *Bioconjugate Chemistry*, vol. 23, no. 4, pp. 805–813, 2012.

[24] C. R. Fischer, V. Groehn, J. Reber, R. Schibli, S. M. Ametamey, and C. Muller, "Improved PET imaging of tumors in mice using a novel ^{18}F-folate conjugate with an albumin-binding entity," *Molecular Imaging and Biology*, vol. 15, no. 6, pp. 649–654, 2013.

[25] V. Hugenberg, H.-J. Breyholz, B. Riemann et al., "A new class of highly potent matrix metalloproteinase inhibitors based on triazole-substituted hydroxamates: (radio)synthesis and in vitro and first in vivo evaluation," *Journal of Medicinal Chemistry*, vol. 55, no. 10, pp. 4714–4727, 2012.

[26] A. Banerjee, S. Maschauer, H. Hübner, P. Gmeiner, and O. Prante, "Click chemistry based synthesis of dopamine D4 selective receptor ligands for the selection of potential PET tracers," *Bioorganic & Medicinal Chemistry Letters*, vol. 23, no. 22, pp. 6079–6082, 2013.

[27] S. Maschauer, K. Michel, P. Tripal et al., "Synthesis and in vivo evaluation of an ^{18}F-labeled glycoconjugate of PD156707 for imaging ETA expression in thyroid carcinoma by positron emission tomography," *American Journal of Nuclear Medicine and Molecular Imaging*, vol. 3, no. 5, pp. 425–436, 2013.

[28] C. Lang, S. Maschauer, H. H. übner, P. Gmeiner, and O. Prante, "Synthesis and evaluation of a ^{18}F-labeled diarylpyrazole glycoconjugate for the imaging of NTS1-positive tumors," *Journal of Medicinal Chemistry*, vol. 56, no. 22, pp. 9361–9365, 2013.

[29] F. Pisaneschi, R. L. Slade, L. Iddon et al., "Synthesis of a new fluorine-18 glycosylated "click" cyanoquinoline for the imaging of epidermal growth factor receptor," *Journal of Labelled Compounds and Radiopharmaceuticals*, vol. 57, no. 2, pp. 92–96, 2014.

[30] S. Maschauer, R. Haubner, T. Kuwert, and O. Prante, "^{18}F-Glyco-RGD peptides for PET imaging of integrin expression: efficient radiosynthesis by click chemistry and modulation of biodistribution by glycosylation," *Molecular Pharmaceutics*, vol. 11, no. 2, pp. 505–515, 2014.

[31] F. Wuest, M. Berndt, R. Bergmann, J. D. Van Hoff, and J. Pietzsch, "Synthesis and application of [^{18}F]FDG-maleimide-hexyloxime ([^{18}F]FDG-MHO): a [^{18}F]FDG-based prosthetic group for the chemoselective ^{18}F-labeling of peptides and proteins," *Bioconjugate Chemistry*, vol. 19, no. 6, pp. 1202–1210, 2008.

[32] M. Namavari, Z. Cheng, R. Zhang et al., "A novel method for direct site-specific radiolabeling of peptides using [^{18}F]FDG," *Bioconjugate Chemistry*, vol. 20, no. 3, pp. 432–436, 2009.

[33] C. Hultsch, M. Schottelius, J. Auernheimer, A. Alke, and H.-J. Wester, "^{18}F-Fluoroglucosylation of peptides, exemplified on cyclo(RGDfK)," *European Journal of Nuclear Medicine and Molecular Imaging*, vol. 36, no. 9, pp. 1469–1474, 2009.

[34] I. Al Jammaz, B. Al-Otaibi, S. Amer, N. Al-Hokbany, and S. Okarvi, "Novel synthesis and preclinical evaluation of folic acid derivatives labeled with ^{18}F-FDG for PET imaging of folate receptor-positive tumors," *Nuclear Medicine and Biology*, vol. 39, no. 6, pp. 864–870, 2012.

[35] F. Wuest, C. Hultsch, M. Berndt, and R. Bergmann, "Direct labelling of peptides with 2-[^{18}F]fluoro-2-deoxy-d-glucose ([^{18}F]FDG)," *Bioorganic and Medicinal Chemistry Letters*, vol. 19, no. 18, pp. 5426–5428, 2009.

[36] S. Dall'Angelo, Q. Zhang, I. N. Fleming et al., "Efficient bioconjugation of 5-fluoro-5-deoxy-ribose (FDR) to RGD peptides for positron emission tomography (PET) imaging of $\alpha_v\beta_3$ integrin receptor," *Organic and Biomolecular Chemistry*, vol. 11, no. 27, pp. 4551–4558, 2013.

[37] X. -G. Li, A. Autio, H. Ahtinen et al., "Translating the concept of peptide labeling with 5-deoxy-5-[^{18}F]fluororibose into preclinical practice: ^{18}F-labeling of Siglec-9 peptide for PET imaging of inflammation," *Chemical Communications*, vol. 49, no. 35, pp. 3682–3684, 2013.

[38] S. Frau, S. Dall'Angelo, G. L. Baillie et al., "Pyrazole-type cannabinoid ligands conjugated with fluoro-deoxy-carbohydrates as potential PET-imaging agents: synthesis and CB1/CB2 receptor affinity evaluation," *Journal of Fluorine Chemistry*, vol. 152, pp. 166–172, 2013.

[39] O. Prante, K. Hamacher, and H. H. Coenen, "Chemo-enzymatic n.c.a. synthesis of the coenzyme uridine diphospho-2-deoxy-2-[^{18}F]fluoro-α-D-glucose," *Journal of Labelled Compounds and Radiopharmaceuticals*, vol. 42, no. 1, pp. S111–S112, 1999.

[40] O. Prante, K. Hamacher, and H. H. Coenen, "Chemoenzymatic n.c.a synthesis of the coenzyme UDP-2-deoxy-2-(^{18}F)fluoro-α-D-glucopyranose as substrate of glycosyltransferases," *Journal of Labelled Compounds and Radiopharmaceuticals*, vol. 50, no. 1, pp. 55–63, 2007.

[41] G. Bormans and A. Verbruggen, "Enzymatic synthesis and biodistribution in mice of β-O-D-galactopyranosyl-(1,4′)-2′-[^{18}F]fluoro-2′-deoxy-D-glucopyranose (2′-[^{18}F]fluorodeoxylactose)," *Journal of Labelled Compounds and Radiopharmaceuticals*, vol. 44, no. 6, pp. 417–423, 2001.

[42] C. P. Phenix, B. P. Rempel, K. Colobong et al., "Imaging of enzyme replacement therapy using PET," *Proceedings of the National Academy of Sciences of the United States of America*, vol. 107, no. 24, pp. 10842–10847, 2010.

[43] M. Patt, D. Sorger, M. Scheunemann, and G. Stöcklin, "Adduct of 2-[^{18}F]FDG and 2-nitroimidazole as a putative radiotracer for the detection of hypoxia with PET: synthesis, in vitro- and in vivo-characterization," *Applied Radiation and Isotopes*, vol. 57, no. 5, pp. 705–712, 2002.

[44] O. Prante, J. Einsiedel, R. Haubner et al., "3,4,6-Tri-O-acetyl-2-deoxy-2-[^{18}F]fluoroglucopyranosyl phenylthiosulfonate: a thiol-reactive agent for the chemoselective ^{18}F-glycosylation of peptides," *Bioconjugate Chemistry*, vol. 18, no. 1, pp. 254–262, 2007.

[45] O. Boutureira, G. J. L. Bernardes, F. D'Hooge, and B. G. Davis, "Direct radiolabelling of proteins at cysteine using [^{18}F]-fluorosugars," *Chemical Communications*, vol. 47, no. 36, pp. 10010–10012, 2011.

[46] F. Ozkaya, P. Unak, E. I. Medine, S. Sakarya, G. Unak, and S. Timur, "^{18}FDG conjugated magnetic nanoparticle probes: synthesis and in vitro investigations on MCF-7 breast cancer cells," *Journal of Radioanalytical and Nuclear Chemistry*, vol. 295, no. 3, pp. 1789–1796, 2013.

[47] G. Unak, F. Ozkaya, E. Ilker Medine et al., "Gold nanoparticle probes: design and in vitro applications in cancer cell culture," *Colloids and Surfaces B: Biointerfaces*, vol. 90, no. 1, pp. 217–226, 2012.

[48] V. V. Rostovtsev, L. G. Green, V. V. Fokin, and K. B. Sharpless, "A stepwise Huisgen cycloaddition process: copper(I)-catalyzed regioselective "ligation" of azides and terminal alkynes," *Angewandte Chemie International Edition*, vol. 41, no. 14, pp. 2596–2599, 2002.

[49] C. W. Tornøe, C. Christensen, and M. Meldal, "Peptidotriazoles on solid phase: [1,2,3]-triazoles by regiospecific copper(I)-catalyzed 1,3-dipolar cycloadditions of terminal alkynes to

azides," *Journal of Organic Chemistry*, vol. 67, no. 9, pp. 3057–3064, 2002.

[50] M. Pretze, D. Pietzsch, and C. Mamat, "Recent trends in bioorthogonal click-radiolabeling reactions using fluorine-18," *Molecules*, vol. 18, no. 7, pp. 8618–8665, 2013.

[51] L. Mirfeizi, L. Campbell-Verduyn, R. A. Dierckx, B. L. Feringa, and P. H. Elsinga, "Application of click chemistry for PET," *Current Organic Chemistry*, vol. 17, no. 19, pp. 2108–2118, 2013.

[52] S. Liu, Z. Liu, K. Chen et al., "^{18}F-labeled galacto and PEGylated RGD dimers for PET imaging of $\alpha_v\beta_3$ integrin expression," *Molecular Imaging and Biology*, vol. 12, no. 5, pp. 530–538, 2010.

[53] J. Guo, L. Lang, S. Hu et al., "Comparison of three dimeric ^{18}F-AlF-NOTA-RGD tracers," *Molecular Imaging and Biology*, vol. 16, no. 2, pp. 274–283, 2014.

[54] Y. Li, Z. Liu, J. Lozada et al., "Single step ^{18}F-labeling of dimeric cycloRGD for functional PET imaging of tumors in mice," *Nuclear Medicine and Biology*, vol. 40, no. 8, pp. 959–966, 2013.

[55] X. G. Li, S. Dall'Angelo, L. F. Schweiger, M. Zanda, and D. O. 'Hagan, "[^{18}F]-5-Fluoro-5-deoxyribose, an efficient peptide bioconjugation ligand for positron emission tomography (PET) imaging," *Chemical Communications*, vol. 48, no. 43, pp. 5247–5249, 2012.

[56] X. G. Li, K. Helariutta, A. Roivainen, S. Jalkanen, J. Knuuti, and A. J. Airaksinen, "Using 5-deoxy-5-[^{18}F]fluororibose to glycosylate peptides for positron emission tomography," *Nature Protocols*, vol. 9, no. 1, pp. 138–145, 2014.

[57] G. Zemplén and E. Pascu, "Über die Verseifung acetylierter Zucker und verwandter Substanzen," *Berichte der Deutschen Chemischen Gesellschaft (A und B Series)*, vol. 62, pp. 1613–1618, 1929.

[58] S. Maschauer, T. Kuwert, and O. Prante, "^{18}F-glycosylation using Koenigs-Knorr conditions: a comparative study," *Journal of Labelled Compounds and Radiopharmaceuticals*, vol. 49, no. 2, pp. 101–108, 2006.

[59] S. Maschauer, M. Pischetsrieder, T. Kuwert, and O. Prante, "Utility of 1,3,4,6-tetra-O-acetyl-2-deoxy-2-[^{18}F]fluoroglucopyranoside for no-carrier-added ^{18}F-glycosylation of amino acids," *Journal of Labelled Compounds and Radiopharmaceuticals*, vol. 48, no. 10, pp. 701–719, 2005.

Hindawi Publishing Corporation
BioMed Research International
Volume 2014, Article ID 674063, 12 pages
http://dx.doi.org/10.1155/2014/674063

Review Article

6-[^{18}F]Fluoro-L-DOPA: A Well-Established Neurotracer with Expanding Application Spectrum and Strongly Improved Radiosyntheses

M. Pretze,[1] C. Wängler,[2] and B. Wängler[1]

[1] *Molecular Imaging and Radiochemistry, Department of Clinical Radiology and Nuclear Medicine, Medical Faculty Mannheim of Heidelberg University, Theodor-Kutzer-Ufer 1-3, 68167 Mannheim, Germany*
[2] *Biomedical Chemistry, Department of Clinical Radiology and Nuclear Medicine, Medical Faculty Mannheim of Heidelberg University, 68167 Mannheim, Germany*

Correspondence should be addressed to B. Wängler; bjoern.waengler@medma.uni-heidelberg.de

Received 26 February 2014; Revised 17 April 2014; Accepted 18 April 2014; Published 28 May 2014

Academic Editor: Olaf Prante

For many years, the main application of [^{18}F]F-DOPA has been the PET imaging of neuropsychiatric diseases, movement disorders, and brain malignancies. Recent findings however point to very favorable results of this tracer for the imaging of other malignant diseases such as neuroendocrine tumors, pheochromocytoma, and pancreatic adenocarcinoma expanding its application spectrum. With the application of this tracer in neuroendocrine tumor imaging, improved radiosyntheses have been developed. Among these, the no-carrier-added nucleophilic introduction of fluorine-18, especially, has gained increasing attention as it gives [^{18}F]F-DOPA in higher specific activities and shorter reaction times by less intricate synthesis protocols. The nucleophilic syntheses which were developed recently are able to provide [^{18}F]F-DOPA by automated syntheses in very high specific activities, radiochemical yields, and enantiomeric purities. This review summarizes the developments in the field of [^{18}F]F-DOPA syntheses using electrophilic synthesis pathways as well as recent developments of nucleophilic syntheses of [^{18}F]F-DOPA and compares the different synthesis strategies regarding the accessibility and applicability of the products for human *in vivo* PET tumor imaging.

1. Introduction

The ^{18}F-radiolabeled nonproteinogenic amino acid 3,4-dihydroxy-6-[^{18}F]fluoro-L-phenylalanine ([^{18}F]F-DOPA) (Figure 1) has been used for over 30 years to image the presynaptic dopaminergic system in the human brain in order to investigate a number of CNS disorders, in particular schizophrenia [1, 2] and Parkinson's disease with positron emission tomography (PET) [3, 4]. As DOPA is the precursor of the neurotransmitter dopamine, the extent of accumulation of [^{18}F]F-DOPA in the brain reflects the functional integrity of the presynaptic dopaminergic synthesis [5] and visualizes the activity of aromatic amino acid decarboxylase (AADC), which converts [^{18}F]F-DOPA to ^{18}F-dopamine. Likewise, the [^{18}F]F-DOPA uptake can also be relevant for determining the effects of treatment of the underlying pathophysiology. For example, its uptake in the striatum is increased during dopamine replacement therapies in Parkinson's disease [6] and modulated by administration of dopamine D_2 receptor antagonist-based antipsychotic compounds [7, 8]. As a diagnostic tool for the investigation of the neuronal dopaminergic metabolism, a high specific activity (SA) of [^{18}F]F-DOPA is not mandatory.

Incidental findings in a patient undergoing a movement disorder diagnosis resulted in a coincidental discovery of a malignant glioma, indicating the potential applicability of [^{18}F]F-DOPA also for glioma imaging [9]. In the following, numerous studies were conducted establishing [^{18}F]F-DOPA as the main diagnostic tool for brain tumor imaging giving more favorable diagnostic results than [^{18}F]FDG [10] (Figure 1) due to a significantly lower background accumulation. Also other alternatives based on amino acids were developed for the imaging of brain malignancies such

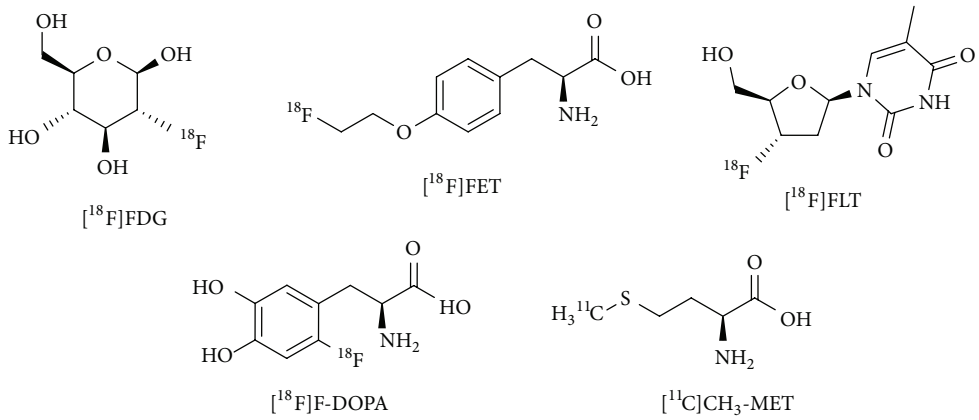

Figure 1: Selected radiotracers applicable in (brain-)tumor imaging.

as [^{11}C]methyl-L-methionine ([^{11}C]CH_3-MET) [11–13], 3′-deoxy-3′-L-[^{18}F]fluorothymidine ([^{18}F]FLT) [14, 15], or [^{18}F]fluoroethyl-L-tyrosine ([^{18}F]FET) [16–19] (Figure 1) which also exhibit the advantage to show a low physiological accumulation in normal cerebral tissue and inflamed lesions compared to [^{18}F]FDG, thus giving more favorable results in brain tumor imaging. Among these tracers used for neurooncologic imaging, [^{18}F]F-DOPA shows a high uptake in the malignant tissues, thus allowing a very sensitive tumor detection via PET imaging.

Beyond glioma imaging, recent studies have also shown the increasing importance of [^{18}F]F-DOPA for the visualization of various peripheral tumor entities via PET [20] which can be attributed to the upregulation of amino acid transporters in malignant tissues due to an often increased proliferation [21, 22]. [^{18}F]F-DOPA, which is transported via the dopamine transporter (DAT) into cells, has thus shown diagnostic advantages in the imaging of high- and low-grade malignancies like neuroendocrine tumors [23–27], pheochromocytoma [28, 29], and pancreatic adenocarcinoma [30–32] regarding diagnostic efficiency and sensitivity. [^{18}F]FDG on the contrary is taken up by the glucose transporter not only by malignant tissues but also by inflamed and healthy tissues exhibiting a high glucose metabolism, resulting in low tumor-to-background ratios [10] in CNS malignancies. The proliferation marker [^{18}F]FLT which accumulates in malignant tissues due to an enhanced activity of TK1 however often shows relatively low tumor uptakes [15], favoring [^{18}F]F-DOPA for the PET imaging of malignancies.

Due to its increasing importance for human tumor imaging, the synthesis of [^{18}F]F-DOPA becomes a critical measure regarding its dissemination in clinical routine. Ideally, the radiotracer should be easily accessible in high radiochemical yields (RCYs) and specific activities (SAs) as well as in short synthesis times by an automated process. Furthermore, as it was demonstrated that D-amino acids lack a permeability through the blood-brain barrier, an enantioselective synthesis for [^{18}F]F-DOPA is mandatory [33].

The following review outlines the developments in the field of [^{18}F]F-DOPA radiosyntheses via electrophilic synthesis routes and the more recent synthesis improvements via nucleophilic syntheses. The main focus of this work is to compare the radiochemical yields (RCYs), radiochemical purities (RCPs), enantiomeric excess (ee), synthesis times, reliability, and a potential for automation of the different radiosynthesis pathways.

2. Synthesis Routes for the Production of [^{18}F]F-DOPA

2.1. First Attempts to Synthesize [^{18}F]F-DOPA. One of the first fluorine-18-labeled DOPA derivatives was 5-[^{18}F]F-DOPA [^{18}**F**]**4**, synthesized via isotopic exchange by Firnau et al. in 1973 [34] (Figure 2). In a swimming pool reactor ^{6}Li(n, ^{4}He)^{3}H and ^{16}O(^{3}H, n)^{18}F nuclear reactions were utilized to produce fluorine-18 in a mixture of Li_2CO_3 in H_2SO_4 and H_2O. The resulting [^{18}F]fluoride was subsequently distilled twice and the diazonium fluoroborate precursor **1** was added to this solution. After the isotopic exchange reaction has occurred, the water was removed and the residue was dried over P_2O_5. The dried residue [^{18}**F**]**2** was redissolved in dioxane, filtered, and heated to 80°C. After adding xylene, the solution was further heated to 132°C for the pyrolysis of the diazonium[^{18}F]fluoroborate [^{18}**F**]**2** for 30 min. After solvent evaporation, HBr (48%) was added to hydrolyze [^{18}**F**]**3** to the final product 5-[^{18}F]F-DOPA.

The resulting product [^{18}**F**]**4** was obtained in high radiochemical purities of >95% but very low specific activities between 2.2 and 22 kBq/μmol (0.2–2.0 μCi/mg). Furthermore, the enantiomeric purity of the product was not determined, limiting the applicability of this cumbersome synthesis route.

A significant limitation for the use of 5-[^{18}F]F-DOPA for *in vivo* imaging purposes is the accelerated *O*-methylation of 5-[^{18}F]F-DOPA in contrast to 6-[^{18}F]F-DOPA ([^{18}**F**]**7**, Figure 3). This increased *O*-methylation rate is caused by the fluorine atom in position 5 in direct vicinity to the hydroxyl group in position 4 [35] and results in a significantly lower *in vivo* stability of 5-[^{18}F]F-DOPA ([^{18}**F**]**4**, Figure 2). The same group presented the reaction of [^{18}F]F_2 and L-DOPA

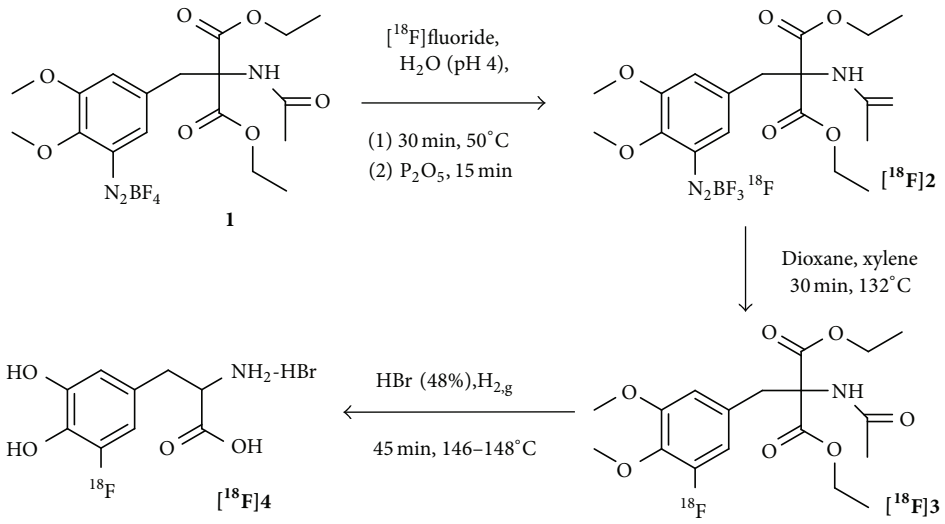

Figure 2: Isotopic exchange reaction pathway for the synthesis of 5-[^{18}F]F-DOPA [34].

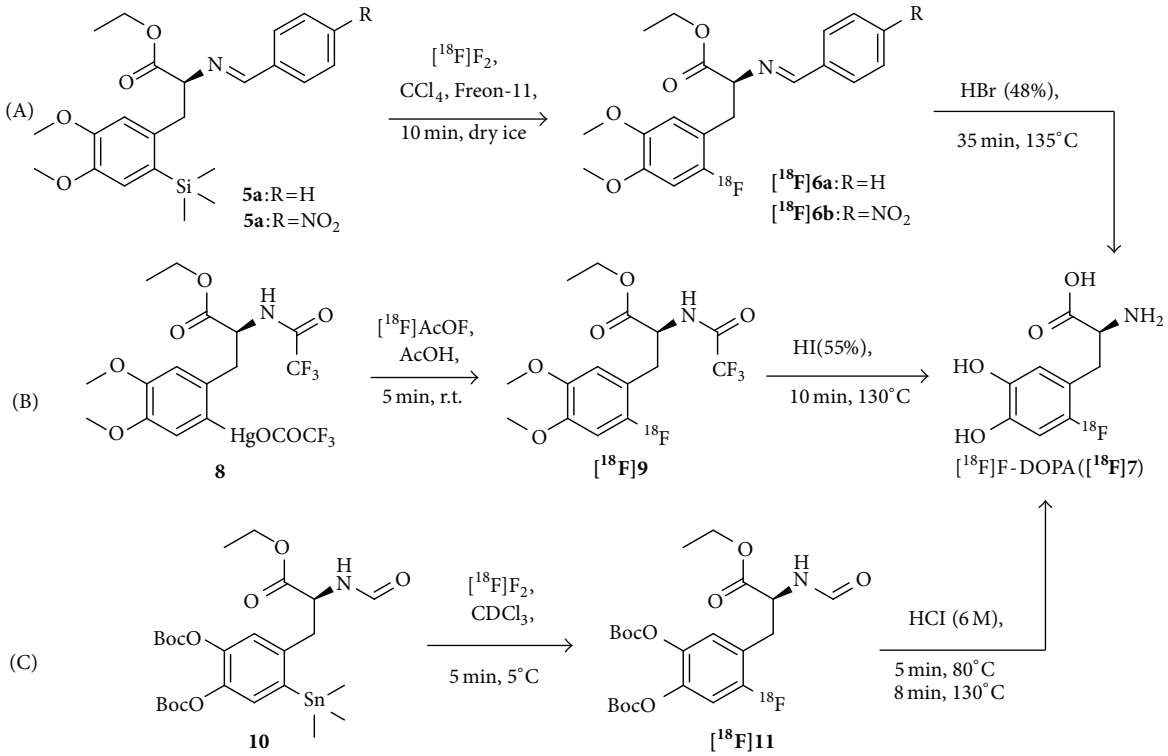

Figure 3: Examples for different demetallation synthesis routes for production of carrier-added [^{18}F]F-DOPA ([^{18}**F**]**7**) via desilylation (A) [42], demercuration (B) [44], and destannylation (C) [95].

in liquid hydrogen fluoride in 1984, yielding a mixture of 2-, 5-, and 6-[^{18}F]F-DOPA in low radiochemical yields: 3.7 GBq [^{18}F]F_2 was produced from a Ne-target by a tandem Van de Graaff accelerator to give 111 MBq (3%) 6-[^{18}F]F-DOPA, limiting the applicability of this synthesis pathway for a routine production [36].

2.2. Electrophilic Syntheses. Twenty years ago, the main route to produce [^{18}F]F_2 for electrophilic fluorination reactions was to utilize the nuclear reaction ^{20}Ne$(d,\alpha)^{18}$F and a F_2-passivated Ni-target [37]. However, this reaction was limited to facilities with a deuterium accelerator and was thus mostly replaced by the ^{18}O$(p,n)^{18}$F nuclear reaction using

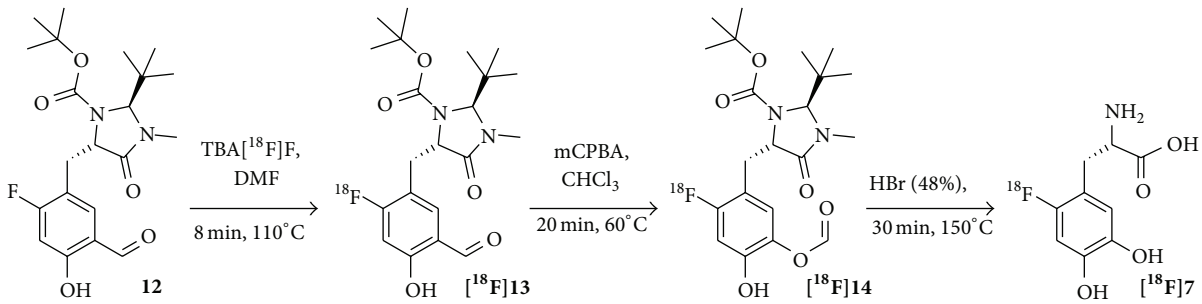

Figure 4: Isotopic exchange reaction for the synthesis of carrier-added [^{18}F]F-DOPA [59].

a respective ^{18}O gas target as this latter method enables the production of higher ^{18}F activities [37–39].

To overcome the problem with regioselectivity [40, 41] and the low radiochemical yields obtained by isotopic exchange reactions, radiodemetallation reactions were proposed by several groups. Thus, desilylation [42] and demercuration [43–46] as well as destannylation [47–52] reactions were developed (Figure 3), of which demercuration and destannylation gave the best results and were also adopted to the automated routine production of [^{18}F]F-DOPA [53]. Table 1 compares some of the most promising approaches. Multiple purification steps utilizing cartridges, HPLC, and sterile membrane filters were used to remove traces of toxic metal contaminations in the final product solutions to obtain the radiolabeled products in acceptable purities. Nevertheless, using demetallation reactions in a clinical radiotracer production, the final quality control has to include a test for metal contaminants.

Utilizing the carrier-added electrophilic introduction of fluorine-18, the main route to synthesize [^{18}F]F-DOPA ([**^{18}F**]**7**) is by using commercially available and enantiomerically pure mercury or stannyl precursors such as **8** or **10** (Figure 3) in combination with automated synthesis modules [53, 54]. The main advantages are a high enantiomeric purity (ee >99%), short reaction times (about 50 min), and a simplified synthesis setup [54]. However, remaining limitations are the achievable radiochemical yields (25 ± 3%; 0.6–2.6 GBq due to the low production yields of [^{18}F]F_2 from the cyclotron and the substantial loss of at least 50% of activity) and specific activities (4–25 MBq/μmol). As [^{18}F]F_2 can normally be obtained in specific activities of up to 350–600 MBq/μmol [55], the [^{18}F]F-DOPA production is not possible in high specific activities by the electrophilic method. Another limitation is the cumbersome transport of gaseous [^{18}F]F_2. Further, the preparation of the precursor compounds is expensive and the radiofluorination of the stannyl precursors gives many side products. In order to obtain [^{18}F]F-DOPA in higher SAs and RCYs, it was thus mandatory to develop another synthesis approach. The most promising one is the nucleophilic labeling using no-carrier-added [^{18}F]fluoride as it can be obtained in very high specific activities of up to 314–43,000 GBq/μmol [56].

3. Nucleophilic Synthesis Strategies for the Production of [^{18}F]F-DOPA

As a tracer for the amino acid metabolism in brain malignancies, a high specific activity is not mandatory for [^{18}F]F-DOPA. However, the increasing importance of [^{18}F]F-DOPA for peripheral oncologic diagnosis and the need to produce the radiotracer in higher radiochemical yields and specific activities (as too low SAs of [^{18}F]F-DOPA were shown to produce pharmacologic effects such as carcinoid crisis by local conversion in tumor tissue of [^{18}F]F-DOPA to noradrenaline, induced by the enzymes aromatic acid decarboxylase and dopamine β-hydroxylase [57]) resulted in efforts to develop no-carrier-added nucleophilic labeling methods.

3.1. Isotopic Exchange. In 2001, Tierling et al. presented the first utilization of an isotopic exchange reaction for the synthesis of [^{18}F]F-DOPA [58]. This approach yielded [^{18}F]F-DOPA in RCYs of 8–10% (n. d. c.) and an ee of >85% within 70 min. Based on these results, Wagner et al. described the utilization of the isotopic exchange reaction for the radiofluorination of a ^{19}F-precursor **12** with tetrabutylammonium[^{18}F]fluoride to produce [^{18}F]F-DOPA in high specific activities (Figure 4) [59]. Specific activities in the range of 1.5–2.5 GBq/μmol and RCYs of 22% were calculated to be achievable from a theoretical starting activity of 100 GBq [^{18}F]fluoride [60] and ^{19}F-precursor amounts of 23 μmol. However, as the reaction was only shown for a starting activity of 370 MBq [^{18}F]fluoride and 5.7 μmol ^{19}F-precursor and no further isotopic exchange experiments with higher starting activities were demonstrated, the calculated achievable yields of up to 2.5 GBq/μmol remain to be shown.

In 2013, Martin et al. implemented the method of Wagner et al. to a GE TRACERlab MX_{FDG}. In preliminary experiments, the automated synthesis of [^{18}F]F-DOPA resulted in reproducible RCYs of 10–15% (n. d. c.), RCPs of >95%, and ee of >98% without giving other synthesis details such as reaction times and starting activities [61].

3.2. Nucleophilic Syntheses and Aspects of Automation. In nucleophilic substitution reactions on aromatic rings using [^{18}F]fluoride, the standard leaving groups are mainly nitro-

Table 1: Selected synthesis details from electrophilic fluorination reactions for the synthesis of [^{18}F]F-DOPA.

Radiolabeling method	Time [min]	RCY [%][a]	Impurities in product	SA [MBq/μmol]	ee [%]	Citation
Desilylation	60	8[b]	n. d.	25.2	100	Diksic and Farrokhzad '85 [42]
L-DOPA + BF_3	120	18	n. d.	n. d.	100	Chirakal et al. '86 [92]
Demercuration	65	12	<10 ppb Hg	n. d.	97	Adam and Jivan '88 [43]
Demercuration	50	11	<20 ppb Hg	2.6	>99	Luxen et al. '90 [44]
Destannylation	60	25	<15 ppb Sn	n. d.	>99	Namavari et al. '92 [47]
O-Pivaloyl ester of L-DOPA	60	17 ± 1.9	n. d.	17 ± 2.5	100	Ishiwata et al. '93 [93]
Demercuration	45–50	14[b]	<0.05 μg/mL Hg	17–19	>98	Chaly et al. '93 [94]
Destannylation	45–50	26	1.5–2.5 ppm Sn	4.4	>99	Dollé et al. '98 [48]
Destannylation	50	25 ± 3	<1 μg/mL $CDCl_3$	30 ± 2	96 ± 1	Füchtner et al. '08 [95]

[a]Unless otherwise stated, RCYs are given decay corrected (d. c.) and [b]nondecay corrected (n. d. c.).

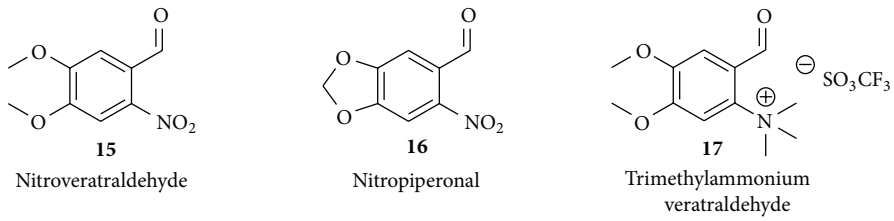

Figure 5: Most common precursors for no-carrier-added nucleophilic radiofluorination reactions producing [^{18}F]F-DOPA.

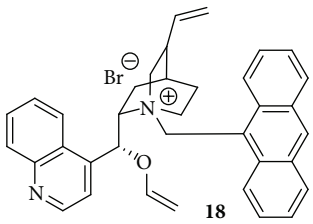

Figure 6: Chiral phase-transfer catalyst *O*-ally-*N*-9-anthracenylmethyl-cinchonidinium bromide **18**.

or trimethylammonium moieties (Figure 5) in combination with electron withdrawing groups such as –CO, –CN, and –NO_2 to enable an efficient reaction. Further, halogen exchange reactions with substituted veratraldehyde (–Cl, –Br, and –F) were evaluated [62]. The first nucleophilic approaches for the synthesis of [^{18}F]F-DOPA gave racemates of D- and L-isomers of the tracer which were purified by chiral HPLC resulting in a significant loss of activity [63, 64].

To overcome these problems, new radiosyntheses were developed based on enantiomerically pure chiral precursors or chiral auxiliaries [65–70]. The radiolabeling reactions using these precursors provide the product in moderate to good RCYs accompanied by a high enantiomeric excess of >96%. The most promising approach was published by Lemaire et al. giving [^{18}F]F-DOPA in a RCY of 17–29% (d. c.) and a SA of >37 GBq/μmol [66]. In Table 2, selected syntheses using different enantiomerically pure chiral precursors or chiral auxiliaries are compared.

In addition, asymmetric synthesis routes were developed for the radiosynthesis of [^{18}F]F-DOPA with higher enantiomeric selectivity and higher RCYs comprising approaches with the precursors depicted in Figure 5 and enantioselective reactions utilizing different chiral phase-transfer catalysts (cPTC). The results from these asymmetric approaches are shown in Table 3.

A very promising approach for the nucleophilic synthesis of [^{18}F]F-DOPA yielding the product in high enantiomeric purities was the utilization of the chiral phase-transfer catalyst *O*-ally-*N*-9-anthracenylmethyl-cinchonidinium bromide (**18**, Figure 6) described by Corey et al. in 1997 [71]. Based on the preliminary results of Lemaire et al. in 1999 [72] and Guillouet et al. in 2001 [73], Zhang et al. adopted the method in 2002 [74] and presented a promising synthesis route utilizing this cPTC **18** for the enantioselective radiosynthesis of [^{18}F]F-DOPA in RCYs of 7–15%, radiochemical purities of >99%, and an ee of 90% within 80–85 min synthesis time. However, special care has to be taken concerning the trimethylammonium veratraldehyde precursor **17** which exhibits a limited stability upon storage of the precursor for more than six months at 0–4°C resulting in a decreasing RCY for the radiofluorination of **17** from 40% to <10% [75].

A limitation for this synthesis route is the achievable enantiomeric purities as, according to the European Pharmacopoeia monograph, the limit of the D-enantiomer in the final solution is 2% (ee 96%) [76]. Thus, the synthesis had to be further improved to comply with this limit. A promising

Table 2: Selected synthesis parameters using chiral auxiliaries or precursors.

Precursor	Time [min]	RCY [%] ^{18}F-label.	RCY [%] overall[a]	SA [GBq/μmol]	ee [%]	Citation
16	100–110	51	12[b]	n. d.	n. d.	Ding et al. '90 [63]
15 or **16**	120	n. d.	5–10	n. d.	50 (rac.)	Lemaire et al. '91 [65]
15	110	n. d.	5–10[b]	n. d.	83–96	Lemaire et al. '93 [67]
15 or **16**	120	20–35; ~50	3–5[b]	n. d.	>99	Reddy et al. '93 [68]
15	90	45 ± 5	17–29	>37	>96	Lemaire et al. '94 [66]
15 or **16**	125	n. d.	4-5[b]	>74	98	Horti et al. '95 [69]
15	85	~50	6–13[b]	>7.4	98	Najafi '95 [70]

[a]Unless otherwise stated, RCYs are given decay corrected (d. c.) and [b]nondecay corrected (n. d. c.).

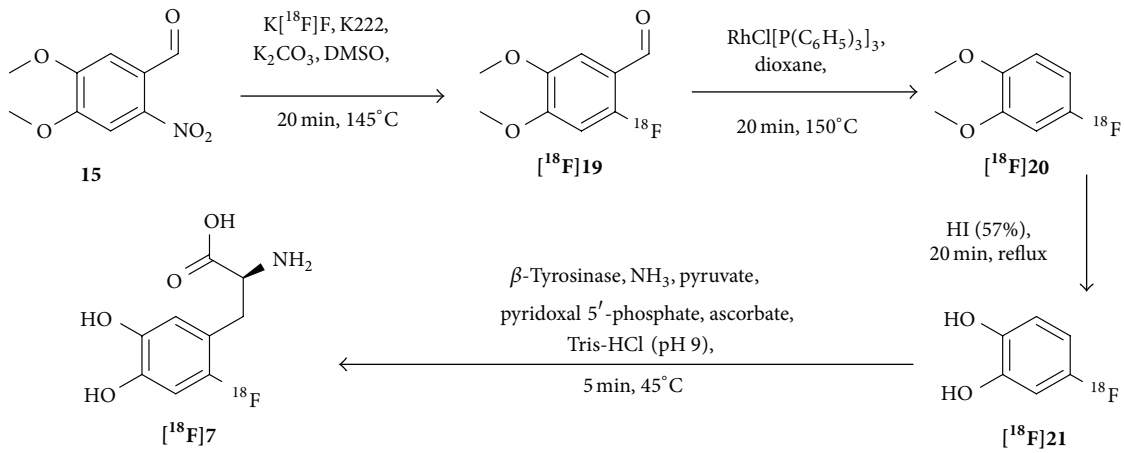

Figure 7: Synthesis pathway for the enzymatic preparation of [^{18}F]F-DOPA according to Kaneko et al. [77].

approach was presented by Kaneko et al. in 1999 (Figure 7) [77]. The enzymatic reaction step was evaluated carefully and provided a conversion rate of 58% from [^{18}F]fluorocatechol ([^{18}**F**]**21**) to [^{18}F]F-DOPA ([^{18}**F**]**7**) under optimized conditions. Despite the efficient enzymatic conversion of [^{18}F]F-catechol to the product, the overall RCY of [^{18}F]F-DOPA that could be obtained was only 2.0% but resulted in the formation of the product in high SAs of >200 GBq/μmol within 150 min synthesis time. The enantiomeric excess was assumed to be 100% due to the enzymatic character of the reaction although being not confirmed.

The automation of radiotracer syntheses is mandatory for their wide clinical distribution as an automated process gives the product in reproducible quality and limits the radiation exposure to the operating personnel, enabling high starting activities and thus the possibility to synthesize several patient doses in one radiosynthesis.

Therefore, Lemaire et al. optimized the enantioselective reaction using the chiral phase-transfer catalysts **18** and were able to obtain enantiomeric excesses of about 96% when performing the reaction in toluene at 0°C [78]. However, this reaction setup is difficult to realize in automated processes, due to cooling and heating steps in the same synthesis process. Thus, an optimized synthesis route was developed, preventing the use of diiodosilane. Aldehyde [^{18}**F**]**19** and its precursor **17** (Figure 5) were trapped on a C18 cartridge, the precursor **17** was removed with water from the solid support, and [^{18}**F**]**19** was reduced by aqueous $NaBH_4$ and subsequently halogenated by HBr or HI on solid support, resulting in a synthesis setup that could be transferred to an automated synthesis module. Recently, this reaction setup was applied for the radiosynthesis and online conversion from aldehyde [^{18}**F**]**19** to different benzyl halides [79].

Another very promising approach was presented in 2004 by Krasikova et al. [80]. An automated enantioselective radiosynthesis utilizing a novel substrate/catalyst pair, namely, NiPBPGly **25** and (*S*)-NOBIN **26** (Figure 8), was developed. In the key alkylation step, the electrophilic bromide [^{18}**F**]**2** reacts with the nickel complex **25** in the presence of (*S*)-NOBIN to form the (*S*)-complex [^{18}**F**]**27**. This enantioselective reaction step was accomplished at room temperature, which is favorable in terms of automation. Subsequently, the alkylation was quenched by HI or acetic acid before the solvent was removed in order to prevent racemization of the (*S*)-complex. Different purification steps were optimized to remove any potentially toxic substances present during the synthesis (Ni, Br, P, or B) which was confirmed by ICP-MS analysis of the final product. Using this method, [^{18}F]F-DOPA was synthesized in an ee of 96% and RCYs of 16 ± 5% [80] in a total synthesis time of 110–120 min. Although this approach seems to be promising, it has not found a widespread application so far which may

Table 3: Selected synthesis parameters utilizing chiral phase-transfer catalysts (cPTC) or asymmetric synthesis routes.

Precursor	Method	Time [min]	RCY [%] ^{18}F-label.	RCY [%] overall[a]	SA [GBq/μmol]	ee [%]	Citation
15	Enzymatic	150	27	2	>200	>99	Kaneko et al. '99 [77]
17	cPTC **18**[c]	110	n. d.	10–15[b]	74–185	95	Guillouet et al. '01 [73]
17	cPTC **18**	80–85	10–40	7–15	n. d.	90	Zhang et al. '02 [74]
16	Catalyst **25**[d]	120	53	16 ± 5	n. d.	96	Krasikova et al. '04 [80]
17	cPTC **18**	100	40–50	25–30	n. d.	96	Lemaire et al. '04 [78]
15	cPTC **18**	120	71	20 ± 4	>50	≥95	Shen et al. '09 [83]
17	cPTC **31**[e]	63	50	36 ± 3	>750	>97	Libert et al. '13 [86]

[a]Unless otherwise stated, RCYs are given decay corrected (d. c.) and [b]nondecay corrected (n. d. c.); [c]see Figure 6; [d]see Figure 8; [e]see Figure 10.

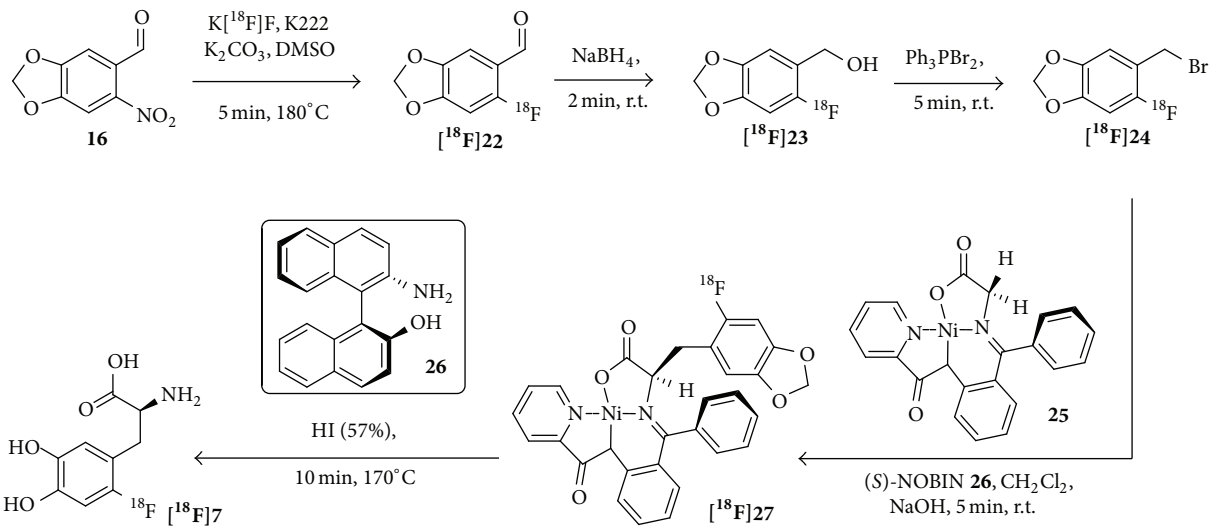

Figure 8: Schematic depiction of the synthesis pathway utilizing NiPBPGly **25** and (*S*)-NOBIN **26** as a novel substrate/catalyst pair for the enantioselective radiosynthesis of [^{18}F]F-DOPA by Krasikova et al. [80].

be due to the laborious synthesis of the catalyst pair [81, 82] and the challenging purification procedures required for the synthesis which include self-made columns/cartridges in order to remove intermediate reagents and side products.

The optimization efforts towards an automation for the routine production of [^{18}F]F-DOPA finally resulted in promising synthesis approaches recently. In 2009, Shen et al. presented a method for the fully automated synthesis for [^{18}F]F-DOPA [83] utilizing the cPTC **18** which can be performed at ambient temperature (Figure 9), combining the methods described by Zhang et al. [74] and Lemaire et al. [78]. By optimization of the amounts of reagents during the alkylation process, they were able to obtain [^{18}F]F-DOPA in RCYs of 20±4%, SAs of ~50 GBq/μmol, and ee of ≥95% within 120 min synthesis time. In order to obtain higher RCYs, it is important to radiolabel the nitro precursor **15** in DMF instead of DMSO due to oxidation processes of the aldehyde **15** occurring in DMSO [84, 85]. Furthermore, the utilization of HBr in combination with KI in the deprotection step resulted in higher RCYs compared to HI alone. However, as noncharacterized substances precipitate during the synthesis, a limitation of this method is the cumbersome maintenance of the synthesis module after each synthesis. To overcome this obstacle, the use of a cassette module would be favorable as this approach would not require the elaborate purification of the module after each use.

Libert and coworkers investigated different cPTC regarding their potential to produce [^{18}F]F-DOPA in the highest enantiomeric excesses and high enantiomeric purities of >97% could be obtained under mild reaction conditions within short reaction times [86]. Together with the use of a structurally optimized chiral phase-transfer catalyst (**31**) [71, 87] (Figure 10), a much simplified synthesis setup for automation was enabled. With this optimization, the group of Libert and Lemaire was able to establish a fast automated synthesis and reported product amounts of >45 GBq obtained in RCYs of 24% (n. d. c.) and specific activities of >750 GBq/μmol [86] within 63 minutes (Figure 10). Furthermore, utilizing cPTC **31** as the catalyst, an ee of >97% could be achieved.

3.3. Miscellaneous. In this chapter, some unconventional approaches for the production of [^{18}F]F-DOPA are described.

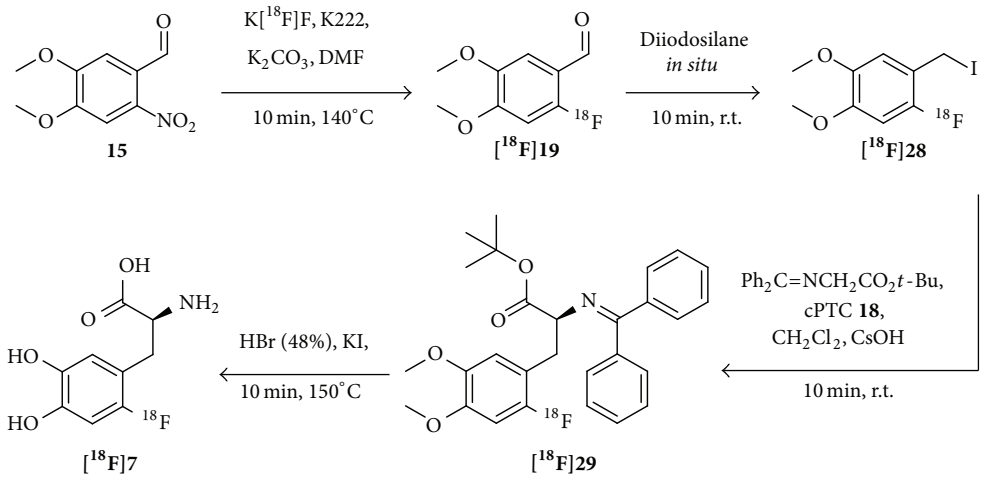

Figure 9: Automated radiosynthesis procedure for [^{18}F]F-DOPA using the chiral phase transfer catalyst **18** [83].

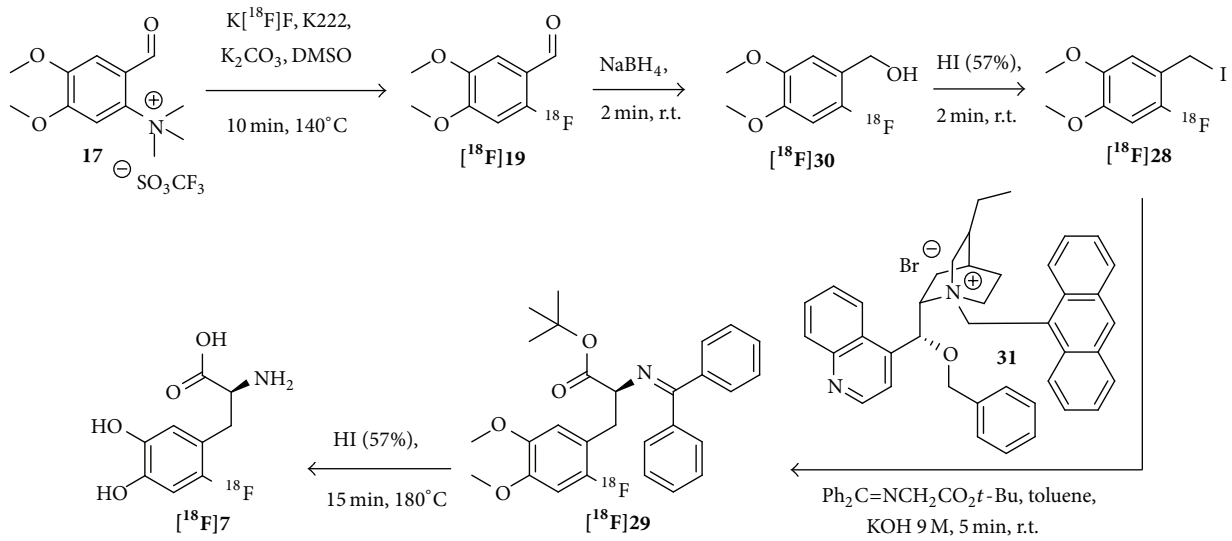

Figure 10: Schematic depiction of the automated synthesis pathway using the chiral phase-transfer catalyst **31** [86].

In 2008, Forsback et al. presented an electrophilic labeling approach for the production of [^{18}F]F-DOPA in RCYs of 6.4 ± 1.7% (d. c.) and SAs of 3.7 ± 0.9 GBq/μmol [88]. The key step was the synthesis of [^{18}F]F_2 in an electrical discharge chamber by a ^{18}F/^{19}F-exchange reaction. The ^{18}F-source was [^{18}F]fluoromethane, which was mixed with a low amount (1 μmol) of carrier fluorine in neon (Ne/0.5% F_2) inside the discharge chamber. [^{18}F]Fluoromethane was produced from methyliodide by a nucleophilic substitution reaction with K[^{18}F]F/K222 in acetonitrile. Deuterated solvents for the synthesis of [^{18}F]F-DOPA like $CDCl_3$, CD_2Cl_2, and C_3D_6O were also investigated providing significantly higher yields than Freon-11 [89].

In 2012, Lee et al. presented a very fast oxidative fluorination approach for ^{18}F-aryl compounds utilizing a nickel-complex **32** and [^{18}F]fluoride (Figure 11). Nickel complex **32** (1 mg), a hypervalent iodine oxidant **33** (1 eq.), an aqueous solution of [^{18}F]fluoride (2–5 μL, 3.7–18.5 MBq), and K222 (2.0 mg) in acetonitrile (200–500 μL) at 23°C yielded a Boc-protected [^{18}F]F-DOPA-analogue [^{18}**F**]**34** in RCYs of 15 ± 7% (n. d. c.) in less than 1 minute [90]. This might be also a useful approach for a very fast synthesis of [^{18}F]F-DOPA.

In 2013, Stenhagen et al. presented an Ag-mediated electrophilic [^{18}F]fluorination of an enantiomerically pure precursor. The protected arylboronic ester was transformed to a 6-Ag-DOPA derivative with silver triflate. Next, [^{18}F]selectfluor bis(triflate) in acetone-d_6 was added. [^{18}F]F-DOPA was obtained after 20 min reaction at ambient temperature and 5 min deprotection in RCYs of 19 ± 12% and SAs of 2.6 ± 0.3 GBq/μmol [91]. These results are comparable with the best known electrophilic approaches and could also serve for an automated synthesis.

In summary, radiosynthesis procedures for [^{18}F]F-DOPA were developed which can give the radiotracer in high RCYs,

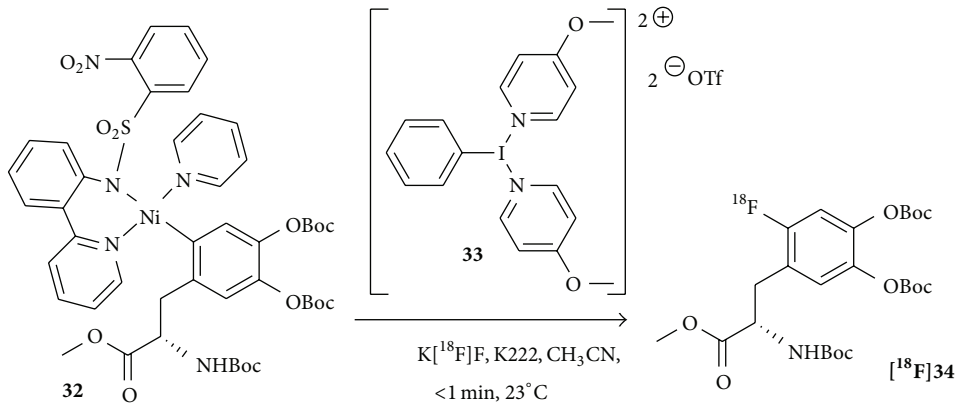

Figure 11: Schematic depiction of an oxidative fluorination approach using the nickel complex **32** and a hypervalent iodine oxidant **33** giving the Boc-protected [^{18}F]F-DOPA-analogue **[^{18}F]34** [90].

SAs, and enantiomeric excesses in short reaction times. Future efforts to even further improve these results could include the utilization of nonoxidizing solvents and microwave conditions in order to achieve even higher [^{18}F]fluoride incorporation rates. Up to now, automated systems based on the radiochemistry described by, for example, Wagner et al. [59], Martin et al. [61], and Libert et al. [86] are commercially available.

4. Conclusion

In over 30 years, the radiosynthesis of [^{18}F]F-DOPA was performed via electrophilic and isotopic exchange routes, when the tracer was mainly applied for the *in vivo* PET imaging of central motor disorders and metabolism imaging purposes. However, the main production route with [^{18}F]F_2 and commercially available stannyl precursors provides [^{18}F]F-DOPA in relatively low RCYs and SAs, limiting the use of this promising radiotracer to the imaging of neuronal function and brain malignancies, which is still its main application.

With the discovery of the potential of [^{18}F]F-DOPA as radiotracer for the imaging of peripheral malignancies such as neuroendocrine tumors, new radiosynthesis approaches based on nucleophilic substitution reactions were developed, yielding [^{18}F]F-DOPA in higher RCYs and SAs as well as shorter synthesis times. Here, two main approaches were followed: one comprises the introduction of nucleophilic [^{18}F]fluoride into complex chiral precursors, followed by deprotection and purification, and the other approach starts with introduction of [^{18}F]fluoride into simple precursors followed by the utilization of chiral phase-transfer catalysts for an enantioselective synthesis of the product. These processes can also be transferred to automated synthesis modules allowing for a broader dissemination of this favorable radiotracer extending the palette of radiotracers towards a patient-individualized precision medicine.

Conflict of Interests

The authors declare no conflict of interests.

Acknowledgment

The funding from "Perspektivförderung des Ministeriums für Wissenschaft und Kunst Baden-Württemberg" is gratefully acknowledged.

References

[1] O. D. Howes, A. J. Montgomery, M.-C. Asselin, R. M. Murray, P. M. Grasby, and P. K. Mcguire, "Molecular imaging studies of the striatal dopaminergic system in psychosis and predictions for the prodromal phase of psychosis," *British Journal of Psychiatry*, vol. 191, no. 51, supplement, pp. S13–S18, 2007.

[2] S. K. Bose, F. E. Turkheimer, O. D. Howes et al., "Classification of schizophrenic patients and healthy controls using [^{18}F] fluorodopa PET imaging," *Schizophrenia Research*, vol. 106, no. 2-3, pp. 148–155, 2008.

[3] D. J. Brooks, "PET studies on the function of dopamine in health and Parkinson's disease," *Annals of the New York Academy of Sciences*, vol. 991, pp. 22–35, 2003.

[4] D. J. Brooks, K. A. Frey, K. L. Marek et al., "Assessment of neuroimaging techniques as biomarkers of the progression of Parkinson's disease," *Experimental Neurology*, vol. 184, no. 1, pp. S68–S79, 2003.

[5] P. Cumming, P. Deep, O. Rousset, A. Evans, and A. Gjedde, "On the rate of decarboxylation of Dopa to Dopamine in living mammalian brain," *Annals of the New York Academy of Sciences*, vol. 835, pp. 274–308, 1997.

[6] T. Nakamura, V. Dhawan, T. Chaly et al., "Blinded positron emission tomography study of dopamine cell implantation for Parkinson's disease," *Annals of Neurology*, vol. 50, no. 2, pp. 181–187, 2001.

[7] J. Tedroff, R. Torstenson, P. Hartvig et al., "Effects of the substituted (*S*)-3-phenylpiperidine (−)-OSU6162 on PET measurements in subhuman primates: evidence for tone-dependent normalization of striatal dopaminergic activity," *Synapse*, vol. 28, pp. 280–287, 1998.

[8] R. Torstenson, P. Hartvig, B. Långström, S. Bastami, G. Antoni, and J. Tedroff, "Effect of apomorphine infusion on dopamine synthesis rate relates to dopaminergic tone," *Neuropharmacology*, vol. 37, no. 8, pp. 989–995, 1998.

[9] W. D. Heiss, K. Wienhard, R. Wagner et al., "F-Dopa as an amino acid tracer to detect brain tumors," *Journal of Nuclear Medicine*, vol. 37, pp. 1180–1182, 1996.

[10] W. Chen, D. H. S. Silverman, S. Delaloye et al., " ^{18}F-FDOPA PET imaging of brain tumors: comparison study with ^{18}F-FDG PET and evaluation of diagnostic accuracy," *Journal of Nuclear Medicine*, vol. 47, no. 6, pp. 904–911, 2006.

[11] S. Oka, H. Okudaira, M. Ono et al., "Differences in transport mechanisms of *trans*-1-amino-3-[^{18}F]fluorocyclobutanecarboxylic acid in inflammation, prostate cancer, and glioma cells: comparison with L-[Methyl-^{11}C]methionine and 2-deoxy-2-[^{18}F]fluoro-D-glucose," *Molecular Imaging and Biology*, vol. 16, no. 3, pp. 322–329, 2013.

[12] Y. Okochi, T. Nihashi, M. Fujii et al., "Clinical use of ^{11}C-methionine and ^{18}F-FDG-PET for germinoma in central nervous system," *Annals of Nuclear Medicine*, vol. 28, no. 2, pp. 94–102, 2013.

[13] S. Takenaka, Y. Asano, J. Shinoda et al., "Comparison of ^{11}C-methionine, ^{11}C-chlorine, and ^{18}F-fluorodeoxyglucose-PET for distinguishing glioma recurrence from radiation necrosis," *Neurologia Medico-Chirurgica*, vol. 54, no. 4, pp. 280–289, 2014.

[14] W. Chen, T. Cloughesy, N. Kamdar et al., "Imaging proliferation in brain tumors with ^{18}F-FLT PET: comparison with ^{18}F-FDG," *Journal of Nuclear Medicine*, vol. 46, no. 6, pp. 945–952, 2005.

[15] L. B. Been, A. J. H. Suurmeijer, D. C. P. Cobben, P. L. Jager, H. J. Hoekstra, and P. H. Elsinga, "[^{18}F]FLT-PET in oncology: current status and opportunities," *European Journal of Nuclear Medicine and Molecular Imaging*, vol. 31, no. 12, pp. 1659–1672, 2004.

[16] N. Galldiks, G. Stoffels, M. I. Ruge et al., "Role of *O*-(2-^{18}F-fluoroethyl)-L-tyrosine PET as a diagnostic tool for detection of malignant progression in patients with low-grade glioma," *Journal of Nuclear Medicine*, vol. 54, no. 12, pp. 2046–2054, 2013.

[17] M. D. Piroth, J. Prasath, A. Willuweit et al., "Uptake of *O*-(2-[^{18}F]fluoroethyl)-L-tyrosine in reactive astrocytosis in the vicinity of cerebral gliomas," *Nuclear Medicine and Biology*, vol. 40, pp. 795–800, 2013.

[18] K. K. Sai, C. Huang, L. Yuan et al., " ^{18}F-AFETP, ^{18}F-FET, and ^{18}F-FDG imaging of mouse DBT gliomas," *Journal of Nuclear Medicine*, vol. 54, no. 7, pp. 1120–1126, 2013.

[19] K. Zhang, K. J. Langen, I. Neuner et al., "Relationship of regional cerebral blood flow and kinetic behaviour of *O*-(2-^{18}F-fluoroethyl)-L-tyrosine uptake in cerebral gliomas," *Nuclear Medicine Communications*, vol. 35, no. 3, pp. 245–251, 2014.

[20] J. P. Seibyl, W. Chen, and D. H. S. Silverman, "3,4-dihydroxy-6-[^{18}F]-fluoro-L-phenylalanine positron emission tomography in patients with central motor disorders and in evaluation of brain and other tumors," *Seminars in Nuclear Medicine*, vol. 37, no. 6, pp. 440–450, 2007.

[21] K. J. Isselbacher, "Sugar and amino acid transport by cells in culture: differences between normal and malignant cells," *The New England Journal of Medicine*, vol. 286, no. 17, pp. 929–933, 1972.

[22] H. Busch, J. R. Davis, G. R. Honig, D. C. Anderson, P. V. Nair, and W. L. Nyhan, "The uptake of a variety of amino acids into nuclear proteins of tumors," *Cancer Research*, vol. 19, pp. 1030–1039, 1959.

[23] O. C. Neels, K. P. Koopmans, P. L. Jager et al., "Manipulation of [^{11}C]-5-hydroxytryptophan and 6-[^{18}F]fluoro-3,4-dihydroxy-L-phenylalanine accumulation in neuroendocrine tumor cells," *Cancer Research*, vol. 68, no. 17, pp. 7183–7190, 2008.

[24] H. Minn, S. Kauhanen, M. Seppänen, and P. Nuutila, " ^{18}F-FDOPA: a multiple-target molecule," *Journal of Nuclear Medicine*, vol. 50, no. 12, pp. 1915–1918, 2009.

[25] P. L. Jager, R. Chirakal, C. J. Marriott, A. H. Brouwers, K. P. Koopmans, and K. Y. Gulenchyn, "6-L-^{18}F-fluorodihydroxyphenylalanine pet in neuroendocrine tumors: basic aspects and emerging clinical applications," *Journal of Nuclear Medicine*, vol. 49, no. 4, pp. 573–586, 2008.

[26] S. Balogova, J.-N. Talbot, V. Nataf et al., "^{18}F-Fluorodihydroxyphenylalanine vs other radiopharmaceuticals for imaging neuroendocrine tumours according to their type," *European Journal of Nuclear Medicine and Molecular Imaging*, vol. 40, no. 6, pp. 943–966, 2013.

[27] S. Chondrogiannis, G. Grassetto, M. C. Marzola et al., "^{18}F-DOPA PET/CT biodistribution consideration in 107 consecutive patients with neuroendocrine tumours," *Nuclear Medicine Communications*, vol. 33, no. 2, pp. 179–184, 2012.

[28] L. Martiniova, S. Cleary, E. W. Lai et al., "Usefulness of [^{18}F]-DA and [^{18}F]-DOPA for PET imaging in a mouse model of pheochromocytoma," *Nuclear Medicine and Biology*, vol. 39, no. 2, pp. 215–226, 2012.

[29] H. C. Rischke, M. R. Benz, D. Wild et al., "Correlation of the genotype of paragangliomas and pheochromocytomas with their metabolic phenotype on 3,4-dihydroxy-6-^{18}F-fluoro-L-phenylalanin PET," *Journal of Nuclear Medicine*, vol. 53, no. 9, pp. 1352–1358, 2012.

[30] J. Tuomela, S. Forsback, L. Haavisto et al., "Enzyme inhibition of dopamine metabolism alters 6-[^{18}F]FDOPA uptake in orthotopic pancreatic adenocarcinoma," *EJNMMI Research*, vol. 3, no. 1, article 18, pp. 1–10, 2013.

[31] H. Jadvar, "Hepatocellular carcinoma and gastroenteropancreatic neuroendocrine tumors: potential role of other positron emission tomography radiotracers," *Seminars in Nuclear Medicine*, vol. 42, no. 4, pp. 247–254, 2012.

[32] K. P. Koopmans, O. C. Neels, I. P. Kema et al., "Improved staging of patients with carcinoid and islet cell tumors with ^{18}F-dihydroxy-phenyl-alanine and ^{11}C-5-hydroxy-tryptophan positron emission tomography," *Journal of Clinical Oncology*, vol. 26, no. 9, pp. 1489–1495, 2008.

[33] W. H. Oldendorf, "Stereospecificity of blood-brain barrier permeability to amino acids," *The American Journal of Physiology*, vol. 224, no. 4, pp. 967–969, 1973.

[34] G. Firnau, C. Nahmias, and S. Garnett, "The preparation of [^{18}F]5-fluoro-DOPA with reactor-produced fluorine-^{18} ," *The International Journal of Applied Radiation and Isotopes*, vol. 24, no. 3, pp. 182–184, 1973.

[35] G. Firnau, S. Sood, R. Pantel, and S. Garnett, "Phenol ionization in dopa determines the site of methylation by catechol-*O*-methyltransferase," *Molecular Pharmacology*, vol. 19, no. 1, pp. 130–133, 1981.

[36] G. Firnau, R. Chirakal, and E. S. Garnett, "Aromatic radiofluorination with [^{18}F]fluorine gas: 6-[^{18}F]fluoro-L-dopa," *Journal of Nuclear Medicine*, vol. 25, no. 11, pp. 1228–1233, 1984.

[37] R. J. Nickles, M. E. Daube, and T. J. Ruth, "An $^{18}O_2$ target for the production of [^{18}F]F_2," *International Journal of Applied Radiation and Isotopes*, vol. 35, no. 2, pp. 117–122, 1984.

[38] A. D. Roberts, T. R. Oakes, and R. J. Nickles, "Development of an improved target for [^{18}F]F_2 production," *Applied Radiation and Isotopes*, vol. 46, no. 2, pp. 87–91, 1995.

[39] E. Hess, S. Sichler, A. Kluge, and H. H. Coenen, "Synthesis of 2-[^{18}F]fluoro-L-tyrosine via regiospecific fluoro-de-stannylation," *Applied Radiation and Isotopes*, vol. 57, no. 2, pp. 185–191, 2002.

[40] K. Hatano, K. Ishiwata, and T. Yanagisawa, "Co production of 2, 6-[^{18}F]difluoroDOPA during electrophilic synthesis of 6-[^{18}F]fluoro-L-DOPA," *Nuclear Medicine and Biology*, vol. 23, pp. 101–103, 1996.

[41] H. H. Coenen, K. Franken, P. Kling, and G. Stöcklin, "Direct electrophilic radiofluorination of phenylalanine, tyrosine and dopa," *Applied Radiation and Isotopes*, vol. 39, no. 12, pp. 1243–1250, 1988.

[42] M. Diksic and S. Farrokhzad, "New synthesis of fluorine-18-labeled 6-fluoro-L-dopa by cleaving the carbon-silicon bond with fluorine," *Journal of Nuclear Medicine*, vol. 26, no. 11, pp. 1314–1318, 1985.

[43] M. J. Adam and S. Jivan, "Synthesis and purification of L-6-[^{18}F]fluorodopa," *Applied Radiation and Isotopes*, vol. 39, no. 12, pp. 1203–1206, 1988.

[44] A. Luxen, M. Perlmutter, G. T. Bida et al., "Remote, semiautomated production of 6-[^{18}F]fluoro-L-dopa for human studies with PET," *Applied Radiation and Isotopes*, vol. 41, no. 3, pp. 275–281, 1990.

[45] A. Bishop, N. Satyamurthy, G. Bida, and J. R. Barrio, "Chemical reactivity of the ^{18}F electrophilic reagents from the $^{18}O(p, n)^{18}$F gas target systems," *Nuclear Medicine and Biology*, vol. 23, no. 5, pp. 559–565, 1996.

[46] T. Chaly, D. Bandyopadhyay, R. Matacchieri et al., "A disposable synthetic unit for the preparation of 3-*O*-methyl-6-[^{18}F]fluorodopa using a regioselective fluorodemercuration reaction," *Applied Radiation and Isotopes*, vol. 45, no. 1, pp. 25–30, 1994.

[47] M. Namavari, A. Bishop, N. Satyamurthy, G. Bida, and J. R. Barrio, "Regioselective radiofluorodestannylation with [^{18}F]F_2 and [^{18}F]CH_3COOF: a high yield synthesis of 6-[^{18}F]fluoro-L-dopa," *Applied Radiation and Isotopes*, vol. 43, no. 8, pp. 989–996, 1992.

[48] F. Dollé, S. Demphel, F. Hinnen, D. Fournier, F. Vaufrey, and C. Crouzel, "6-[^{18}F]fluoro-L-DOPA by radiofluorodestannylation: a short and simple synthesis of a new labelling precursor," *Journal of Labelled Compounds and Radiopharmaceuticals*, vol. 41, no. 2, pp. 105–114, 1998.

[49] F. Füchtner, P. Angelberger, H. Kvaternik, F. Hammerschmidt, B. P. Simovc, and J. Steinbach, "Aspects of 6-[^{18}F]fluoro-L-DOPA preparation: precursor synthesis, preparative HPLC purification and determination of radiochemical purity," *Nuclear Medicine and Biology*, vol. 29, no. 4, pp. 477–481, 2002.

[50] F. Füchtner and J. Steinbach, "Efficient synthesis of the ^{18}F-labelled 3-*O*-methyl-6-[^{18}F]fluoro-L-DOPA," *Applied Radiation and Isotopes*, vol. 58, no. 5, pp. 575–578, 2003.

[51] C. W. Chang, H. E. Wang, H. M. Lin, C. S. Chtsai, J. B. Chen, and R.-S. Liu, "Robotic synthesis of 6-[^{18}F]fluoro-L-dopa," *Nuclear Medicine Communications*, vol. 21, no. 9, pp. 799–802, 2000.

[52] M. J. Adam, J. Lu, and S. Jivan, "Stereoselective synthesis of 3-*O*-methyl-6-[^{18}F]fluorodopa via fluorodestannylation," *Journal of Labelled Compounds and Radiopharmaceuticals*, vol. 34, no. 6, pp. 565–570, 1994.

[53] E. F. J. de Vries, G. Luurtsema, M. Brüssermann, P. H. Elsinga, and W. Vaalburg, "Fully automated synthesis module for the high yield one-pot preparation of 6-[^{18}F]fluoro-L-DOPA," *Applied Radiation and Isotopes*, vol. 51, no. 4, pp. 389–394, 1999.

[54] A. Luxen, M. Guillaume, W. P. Melega, V. W. Pike, O. Solin, and R. Wagner, "Production of 6-[^{18}F]fluoro-L-DOPA and its metabolism in vivo: a critical review," *Nuclear Medicine and Biology*, vol. 19, no. 2, pp. 149–158, 1992.

[55] E. Hess, G. Blessing, H. H. Coenen, and S. M. Qaim, "Improved target system for production of high purity [^{18}F]fluorine via the $^{18}O(p,n)^{18}$F reaction," *Applied Radiation and Isotopes*, vol. 52, no. 6, pp. 1431–1440, 2000.

[56] F. Füchtner, S. Preusche, P. Mäding, J. Zessin, and J. Steinbach, "Factors affecting the specific activity of [^{18}F]fluoride from a [^{18}O]water target," *Nuklearmedizin*, vol. 47, no. 3, pp. 116–119, 2008.

[57] K. P. Koopmans, A. H. Brouwers, M. N. De Hooge et al., "Carcinoid crisis after injection of 6-^{18}F- fluorodihydroxyphenylalanine in a patient with metastatic carcinoid," *Journal of Nuclear Medicine*, vol. 46, no. 7, pp. 1240–1243, 2005.

[58] T. Tierling, K. Hamacher, and H. H. Coenen, "A new nucleophilic asymmetric synthesis of 6-[^{18}F]fluoro-dopa," *Journal of Labelled Compounds and Radiopharmaceuticals*, vol. 44, supplement, pp. S146–S147, 2001.

[59] F. M. Wagner, J. Ermert, and H. H. Coenen, "Three-step, "one-pot" radiosynthesis of 6-fluoro-3,4-dihydroxy-l-phenylalanine by isotopic exchange," *Journal of Nuclear Medicine*, vol. 50, no. 10, pp. 1724–1729, 2009.

[60] F. M. Wagner, *Zur Synthese radiofluorierter aromatischer Aminosäuren mittels Isotopenaustausch am Beispiel von 6-[^{18}F]Fluor-L-DOPA, " [Ph.D. thesis]*, Forschungszentrum Jülich, Universität zu Köln, 2007.

[61] R. Martin, D. Baumgart, S. Hübner et al., "Automated nucleophilic one-pot synthesis of ^{18}F-L-DOPA with high specific activity using the GE TRACERlab MX*FDG*," *Journal of Labelled Compounds and Radiopharmaceuticals*, vol. 56, supplement S126, 2013.

[62] A. Al-Labadi, K.-P. Zeller, and H.-J. Machulla, "Synthesis of 6-[^{18}F]fluoroveratraldehyde by nucleophilic halogen exchange at electron-rich precursors," *Journal of Radioanalytical and Nuclear Chemistry*, vol. 270, no. 2, pp. 313–318, 2006.

[63] Y.-S. Ding, C.-Y. Shiue, J. S. Fowler, A. P. Wolf, and A. Plenevaux, "No-carrier-added (NCA) aryl [^{18}F]fluorides via the nucleophilic aromatic substitution of electron-rich aromatic rings," *Journal of Fluorine Chemistry*, vol. 48, no. 2, pp. 189–206, 1990.

[64] C. Lemaire, M. Guillaume, R. Cantineau, and L. Christiaens, "No-carrier-added regioselective preparation of 6-[^{18}F]fluoro-L-dopa," *Journal of Nuclear Medicine*, vol. 31, no. 7, pp. 1247–1251, 1990.

[65] C. Lemaire, M. Guillaume, R. Cantineau, A. Plenevaux, and L. Christiaens, "An approach to the asymmetric synthesis of L-6-[^{18}F]fluorodopa via NCA nucleophilic fluorination," *Applied Radiation and Isotopes*, vol. 42, no. 7, pp. 629–635, 1991.

[66] C. Lemaire, P. Damhaut, A. Plenevaux, and D. Comar, "Enantioselective synthesis of 6-[fluorine-18]-fluoro-L-dopa from no-carrier-added fluorine-18-fluoride," *Journal of Nuclear Medicine*, vol. 35, no. 12, pp. 1996–2002, 1994.

[67] C. Lemaire, A. Plenevaux, R. Cantineau, L. Christiaens, M. Guillaume, and D. Comar, "Nucleophilic enantioselective synthesis of 6-[^{18}F]fluoro-L-dopa via two chiral auxiliaries," *Applied Radiation and Isotopes*, vol. 44, no. 4, pp. 737–744, 1993.

[68] G. N. Reddy, M. Haeberli, H.-F. Beer, and A. P. Schubiger, "An improved synthesis of no-carrier-added (NCA) 6-[^{18}F]fluoro-L-DOPA and its remote routine production for PET investigations of dopaminergic systems," *Applied Radiation and Isotopes*, vol. 44, no. 4, pp. 645–649, 1993.

[69] A. Horti, D. E. Redmond Jr., and R. Soufer, "No-carrier-added (NCA) synthesis of 6-[^{18}F]fluoro-L-DOPA using 3,5,6,7,8,8a-hexahydro-7,7,8a-trimethyl-[6*S*-(6α, 8α, 8$\alpha\beta$)]-6,8-methano-2*H*-1,4-benzoxazin-2-one," *Journal of Labelled Compounds and Radiopharmaceuticals*, vol. 36, no. 5, pp. 409–423, 1995.

[70] A. Najafi, "Measures and pitfalls for successful preparation of "no carrier added" asymmetric 6-[^{18}F]fluor-L-dopa from ^{18}F-fluoride ion," *Nuclear Medicine and Biology*, vol. 22, no. 3, pp. 395–397, 1995.

[71] E. J. Corey, F. Xu, and M. C. Noe, "A rational approach to catalytic enantioselective enolate alkylation using a structurally rigidified and defined chiral quaternary ammonium salt under phase transfer conditions," *Journal of the American Chemical Society*, vol. 119, no. 50, pp. 12414–12415, 1997.

[72] C. Lemaire, S. Guillouet, A. Plenevaux, C. Brihaye, J. Aerts, and A. Luxen, "The synthesis of 6-[^{18}F]fluoro-L-dopa by chiral catalytic phase-transfer alkylation," *Journal of Labelled Compounds and Radiopharmaceuticals*, vol. 42, supplement 1, pp. S113–S115, 1999.

[73] S. Guillouet, C. Lemaire, G. Bonmarchand, L. Zimmer, and D. le Bars, "Large scale production of 6-[^{18}F]fluoro-L-DOPA in a semi-automated system," *Journal of Labelled Compounds and Radiopharmaceuticals*, vol. 44, supplement, pp. S868–S870, 2001.

[74] L. Zhang, G. Tang, D. Yin, X. Tang, and Y. Wang, "Enantioselective synthesis of no-carrier-added (NCA) 6-[^{18}F]fluoro-L-DOPA," *Applied Radiation and Isotopes*, vol. 57, no. 2, pp. 145–151, 2002.

[75] D. Yin, L. Zhang, G. Tang, X. Tang, and Y. Wang, "Enantioselective synthesis of no-carrier added (NCA) 6-[^{18}F]Fluoro-L-Dopa," *Journal of Radioanalytical and Nuclear Chemistry*, vol. 257, no. 1, pp. 179–185, 2003.

[76] "Fluorodopa (^{18}F) (prepared by electrophilic substitution) injection," *European Pharmacopoeia*, vol. 6, pp. 990–992, 2008.

[77] S. Kaneko, K. Ishiwata, K. Hatano, H. Omura, K. Ito, and M. Senda, "Enzymatic synthesis of no-carrier-added 6-[^{18}F]fluoro-L-dopa with β- tyrosinase," *Applied Radiation and Isotopes*, vol. 50, no. 6, pp. 1025–1032, 1999.

[78] C. Lemaire, S. Gillet, S. Guillouet, A. Plenevaux, J. Aerts, and A. Luxen, "Highly enantioselective synthesis of no-carrier-added 6-[^{18}F]fluoro-L-dopa by chiral phase-transfer alkylation," *European Journal of Organic Chemistry*, no. 13, pp. 2899–2904, 2004.

[79] C. Lemaire, L. Libert, A. Plenevaux, J. Aerts, X. Franci, and A. Luxen, "Fast and reliable method for the preparation of ortho- and para-[^{18}F]fluorobenzyl halide derivatives: key intermediates for the preparation of no-carrier-added PET aromatic radiopharmaceuticals," *Journal of Fluorine Chemistry*, vol. 138, pp. 48–55, 2012.

[80] R. N. Krasikova, V. V. Zaitsev, S. M. Ametamey et al., "Catalytic enantioselective synthesis of ^{18}F-fluorinated α-amino acids under phase-transfer conditions using (*S*)-NOBIN," *Nuclear Medicine and Biology*, vol. 31, no. 5, pp. 597–603, 2004.

[81] Y. N. Belokon, K. A. Kochetkov, T. D. Churkina et al., "Highly efficient catalytic synthesis of alpha-amino acids under phase-transfer conditions with a novel catalyst/substrate pair," *Angewandte Chemie: International Edition*, vol. 40, pp. 1948–1951, 2001.

[82] M. Smrčina, J. Poláková, Š. Vyskočil, and P. Kočovský, "Synthesis of enantiomerically pure binaphthyl derivatives. Mechanism of the enantioselective, oxidative coupling of naphthols and designing a catalytic cycle," *Journal of Organic Chemistry*, vol. 58, no. 17, pp. 4534–4538, 1993.

[83] B. Shen, W. Ehrlichmann, M. Uebele, H.-J. Machulla, and G. Reischl, "Automated synthesis of n.c.a. [^{18}F]FDOPA via nucleophilic aromatic substitution with [^{18}F]fluoride," *Applied Radiation and Isotopes*, vol. 67, no. 9, pp. 1650–1653, 2009.

[84] B. Shen, D. Löffler, G. Reischl, H.-J. Machulla, and K.-P. Zeller, "Nucleophilic [^{18}F]Fluorination and subsequent decarbonylation of methoxy-substituted nitro- and halogen-benzenes activated by one or two formyl groups," *Journal of Labelled Compounds and Radiopharmaceuticals*, vol. 53, no. 3, pp. 113–119, 2010.

[85] B. Shen, D. Löffler, K.-P. Zeller, M. Übele, G. Reischl, and H.-J. Machulla, "Effect of aldehyde and methoxy substituents on nucleophilic aromatic substitution by [^{18}F]fluoride," *Journal of Fluorine Chemistry*, vol. 128, no. 12, pp. 1461–1468, 2007.

[86] L. C. Libert, X. Franci, A. R. Plenevaux et al., "Production at the Curie level of no-carrier-added 6-^{18}F-fluoro-L-dopa," *Journal of Nuclear Medicine*, vol. 54, no. 7, pp. 1154–1161, 2013.

[87] S.-S. Jew and H.-G. Park, "Cinchona-based phase-transfer catalysts for asymmetric synthesis," *Chemical Communications*, no. 46, pp. 7090–7103, 2009.

[88] S. Forsback, O. Eskola, M. Haaparanta, J. Bergman, and O. Solin, "Electrophilic synthesis of 6-[^{18}F]fluoro-L-DOPA using post-target produced [^{18}F]F2," *Radiochimica Acta*, vol. 96, no. 12, pp. 845–848, 2008.

[89] S. Forsback, O. Eskola, J. Bergman, M. Haaparanta, and O. Solin, "Alternative solvents for electrophilic synthesis of 6-[^{18}F] fluoro-L-DOPA," *Journal of Labelled Compounds and Radiopharmaceuticals*, vol. 52, no. 7, pp. 286–288, 2009.

[90] E. Lee, J. M. Hooker, and T. Ritter, "Nickel-mediated oxidative fluorination for PET with aqueous [^{18}F] fluoride," *Journal of the American Chemical Society*, vol. 134, no. 42, pp. 17456–17458, 2012.

[91] I. S. R. Stenhagen, A. K. Kirjavainen, S. J. Forsback et al., "Fluorination of an arylboronic ester using [^{18}F]selectfluor bis(triflate): application to 6-[^{18}F]fluoro-l-DOPA," *Chemical Communications*, vol. 49, no. 14, pp. 1386–1388, 2013.

[92] R. Chirakal, G. Firnau, and E. S. Garnett, "High yield synthesis of 6-[^{18}F]fluoro-L-dopa," *Journal of Nuclear Medicine*, vol. 27, no. 3, pp. 417–421, 1986.

[93] K. Ishiwata, S. Ishii, M. Senda, Y. Tsuchiya, and K. Tomimoto, "Electrophilic synthesis of 6-[^{18}F]fluoro-L-DOPA: use of 4-*O*-pivaloyl-L-DOPA as a suitable precursor for routine production," *Applied Radiation and Isotopes*, vol. 44, no. 4, pp. 755–759, 1993.

[94] T. Chaly, J. R. Dahl, R. Matacchieri et al., "Synthesis of 6-[^{18}F]fluorodopamine with a synthetic unit made up of primarily sterile disposable components and operated by a master slave manipulator," *Applied Radiation and Isotopes*, vol. 44, no. 5, pp. 869–873, 1993.

[95] F. Füchtner, J. Zessin, P. Mäding, and F. Wüst, "Aspects of 6-[^{18}F]fluoro-L-DOPA preparation," *Nuklearmedizin*, vol. 47, pp. 62–64, 2008.

Hindawi Publishing Corporation
BioMed Research International
Volume 2014, Article ID 203601, 13 pages
http://dx.doi.org/10.1155/2014/203601

Review Article

Zirconium-89 Labeled Antibodies: A New Tool for Molecular Imaging in Cancer Patients

Floor C. J. van de Watering,[1] Mark Rijpkema,[1] Lars Perk,[2] Ulrich Brinkmann,[3] Wim J. G. Oyen,[1] and Otto C. Boerman[1]

[1] *Department of Radiology and Nuclear Medicine, Radboud University Medical Center, Geert Grooteplein Zuid 10, 6525 GA, Nijmegen, The Netherlands*
[2] *Radboud Translational Medicine B.V., Reinier Postlaan 2, 6525 GC, Nijmegen, The Netherlands*
[3] *Roche Pharma Research & Early Development, Large Molecule Research, Nonnenwald 2, 82377 Penzberg, Germany*

Correspondence should be addressed to Otto C. Boerman; otto.boerman@radboudumc.nl

Received 14 March 2014; Accepted 23 April 2014; Published 28 May 2014

Academic Editor: Roland Haubner

Antibody based positron emission tomography (immuno-PET) imaging is of increasing importance to visualize and characterize tumor lesions. Additionally, it can be used to identify patients who may benefit from a particular therapy and monitor the therapy outcome. In recent years the field is focused on ^{89}Zr, a radiometal with near ideal physical and chemical properties for immuno-PET. In this review we will discuss the production of ^{89}Zr, the bioconjugation strategies, and applications in (pre-)clinical studies of ^{89}Zr-based immuno-PET in oncology. To date, ^{89}Zr-based PET imaging has been investigated in a wide variety of cancer-related targets. Moreover, clinical studies have shown the feasibility for ^{89}Zr-based immuno-PET to predict and monitor treatment, which could be used to tailor treatment for the individual patient. Further research should be directed towards the development of standardized and robust conjugation methods and improved chelators to minimize the amount of released Zr^{4+} from the antibodies. Additionally, further validation of the imaging method is required. The ongoing development of new ^{89}Zr-labeled antibodies directed against novel tumor targets is expected to expand applications of ^{89}Zr-labeled immuno-PET to a valuable method in the medical imaging.

1. Introduction

Molecular biomarkers can be used to monitor, image, and measure biological processes at molecular or cellular level. Different types of biomarkers are known, including diagnostic, prognostic, and predictive biomarkers, or a combination of these [1]. Extensive research has been done on the development of molecular imaging biomarkers in the field of cancer. This has led to tools that can be used to visualize and characterize tumor lesions. An advantage of using molecular imaging agents is the noninvasive nature of these procedures, whereas in conventional methods a more invasive procedure is used (e.g., blood sample or biopsy). Various imaging modalities can be used for tumor visualization such as fluorescent imaging, magnetic resonance imaging (MRI) or radionuclide imaging with positron emission tomography (PET), or single photon emission computed tomography (SPECT). In most cases, the use of PET is preferred over SPECT since higher spatial resolution images can be obtained and images can be analyzed quantitatively more accurately with PET. Specific uptake of molecular biomarkers can be achieved using radiolabeled targeting agents such as antibodies, directed against tumor-associated antigens like epidermal growth factor receptor (EGFR) [2], human epidermal growth factor receptor 2 (HER2), and many others. The high specificity and affinity of radiolabeled antibodies make them attractive candidates as an imaging agent. For example, ^{89}Zr-labeled anti-HER2 antibodies can be used to differentiate between $HER2^+$ and $HER2^-$ tumors [3], also appreciating intra- and intertumoral heterogeneity. An additional application of radiolabeled antibodies is to identify patients who may benefit from a particular therapy and monitor therapy outcome based on the level of tumor-associated antigen expression [4]. However, the relative slow pharmacokinetics of intact antibodies

($t_{1/2}$ = 3-4 days) requires the use of radionuclides with long half-lives (e.g., ^{111}In (2.8 days) for SPECT or ^{89}Zr (3.3 days) and ^{124}I (4.2 days) for PET [5]). For antibody based PET imaging (immune-PET) ^{89}Zr has several advantages: ^{89}Zr has a half-life of 78.4 h which matches the pharmacokinetics of antibodies and it has a relative low average positron energy of 395 keV, making it an ideal candidate for high resolution PET imaging of slow-accumulating biomolecules. In addition, ^{89}Zr-based agents are safer to handle and more stable *in vivo* making them better candidates than ^{124}I-based agents for clinical applications. Due to the numerous advantages of ^{89}Zr-based immuno-PET, the field is progressing at a rapid and exciting pace. In this review, the potential of ^{89}Zr-based immuno-PET in oncology will be reviewed. The production of ^{89}Zr, the bioconjugation strategies, and applications in (pre-)clinical studies are discussed.

2. Radiochemical Properties of ^{89}Zr

^{89}Zr decays (half-life of 78.4 h) first via positron emission and electron capture to ^{89m}Y (half-life of 15.7 s) which in turn decays via gamma ray emission (909 keV) to the stable ^{89}Y. With its relatively low energy positrons (average energy 395 keV) ^{89}Zr provides high resolution PET images. In addition, the energy disparity between the photons (511 keV) and the gamma rays (909 keV) prevents the latter from interfering with the detection of 511 keV photons. In contrast, its halogen competitor, ^{124}I, produces high energy photons of different energies (603 keV (63.0%), 1691 keV (10.9%), and 723 keV (10.4%) [6]) which may result in random and scatter coincidences and therefore in more background noise as compared to ^{89}Zr. Hence, reconstruction of ^{89}Zr-based PET scans is more straightforward to attain good image quality compared to ^{124}I. Although ^{89}Zr has many advantages over other PET radionuclides, some essential shielding requirements during transport and handling of ^{89}Zr are needed (half-value layer of ^{89}Zr in lead is roughly 10 mm). High energy and highly penetrating photons (909 keV) are emitted during ^{89}Zr decay in high abundance.

3. Production of ^{89}Zr

The first production of ^{89}Zr was done by Link et al. [7] by a (p,n) nuclear reaction by bombarding ^{89}Y on Y foil with 13 MeV protons [5]. The produced ^{89}Zr needed several purification steps and was obtained in 80% yield with radionuclidic purity exceeding 99%. Nowadays, many medical centers are able to produce medical isotopes using low-energy cyclotrons that are capable of bombarding targets with protons of low energy (<20 MeV). Therefore, the most common route to produce ^{89}Zr is via the ^{89}Y (p, n) ^{89}Zr reaction on commercially available ^{89}Y target foils. The above route will in general result in high yields (94-95%) and high radionuclidic purities (>99%). Competing nuclear reaction, like (p, 2n) reactions, can result in small amounts radionuclidic byproducts, such as ^{88}Zr and ^{88}Y [8]. Several separation and purification techniques with variable outcomes are used including anion exchange, cation exchange, and solvent extraction [9–11]. For synthesizing such radiopharmaceuticals for patients, automated units for a clean, fast, safe, and reproducible radionuclide synthesis according to good manufacturing practice (GMP) are necessary. Several groups have designed and built automated systems for ^{89}Zr [12, 13]. For example Wooten et al. [14] reported a custom-made system to safely and routinely produce ^{89}Zr with high radionuclidic purity (>99.99%) and satisfactory effective specific activity (5–353 mCi·μmol^{-1} (0.01%–0.88% of theoretical specific activity)) based on previous developments in separation and purification techniques [9–11, 15].

4. The Need for Efficient Chelators

The release of $^{89}Zr^{4+}$ from the antibodies needs to be prevented, because the free radionuclide can accumulate in the mineral bone and can associate with plasma proteins. This leads to depositing significant doses to the bone marrow [16]. Therefore, an appropriate chelator system is necessary to minimize the disassociation of ^{89}Zr from the antibodies. Over the years, several chelators have been used with different success, such as diethylenetriaminepentaacetic acid (DTPA), ethylenediaminetetraacetic acid (EDTA), 1,4,7,10-tetraacetic acid (DOTA), and desferoxamine (DFO) [17]. The stability of Zr-DOTA, Zr-DTPA, and Zr-EDTA was found to be limited. The thermodynamic stability of Zr-DTPA is slightly higher than that of Zr-EDTA, most likely because DTPA coordinatively saturates the Zr^{4+}, while EDTA requires exogenous water molecules [18]. DFO is the most prominent chelator of Zr^{4+}. DFO is a hexadentate siderophore containing three hydroxamate groups for chelating metals and a primary amine tail for conjugation to a biomolecule (Figure 1). Besides a zirconium chelator, it is a chelating agent for several other metal ions [19]. It demonstrated good stability, releasing less than 0.2% of Zr^{4+} after 24 h in serum [20] and after seven days in serum still less than 2% demetallation occurs [21]. Several proof-of-principle preclinical studies have been conducted using DFO to label antibodies with ^{89}Zr; however, the *in vivo* stability of this complex remains an issue, because free ^{89}Zr is observed in the bone dependent on the *in vivo* behavior of the antibody [22]. Several studies have attempted to improve the linkage between DFO and the antibody [9, 23], whereas others have focused on improving the chelate itself [24]. Eventually, a ligand that is both octadentate and oxygen-rich is believed to be the most stable Zr^{4+} chelator, since it would be able to incorporate all eight coordination sites of zirconium [22]. This novel high stability Zr^{4+} ligand would in theory minimize the uptake of liberated Zr^{4+} in the bone and other nontargeted tissues. To date, the design, synthesis, and the evaluation of such a Zr^{4+} chelate requires further research.

4.1. Conjugation of Antibodies with DFO. As DFO is currently the most promising chelator for $^{89}Zr^{4+}$, conjugation of antibodies with DFO will be discussed here in detail (Figure 1). Several methods are available to conjugate DFO based on

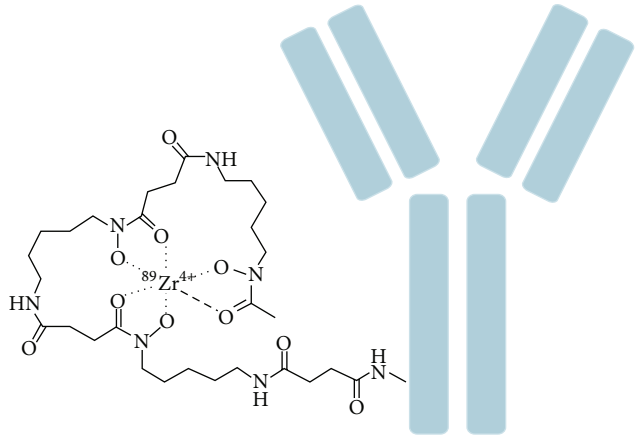

Figure 1: Schematic overview of ^{89}Zr-labeled antibody using DFO as chelator.

the reaction of an activated bifunctional chelator with a lysine or cysteine residue of the antibody. The different conjugation techniques do not only have different conjugation efficiencies, but also affect the biodistribution of the radiolabeled antibody [22].

The earliest reports on conjugation of DFO to bioactive molecules is based on the addition of thiols to the amino group of DFO [20]. In this approach DFO was modified by *N*-succinimidyl-S-acetylthioacetate (SATA), resulting in an S-acetyl-protected thiol derivatized form of chelator. In parallel, maleimide moieties were introduced in the antibody by the reaction with 4-(*N*-maleimidomethyl) cyclohexane carboxylic acid N-hydroxysuccinimide ester (SMCC). Next, the two formed compounds were combined and in the presence of hydroxylamine at physiological pH the DFO-antibody conjugate was formed. Following this early work, Verel et al. introduced a novel conjugation approach, which was based on an activated 2,3,5,6-tetrafluorophenol (TFP) chelate ester which can form a stable amide bond with the ε-amino-groups of the lysine residues of the monoclonal antibody (mAb) [9]. This laborious approach consisted of 5 steps which involve (i) the extension of DFO with succinyl anhydride, (ii) protection of side-reactions of the hydroxamate groups of the ligand by complexation with Fe^{3+}, (iii) formation of activated TFP ester, (iv) conjugation of activated DFO-ester to the unmodified antibody, and (v) removal of Fe^{3+} from the chelator. Nowadays the most widely used method in preclinical ^{89}Zr-based immuno-PET uses the conjugation strategy with *N*-succinimidyl-DFO, which addresses ε-amino groups of lysine side chains [22, 25–30]. Since the Zr^{4+} field is rapidly growing and becoming more mainstream in the clinical setting, simple methods for DFO conjugation preferably using commercial available starting materials are essential. Perk et al. introduced a simplified method using a commercially available *p*-isothiocyanatobenzyl-DFO (DFO-Bz-NCS) chelate, which can be directly attached to the ε-aminogroups of the lysine residues of an antibody by forming a stable thiourea linkage [23]. Despite the fact that this method is simpler than the *N*-succinimidyl-DFO chemistry, it requires more expertise mainly because of the limited water solubility of the chelator precursor.

A limitation of the conjugation of DFO to antibodies is compromised immunoreactivity, because the chelator may interfere with the antigen-binding domain of the antibody, especially if there are lysines in or close to the complementarity determining regions of the antibody. To overcome these limitations site-specific strategies using engineered cysteine residues can be used in combination with thiol-reactive DFO derivatives such as bromoacetamido-desferrioxamine (DFO-Bac), iodoacetamido-desferrioxamine (DFO-Iac), and maleimidocyclohexyl-desferrioxamine (DFO-CHX-Mal) [31]. The radiolabeled antibodies using these thiol-reactive DFO derivatives were stable and showed similar characteristics as the lysine-linked complexes. Remarkably, no significant difference was observed between the immunoreactivity of the site-specific complex and the lysine-linked complexes.

Another novel conjugation approach for effective labeling of ^{89}Zr to antibodies is the use of click chemistry between an acetylene group and an azide. This approach might not significantly improve the targeting of tumors compared with DFO-based conjugation strategies; however, with this approach it is possible to fully tailor the constructs. Furthermore, the modular system can be used for direct comparison of bioconjugates with different radiometals as the the chelator-modified antibodies are synthesized using identical ligation conditions resulting in similar immunoreactivity and chelator/antibody ratios [32]. Several studies have been reported on bioorthogonal click chemistry [32], Staudinger ligation [33], or catalyst-free click chemistry [34]. The click chemistry as specialized conjugation method is expected to expand the scope of ^{89}Zr-based PET.

5. Preclinical Studies with ^{89}Zr

Over the last years several ^{89}Zr-labeled antibodies directed against different tumor types have been evaluated in preclinical studies (e.g., [9, 18, 22, 35, 36]; see Table 1). Here these developments of ^{89}Zr-labeled antibodies in preclinical studies will be discussed based on their tumor target.

5.1. Targeting CD20. The glycosylated phosphoprotein, CD20, is expressed on the surface of B-cell lymphomas, hairy

Table 1: Overview of the described preclinical and clinical studies using ^{89}Zr-labeled antibodies.

Target	Type of tumor	Targeting vector
CD147	Pancreas	059-053
CD20*	Non-Hodgkin's lymphoma	ibritumomab tiuxetan
CD44v6*	Head and neck squamous cell carcinoma	cmAb U36
EGFR	Multiple	Cetuximab
EGP-1	Prostate	hRS7
GPC3	Liver	αGPC3
HER1	Colorectal	Panitumunmab
HER2*	Breast and ovarian	Trastuzumab
IGF-1R	Triple negative breast cancer	R1507
MET	Head and neck squamous cell carcinoma and gastric	DN30
MN/CA IX	Renal cell carcinoma	cG250
PSMA	Prostate	7E11
PIGF	Liver	RO5323441
VEGF*	Breast, head, and neck squamous cell carcinoma and ovarian	Bevacizumab

*Targets evaluated in clinical studies.

leukemia, B-cell chronic lymphocytic leukemia, and melanoma cells. ^{89}Zr-labeled antibodies directed against CD20 might be useful to measure and monitor the therapeutic effect of non-Hodgkin's lymphoma (NHL) therapy [18, 37]. The ^{89}Zr-Desferrioxamine-rituximab, an antibody directed against CD20, specifically targeted the human CD20 antigen in a humanized CD20-expressing transgenic mouse model (huCD20TM). ^{90}Y-labeled anti-CD20 mAb ibritumomab tiuxetan (Zevalin) is approved for treatment of patients with relapsed and refractory NHL. In a pilot study, ^{89}Zr-labeled ibritumomab tiuxetan was shown to have a nearly identical biodistribution compared to ^{90}Y-labeled counterpart [18]. This indicated that a scout scan with ^{89}Zr-ibritumomab immuno-PET can be used to assess, predict, and quantify the biodistribution of ^{90}Y-ibritumomab tiuxetan.

5.2. Targeting CD44. The cell-surface glycoprotein, CD44, is involved in many biological processes including adhesion of cells to extracellular matrix proteins, lymphocyte-endothelial cell interactions, metastasis formation, migration of cells, and T cell activation/adherence [38]. The v6 splice variant of CD44 is involved in tumorigenesis, tumor cell invasion, and metastasis and is expressed preferentially in squamous cell carcinomas [39]. Preclinical studies using ^{89}Zr-labeled anti-CD44v6 chimeric monoclonal antibody cU36 demonstrated that the tracer was able to detect small tumors in nude mice with HNSCC xenografts [9, 40]. In addition, it was reported that ^{89}Zr-cU36 PET imaging was a suitable candidate for scouting of therapeutic doses of ^{90}Y-cU36 [40, 41]. Recently, evaluation of ^{89}Zr-RG7356, an antibody directed against the constant part of CD44, was performed in mice bearing tumor xenografts with different levels of CD44 expression and RG7356 responsiveness, namely, MDA-MB-231 (CD44+, responsive), PL45 (CD44+, nonresponsive), and HepG2 (CD44−, nonresponsive) [42]. ^{89}Zr-RG7356 selectively targeted CD44+ responsive and nonresponsive tumors in mice. ^{89}Zr-RG7356 whole body immuno-PET in healthy cynomolgus monkeys revealed antibody uptake in spleen, salivary gland, and bone marrow, which might be related to the expression of CD44 in these organs. The ^{89}Zr-RG7356 uptake in the normal organs decreased with increasing dose of unlabeled RG7356, indicating saturable targeting of CD44 in these animals.

5.3. Targeting EGFR. The epidermal growth factor receptor (EGFR) is a member of the ErbB family. It plays a crucial role in differentiation, proliferation, and survival of many different tumor types, including breast, lung bladder, and colon carcinoma [2]. The overexpression of EGFR is associated with more aggressive tumors and poor prognosis due to the resistance of treatment [43, 44]. Many mAbs have been developed to inhibit the EGFR activation [2]. A well-known example is cetuximab (Erbitux), a chimeric IgG, which upon binding to the ligand-binding domain induces internalization of EGFR and thereby blocking downstream signalling [45, 46]. Several studies showed tumor regression upon treatment with cetuximab [47–50].

^{89}Zr-labeled cetuximab was evaluated for scouting the biodistribution of ^{90}Y- and ^{177}Lu-cetuximab in tumor bearing mouse and thus potentially allowing the estimation of the radiation dose delivered to tumors and normal tissues during radioimmunotherapy with ^{90}Y- and ^{177}Lu-cetuximab [51]. It was reported that the ^{89}Zr-immuno-PET could be used for *in vivo* scouting of ^{90}Y- and ^{177}Lu-labeled mAbs. However, an increased bone uptake of ^{89}Zr-cetuximab, compared with ^{90}Y- and ^{177}Lu labeled cetuximab, was observed indicating that ^{89}Zr is more efficiently incorporated in the bone compared to the other radiometals (^{90}Y- and ^{177}Lu). Therefore estimating bone marrow doses based on ^{89}Zr-bone uptake is not straightforward. Another study investigated the relation between the *in vivo* expression of EGFR and the tumor uptake of ^{89}Zr-cetuximab [52]. In this study no clear-cut relationship was found, suggesting that apart from antigen

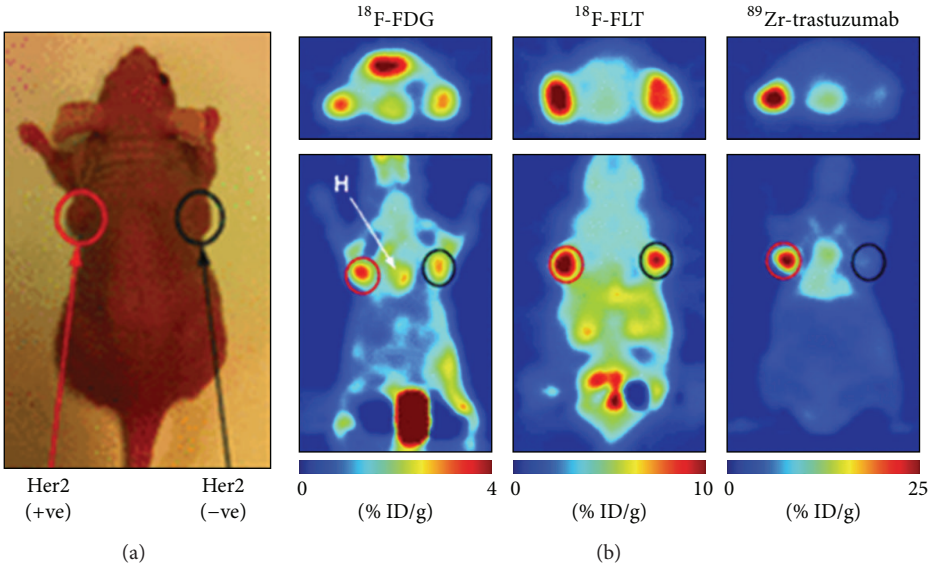

Figure 2: Specificity of ^{89}Zr-trastuzumab for HER2-positive tumors. Coronal ^{89}Zr-trastuzumab, ^{18}F-FDG, and ^{18}F-FLT PET images of athymic nude mice bearing subcutaneous HER2-positive NCI-N87 (left) and HER2-negative MKN-74 (right) are shown. ROIs (%ID/g) for ^{89}Zr-trastuzumab, ^{18}F-FDG, and ^{18}F-FLT are indicated. +ve = positive; −ve = negative. This research was originally published in [3]. © by the Society of Nuclear Medicine and Molecular Imaging, Inc.

expression other parameters determine the tumor uptake of ^{89}Zr-cetuximab.

Another approved mAb to inhibit the EGFR signalling is panitumumab. It was the first recombinant human monoclonal antibody (IgG2) approved by the FDA for the treatment of patients with EGFR-expressing metastatic colorectal cancer (mCRC) [53]. In several studies the use of panitumumab for noninvasive, *in vivo* imaging of HER1 expression in tumors is reported [54–58]. The use of ^{89}Zr-panitumumab for immuno-PET of HER1 expression was recently evaluated in a direct comparison with ^{111}In-panitumumab. The organ biodistribution between ^{111}In- and ^{89}Zr-panitumumab was almost identical [55]. In addition, the targeting of ^{89}Zr-panitumumab correlated well with the HER1 expression. Recently, a standardized and straightforward stepwise ~5 h production method was reported for the production of clinical-grade ^{89}Zr-panitumumab [59]. In this method clinical-grade panitumumab is conjugated with DFO chelate and subsequently radiolabeled with ^{89}Zr resulting in high yields (>70%) and high radiochemical purity (>98%).

5.4. Targeting HER2. Human epidermal growth factor receptor 2 (HER2) is another member of the ErbB family. It is involved in angiogenesis, differentiation, metastasis, proliferation, and cell survival upon heterodimerization with other members of the EGF receptor family [60]. HER2 overexpression is found in many types of tumors including breast and ovarian cancer. The FDA approved anti-HER2 mAb trastuzumab (Herceptin, Genentech, CA, USA) to be used for the treatment of HER2 positive breast tumors, since it blocks the HER2 activation [60]. The efficacy of the treatment is dependent on the HER2 expression level. The HER2 expression level in a tumor is not static and may vary over time [60]. In addition, the HER2 expression is found to be different between the primary lesion and the distant metastatic lesions in the same patient. Noninvasive *in vivo* imaging to visualize HER2 expressing using radiolabeled trastuzumab has been extensively investigated [29, 30, 61]. PET imaging using ^{89}Zr-trastuzumab has been performed in different murine tumor models and accumulation of the tracer was found to be HER2 specific [29, 30, 61]. For example, the tumor uptake of ^{89}Zr-trastuzumab in nude mice with a subcutaneous human ovarian cancer xenografts (SK-OV-3) was high (~30% ID/g) and the biodistribution was similar to that of ^{111}In-trastuzumab [29]. Recently, the specificity of ^{89}Zr-trastuzumab, ^{18}F-FDG, and ^{18}F-FLT PET for HER2-positive gastric cancer was evaluated ([3]; Figure 2). The study revealed a high specific uptake of ^{89}Zr-trastuzumab in HER2-positive tumors, whereas ^{18}F-FDG and ^{18}F-FLT PET were unable to differentiate between HER2-positive and HER2-negative tumors. In addition, ^{89}Zr-trastuzumab was used to quantitatively determine the HER2 expression level after treatment. For example, after treatment with a heat shock protein 90 (hsp90) inhibitor a significant decrease in HER2 expression could be measured based on the ^{89}Zr-trastuzumab tumor targeting [30, 62]. A combination treatment of hsp90 inhibitor 17AAG and the EGFR/HER2 tyrosine kinase inhibitor, lapatinib, revealed an even stronger reduction of the HER2 expression levels using ^{89}Zr-Trastuzumab-F(ab$'$)$_2$ fragment as probe [63]. Additionally, the biological effect of afatinib, an EGFR/HER2/HER4 inhibitor, in a HER2-positive gastric xenograft models was evaluated [3]. In this model the uptake of ^{18}F-FDG did not change after afatinib therapy,

whereas a decrease in ^{89}Zr-trastuzumab uptake was observed upon treatment. The lower uptake of the ^{89}Zr-trastuzumab correlated with the decreased HER2 expression as determined by immunoblots and immunohistochemistry. Thus, ^{89}Zr-trastuzumab PET might be useful for the characterization, treatment planning, and treatment monitoring of HER-2 positive cancers.

5.5. Targeting VEGF. Vascular endothelial growth factor (VEGF) is a proangiogenic factor in both normal tissues and in tumors. The overexpression of VEGF and its receptors (VEGFR) are associated with poor prognosis [64]. The humanized anti-VEGF mAb, bevacizumab (Avastin, Genentech/Hoffmann-La Roche), is capable of blocking angiogenesis by depleting VEGF and thereby preventing its binding to the VEGFR. This neutralizes VEGF actions (see, e.g., [65–72]). A direct comparison between ^{89}Zr-bevacizumab and an irrelevant ^{89}Zr-labeled IgG revealed a significantly higher tumor uptake of ^{89}Zr-bevacizumab in nude mice with human ovarian SK-OV-3 tumors [73]. Besides using ^{89}Zr-bevacizumab as PET tracer for non-invasive *in vivo* imaging of VEGF expression in the tumor microenvironment, potentially it can also be used to predict or monitor an antiangiogenic response. For example, hsp90 is crucial player in VEGF transcription and can be used to treat ovarian tumors. In nude mice with a subcutaneous human ovarian cancer xenografts (A2780), uptake of ^{89}Zr-bevacizumab in the tumors correlated with the therapeutic effect of the hsp90 inhibitor, NVP-AUY922, [74]. In another study the effect of the mTOR inhibitor, everolimus, on the VEGF production was evaluated [75]. Everolimus treatment caused decreased ^{89}Zr-bevacizumab uptake in subcutaneous A2780 human ovarian tumor. The results were in line with the lower VEGF-A protein levels in tumor lysates of treated versus untreated tumors. These results indicate ^{89}Zr-bevacizumab can be used to monitor tumor VEGF-A levels as an early biomarker of the antiangiogenic effect of mTOR inhibitor treatment.

^{89}Zr-labeled ranibizumab, a monoclonal antibody fragment (Fab) derivative of bevacizumab, was used to detect and monitor the early antiangiogenic response to treatment with sunitinib, a VEGFR tyrosine kinase inhibitor, in nude mice bearing a subcutaneous A2780 human ovarian tumor or Colo205 human colon cancer xenografts. ^{89}Zr-ranibizumab PET matched better with the observed results obtained by histology, immunohistochemistry, and tumor proliferation and vascularization assays, than ^{18}F-FDG PET and ^{15}O-water PET. Since ranibizumab has a serum half-life of only 2 to 6 hours, rapid and sequential follow-up PET scans are feasible with ^{89}Zr-ranibizumab [76]. Therefore, in contrast to ^{89}Zr-bevacizumab, ^{89}Zr-ranibizumab can be used for imaging of rapid dynamic alterations in VEGF response in tumors.

5.6. Targeting PIGF. The clinical benefits of angiogenesis inhibitors can be compromised by the upregulation of proangiogenic factors such as the placental growth factor (PIGF). PIGF, a VEGF homolog, is expressed in low levels in normal tissue and can be overexpressed in tumor cells. PIGF contributes to angiogenesis in pregnancy, wound healing, ischemic conditions, and tumor growth [77, 78]. PIGF inhibitors are able to reduce the angiogenesis and tumor cell motility. The antitumor activity of a humanized mAb directed against PIGF-1 and PIGF-2, RO5323441, in human tumor xenograft models has been reported [79]. To further explore and validate the use of RO5323441, the tumor and normal tissue uptake of ^{89}Zr-RO5323441 at different time points was evaluated in mice bearing human PlGF-expressing Huh7 hepatocellular cancer xenografts. Tumor accumulation of ^{89}Zr-RO5323441 was specific and time- and dose-dependent.

5.7. Targeting PSMA. Prostate-specific membrane antigen (PSMA) is a transmembrane glycoprotein which is associated with increased tumor progression, development of castration resistance, and/or resistance to hormone-based treatments [80–82]. PMSA is expressed in a limited range of normal tissues including benign prostatic epithelium, renal proximal tubule, small bowel, and the brain; however, the expression level is 2 to 3 times lower than in prostate cancer specimens [83]. ^{89}Zr-labeled anti-PSMA mAb, J591, was able to differentiate between subcutaneous PSMA positive and negative tumors in athymic nude mice [21], making it a potential target for clinical noninvasive identification and quantification of PSMA-positive tumors.

5.8. Targeting CD147. CD147, a member of the immunoglobulin superfamily, is involved in many physiological functions including embryo implantation, early stage neural network formation, and spermatogenesis [85]. Overexpression of CD147 is found in many types of cancer including pancreatic cancer and induces expression of matrix metalloproteinases (MMPs) and VEGF [86, 87]. Several (pre-)clinical studies have been performed using anti-CD147 antibodies to inhibit the actions of CD147 and revealed a reduction in proliferation, invasion and metastasis of tumors [88–90]. Almost 90% of the pancreatic cancers have high CD147 expression levels [86]. Sugyo et al. evaluated the CD147 expression in four pancreatic cancer cell lines (MIA Paca-2, PANC-1, BxPC-3, and AsPC-1) using the human ^{125}I-, ^{67}Ga-, or ^{89}Zr-labeled anti-CD147 mAb (059-053) [84]. Additionally, the *in vivo* CD147 expression was evaluated using ^{125}I- or ^{89}Zr-labeled 059-053 in mice with s.c. and orthotopic MIA Paca-2 and A4 (non-CD147-expressing) tumors. The biodistribution data revealed significantly higher tumor uptake of ^{89}Zr-059-053 in MIA Paca-2 tumors than in the A4 tumors (Figure 3). PET/CT imaging demonstrated that orthotopic MIA Paca-2 tumors could be visualized with ^{89}Zr-059-053 PET. High expression of CD147 is not only restricted to pancreatic cancer, but is also found in other types of cancer including bladder, breast, colorectal, cervical, liver, and ovarian cancer [84–86]. Therefore, ^{89}Zr-059-053 might also be applied in patients with these cancer types.

5.9. Targeting CAIX. Hypoxia in tumors is associated with a poor prognosis in many tumor types since it is associated with resistance to radiotherapy and chemotherapy. In many tumor types carbonic anhydrase IX (CAIX) has been validated as

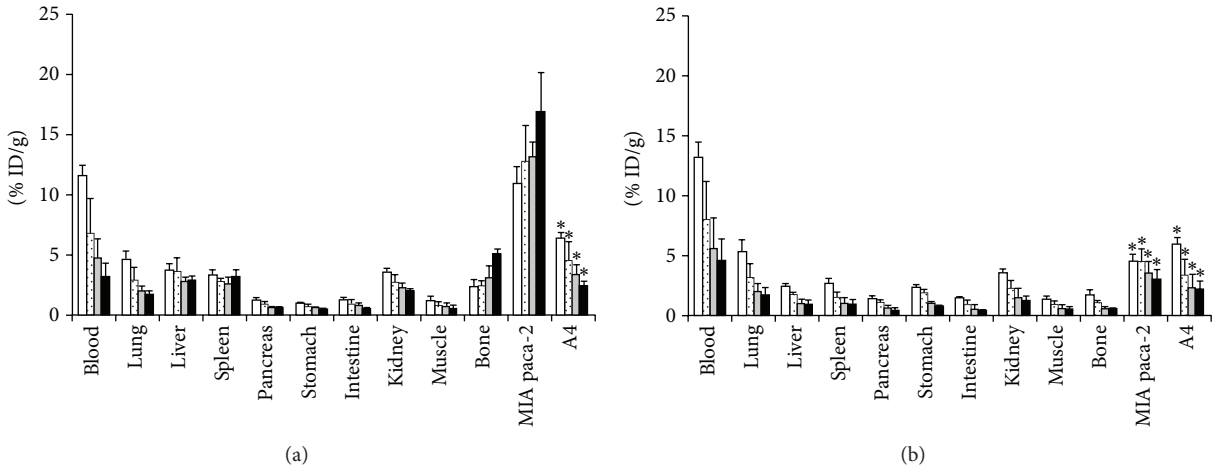

Figure 3: *In vivo* biodistribution experiments in nude mice bearing MIA PaCa-2 and A4 xenografts of radiolabeled anti-CD147 antibody 059-053. Samples were collected and weighted, and radioactivity was measured at days 1 (white bars), 2 (dot bars), 4 (gray bars), and 6 (black bars) after intravenous injection of 37 kBq each of ^{89}Zr-059-053 (a) and ^{125}I-059-053 (b). Data are expressed as mean ± SD ($n = 5$). $^{*}P < 0.01$ versus ^{89}Zr-059-053 tumor uptake at each time point analyzed by ANOVA with the Student-Newman-Keuls method multiple comparison test. This research was originally published in [84].

an intrinsic hypoxia-related cell marker [91]. Using antibodies directed against CAIX it is possible to select patients for hypoxia-targeting or -modifying treatment combined with radiotherapy. For example, it is possible to visualize tumor hypoxia in mice bearing s.c. SCCNij3 head and neck squamous cell carcinomas using ^{89}Zr-cG250-F(ab′)$_2$, an anti-CAIX antibody fragment [92]. In a direct comparison, the tumor uptake of mAb ^{89}Zr-cG250 in mice with CAIX-expressing clear cell renal cell carcinoma (ccRCC) xenografts (NU-12) was significantly higher compared to that of ^{124}I-cG250 [93]. This indicates that PET imaging of ccRCC tumors with ^{89}Zr-cG250 could be more sensitive than ^{124}I-cG250-PET. CAIX targeted ^{89}Zr-PET imaging is a candidate for imaging hypoxia in different types of tumors and deserves further exploration.

5.10. Targeting IGF-1R. The insulin like growth factor 1 receptor (IGF-1R) is a transmembrane receptor expressed in many human cancers, including in ~35% of all triple-negative breast carcinomas. It is involved in the proliferation, apoptosis, angiogenesis, and tumor invasion. Heskamp et al. reported excellent tracer uptake of ^{111}In-R1507 and ^{89}Zr-R1507, a human mAb directed against IGF-1R, in mice with s.c. SUM149 triple-negative breast cancer xenografts [94]. This suggests that the use of ^{89}Zr-R1507 in patient selection of IGF-1R-targeted therapy is possible.

5.11. Targeting Met. The expression of hepatocyte growth factor receptor tyrosine kinase (Met) was measured by PET using ^{76}Br or ^{89}Zr-labeled-onartuzumab, a mAb against Met [95]. Both tracers specifically targeted Met; however, at later time points a higher tumor uptake was observed with ^{89}Zr-Onartuzumab. This suggests that ^{89}Zr-onartuzumab is the preferred tracer to identify Met expression in cancer patients and possibly to predict and monitor the treatment with Met-targeted therapeutics. In another study, the potential of immune-PET using ^{89}Zr (residualising radionuclide) or ^{124}I-labeled (non-residualising radionuclide) anti-Met mAb DN30 was evaluated in mice with s.c. GLT-16 (high Met expression) and FaDu (low Met expression) tumors [96]. The biodistribution data revealed significantly higher tumor uptake of ^{89}Zr-DN30 than ^{124}I-DN30 in GTL-16 tumor-bearing mice. Similar blood levels were found indicating that DN30 is internalized. ^{89}Zr-DN30 immuno-PET imaging was able to visualize small tumor lesions with a higher ^{89}Zr tumor uptake in GTL-16 than FaDu tumor-bearing mice. Additionally, the correlation was high for PET-image-derived ^{89}Zr tumor uptake and the *ex vivo*-assessed ^{89}Zr tumor uptake. This indicates that ^{89}Zr-labeled immuno-PET is an attractive method to evaluate Met-targeted therapeutics.

5.12. Targeting GPC3. The glypican-3 (GPC3) is a hepatocellular-specific cell surface proteoglycan overexpressed in most hepatocellular carcinomas (HCC). Sham et al. reported excellent tracer uptake of ^{89}Zr-αGPC3, a mAb directed against GPC3, in mice with GPC3-expressing HepG2 liver tumors [97]. This suggests that the use of ^{89}Zr-αGPC3 to image HCC in the liver is possible.

6. Clinical Translation of ^{89}Zr Immuno-PET

The ^{89}Zr-labeled antibodies against the targets mentioned above all show promising results for clinical translation. To date, several clinical investigations using ^{89}Zr-labeled antibody constructs have been reported [1, 22, 98]. Here these recent clinical studies will be discussed.

6.1. ^{89}Zr-Labeled cU36. The first clinical trial using the ^{89}Zr-cU36 PET to target CD44 expressing tumors showed that

the tracer was able to detect primary tumors as well as metastases in the neck region with similar sensitivity as computed tomography (CT) and magnetic resonance imaging (MRI) [99]. The results are promising, although several issues remain to be addressed. In the clinical study micrometastases were missed with ^{89}Zr-cU36 PET, so immuno-PET may be less suited as a staging tool, but more suitable to characterize tumors. Moreover, 2 out of the 20 patients developed antibodies against the chimeric cU36 antibody (HACA), which may hinder repetitive imaging procedures.

6.2. ^{89}Zr-Ibritumomab. A clinical prospective study was conducted to evaluate the biodistribution and radiation dosimetry of CD20-targeting ^{90}Y-ibritumomab tiuxetan using ^{89}Zr-ibritumomab tiuxetan [100]. Patients with relapsed or refractory aggressive B-cell (CD20-positive) NHL underwent a PET scan at 1, 72 and 144 h after injection of 70 MBq ^{89}Zr-ibritumomab tiuxetan and again 2 weeks later after coinjection of 15 MBq/kg or 30 MBq/kg ^{90}Y-ibritumomab tiuxetan. The results revealed that simultaneous therapy of ^{90}Y-ibritumomab tiuxetan did not affect the biodistribution of ^{89}Zr-ibritumomab. A second aim of the study was to estimate the radiation doses during radioimmunotherapy with ^{90}Y-ibritumomab tiuxetan based on ^{89}Zr-ibritumomab PET. The highest ^{90}Y absorbed dose was observed in liver (3.2 ± 1.8 mGy/MBq) followed by the spleen (2.9 ± 0.7 mGy/MBq). Additionally, the correlation was high for standardized uptake value (SUV) of ^{89}Zr-ibritumomab tiuxetan and absorbed dose of ^{90}Y-ibritumomab tiuxetan in the liver at 72 h p.i. and 144 h p.i. This suggests that in the future a single ^{89}Zr-ibritumomab tiuxetan PET scan is sufficient to optimize the administered amount of ^{90}Y-ibritumomab tiuxetan RIT for individual patients

6.3. ^{89}Zr-Trastuzumab. In 2010, the first-in-man report of ^{89}Zr-trastuzumab for imaging of HER2-positive lesions in patients with metastatic breast cancer was published [101]. 14 Patients were included in the study that either received 10 (n = 2) or 50 (n = 5) mg ^{89}Zr-trastuzumab if trastuzumab-naïve and 10 mg ^{89}Zr-trastuzumab (n = 7) if on trastuzumab treatment (37 MBq ^{89}Zr-trastuzumab). Per patient at least two PET scans were acquired between day 2 and day 5 after injection of ^{89}Zr-trastuzumab. The trastuzumab-naïve patients required a 50 mg dose for effective imaging whereas 10 mg was sufficient in the trastuzumab-treated patients. A higher dose in the trastuzumab-naïve patients was required as an increased ^{89}Zr-trastuzumab clearance was observed at lower doses due to presence of extracellular domains of the HER2 receptor in the circulation [102]. After binding of ^{89}Zr-trastuzumab to these extracellular domains, the immune complex was cleared by the liver and excreted in the intestines. In patients treated with trastuzumab at the time of injection, higher doses of ^{89}Zr-trastuzumab did not improve imaging since complex formation was minimal. Overall, the uptake of ^{89}Zr-trastuzumab in the tumor lesions was high. The best time to assess tumor uptake was 4 to 5 days after injection of ^{89}Zr-trastuzumab (Figure 4). All the known and even some unknown lesions were detected with PET. Of interest, metastatic brain lesions were detected in several patients, despite the fact that trastuzumab cannot penetrate the blood-brain barrier. This is probably because the blood-brain barrier in patients with brain metastasis is disrupted allowing ^{89}Zr-trastuzumab to pass. In this study HER2 overexpressing lesions could be distinguished from non-HER2 expressing lesions. These data indicate the potential use of ^{89}Zr-trastuzumab to improve the diagnosis of patients with HER2-positive breast cancer especially when lesions are inaccessible for biopsy.

6.4. ^{89}Zr-Bevacizumab. Recently, a clinical study was performed to assess the use of ^{89}Zr-bevacizumab for the visualization of VEGF-A in primary breast cancer [103]. In 23 patients, 26 tumors were detected by conventional imaging modalities mammography (n = 22), ultrasound (n = 25), or MRI (n = 1). Prior to surgery and 4 days p.i. of 37 MBq of ^{89}Zr-bevacizumab the patients underwent a PET/CT scan of the breasts and the axillary regions (Figure 5(a)). 25 of the 26 breast cancer nodules (96.1%) were detected using ^{89}Zr-bevacizumab. Also, a correlation between the VEGF-A protein level in the tumors observed as measured by VEGF-A ELISA and the tumor uptake ^{89}Zr-bevacizumab was found (Figure 5(b)). This study provides evidence that ^{89}Zr-bevacizumab might be a potential candidate for the classification of breast tumors and to predict and monitor the effect of VEGF-A targeted therapies.

7. Conclusions

Clinical studies revealed that the use of ^{89}Zr-based immuno-PET results in high spatial resolution images with high tumor uptake and a good signal to noise ratio. Therefore, the use of ^{89}Zr-labeled antibodies is very promising for noninvasive visualization of tumor-associated antigens before, during, and after therapy. This makes ^{89}Zr-based immuno-PET an excellent imaging modality to predict and monitor treatment and to tailor treatment for individual patients. However, to fully integrate ^{89}Zr-based immuno-PET in the clinic several hurdles still need to be overcome. For example, standardized and robust methods for stable conjugation of DFO to antibodies should become available to obtain clinical-grade conjugates. In addition, research should focus on the development of improved chelators to minimize the amount of liberated Zr^{4+}. Although some direct comparison studies between ^{89}Zr-based immuno-PET and immuno-PET using other PET isotopes have been performed, and supplementary quantitative and comprehensive comparison studies are needed to evaluate the value of ^{89}Zr-based immuno-PET. Additionally, the radiation dose for patients undergoing a ^{89}Zr-based immuno-PET (75 MBq of ^{89}Zr-cmAb U36) was found to result in a mean effective dose of 0.53 to 0.66 mSv/MBq [104] which is significantly higher compared to the mean effective dose of clinically used ^{111}In- and ^{99}Tcm-based tracers (^{111}In-IgG (75 MBq) was 0.25 mSv/MBq and ^{99}Tcm-IgG (750 MBq) was mu Sv/MBq) [105]. The high

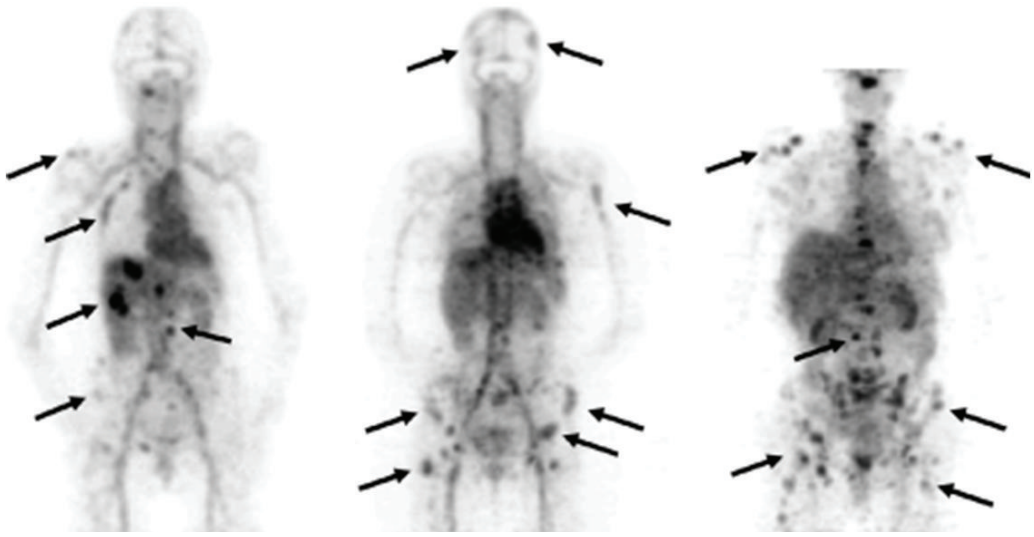

(a) (b) (c)

Figure 4: Examples of ^{89}Zr-trastuzumab uptake 5 days after the injection: (a) a patient with liver and bone metastases and ((b) and (c)) two patients with multiple bone metastases. A number of lesions have been specifically indicated by arrows. This research was originally published in [101].

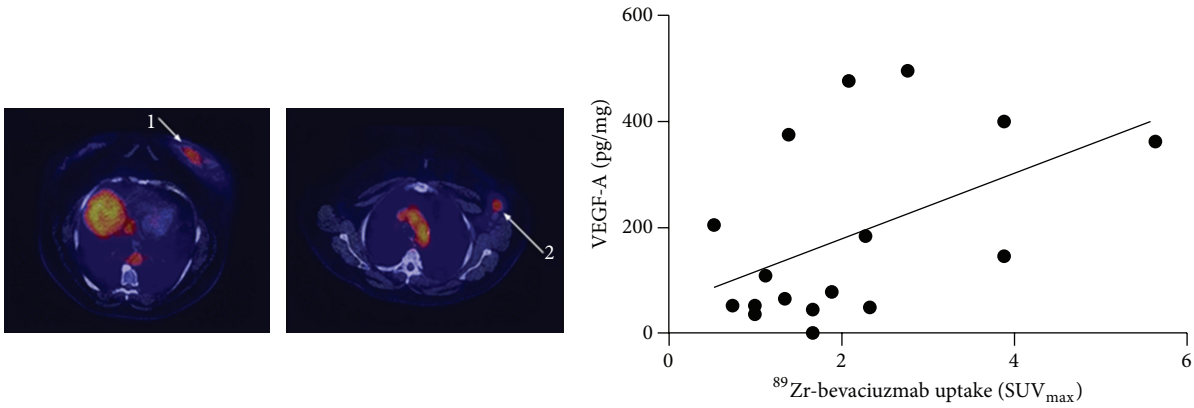

(a) (b)

Figure 5: (a) Axial slices of ^{89}Zr-bevacizumab PET from patient with primary breast tumor (1) and lymph node metastasis (2). (b) Correlation between ^{89}Zr-bevacizumab tumor uptake (x-axis) and tumor VEGF-A (y-axis) levels as measured by ELISA (Pearson $r = 0.49$, $P = 0.04$). This research was originally published in [103]. © by the Society of Nuclear Medicine and Molecular Imaging, Inc.

radiation dose for patients will limit repeated application of ^{89}Zr-based immuno-PET [104]. However, introducing new PET/CT scanners to allow better-quality immuno-PET images to be obtained with a lower ^{89}Zr radioactivity (37 MBq) dose have reduced the radiation dose [102, 103]. Furthermore, research is focusing on combining ^{89}Zr-based immuno-PET with other imaging modalities. For example, the use of ^{89}Zr-immuno-PET in combination with near-infrared fluorescence (NIRF) imaging has been reported by several groups [106–108]. The ongoing development of new ^{89}Zr-labeled antibodies directed against novel tumor targets is believed to rapidly expand applications of ^{89}Zr-labeled immuno-PET to a valuable method in the medical imaging.

Conflict of Interests

The authors declare that there is no conflict of interests regarding the publication of this paper.

References

[1] Y. Zhang, H. Hong, and W. Cai, "PET tracers based on zirconium-89," *Current Radiopharmaceuticals*, vol. 4, no. 2, pp. 131–139, 2011.

[2] R. S. Herbst and D. M. Shin, "Monoclonal antibodies to target epidermal growth factor receptor-positive tumors: a new paradigm for cancer therapy," *Cancer*, vol. 94, no. 5, pp. 1593–1611, 2002.

[3] Y. Y. Janjigian, N. Viola-Villegas, J. P. Holland et al., "Monitoring afatinib treatment in HER2-positive gastric cancer with 18F-FDG and ^{89}Zr-trastuzumab PET," *Journal of Nuclear Medicine*, vol. 54, no. 6, pp. 936–943, 2013.

[4] C. H. Muselaers, A. B. Stillebroer, I. M. Desar et al., "Tyrosine kinase inhibitor sorafenib decreases ^{111}In-girentuximab uptake in patients with clear cell renal cell carcinoma," *Journal of Nuclear Medicine*, vol. 55, no. 2, pp. 242–247, 2014.

[5] T. J. Wadas, E. H. Wong, G. R. Weisman, and C. J. Anderson, "Coordinating radiometals of copper, gallium, indium, yttrium, and zirconium for PET and SPECT imaging of disease," *Chemical Reviews*, vol. 110, no. 5, pp. 2858–2902, 2010.

[6] M. Lubberink and H. Herzog, "Quantitative imaging of ^{124}I and ^{86}Y with PET," *European Journal of Nuclear Medicine and Molecular Imaging*, vol. 38, supplement 1, pp. S10–S18, 2011.

[7] J. M. Link, K. A. Krohn, J. F. Eary et al., "Sixth international symposium on radiopharmaceutical chemistry. Abstracts. Part III," *Journal of Labelled Compounds and Radiopharmaceuticals*, vol. 23, no. 10-12, p. 1297, 1986.

[8] A. Kasbollah, P. Eu, S. Cowell, and P. Deb, "Review on production of ^{89}Zr in a medical cyclotron for PET radiopharmaceuticals," *Journal of Nuclear Medicine Technology*, vol. 41, no. 1, pp. 35–41, 2013.

[9] I. Verel, G. W. Visser, R. Boellaard, M. Stigter-van Walsum, G. B. Snow, and G. A. van Dongen, "^{89}Zr immuno-PET: comprehensive procedures for the production of ^{89}Zr-labeled monoclonal antibodies," *Journal of Nuclear Medicine*, vol. 44, no. 8, pp. 1271–1281, 2003.

[10] W. E. Meijs, J. D. M. Herscheid, H. J. Haisma et al., "Production of highly pure no-carrier added ^{89}Zr for the labelling of antibodies with a positron emitter," *Applied Radiation and Isotopes*, vol. 45, no. 12, pp. 1143–1147, 1994.

[11] J. P. Holland, Y. Sheh, and J. S. Lewis, "Standardized methods for the production of high specific-activity zirconium-89," *Nuclear Medicine and Biology*, vol. 36, no. 7, pp. 729–739, 2009.

[12] A. L. Wooten, G. D. Schweitzer, L. A. Lawrence, E. Madrid, and S. E. Lapi, "An automated system for production of ^{89}Zr," in *Proceedings of the 14th International Workshop on Targetry and Target Chemistry (WTTC '12)*, vol. 1509 of *AIP Conference*, pp. 201–205, Playa del Carmen, México, August 2012.

[13] J. Siikanen, M. Peterson, T. A. Tran, P. Roos, T. Ohlsson, and A. Sandell, "A peristaltic pump driven ^{89}Zr separation module," in *Proceedings of the 14th International Workshop on Targetry and Target Chemistry (WTTC '12)*, vol. 1509 of *AIP Conference*, pp. 206–210, Playa del Carmen, México, August 2012.

[14] A. L. Wooten, E. Madrid, and G. D. Schweitzer, "Routine production of ^{89}Zr using an automated module," *Applied Sciences*, vol. 3, no. 3, pp. 593–613, 2013.

[15] J. D. M. Herscheid, C. M. Vos, and A. Hoekstra, "Manganese-52m for direct application: a new 52Fe/52mMn generator based on a hydroxamate resin," *The International Journal of Applied Radiation and Isotopes*, vol. 34, no. 6, pp. 883–886, 1983.

[16] D. S. Abou, T. Ku, and P. M. Smith-Jones, "*In vivo* biodistribution and accumulation of ^{89}Zr in mice," *Nuclear Medicine and Biology*, vol. 38, no. 5, pp. 675–681, 2011.

[17] W. M. Al Lawati, J. S. Jean, T. R. Kulp et al., "Characterisation of organic matter associated with groundwater arsenic in reducing aquifers of Southwestern Taiwan," *Journal of Hazardous Materials*, vol. 262, pp. 970–979, 2013.

[18] L. R. Perk, O. J. Visser, M. Stigter-van Walsum et al., "Preparation and evaluation of ^{89}Zr-Zevalin for monitoring of ^{90}Y-Zevalin biodistribution with positron emission tomography," *European Journal of Nuclear Medicine and Molecular Imaging*, vol. 33, no. 11, pp. 1337–1345, 2006.

[19] T. Kiss and E. Farkas, "Metal-binding ability of desferrioxamine B," *Journal of Inclusion Phenomena and Molecular Recognition in Chemistry*, vol. 32, no. 2-3, pp. 385–403, 1998.

[20] W. E. Meijs, J. D. Herscheid, H. J. Haisma, and H. M. Pinedo, "Evaluation of desferal as a bifunctional chelating agent for labeling antibodies with Zr-89," *International Journal of Radiation Applications and Instrumentation A: Applied Radiation and Isotopes*, vol. 43, no. 12, pp. 1443–1447, 1992.

[21] J. P. Holland, V. Divilov, N. H. Bander, P. M. Smith-Jones, S. M. Larson, and J. S. Lewis, "^{89}Zr-DFO-J591 for immunoPET of prostate-specific membrane antigen expression *in vivo*," *Journal of Nuclear Medicine*, vol. 51, no. 8, pp. 1293–1300, 2010.

[22] M. A. Deri, B. M. Zeglis, L. C. Francesconi, and J. S. Lewis, "PET imaging with ^{89}Zr: from radiochemistry to the clinic," *Nuclear Medicine and Biology*, vol. 40, no. 1, pp. 3–14, 2013.

[23] L. Perk, M. W. D. Vosjan, G. W. Visser et al., "*p*-isothiocyanatobenzyl-desferrioxamine: a new bifunctional chelate for facile radiolabeling of monoclonal antibodies with zirconium-89 for immuno-PET imaging," *European Journal of Nuclear Medicine and Molecular Imaging*, vol. 37, no. 2, pp. 250–259, 2010.

[24] F. Guerard, Y.-S. Lee, R. Tripier, L. P. Szajek, J. R. Deschamps, and M. W. Brechbiel, "Investigation of Zr(IV) and ^{89}Zr(IV) complexation with hydroxamates: progress towards designing a better chelator than desferrioxamine B for immuno-PET imaging," *Chemical Communications*, vol. 49, no. 10, pp. 1002–1004, 2013.

[25] S. Bhattacharyya, K. Kurdziel, L. Wei et al., "Zirconium-89 labeled panitumumab: a potential immuno-PET probe for HER1-expressing carcinomas," *Nuclear Medicine and Biology*, vol. 40, no. 4, pp. 451–457, 2013.

[26] D. J. Vugts, G. W. Visser, and G. A. van Dongen, "^{89}Zr-PET radiochemistry in the development and application of therapeutic monoclonal antibodies and other biologicals," *Current Topics in Medicinal Chemistry*, vol. 13, no. 4, pp. 446–457, 2013.

[27] K. Leung, "^{89}Zr-desferrioxamine b-j591 anti-prostate-specific membrane antigen monoclonal antibody," in *Molecular Imaging and Contrast Agent Database (MICAD)*, National Center for Biotechnology Information, Bethesda, Md, USA, 2004.

[28] A. Chopra, "^{89}Zr-labeled *p*-isothiocyanatobenzyl-desferrioxamine b (df-bz-ncs)-conjugated panitumumab, a fully human monoclonal antibody directed against the extracellular domain III of the epidermal growth factor receptor," in *Molecular Imaging and Contrast Agent Database (MICAD)*, National Center for Biotechnology Information, Bethesda, Md, USA, 2004.

[29] E. C. Dijkers, J. G. Kosterink, A. P. Rademaker et al., "Development and characterization of clinical-grade ^{89}Zr- trastuzumab for HER2/*neu* immunoPET imaging," *Journal of Nuclear Medicine*, vol. 50, no. 6, pp. 974–981, 2009.

[30] T. H. Oude Munnink, M. A. de Korte, W. B. Nagengast et al., "^{89}Zr-trastuzumab PET visualises HER2 downregulation by the HSP90 inhibitor NVP-AUY922 in a human tumour xenograft," *European Journal of Cancer*, vol. 46, no. 3, pp. 678–684, 2010.

[31] J. N. Tinianow, H. S. Gill, A. Ogasawara et al., "Site-specifically ^{89}Zr-labeled monoclonal antibodies for ImmunoPET," *Nuclear Medicine and Biology*, vol. 37, no. 3, pp. 289–297, 2010.

[32] B. M. Zeglis, P. Mohindra, G. I. Weissmann et al., "Modular strategy for the construction of radiometalated antibodies for positron emission tomography based on inverse electron

demand diels-alder click chemistry," *Bioconjugate Chemistry*, vol. 22, no. 10, pp. 2048–2059, 2011.

[33] D. J. Vugts, A. Vervoort, M. Stigter-van Walsum et al., "Synthesis of phosphine and antibody-azide probes for *in vivo* staudinger ligation in a pretargeted imaging and therapy approach," *Bioconjugate Chemistry*, vol. 22, no. 10, pp. 2072–2081, 2011.

[34] B. M. Zeglis, C. B. Davis, R. Aggeler et al., "Enzyme-mediated methodology for the site-specific radiolabeling of antibodies based on catalyst-free click chemistry," *Bioconjugate Chemistry*, vol. 24, no. 6, pp. 1057–1067, 2013.

[35] G. Fischer, U. Seibold, R. Schirrmacher, B. Wängler, and C. Wängler, "^{89}Zr, a radiometal nuclide with high potential for molecular imaging with pet: chemistry, applications and remaining challenges," *Molecules*, vol. 18, no. 6, pp. 6469–6490, 2013.

[36] H. H. Yeh, K. Ogawa, J. Balatoni et al., "Molecular imaging of active mutant L858R EGF receptor (EGFR) kinase-expressing nonsmall cell lung carcinomas using PET/CT," *Proceedings of the National Academy of Sciences of the United States of America*, vol. 108, no. 4, pp. 1603–1608, 2011.

[37] A. Natarajan, F. Habte, and S. S. Gambhir, "Development of a novel long-lived immunoPET tracer for monitoring lymphoma therapy in a humanized transgenic mouse model," *Bioconjugate Chemistry*, vol. 23, no. 6, pp. 1221–1229, 2012.

[38] D. S. Webb, Y. Shimizu, G. A. van Seventer, S. Shaw, and T. L. Gerrard, "LFA-3, CD44, and CD45: physiologic triggers of human monocyte TNF and IL-1 release," *Science*, vol. 249, no. 4974, pp. 1295–1297, 1990.

[39] J. W. Mulder, P. M. Kruyt, M. Sewnath et al., "Colorectal cancer prognosis and expression of exon-v6-containing CD44 proteins," *The Lancet*, vol. 344, no. 8935, pp. 1470–1472, 1994.

[40] I. Verel, G. W. Visser, R. Boellaard et al., "Quantitative ^{89}Zr immuno-PET for *in vivo* scouting of 90Y-labeled monoclonal antibodies in xenograft-bearing nude mice," *Journal of Nuclear Medicine*, vol. 44, no. 10, pp. 1663–1670, 2003.

[41] I. Verel, G. W. Visser, O. C. Boerman et al., "Long-lived positron emitters zirconium-89 and iodine-124 for scouting of therapeutic radioimmunoconjugates with PET," *Cancer Biotherapy and Radiopharmaceuticals*, vol. 18, no. 4, pp. 655–661, 2003.

[42] D. Vugts, D. Heuveling, M. Stigter-van Walsum et al., "Preclinical evaluation of ^{89}Zr-labeled anti-CD44 monoclonal antibody RG7356 in mice and cynomolgus monkeys: prelude to phase 1 clinical studies," *MAbs*, vol. 6, no. 2, pp. 567–575, 2013.

[43] F. Meric-Bernstam and M.-C. Hung, "Advances in targeting human epidermal growth factor receptor-2 signaling for cancer therapy," *Clinical Cancer Research*, vol. 12, no. 21, pp. 6326–6330, 2006.

[44] H. J. Burstein, "The distinctive nature of HER2-positive breast cancers," *The New England Journal of Medicine*, vol. 353, no. 16, pp. 1652–1654, 2005.

[45] B. A. W. Hoeben, J. D. M. Molkenboer-Kuenen, W. J. G. Oyen et al., "Radiolabeled cetuximab: dose optimization for epidermal growth factor receptor imaging in a head-and-neck squamous cell carcinoma model," *International Journal of Cancer*, vol. 129, no. 4, pp. 870–878, 2011.

[46] L. Koi, R. Bergmann, K. Brüchner et al., "Radiolabeled anti-EGFR-antibody improves local tumor control after external beam radiotherapy and offers theragnostic potential," *Radiotherapy and Oncology*, vol. 110, no. 2, pp. 362–369, 2014.

[47] P. Specenier and J. B. Vermorken, "Cetuximab: its unique place in head and neck cancer treatment," *Biologics*, vol. 7, no. 1, pp. 77–90, 2013.

[48] C. Jones, M. A. Taylor, and B. McWilliams, "The role of cetuximab as first-line treatment of colorectal liver metastases," *HPB*, vol. 15, no. 1, pp. 11–17, 2013.

[49] K. Boyd, S. M. Shea, and J. Patterson, "Cetuximab for treatment of advanced squamous cell carcinoma in solid organ transplant recipients," *Wiener Medizinische Wochenschrift*, vol. 163, no. 15-16, pp. 372–375, 2013.

[50] K. Unger, U. Niehammer, A. Hahn et al., "Treatment of metastatic colorectal cancer with cetuximab: influence on the quality of life," *Zeitschrift für Gastroenterologie*, vol. 51, no. 8, pp. 733–739, 2013.

[51] L. R. Perk, G. W. Visser, M. J. Vosjan et al., "^{89}Zr as a PET surrogate radioisotope for scouting biodistribution of the therapeutic radiometals ^{90}Y and ^{177}Lu in tumor-bearing nude mice after coupling to the internalizing antibody cetuximab," *Journal of Nuclear Medicine*, vol. 46, no. 11, pp. 1898–1906, 2005.

[52] H. J. Aerts, L. Dubois, L. Perk et al., "Disparity between *in vivo* EGFR expression and ^{89}Zr-labeled cetuximab uptake assessed with PET," *Journal of Nuclear Medicine*, vol. 50, no. 1, pp. 123–131, 2009.

[53] M. Wu, A. Rivkin, and T. Pham, "Panitumumab: human monoclonal antibody against epidermal growth factor receptors for the treatment of metastatic colorectal cancer," *Clinical Therapeutics*, vol. 30, no. 1, pp. 14–30, 2008.

[54] K. E. Day, L. Sweeny, B. Kulbersh, K. R. Zinn, and E. L. Rosenthal, "Preclinical comparison of near-infrared-labeled cetuximab and panitumumab for optical imaging of head and neck squamous cell carcinoma," *Molecular Imaging and Biology*, vol. 15, no. 6, pp. 722–729, 2013.

[55] A. J. Chang, R. A. de Silva, and S. E. Lapi, "Development and characterization of ^{89}Zr-labeled panitumumab for immunopositron emission tomographic imaging of the epidermal growth factor receptor," *Molecular Imaging*, vol. 12, no. 1, pp. 17–27, 2013.

[56] L. Shan, "Activatable alexa fluor680-conjugated panitumumab and indocyanine green-conjugated trastuzumab cocktail," in *Molecular Imaging and Contrast Agent Database (MICAD)*, National Center for Biotechnology Information, Bethesda, Md, USA, 2004.

[57] A. Chopra, "^{111}In-labeled panitumumab, a fully human monoclonal antibody directed against the extracellular domain III of the epidermal growth factor receptor," in *Molecular Imaging and Contrast Agent Database (MICAD)*, National Center for Biotechnology Information, Bethesda, Md, USA, 2004.

[58] K. J. Wong, K. E. Baidoo, T. K. Nayak, K. Garmestani, M. W. Brechbiel, and D. E. Milenic, "*In vitro* and *in vivo* pre-clinical analysis of a $F(ab')_2$ fragment of panitumumab for molecular imaging and therapy of HER1-positive cancers," *EJNMMI Research*, vol. 1, no. 1, pp. 1–15, 2011.

[59] L. Wei, J. Shi, G. Afari, and S. Bhattacharyya, "Preparation of clinical-grade ^{89}Zr-panitumumab as a positron emission tomography biomarker for evaluating epidermal growth factor receptor-targeted therapy," *Journal of Labelled Compounds and Radiopharmaceuticals*, vol. 57, no. 1, pp. 25–35, 2014.

[60] M. E. Gross, R. L. Shazer, and D. B. Agus, "Targeting the HER-kinase axis in cancer," *Seminars in Oncology*, vol. 31, supplement 3, no. 1, pp. 9–20, 2004.

[61] A. J. Chang, R. DeSilva, S. Jain, K. Lears, B. Rogers, and S. Lapi, "^{89}Zr-radiolabeled trastuzumab imaging in orthotopic and metastatic breast tumors," *Pharmaceuticals*, vol. 5, no. 1, pp. 79–93, 2012.

[62] J. P. Holland, E. Caldas-Lopes, V. Divilov et al., "Measuring the pharmacodynamic effects of a novel Hsp90 inhibitor on HER2/*neu* expression in mice using ^{89}Zr-DFO-trastuzumab," *PLoS ONE*, vol. 5, no. 1, Article ID e8859, 2010.

[63] T. H. Oude Munnink, E. G. de Vries, S. R. Vedelaar et al., "Lapatinib and 17AAG reduce ^{89}Zr-trastuzumab-F(ab′)^2 uptake in SKBR3 tumor xenografts," *Molecular Pharmaceutics*, vol. 9, no. 11, pp. 2995–3002, 2012.

[64] I. S. Moreira, P. A. Fernandes, and M. J. Ramos, "Vascular endothelial growth factor (VEGF) inhibition: a critical review," *Anti-Cancer Agents in Medicinal Chemistry*, vol. 7, no. 2, pp. 223–245, 2007.

[65] J. Lin and W. K. Kelly, "Targeting angiogenesis as a promising modality for the treatment of prostate cancer," *Urologic Clinics of North America*, vol. 39, no. 4, pp. 547–560, 2012.

[66] D. Maru, A. P. Venook, and L. M. Ellis, "Predictive biomarkers for bevacizumab: are we there yet?" *Clinical Cancer Research*, vol. 19, no. 11, pp. 2824–2827, 2013.

[67] M. T. Schweizer and M. A. Carducci, "From bevacizumab to tasquinimod: angiogenesis as a therapeutic target in prostate cancer," *Cancer Journal*, vol. 19, no. 1, pp. 99–106, 2013.

[68] A. Argiris, A. P. Kotsakis, T. Hoang et al., "Cetuximab and bevacizumab: preclinical data and phase II trial in recurrent or metastatic squamous cell carcinoma of the head and neck," *Annals of Oncology*, vol. 24, no. 1, pp. 220–225, 2013.

[69] J. A. Chan, K. Stuart, C. C. Earle et al., "Prospective study of bevacizumab plus temozolomide in patients with advanced neuroendocrine tumors," *Journal of Clinical Oncology*, vol. 30, no. 24, pp. 2963–2968, 2012.

[70] J. R. Kroep and J. W. Nortier, "The role of bevacizumab in advanced epithelial ovarian cancer," *Current Pharmaceutical Design*, vol. 18, no. 25, pp. 3775–3783, 2012.

[71] P. G. Morris, "Bevacizumab is an active agent for recurrent high-grade glioma, but do we need randomized controlled trials?" *Anti-Cancer Drugs*, vol. 23, no. 6, pp. 579–583, 2012.

[72] S. Sato and H. Itamochi, "Bevacizumab and ovarian cancer," *Current Opinion in Obstetrics and Gynecology*, vol. 24, no. 1, pp. 8–13, 2012.

[73] W. B. Nagengast, E. G. de Vries, G. A. Hospers et al., "*In vivo* VEGF imaging with radiolabeled bevacizumab in a human ovarian tumor xenograft," *Journal of Nuclear Medicine*, vol. 48, no. 8, pp. 1313–1319, 2007.

[74] W. B. Nagengast, M. A. de Korte, T. H. Oude Munnink et al., "^{89}Zr-bevacizumab PET of early antiangiogenic tumor response to treatment with HSP90 inhibitor NVP-AUY922," *Journal of Nuclear Medicine*, vol. 51, no. 5, pp. 761–767, 2010.

[75] A. R. van der Bilt, A. G. T. van Scheltinga, H. Timmer-Bosscha et al., "Measurement of tumor VEGF-A levels with ^{89}Zr-bevacizumab PET as an early biomarker for the antiangiogenic effect of everolimus treatment in an ovarian cancer xenograft model," *Clinical Cancer Research*, vol. 18, no. 22, pp. 6306–6314, 2012.

[76] W. B. Nagengast, M. N. Lub-de Hooge, S. F. Oosting et al., "VEGF-PET imaging is a noninvasive biomarker showing differential changes in the tumor during sunitinib treatment," *Cancer Research*, vol. 71, no. 1, pp. 143–153, 2011.

[77] P. Carmeliet, L. Moons, A. Luttun et al., "Synergism between vascular endothelial growth factor and placental growth factor contributes to angiogenesis and plasma extravasation in pathological conditions," *Nature Medicine*, vol. 7, no. 5, pp. 575–583, 2001.

[78] J. M. Rakic, V. Lambert, L. Devy et al., "Placental growth factor, a member of the VEGF family, contributes to the development of choroidal neovascularization," *Investigative Ophthalmology and Visual Science*, vol. 44, no. 7, pp. 3186–3193, 2003.

[79] T. H. Oude Munnink, K. R. Tamas, M. N. Lub-de Hooge et al., "Placental growth factor (PlGF)-specific uptake in tumor microenvironment of ^{89}Zr-labeled PlGF antibody RO5323441," *Journal of Nuclear Medicine*, vol. 54, no. 6, pp. 929–935, 2013.

[80] J. R. Osborne, N. H. Akhtar, S. Vallabhajosula, A. Anand, K. Deh, and S. T. Tagawa, "Prostate-specific membrane antigen-based imaging," *Urologic Oncology*, vol. 31, no. 2, pp. 144–154, 2013.

[81] Y. Zhang, Z. Guo, T. Du et al., "Prostate specific membrane antigen (PSMA): a novel modulator of p38 for proliferation, migration, and survival in prostate cancer cells," *Prostate*, vol. 73, no. 8, pp. 835–841, 2013.

[82] A. Afshar-Oromieh, A. Malcher, M. Eder et al., "PET imaging with a [^{68}Ga]gallium-labelled PSMA ligand for the diagnosis of prostate cancer: biodistribution in humans and first evaluation of tumour lesions," *European Journal of Nuclear Medicine and Molecular Imaging*, vol. 40, no. 4, pp. 486–495, 2013.

[83] M. J. Manyak, "Indium-111 capromab pendetide in the management of recurrent prostate cancer," *Expert Review of Anticancer Therapy*, vol. 8, no. 2, pp. 175–181, 2008.

[84] A. Sugyo, A. B. Tsuji, H. Sudo et al., "Evaluation of ^{89}Zr-labeled human anti-CD147 monoclonal antibody as a positron emission tomography probe in a mouse model of pancreatic cancer," *PLoS ONE*, vol. 8, no. 4, Article ID e61230, 2013.

[85] U. H. Weidle, W. Scheuer, D. Eggle, S. Klostermann, and H. Stockinger, "Cancer-related issues of CD147," *Cancer Genomics and Proteomics*, vol. 7, no. 3, pp. 157–169, 2010.

[86] S. Riethdorf, N. Reimers, V. Assmann et al., "High incidence of EMMPRIN expression in human tumors," *International Journal of Cancer*, vol. 119, no. 8, pp. 1800–1810, 2006.

[87] S. Zucker, M. Hymowitz, E. E. Rollo et al., "Tumorigenic potential of extracellular matrix metalloproteinase inducer," *The American Journal of Pathology*, vol. 158, no. 6, pp. 1921–1928, 2001.

[88] Z. N. Chen, L. Mi, J. Xu et al., "Targeting radioimmunotherapy of hepatocellular carcinoma with iodine (131I) metuximab injection: clinical phase I/II trials," *International Journal of Radiation Oncology Biology Physics*, vol. 65, no. 2, pp. 435–444, 2006.

[89] Z. Zhang, H. Bian, Q. Feng et al., "Biodistribution and localization of iodine-131-labeled Metuximab in patients with hepatocellular carcinoma," *Cancer Biology and Therapy*, vol. 5, no. 3, pp. 318–322, 2006.

[90] J. Xu, Z. Y. Shen, X. G. Chen et al., "A randomized controlled trial of licartin for preventing hepatoma recurrence after liver transplantation," *Hepatology*, vol. 45, no. 2, pp. 269–276, 2007.

[91] P. Swietach, A. Hulikova, R. D. Vaughan-Jones, and A. L. Harris, "New insights into the physiological role of carbonic anhydrase IX in tumour pH regulation," *Oncogene*, vol. 29, no. 50, pp. 6509–6521, 2010.

[92] B. A. W. Hoeben, J. H. A. M. Kaanders, G. M. Franssen et al., "PET of hypoxia with ^{89}Zr-labeled cG250-F(ab′)$_2$ in head and neck tumors," *Journal of Nuclear Medicine*, vol. 51, no. 7, pp. 1076–1083, 2010.

[93] A. M. Stillebroer, G. M. Franssen, P. F. A. Mulders et al., "ImmunoPET imaging of renal cell carcinoma with 124I- and ^{89}Zr-Labeled Anti-CAIX monoclonal antibody cG250 in mice," *Cancer Biotherapy & Radiopharmaceuticals*, vol. 28, no. 7, pp. 510–515, 2013.

[94] S. Heskamp, H. W. Van Laarhoven, J. D. Molkenboer-Kuenen et al., "ImmunoSPECT and immunoPET of IGF-1R expression with the radiolabeled antibody R1507 in a triple-negative breast cancer model," *Journal of Nuclear Medicine*, vol. 51, no. 10, pp. 1565–1572, 2010.

[95] E. M. Jagoda, L. Lang, V. Bhadrasetty et al., "Immuno-PET of the hepatocyte growth factor receptor met using the 1-armed antibody onartuzumab," *Journal of Nuclear Medicine*, vol. 53, no. 10, pp. 1592–1600, 2012.

[96] L. R. Perk, M. Stigter-van Walsum, G. W. Visser et al., "Quantitative PET imaging of Met-expressing human cancer xenografts with ^{89}Zr-labelled monoclonal antibody DN30," *European Journal of Nuclear Medicine and Molecular Imaging*, vol. 35, no. 10, pp. 1857–1867, 2008.

[97] J. G. Sham, F. M. Kievit, J. R. Grierson et al., "Glypican-3-targeted ^{89}Zr PET imaging of hepatocellular carcinoma," *Journal of Nuclear Medicine*, vol. 55, no. 5, pp. 799–804, 2014.

[98] J. L. Seitchik, J. C. Peeler, M. T. Taylor et al., "Genetically encoded tetrazine amino acid directs rapid site-specific *in vivo* bioorthogonal ligation with trans-cyclooctenes," *Journal of the American Chemical Society*, vol. 134, no. 6, pp. 2898–2901, 2012.

[99] P. K. Börjesson, Y. W. Jauw, R. Boellaard et al., "Performance of immuno-positron emission tomography with zirconium-89-labeled chimeric monoclonal antibody U36 in the detection of lymph node metastases in head and neck cancer patients," *Clinical Cancer Research*, vol. 12, no. 7, part 1, pp. 2133–2140, 2006.

[100] S. N. Rizvi, O. J. Visser, M. J. W. Vosjan et al., "Biodistribution, radiation dosimetry and scouting of 90Y- ibritumomab tiuxetan therapy in patients with relapsed B-cell non-Hodgkin's lymphoma using ^{89}Zr-ibritumomab tiuxetan and PET," *European Journal of Nuclear Medicine and Molecular Imaging*, vol. 39, no. 3, pp. 512–520, 2012.

[101] E. C. Dijkers, T. H. Oude Munnink, J. G. Kosterink et al., "Biodistribution of ^{89}Zr-trastuzumab and PET imaging of HER2-positive lesions in patients with metastatic breast cancer," *Clinical Pharmacology and Therapeutics*, vol. 87, no. 5, pp. 586–592, 2010.

[102] R. Bruno, C. B. Washington, J. Lu, G. Lieberman, L. Banken, and P. Klein, "Population pharmacokinetics of trastuzumab in patients with HER2+ metastatic breast cancer," *Cancer Chemotherapy and Pharmacology*, vol. 56, no. 4, pp. 361–369, 2005.

[103] S. B. M. Gaykema, A. H. Brouwers, M. N. L. Hooge et al., "^{89}Zr-bevacizumab PET imaging in primary breast cancer," *Journal of Nuclear Medicine*, vol. 54, no. 7, pp. 1014–1018, 2013.

[104] P. K. Börjesson, Y. W. Jauw, R. de Bree et al., "Radiation dosimetry of ^{89}Zr-labeled chimeric monoclonal antibody U36 as used for immuno-PET in head and neck cancer patients," *Journal of Nuclear Medicine*, vol. 50, no. 11, pp. 1828–1836, 2009.

[105] W. C. Buijs, W. J. Oyen, E. T. Dams et al., "Dynamic distribution and dosimetric evaluation of human non-specific immunoglobulin G labelled with ^{111}In or 99Tcm," *Nuclear Medicine Communications*, vol. 19, no. 8, pp. 743–751, 1998.

[106] A. G. T. Terwisscha van Scheltinga, G. M. van Dam, W. B. Nagengast et al., "Intraoperative near-infrared fluorescence tumor imaging with vascular endothelial growth factor and human epidermal growth factor receptor 2 targeting antibodies," *Journal of Nuclear Medicine*, vol. 52, no. 11, pp. 1778–1785, 2011.

[107] H. Hong, Y. Zhang, G. W. Severin et al., "Multimodality imaging of breast cancer experimental lung metastasis with bioluminescence and a monoclonal antibody dual-labeled with ^{89}Zr and IRDye 800CW," *Molecular Pharmaceutics*, vol. 9, no. 8, pp. 2339–2349, 2012.

[108] Y. Zhang, H. Hong, G. W. Severin et al., "ImmunoPET and near-infrared fluorescence imaging of CD105 expression using a monoclonal antibody dual-labeled with ^{89}Zr and IRDye 800CW," *American Journal of Translational Research*, vol. 4, no. 3, pp. 333–346, 2012.

Hindawi Publishing Corporation
BioMed Research International
Volume 2014, Article ID 361329, 16 pages
http://dx.doi.org/10.1155/2014/361329

Review Article

^{18}F-Labeling Using Click Cycloadditions

Kathrin Kettenbach,[1] Hanno Schieferstein,[1] and Tobias L. Ross[1,2]

[1] *Institute of Nuclear Chemistry, Johannes Gutenberg University Mainz, 55128 Mainz, Germany*
[2] *Radiopharmaceutical Chemistry, Department of Nuclear Medicine, Hannover Medical School, 30625 Hannover, Germany*

Correspondence should be addressed to Tobias L. Ross; ross.tobias@mh-hannover.de

Received 15 March 2014; Revised 29 April 2014; Accepted 1 May 2014; Published 27 May 2014

Academic Editor: Olaf Prante

Due to expanding applications of positron emission tomography (PET) there is a demand for developing new techniques to introduce fluorine-18 ($t_{1/2}$ = 109.8 min). Considering that most novel PET tracers are sensitive biomolecules and that direct introduction of fluorine-18 often needs harsh conditions, the insertion of ^{18}F in those molecules poses an exceeding challenge. Two major challenges during ^{18}F-labeling are a regioselective introduction and a fast and high yielding way under mild conditions. Furthermore, attention has to be paid to functionalities, which are usually present in complex structures of the target molecule. The Cu-catalyzed azide-alkyne cycloaddition (CuAAC) and several copper-free click reactions represent such methods for radiolabeling of sensitive molecules under the above-mentioned criteria. This minireview will provide a quick overview about the development of novel ^{18}F-labeled prosthetic groups for click cycloadditions and will summarize recent trends in copper-catalyzed and copper-free click ^{18}F-cycloadditions.

1. Introduction

For the application in positron emission tomography (PET) [1], fluorine-18 provides ideal nuclear physical characteristics for *in vivo* imaging. Fluorine-18 offers a half-life of 110 min, a β^+-branch of 97%, and especially a low β^+-energy of 635 keV, which is responsible for a very high spatial resolution [2]. The challenges for researchers are to develop convenient ^{18}F-labeling strategies, which include short reaction times and applicability for sensitive biomolecules. Especially the harsh conditions during direct ^{18}F-labeling pose an exceeding challenge [3, 4]. Therefore, most of the radiolabeling strategies focus on ^{18}F-containing prosthetic groups, which allow a sensitive and bioorthogonal ^{18}F-labeling to treat the multitude of functional groups in those bioactive compounds with respect.

The most established method, which fulfills all mentioned criteria, is given by click reactions. Especially the Cu(I)-catalyzed variant of the Huisgen 1,3-dipolar cycloaddition of terminal alkynes and azides offers a very powerful reaction with high specificity and excellent yields under mild conditions [5]. As a result, numerous PET tracers have been synthesized using CuAAC in a widespread spectrum of structural varieties of the prosthetic group within the last decade. One of the latest investigations deals with a polar clickable amino acid-based prosthetic group to further improve the pharmacokinetic properties of radiotracers, particularly suitable for peptides and proteins [6].

However, the need of cytotoxic copper during CuAAC has led to the necessity of alternative fast and copper-free click reaction strategies for radiofluorination and additionally enabling pretargeting approaches in living systems. Those so-called strain-promoted click reactions can be carried out between cyclooctyne derivatives and azides (strain-promoted azide-alkyne cycloaddition, SPAAC) [7–13] or tetrazines (tetrazine-trans-cyclooctyne (TTCO) ligation) [14–17] as well as between norbornene derivatives and tetrazines [18]. Especially, the TTCO ligation showed promising reaction rates, which makes this click reaction concept very suitable for ^{18}F-labeling and also for *in vivo* application in living systems. Very recently, new versions of ^{18}F-click cycloadditions are added to the range of reactions [19–25]. In this line, the first ^{18}F-labeled β-lactame became available via a new *radio*-Kinugasa reaction [21].

As a consequence, click cycloaddition is one of the most frequently applied methods for ^{18}F-labeling of new bioactive compounds, with or without a catalytic system. This can be

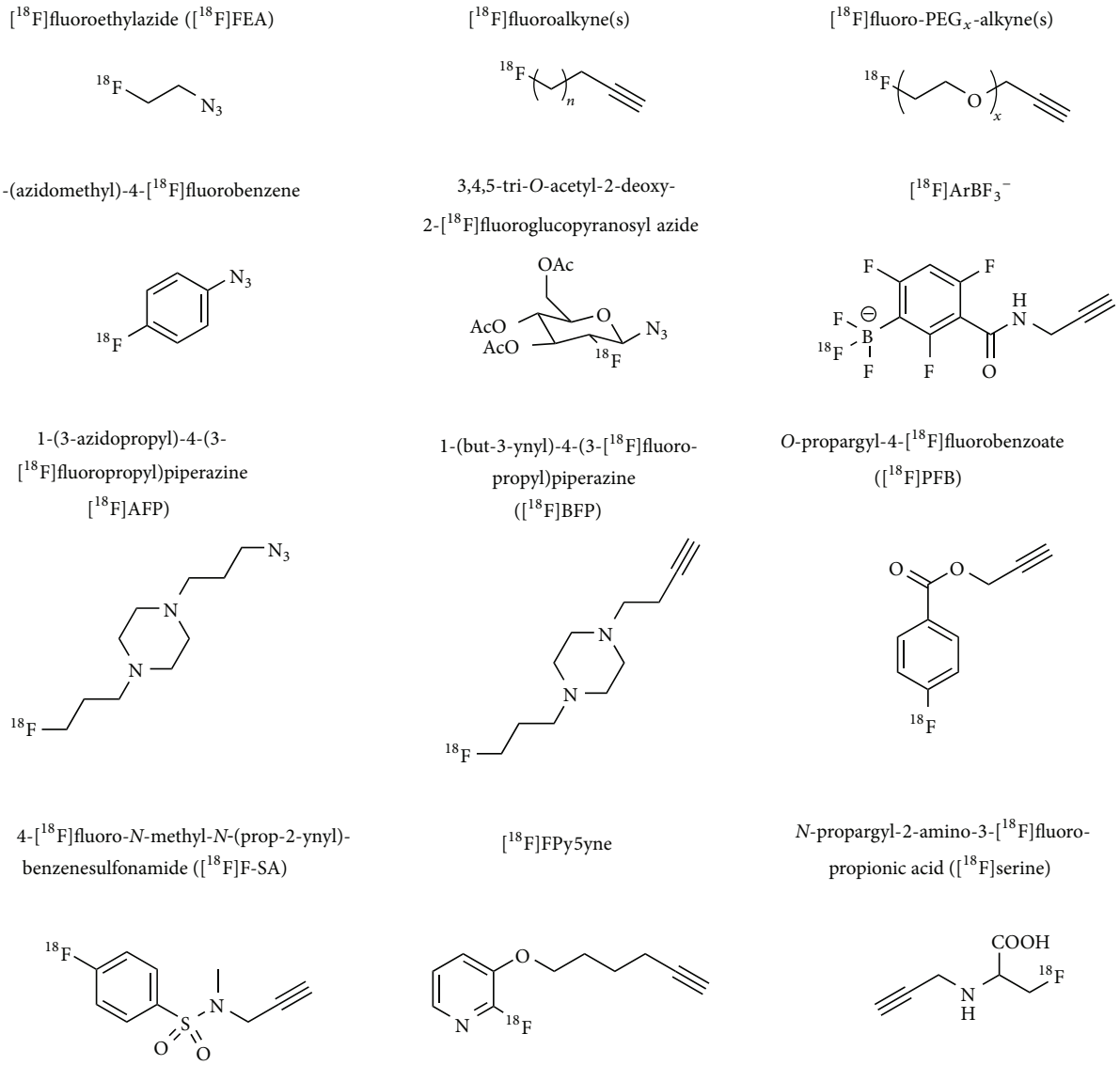

Figure 1: Lead structures of the most important ^{18}F-prosthetic groups applied for copper-catalyzed click ^{18}F-fluorination.

impressively illustrated by the fact that over 50 original papers have been published in this research area within the last eight years.

Tables 1–3 give an overview of the ^{18}F-prosthetic groups, the reaction conditions and reaction partners applied for copper-catalyzed, copper-free and other kinds of ^{18}F-click cycloadditions, respectively. The most important structures of those prosthetic groups are shown in Figures 1, 3, and 5.

2. Copper-Catalyzed ^{18}F-Click Cycloadditions

In the last decade, the copper-catalyzed azide alkyne cycloaddition (CuAAC), which has first been reported independently by Rostovtsev et al. [81] and Tornøe et al. [82] in 2002, has spread over almost all fields of chemistry [83–87], biology [88–90], and material science [91, 92]. The great advantage of this method is given by its outstanding efficiency, its regiospecificity, and fast formation of 1,4-disubstituted 1,2,3-triazoles at ambient temperatures, which is particularly suitable for ^{18}F-labeling of sensitive biomolecules. In particular, the CuAAC enables incorporation of fluorine-18 via a prosthetic group under mild and bioorthogonal conditions [22–25]. 1,2,3-triazoles were first introduced by Michael, who described the formation of a 1,2,3-triazole from a phenylazide in 1893 [93]. Following this pioneering work, Dimroth, Fester, and Huisgen described this type of reaction as a 1,3-dipolar cycloaddition for the first time in 1963 [5].

In 2006, Marik and Sutcliffe published the application of the CuAAC as an ^{18}F-labeling strategy for the first time [26]. They radiolabeled three different alkyne precursors in radiochemical yields (RCY) of 36–81%. Afterwards they were reacted them with azido-functionalized peptides in RCY of 54–99% and an overall reaction time of 30 min. Thus, they could show a new, very fast, efficient, and mild ^{18}F-labeling strategy for complex compounds, especially appropriate for sensitive biomolecules. Only two years later, the suitability of this approach was demonstrated for the ^{18}F-labeling of a folate derivative for *in vivo* tumor imaging with the same

Table 1: Summary of the prosthetic groups, reaction conditions, and reaction partners applied for copper-catalyzed click ^{18}F-fluorination.

^{18}F-prosthetic group	Steps/reaction time[1]	RCY[2]	Reacting agent	Catalytic system	Overall reaction time[1] (CCA)	RCY[2] CCA	Literature
[^{18}F]fluoroalkynes	1 step, 10 min	36–81%	N-(3-azidopropionyl) peptides	CuI/NaAsc/DIPEA	30 min	54–99%	[26]
4-[^{18}F]fluoro-1-butyne	1 step, 15 min (estimated)	n.d.	Glucopyranosyl azide		75–80 min	30%	[27]
4-[^{18}F]Fluoro-1-butyne	1 step, 15 min	45 ± 3%	2,3,4,6-tetra-O-acetyl-b-D-glucopyranosyl azide	Cu(I)/Asc/2,6-lutidine	30 min	27 ± 6%	[28]
5-[^{18}F]fluoro-1-pentyne	1 step, 15 min	59 ± 6%				52 ± 5%	
	1 step, 22 min	86 ± 2%	$\alpha_V\beta_6$ specific peptide A20FMDV2 azide	CuI/Asc	66 min	8.7 ± 2.3%	[29]
6-[^{18}F]fluoro-1-hexyne	1 step, 12 min	70–85%	γ-(4-azido-butyl)-folic acid amide	CuI	1.5 h	25–35%	[30]
[^{18}F]fluoroethyl azide ([^{18}F]FEA)	1 step, 15 min	55%	Terminal alkynes	Excess of Cu^{2+}/Asc or copper powder	1 h	61–98% respectively 15–98% with copper powder	[31] [32]
		n.d.	Caspase 3/7 Selective Isatin	$CuSO_4$/Asc	n.d.	65 ± 6%	[33]
			RGD peptides	Cu^{2+}/Asc		47 ± 8%	[34]
			3-Cyanoquinoline core		3 h	37 ± 3.6%	[35]
			Apoptosis marker ICMT11	$CuSO_4$/Asc/BPDS	n.d.	1–3.4% n.d.c.	[36]
			5-Ethynyl-2′-deoxyuridine	CuI/ascorbic acid/DIPEA		75 ± 10%	[37]
			[Tyr^3]octreotate analogues	$CuSO_4$/Asc/BPDS	30 min (estimated)	40–64%	[38]
			ICMT-11 (automated synthesis)		90 min	3 ± 2.6% n.d.c.	[39]
			Nucleosides	$CuSO_4$/Asc	n.d.	8–12% n.d.c.	[40]
			4-(prop-2-ynyloxy)Benzaldehyde		35 min	90%	[41]
			Haloethylsulfoxides	CuI/ascorbate/DIPEA	n.d.	28.5 ± 2.5%	[42]
		50% n.d.c.	Nitroaromatic substrates	$CuSO_4$/Asc	1 h		[43]
		71 ± 4%	RGDfK		60 min	60 ± 2%	[44]
		55%	Alkyne-func. 6-halopurines	One-pot BPDS-copper(I) ($CuSO_4$/NaAsc.)	1 h	55–75%	[45]
		n.d.	tert-butyl ester of N-Boc-(S)-propargyl glycine		2.5 h	58 ± 4%	[46]
	Precursor: 2 steps [^{18}F]FEA: 15 min.	n.d.	3-Butynyl triphenyl phosphonium bromide	$CuSO_4$, NaAsc	1 h	n.d.	[47]
	1 step, 5–10 min	68–75%	Alkynes of benzene rings		30 min	25–87%	[48]
[^{18}F]FEA from a polyflourinated sulfonate precursor	n.d.	n.d.	FtRGD		70–75 min	10–30% n.d.c.	[49]

Table 1: Continued.

^{18}F-prosthetic group	Steps/reaction time[1]	RCY[2]	Reacting agent	Catalytic system	Overall reaction time[1] (CCA)	RCY[2] CCA	Literature
^{18}F-Fluoro-PEG-Alkyne	1 step, 20 min	85–94%	Various azides	$CuSO_4$/Asc	10–30 min	71–99%	[50]
	1 step, 15 min	65 ± 1.9%	$E(RGDyK)_2$ azide		110 min (estimated)	52 ± 8.3%	[51]
		57%	Nanoparticle azide		1 h (estimated)	58%	[52]
[^{18}F]PEG_3-azide	1 step, 40 min	62 ± 4%	N-alkynylated peptide	$CuSO_4$/Asc/BPDS	2 h (estimated)	31 ± 6%	[53]
		n.d.	ZnO nanoparticle alkynes		n.d.	>95%	[54]
[^{18}F]PEG-azide	Precursor: 2 steps labeling: 1 step	labeling: 58%	γ-(11-azido-3,6,9-trioxaundecanyl)folic acid amide	CuAcetate, NaAsc	2.5 h	8.5%	[55]
4-[^{18}F]fluoro-N-methyl-N-(prop-2-ynyl)-benzenesulfonamide (p[^{18}F]F-SA)	Precursor: 3 steps, labeling: 1 step, 80 min	32 ± 5%	Azide-functionalized neurotensin	Cu(I)-TBTA	n.d.	66%	[56]
			Azide-functionalized human serum albumin (HSA)		100 min	55–60%	[57]
		n.d.	Azide-functionalized phosphopeptide, protein (HAS), oligonucleotide (L-RNA)	$CuSO_4$/Asc	2 h	77%/55–60%/25%	[58]
[^{18}F]FPy5yne	1 step, 15 min	42%	N_3–(CH_2)4–CO–YKRI–OH (BG142)	Tetrakis(acetonitrilo) copper(I) hexa fluorophosphates/TBTA	160 min	18.7%	[59]
			Azide-functionalized DNA	CuBr/TBTA and 2,6-lutidine	276 min	24.6 ± 0.5%	
2-[^{18}F]fluoro-3-pent-4-yn-1-yloxypyridine ([^{18}F]FPyKYNE)	20–25 min	20–35%	Azide-functionalized RGD peptide	$CuSO_4$/Asc	125 min	12–18%	[60]
6-[^{18}F]fluoro-2-etynylpyridine	1 step, 10 min	27.5 ± 6.6%	D-amino acid analogue of WT-pHLIP azide	Cu-Acetate/NaAsc	85 min	5–20%	[61]
propargyl 4-[^{18}F]fluorobenzoate ([^{18}F]PFB)	Precursor: 2 steps, labeling: 1 steps, 15 min	58 ± 31%	Benzyl azide, two lysine derivatives, transglutaminase-reactive peptide	$CuSO_4$/Asc	1 h (estimated)	88 ± 4%, 79 ± 33% and 75 ± 5% 37 ± 31%	[62]
4-[^{18}F]fluoro-3-nitro-N-2-propyn-1-yl-benzamide ([^{18}F]FNPB)	1 step, 40 min	58%	Azido-peptides cRGDfK and D4 peptide		1 h	87–93%	[63]

Table 1: Continued.

^{18}F-prosthetic group	Steps/reaction time[1]	RCY[2]	Reacting agent	Catalytic system	Overall reaction time[1] (CCA)	RCY[2] CCA	Literature
1-(azidomethyl)-4-[^{18}F]-fluorobenzene	4 steps, 75 min	34%	4-Ethynyl-*L*-phenylalanine-peptide	CuI/NaAsc/DIEA	90 min	90%	[64]
	4 steps, 75 min	41%	siRNA alkyne	$CuSO_4$/Asc/TBTA	120 min	15 ± 5%	[65]
	1 step, 45 min	84%	siRNA-linker (two new alkyne-bearing linkers)		120 min	12%	[66]
1-Azido-4-(3-[^{18}F]fluoropropoxy)benzene	4 steps, 75 min	35%		$CuSO_4$/Asc	120 min	15 ± 5%	[65]
[^{18}F](azidomethyl)fluorobenzene	1 step, 94–188 s	around 40%	siRNA alkyne		n.d.	n.d.	[67]
4-[^{18}F]Fluorophenylazide		around 15%					
3,4,6-tri-O-acetyl-2-deoxy-2-[^{18}F]fluorogluco-pyranosyl azide	1 step, 30 min	71 ± 10%	Fmoc-L-propargylglycine	$CuSO_4$/Asc	1.5 h (estimated)	60%	[68]
	2 step, 7.5 min	n.d.	Alkyne-functionalized peptides (RDG, neurotensin peptoid)		75 min	17–20% n.d.c.	[69]
		52%	folate alkyne	Cu-Acetate/NaAsc	3 h	5–25%	[70]
	1 step, 10 min	84%	RGD-peptide alkyne	$CuSO_4$/Asc	70–75 min	16–24%	[71]
		1.3–4.7%	Alkyne-bearing protein	CuBr/TTMA	80–100 min	4.1%	[72]
	1 step	n.d.	ET_AR ligand alkyne	$CuSO_4$/Asc	70 min	20–25% n.d.c.	[73]
			cyanoquinoline (EGFR) alkyne		90 min	8.6 ± 2.3% n.d.c.	[74]
[^{18}F]ArBF$_3^-$	1 step, 20 min	n.d.	Alkyne-functionalized RGD	Cu^I/Asc	1 h	n.d.	[75]
			Alkyne-functionalized bombesin (BBN)			20 ± 10% n.d.c.	[76]
	2 steps,		Alkyne-functionalized RGD-boronate		30 min	15–30%	[77]
piperazine-based [^{18}F]AFP [^{18}F]BFP	AFP: 4 steps, 54 h BFP: 4 steps, 72 h [^{18}F]AFP: 1 step, 40 min [^{18}F]BFP: 1 step, 40 min	[^{18}F]AFP: 29 ± 5% [^{18}F]BFP: 31 ± 9%	N-Fmoc-e-azido-Lnorleucine (amino acid), SNEW peptide	$CuSO_4$, Asc	2 h	Amino acid: 59–79% SNEW peptide: 17–25%	[78]
[^{18}F]serine	2 steps, 125 min	28 ± 5%	cRDG-azide	$CuSO_4$, Asc	145 min	75%	[6]

[1]Calculated as sum from all steps, for the ^{18}F-prosthetic group, respectively, for the overall reaction yielding the click product, starting from fluorine-18.
[2]Radiochemical yields for the ^{18}F-prosthetic group starting from fluorine-18 for the click reaction, respectively; decay corrected, as long as not noted elsewise.
CCA: click cycloaddition; (n.)d.c.: (not) decay corrected; Asc: ascorbate; DIPEA: diisopropylethylamin; TBTA: tris[(1-benzyl-1*H*-1,2,3-triazol-4-yl)methyl]amine; n.d.: no data.

prosthetic group, 6-[^{18}F]fluoro-1-hexyne [30]. The radiofolate was obtained in RCY of 25–35% and was applied to KB-tumor bearing mice. A specific tumor accumulation could be observed by using the folate receptor (FR) targeting concept. Furthermore, Kim et al. used ^{18}F-labeled alkynes as prosthetic groups for the ^{18}F-labeling of 2,3,4,6-tetra-O-acetyl-β-D-glucopyranosyl azide [27], which in turn was employed to label the $\alpha_V\beta_6$ specific peptide A20FMDV2 [28].

Considering all known clickable prosthetic groups for ^{18}F-labeling, [^{18}F]fluoroethyl azide ([^{18}F]FEA) is certainly one of the most investigated clickable ^{18}F-prosthetic groups. Until today, about twenty different manuscripts deal with [^{18}F]FEA to radiolabel a broad variety of biomolecules and compounds. In 2007, Glaser and Årstad [31] mentioned for the first time the preparation of [^{18}F]FEA with a RCY of 55% using 2-azidoethyl-4-toluenesulfonate as precursor. As a proof of concept, they reacted [^{18}F]FEA with different terminal alkynes in very good to excellent RCY of 61–98%. With respect to the catalytic system copper sulfate in combination with ascorbic acid or sodium ascorbate has mainly been used, whereas only in a few approaches copper(I) iodide was used [37, 42]. It has been shown that addition of bathophenanthroline disulfonate (Cu^I stabilizing agent) accelerates the 1,3-dipolar cycloaddition [36, 38, 45]. The very good access to [^{18}F]FEA led to the development of a variety of radiotracers labeled with this prosthetic group, like ^{18}F-deoxyuridine [37], ^{18}F-fluoro-oxothymidine (^{18}F-FOT), or ^{18}F-fluoro-thiothymidine (^{18}F-FTT) [40] as well as apoptosis markers [36] and several peptide systems [34, 44, 49]. In 2012, Smith et al. [40] described the reduction of [^{18}F]FEA using copper wire under acidic conditions, which is a possible explanation of the poor yields during some click reactions.

In 2007, Sirion et al. [50] reported for the first time [^{18}F]fluoro-PEG$_x$-derivatives (x = various polyethylene glycol (PEG) ratios) as new ^{18}F-labeled prosthetic click groups. These compounds showed a reduced volatility and increased polarity compared with other ^{18}F-labeled prosthetic groups like [^{18}F]FEA or [^{18}F]fluoroalkynes. These properties ease their handling as well as improving the *in vivo* behavior of the labeled compounds. The compounds showed a longer circulation time and a reduced renal clearance making them very suitable for *in vivo* application. Sirion et al. described the preparation of different aliphatic and aromatic ^{18}F-PEG-azides and ^{18}F-labeled alkynes in RCY of 85–94%. As a proof of concept, they carried out cycloadditions with the ^{18}F-labeled prosthetic groups and the corresponding alkynes, respectively, azides in high RCY of 71–99%. Several other groups continued this work by using the ^{18}F-labeled PEGylated prosthetic groups for labeling cRGD derivatives [51] and other peptides [53], nanoparticles [52, 54], or folates [55].

To increase the lipophilicity and metabolic stability of radiotracers, [^{18}F]fluoro-aryl-based prosthetic groups have been developed and investigated. In 2007, Ramenda et al. [56] published for the first time a 4-[^{18}F]fluoro-*N*-methyl-*N*-(prop-2-ynyl)-benzenesulfonamide (p-[^{18}F]F-SA), which was obtained in RCY of 32 ± 5%. Subsequently, this prosthetic group was used for radiolabeling an azido-functionalized neurotensin giving a RCY of 66%. Furthermore, the same group used the ^{18}F-aryl prosthetic group for the labeling of human serum albumin (HSA) [57] and other proteins, phosphopeptides, and *L*-RNA [58] in good RCY. A pyridine-based ^{18}F-prosthetic group was first introduced by Inkster et al. [59] in 2008 by reacting [^{18}F]FPy5yne with a model peptide in RCY of 18.7% and an overall reaction time of 160 min. They started from either 2-nitro- or 2-trimethylammonium pyridine to synthesize [^{18}F]FPy5yne with a RCY of 42%. Furthermore, [^{18}F]pyridine derivatives have been used to radiolabel cRGDs [60] and the *D*-amino acid analog of WT-pHLIP [61].

In 2009, Vaidyanathan et al. [62] presented a prosthetic group based on a 4-[^{18}F]fluorobenzoate. Propargyl-4-[^{18}F]fluorobenzoate ([^{18}F]PFB), which could be obtained in RCY of 58 ± 31% within 15 min. To investigate the labeling properties of this new prosthetic group, numerous compounds have been ^{18}F-labeled using [^{18}F]PFB with RCY from 37% to 88% and overall reaction times of about 1 h. Another approach was published by Li et al. in 2012 [63], who synthesized 4-[^{18}F]fluoro-3-nitro-*N*-2-propyn-1-yl-benzamide ([^{18}F]FNPB) for ^{18}F-labeling of cRGDfK and a D4 peptide, which was identified as an EGFR targeting ligand. This approach was followed by the synthesis of 1-(azidomethyl)-4-[^{18}F]fluorobenzene by Thonon et al. [64]. They did a multistep radiosynthesis (4 steps), where the fluorine-18 was introduced in the first step. The desired radiolabeled product could be obtained in a RCY of 34% within 75 min and was used itself to label a 4-ethynyl-*L*-phenylalanine-containing peptide. The same prosthetic group was also employed by Mercier et al. [65] and Flagothier et al. [66] for ^{18}F-labeling of *si*RNA. Other structural analog prosthetic groups have also been developed by Mercier et al. [65] and Chun and Pike [67].

To improve the *in vivo* behavior of peptides with respect to blood clearance and stability, Maschauer and Prante developed ^{18}F-gluco-derivatives for CuAAC-radiolabeling of Fmoc-*L*-propargylglycine with a RCY of 60% [68]. They showed that the ^{18}F-click labeling reaction was more convenient by using the β-anomeric derivative of the azides, respectively, alkynes, giving very high RCY of 71 ± 10%. One year later, they published the first *in vivo* evaluation of an ^{18}F-labeled RGD peptide labeled with [^{18}F]FDG-β-Az in U87MG-tumor bearing mice showing an improved blood clearance and stability [65, 66]. Likewise, Fischer et al. demonstrated in 2012 that a [^{18}F]fluorodeoxyglycosyl folate could be obtained in RCY of 5–25% and subsequent biodistribution and PET-imaging studies showed a high and specific uptake of the radiotracer in FR-positive tumors [70]. The variety of new ^{18}F-labeling strategies using ^{18}F-Fluoroglycosylation is the focus of a review article as a part of this special issue provided by Maschauer and Prante [94].

As another promising approach, Li et al. presented in 2013 an alkyne-functionalized aryltri-[^{18}F]fluoroborate for radiolabeling azido-bombesin and azido-RGD. The major advantage of this method is the two-step, one-pot procedure

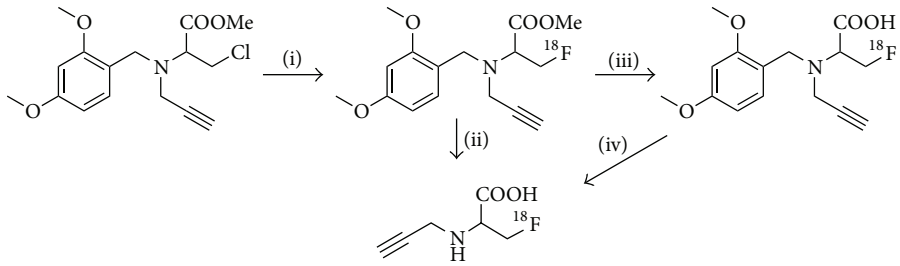

Figure 2: Radiosynthesis of a new amino-acid based ^{18}F-prosthetic group (*N*-propargyl-2-amino-3-[^{18}F]fluoro-propionic acid, "[^{18}F]serine") for ^{18}F-CuAAC-labeling of complex biomolecules. (i) $[K \subset 2.2.2]^+/^{18}F^-$, DMSO, 140°C, 10 min; (ii) hydrochloric acid (3.3 M), 100°C, 15 min; for analytical purposes (sequential deprotection): (iii) sodium hydroxide (3.3 M), 60°C, 5 min; (iv) hydrochloric acid (3.3 M), 100°C, 15 min.

providing a water-soluble and noncoordinating aryltri-[^{18}F]fluoroborate anion, which provided specific activities up to 555 GBq/μmol [75, 76, 95].

Two new piperazine-based prosthetic groups, 1-(but-3-ynyl)-4-(3-[^{18}F]fluoropropyl)piperazine ([^{18}F]BFP) and 1-(3-azidopropyl)-4-(3-[^{18}F]fluoropropyl)piperazine ([^{18}F]AFP), have recently been developed by Pretze and Mamat [78]. Spiro salts were used as precursors, facilitating purification by using solid phase extractions (RP-18 or SiO_2-cartridges). Both prosthetic groups could be obtained in RCY of about 30% using an automated synthesis module. To avoid Glaser coupling, which has been observed by using [^{18}F]BFP for radiolabeling of peptides, [^{18}F]AFP was used instead. An important observation was the fact that the applied peptide formed very strong complexes with the copper catalyst, which required the use of bispidine as a strong chelating agent to remove cytotoxic copper species.

One of the latest developments describes the synthesis of an ^{18}F-labeled alanine derivative as a new prosthetic click group, reported by Schieferstein and Ross [6]. In this case, an amino acid-based prosthetic group has been developed to improve the pharmacokinetic profile of ^{18}F-click-labeled biomolecules. The prosthetic group was obtained in good RCY of 28 ± 5% from a two-step reaction as described in Figure 2. The final ^{18}F-labeled prosthetic group was subsequently reacted with an azido-RGD as model system in RCY of 75% within 20 min.

Considering the above-mentioned prosthetic groups for radiolabeling with fluorine-18, Table 1 summarizes important properties of those components. It has been shown that the integration of an ^{18}F-propyl, ^{18}F-ethyl, or ^{18}F-aryl moiety can provide an improved metabolic profile and that the glycosylation or PEGylation can further improve the *in vivo* behavior. Furthermore, for *in vivo* application a total removal of the copper catalyst is essential. This could be very challenging in the case where peptides or proteins are able to complex copper species from the catalytic system.

3. Copper-Free ^{18}F-Click Cycloadditions

Even though a large number of novel radiotracers using click chemistry have been developed, none of them has entered clinical routine to date, apart from ^{18}F-RGD-K5, which is already used in clinical trials in US. This can be explained by the need of cytotoxic copper during radiotracer syntheses by using copper-catalyzed 1,3-dipolar Huisgen cycloadditions [96]. Thus, there is still a demand for facile (metal-free) and robust ^{18}F-labeling reactions for the syntheses of radiotracers for imaging of malignancies *in vivo*. This leads to the development of catalyst-free click-labeling approaches, which spare copper species during labeling steps and even enable *in vivo* pretargeting concept. Recent developments deal with biocompatible strain-promoted copper-free versions of the alkyne-azide cycloaddition (SPAAC), where the focus has been set on derivatives of cyclooctynes and dibenzocyclooctynes. First approaches focus on the reaction of ^{18}F-labeled cyclooctynes with azide-bearing biomolecules. On the other hand, in further approaches cyclooctyne-carrying bioactive compounds are used, which can be labeled with different ^{18}F-labeled azides. In the beginning, only a few studies have been reported due to the complex and low yielding syntheses of strained cyclooctynes [10, 12, 14]. However, nowadays lots of cyclooctyne derivatives are commercially available, which facilitates the precursor syntheses and opens a wide range of applications.

In 2011 Bouvet et al. [7] published the first example of a SPAAC with ^{18}F-labeled *aza*-dibenzocyclooctyne, [^{18}F]FB-DBCO, and a plethora of azides. The ^{18}F-labeled building block was synthesized via acylation of commercially available *N*-(3-aminopropionyl)-5,6-dihydro-11,12-didehydrodibenzo[*b*,*f*]azocine with *N*-succinimidyl-4-[^{18}F]fluorobenzoate ([^{18}F]SFB), which can be easily prepared in an automated synthesis module [97]. The ^{18}F-labeled cyclooctyne could be obtained in a RCY of 85% and a purity >95% within 60 min. The evaluation of this building block in healthy Balb/C mice showed 60% of intact compound at 60 min p.i. and had a blood clearance half-life of 53 s. Besides, the compound was stable in methanol and phosphate buffer over 60 min. Subsequently, [^{18}F]FB-DBCO was reacted with various azides as proof of principle showing different structural complexities. In all reactions, the formation of two regioisomers (1,4- and 1,5-triazole) has been observed and in some cases a separation of the regioisomers by HPLC was impossible. All ^{18}F-labeled radiotracers were obtained

Table 2: Summary of the prosthetic groups, reaction conditions, and reaction partners applied for copper-free click fluorination.

^{18}F-prosthetic group	Steps/reaction time[1]	RCY[2]	Reacting agent	Reaction type/catalytic system	Overall reaction time[1] (CCA)	RCY[2] CCA	Literature
[^{18}F]COT	1 step, 15 min	71%	3,6-diaryl-*s*-tetrazine	inverse electron-demand DA cyclo-addition	30 min (without HPLC)	>98%	[14]
[^{18}F]FB-DBCO	1 step, 60 min	85%	Various azides	Strain-promoted click 1,3-dipolar cycloaddition	2 h	69–98%	[7]
TCO-derivative: Aza-DBCO-BN (bombesin)	9 steps, —	17%	Three different [^{18}F]azides		30 min (without HPLC)	19–37% (depending on azide)	[8]
[^{18}F]DBCO	1 step, 1 h	21%	Tyr^3-octreotide-N_3(TATE)		1.5 h	95%	[9]
[^{18}F]TCO	[14]	[14]	Tetrazine-RGD	Inverse electron-demand DA cyclo-addition	30 min	90%	[15]
[^{18}F]bifunctional azadibenzocyclo-octyne	1 step, 30 min	24.5%	Alkyl azide	Strain-promoted click 1,3-dipolar cycloaddition	202 ± 34 min	74 ± 4.8%	[10]
[^{18}F]PEG$_4$ azide	1 step, 45 min	63%	cRGD-DBCO		80 min	92%	[11]
[^{18}F]cyclooctyne	6–11 steps, 30–80 h (depending on the derivative)	20–57% (depending on the derivative)	[^{18}F]2-fluoro-ethylazide		30 min.	9.6–97% (depending on COT and solvent)	[12] [79]
[^{18}F]*trans*-cyclooctene ([^{18}F]TCO)	1 step, 102 min	46.1 ± 12.2%	Tetrazine modified exendin-4	Inverse electron-demand DA cycloaddition	3 h	46.7 ± 17.3%	[16]
			Polymer modified tetrazine			89.2% *in vivo*	[80]
[^{18}F]amine-functionalised norbornene	1 step, 52 min	60 ± 17%	Tetrazine (peptide-/bombesin-derivatives)		82 min (without preparation of [^{18}F]SFB)	46–97% (depending on the tetrazine)	[18]
[^{18}F]FBA-C$_6$-DBCO	[10]	[10]	$\alpha_V\beta_6$-specific peptide	Strain-promoted click 1,3-dipolar cycloaddition	click: 40 ± 4 min	11.9 ± 3.2%	[13]

[1]Calculated as sum from all steps, for the ^{18}F-prosthetic group, respectively, for the overall reaction leading to the click product, starting from fluorine-18.
[2]Radiochemical yields for the ^{18}F-prosthetic group starting from fluorine-18 for the click reaction, respectively; decay corrected, as long as not noted elsewise.
CCA: click cycloaddition; DA: Diels Alder; DBCO: *aza*-dibenzocyclooctyne; TCO: *trans*-cyclooctyne.

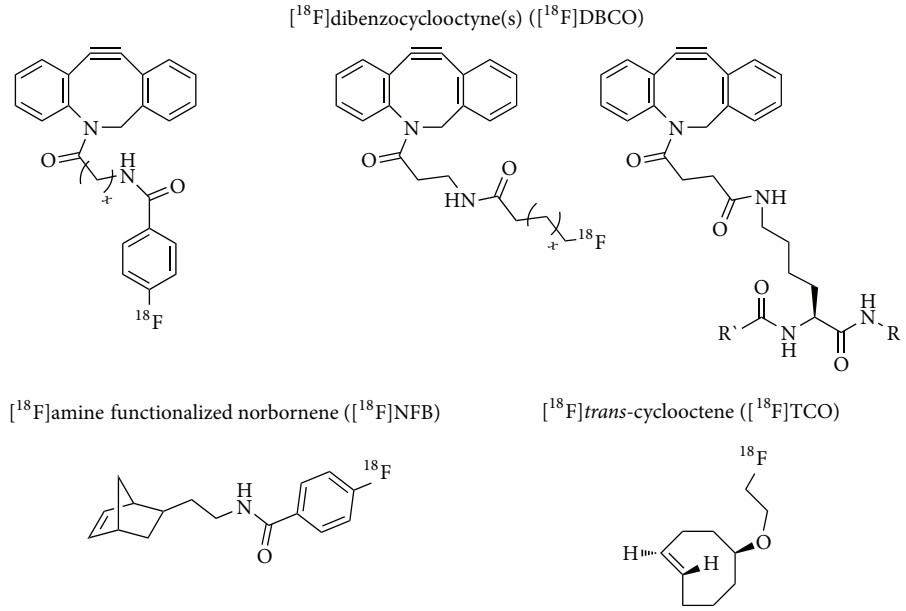

Figure 3: Lead structures of the most important ^{18}F-prosthetic groups applied for copper-free click ^{18}F-fluorination.

in good to excellent RCY of 69–98% within an overall reaction time of about 2 h. However, the reaction rates in these cases were much slower compared to other examples of bioorthogonal reactions, limiting this new approach for *in vivo* pretargeting applications.

A cyclooctyne derivative has been conjugated to bombesin (*aza*-DBCO-BN, 9 steps) with an overall yield of 17% by Campbell-Verduyn et al. [8]. The *aza*-DBCO-BN was reacted with various ^{18}F-azides giving RCY of 19–37% within 30 min. In 2011, Arumugam et al. [9] investigated the direct ^{18}F-labeling of azadibenzocyclooctyne (DBCO) yielding the ^{18}F-labeled prosthetic group (RCY = 36%). The radiolabeling was followed by a click reaction with an *azido*-octreotide leading to the ^{18}F-labeled octreotide in a RCY of 95% within a total reaction time of 1.5 h. In contrast, other working groups used ^{18}F-cyclooctynes for labeling RDG-derivatives [11] as well as further integrin-specific peptides [10, 13].

Another possibility to perform copper-free click reactions is given by the inverse electron demand of the Diels Alder cycloaddition between a cyclooctene and a tetrazine under the release of nitrogen. The so-called tetrazine-*trans*-cyclooctene ligation (TTCO ligation) was first published by Li et al. in 2010 [14]. Concerning the instability of the tetrazines, it is more practical to functionalize the biomolecule with a tetrazine followed by the reaction with an ^{18}F-labeled cyclooctene. The latter are much more suitable for direct ^{18}F-labeling than tetrazines. For this purpose a nosylate precursor was used for ^{18}F-labeling of the cyclooctene providing RCY of 71% within 15 min. To investigate the suitability of the ^{18}F-prosthetic group in click reactions, the ^{18}F-cyclooctene was reacted with a 3,6-di(2-pyridyl)-*S*-tetrazine in an excellent RCY of 98% within 10 s, showing its outstanding feasibility for *in vivo* pretargeting approaches. These fast reaction rates made this approach very attractive that even ^{11}C-labeling reaction was explored using the inverse electron demand Diels Alder cycloaddition between a cyclooctene and a tetrazine [98]. In 2011, ^{18}F-labeled cyclooctene was linked to a tetrazine-RGD derivative by Selvaraj et al. [15] with a RCY of 90% within 5 min at room temperature. The resulting ^{18}F-labeled tracer was tested in *in vivo* experiments showing a high tumor accumulation, which could selectively be blocked. In 2012, the group of Devaraj et al. [80] published for the first time the *in vivo* click reaction of [^{18}F]*trans*-cyclooctene and a polymer-modified tetrazine (PMT). The radiolabeled peptide ^{18}F-PMT10 could be obtained in a RCY of 89.2%. Whole body animal PET scans were carried out 3 h p.i., showing renal clearance and a widespread tissue distribution as can be seen in Figure 4. Previously, the same group described the synthesis of an ^{18}F-labeled cyclooctene with a RCY of 46.1 ± 12.2%. Subsequently, this prosthetic group was clicked with a tetrazine-modified exendin-4 in RCY of 46.7 ± 17.3% [16].

A similar strategy was published by Knight et al. in 2013, where an ^{18}F-labeled amino-functionalized norbornene was reacted with a tetrazine-modified peptide [18]. The ^{18}F-labeled norbornene was obtained using N-succinimicyl-4-[^{18}F]fluorobenzoate ([^{18}F]SFB) in RCY of 60 ± 17% within 52 min. As a proof of concept, two different tetrazines, an asymmetric dipyridyl tetrazine, and a tetrazine-modified bombesin peptide were labeled with ^{18}F-labeled norbornene derivative ([^{18}F]NFB) in 46–97% RCY within 82 min.

Considering the copper-free click labeling of bioactive compounds with fluorine-18, both the strain-promoted alkyne-azide cycloaddition (SPAAC) and the tetrazine-*trans*-cyclooctyne ligation (TTCO ligation) show promising results. Regarding *in vivo* pretargeting approaches, only the TTCO

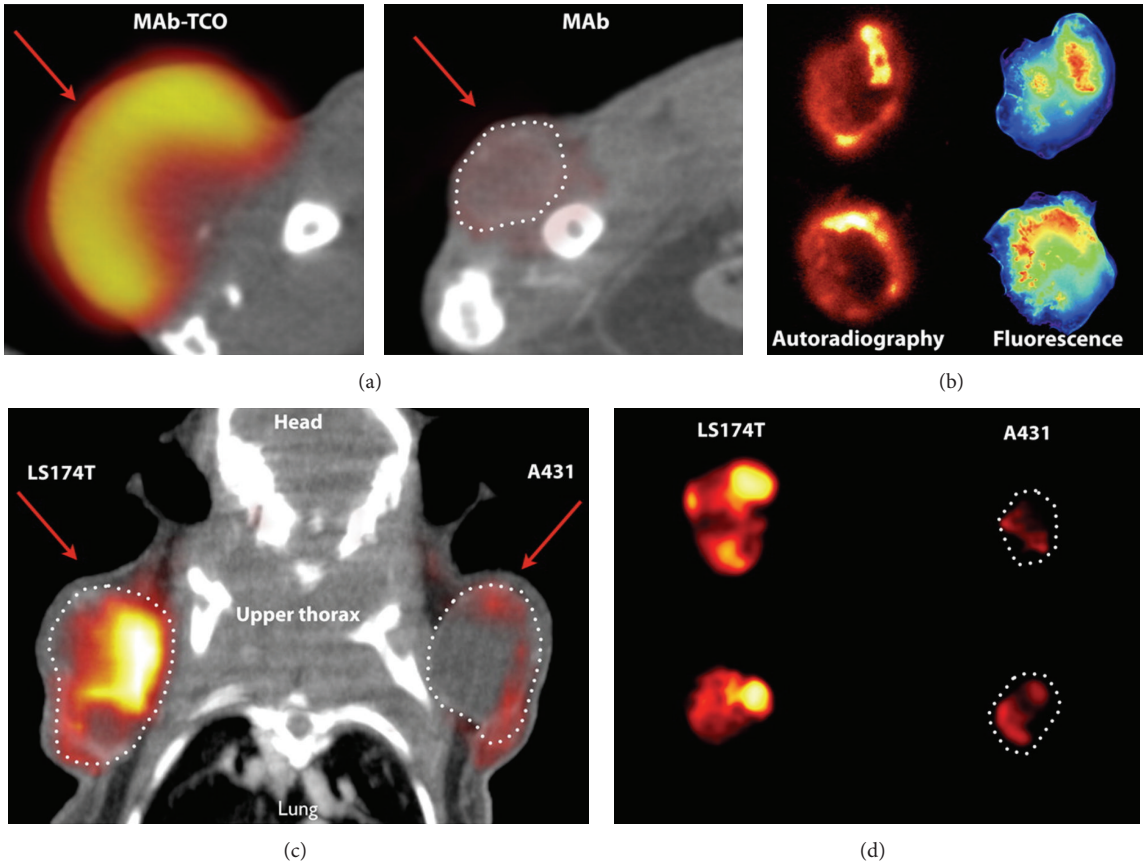

Figure 4: PET and autoradiography using ^{18}F-tetrazine agents. (a) PET/CT fusion of LS174T tumor xenograft labeled using either *trans*-cyclooctene (TCO) monoclonal antibodies (mAb TCO) or control unlabeled antibodies (mAb) followed by ^{18}F-PMT10 (polymer-modified tetrazine). Arrows indicate location of the tumor xenograft. The bladder was omitted for clarity. (b) Imaging using autoradiography (left side) and fluorescence slices after targeting with fluorescence TCO monoclonal antibody and ^{18}F-PMT10. (c) PET/CT fusion of mouse bearing A431 and LS174T tumors after targeting with anti-A33 TCO monoclonal antibodies followed by ^{18}F-PMT10. Arrows indicate location of tumors and the liver was omitted for clarity. (d) Autoradiography of representative 1 mm LS174T and A431 tumor slices after multistep targeting (reprinted with permission from [80]; Copyright 2012 National Academy of Sciences of the United States of America).

ligation showed favorable results and reaction rates, which are suitable for this application [80]. Table 2 summarizes reaction conditions, radiochemical yields, and reaction partners of those components.

4. New Developments in ^{18}F-Click Cycloadditions

The latest developments in metal-free ^{18}F-click cycloadditions have been reported by Zlatopolskiy et al. [19–21] (Table 3). In a first approach, the ^{18}F-labeled building block C-(4-[^{18}F]fluorophenyl)-N-phenyl nitrone was developed to form ^{18}F-isoxazolidines via high-yielding [3+2]cycloadditions with various maleimides [19]. C-(4-[^{18}F]fluorophenyl)-N-phenyl nitrone was obtained from the reaction of 4-[^{18}F]fluorobenzaldehyde and N-phenylhydroxylamine in high RCY of 74% with 10 min. In the subsequent click cycloaddition step, differently substituted maleimides as model dipolarophiles were used to form the corresponding isoxazolidines as endo-/exoisomers in high yields of up to >90% within 10 min. A one-pot strategy with *in situ* generation of C-(4-[^{18}F]fluorophenyl)-N-phenyl nitrone provided the desired ^{18}F-isoxazolidines only in moderate yields of 25% and only after heating to 110°C. Under optimized conditions, ^{18}F-isoxazolidines were obtained from fast ^{18}F-click [3+2]cycloadditions.

In further studies, the same group used 4-[^{18}F]fluorobenzonitrile oxide instead of C-(4-[^{18}F]fluorophenyl)-N-phenyl nitrone as 1,3-dipol for milder reaction conditions [20] (Table 3). 4-[^{18}F]fluorobenzonitrile oxide was obtained in 92% RCY within 10 min from the reaction of 4-[^{18}F]fluorobenzaldehyde (RCY: 30–50%, 50 min [99]) with hydroxylamine and subsequent treatment with phenyl iodine bis(trifluoroacetate).

After the click [3+2]cycloaddition to various ^{18}F-labeled model 2-isoxazolines and isoxazoles was successfully tested, the novel method was applied to three different COX-2 inhibitors (indomethacin conjugates) carrying dipolarophilic

Table 3: New developments in ^{18}F-click [3+2]cycloadditions, showing the 1,3-dipolar ^{18}F-prosthetic groups, reaction type, and conditions.

^{18}F-prosthetic group	Steps/reaction time	RCY	Reacting agent	Reaction type/ catalytic system	Overall reaction time[1] (CCA)	RCY CCA	Literature
C-(4-[^{18}F]fluoro-phenyl)-N-phenyl-nitrone	2 steps/20 min, (labeling of [^{18}F]FB-CHO: 1 step, 50 min)	22–37%[1] ([^{18}F]FB-CHO: 30–50%) (^{18}F-nitrone: 74%)	Various maleimides		80 min (10 min)	87–91%	[19]
			Various dipolarophiles			36–99%	
4-[^{18}F]fluoro-benzonitrile oxide	3 steps/20 min (labeling of [^{18}F]FB-CHO: 1 step, 50 min)	28–46%[1] ([^{18}F]FB-CHO: 30–50%) (^{18}F-nitro oxide: 92%)	Cyclononyne-indomethacins (COX-2 inhibitor)	1,3-dipolar [3+2]cycloaddition, no catalyst	80 min (10 min)	81%	[20]
			Maleimide-indomethacins (COX-2 inhibitor)			55%	
			Propyne-indomethacins (COX-2 inhibitor)			35%	
N-hydroxy-4-[^{18}F]fluorobenz-imidoyl chloride	4 steps/20 min (labeling of [^{18}F]FB-CHO: 1 step, 50 min)	27–45%[1] ([^{18}F]FB-CHO: 30–50%) (^{18}F-nitro oxide: 92%) (^{18}F-benzimidoyl Cl: 99%)	Cyclononyne-β-Ala-Phe-OMe (dipeptide)		85 min (10 min)	88%[2]	
			Norbornene-β-Ala-Phe-OMe (dipeptide)			82%[2]	
C-(4-[^{18}F]fluoro-phenyl)-N-phenyl-nitrone	2 steps/20 min, (labeling of [^{18}F]FB-CHO: 1 step, 50 min)	22–37%[1] ([^{18}F]FB-CHO: 30–50%) (^{18}F-nitrone: 74%)	Terminal alkynes methyl propiolate	*radio*-Kinugasa, $CuSO_4$, AscONa (*L*-histidine)	80 min (10 min)	89% (*trans/cis* = 2 : 3)	[21]
			Terminal alkyne propargyl alcohol	*radio*-Kinugasa, CuI (Cu^I-stabilizing ligands or pyridine)	100 min (30 min)	82% (*trans/cis* = 1 : 5)	
						60% (*trans/cis* = 1 : 5)	
			Terminal alkyne 1-propargyl uracyl (nucleobase chimera)			65% (*trans/cis* = 4 : 1)	
			propiolyl-β-Ala-Phe-OMe (dipeptide)	*radio*-Kinugasa, $CuSO_4$, AscONa (*L*-histidine)	80 min (10 min)	85% (*trans/cis* = 1 : 3)	
			propiolated protein (BSA)			32%	
o-/*p*-[^{18}F]fluoro-phenyl acetylene	n.d.	n.d.	3,6-dihydro-2*H*-1,4-oxazine-4-oxide	*radio*-Kinugasa, CuI (1,10-phenanthroline)	(10 min)	52% (*ortho*) 41% (*para*)	

[1]Calculated as sum from all steps.
[2]Best RCY, obtained only with high precursor amounts.
FB-CHO: 4-fluorobenzaldehyde; CCA: click cycloaddition; PHA: *N*-phenylhydroxylamine; AscONa: sodium ascorbate'; BSA: bovine serum albumin; n.d.: no data.

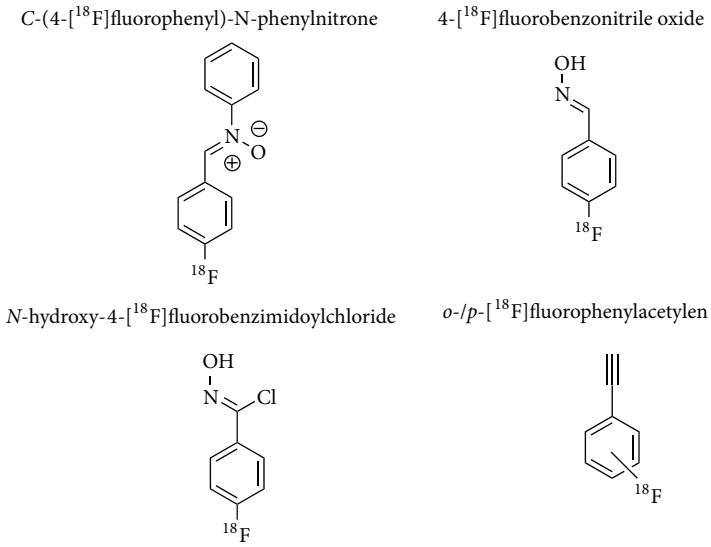

Figure 5: Lead structures of new ^{18}F-prosthetic groups applied for click ^{18}F-fluorination.

moieties of cyclononyne, maleimide, and propyne. The resulting products were obtained in moderate to excellent RCY of 81%, 55%, and 35%, respectively. It is noteworthy that, for the propyne derivative, the milder oxidant [bis(acetoxy)iodo]benzene was used to avoid decomposition. Finally, the method was successfully adapted for ^{18}F-labeling of two model dipeptide conjugates, cyclononyne- and norbornene-β-Ala-Phe-OMe. However, the original cycloaddition using 4-[^{18}F]fluorobenzonitrile oxide did only provide traces of the desired products. Consequently, 4-[^{18}F]fluorobenzonitrile oxide was further treated with chloramine T (CAT) *in situ* forming the more stable building block N-hydroxy-4-[^{18}F]fluorobenzimidoyl chloride. With the use of high precursor (peptides) amounts, the latter enabled excellent RCY of the ^{18}F-labeled dipeptides of up to 88% within 10 min at room temperature [20]. Under optimized conditions low precursor amounts of 5 nmol (cyclononyne) and 50 nmol (norbornene-β-Ala-Phe-OMe) still allowed RCY of 56% and 47%, respectively.

In a very recent report, Zlatopolskiy and coworkers applied their ^{18}F-labeled nitrone, C-(4-[^{18}F]fluorophenyl)-N-phenyl nitrone, for the first formation of ^{18}F-labeled β-lactames via the CuI-catalyzed Kinugasa reaction [21] (Table 3). The optimized reactions went smooth under very mild conditions to give the ^{18}F-labeled model β-lactames in high RCY and various isomeric mixtures of the *trans*- and *cis*-product. In dependency on the reactivity of the terminal alkynes, the reaction parameters needed (individual) optimization regarding catalyst system, solvent, temperature, and CuI-stabilizing ligands. As a biologically relevant molecule the ^{18}Flabeled nucleobase chimera was synthesized as potential PET-imaging agent for bacterial infections.

Moreover, the dipeptide β-Ala-Phe-OMe was propiolated and used in this radio-Kinugasa reaction to give excellent RCY of 85% of the ^{18}F-labeled dipeptide under very mild conditions (aqueous solution, room temperature) [21]. Similarly, this new method was successfully transferred to the ^{18}F-labeling of proteins. Bovine serum albumin (BSA) was conjugated with 3-propiolamidopropyl chloroformate. This propiolated BSA was successfully radiolabeled with fluorine-18 in the radio-Kinugasa reaction.

5. Conclusions

The field of click cycloadditions had and still has a major impact in ^{18}F-labeling chemistry. The very mild reaction conditions mostly applicable and the excellent efficiency of all types of these reactions are particularly suitable for ^{18}F-labeling. Especially, complex and sensitive biomolecules benefit from this methodology. No protection group chemistry is needed and the ^{18}F-click cycloaddition step provides the final radiotracer.

Besides several new ^{18}F-labeled radiotracers are available via click cycloadditions, and the metal-free versions even enabled pretargeting concepts by *in vivo* click. The latest development of a radio-Kinugasa reaction towards the first ^{18}F-β-lactames demonstrates the highly active field and the broad applicability of ^{18}F-click cycloadditions.

Conflict of Interests

The authors declare that there is no conflict of interests regarding the publication of this paper.

References

[1] M. E. Phelps, "Positron emission tomography provides molecular imaging of biological processes," *Proceedings of the National Academy of Sciences of the United States of America*, vol. 97, no. 16, pp. 9226–9233, 2000.

[2] J. S. Fowler and A. P. Wolf, "The synthesis of carbon-11, fluorine-18 and nitrogen-13 labeled radiotracers for biomedical applications," Bnl-31222 de82 013799.

[3] H. H. Coenen, K. Franken, P. Kling, and G. Stocklin, "Direct electrophilic radiofluorination of phenylalanine, tyrosine and dopa," *Applied Radiation and Isotopes*, vol. 39, no. 12, pp. 1243–1250, 1988.

[4] L. Lang and W. C. Eckelman, "One-step synthesis of ^{18}F labeled [^{18}F]-N-succinimidyl 4-(fluoromethyl)benzoate for protein labeling," *Applied Radiation and Isotopes*, vol. 45, no. 12, pp. 1155–1163, 1994.

[5] R. Huisgen, "1.3-dipolare cycloadditionen," *Angewandte Chemie*, no. 13, pp. 604–637, 1963.

[6] H. Schieferstein and T. L. Ross, "A Polar ^{18}F-labeled amino acid derivative for click-labeling of biomolecules," *European Journal of Organic Chemistry*, 2014.

[7] V. Bouvet, M. Wuest, and F. Wuest, "Copper-free click chemistry with the short-lived positron emitter fluorine-18," *Organic & Biomolecular Chemistry*, vol. 9, no. 21, pp. 7393–7399, 2011.

[8] L. S. Campbell-Verduyn, L. Mirfeizi, A. K. Schoonen, R. A. Dierckx, P. H. Elsinga, and B. L. Feringa, "Strain-promoted copper-free "click" chemistry for ^{18}F radiolabeling of bombesin," *Angewandte Chemie International Edition*, vol. 50, no. 47, pp. 11117–11120, 2011.

[9] S. Arumugam, J. Chin, R. Schirrmacher, V. V. Popik, and A. P. Kostikov, "[^{18}F]azadibenzocyclooctyne ([^{18}F]ADIBO): a biocompatible radioactive labeling synthon for peptides using catalyst free [3+2] cycloaddition," *Bioorganic & Medicinal Chemistry Letters*, vol. 21, no. 23, pp. 6987–6991, 2011.

[10] R. D. Carpenter, S. H. Hausner, and J. L. Sutcliffe, "Copper-free click for PET: rapid 1,3-dipolar cycloadditions with a fluorine-18 cyclooctyne," *ACS Medicinal Chemistry Letters*, vol. 2, no. 12, pp. 885–889, 2011.

[11] K. Sachin, V. H. Jadhav, E.-M. Kim et al., "F-18-labeling protocol of peptides based on chemically orthogonal strain-promoted cycloaddition under physiologically friendly reaction conditions," *Bioconjugate Chemistry*, vol. 23, no. 8, pp. 1680–1686, 2012.

[12] H. L. Evans, R. L. Slade, L. Carroll et al., "Copper-free click—a promising tool for pre-targeted PET imaging," *Chemical Communications*, vol. 48, no. 7, pp. 991–993, 2012.

[13] S. H. Hausner, R. D. Carpenter, N. Bauer, and J. L. Sutcliffe, "Evaluation of an integrin $\alpha_v\beta_6$-specific peptide labeled with [^{18}F]fluorine by copper-free, strain-promoted click chemistry," *Nuclear Medicine and Biolology*, vol. 40, no. 2, pp. 233–239, 2013.

[14] Z. Li, H. Cai, M. Hassink et al., "Tetrazine-trans-cyclooctene ligation for the rapid construction of ^{18}F labeled probes," *Chemical Communications*, vol. 46, no. 42, pp. 8043–8045, 2010.

[15] R. Selvaraj, S. Liu, M. Hassink et al., "Tetrazine-trans-cyclooctene ligation for the rapid construction of integrin $\alpha_v\beta_3$ targeted PET tracer based on a cyclic RGD peptide," *Bioorganic & Medicinal Chemistry Letters*, vol. 21, no. 17, pp. 5011–5014, 2011.

[16] E. J. Keliher, T. Reiner, G. M. Thurber, R. Upadhyay, and R. Weissleder, "Efficient ^{18}F-labeling of synthetic exendin-4 analogues for imaging beta cells," *ChemistryOpen*, vol. 1, no. 4, pp. 177–183, 2012.

[17] N. Devaraj, "Advancing tetrazine bioorthogonal reactions through the development of new synthetic tools," *Synlett*, vol. 23, no. 15, pp. 2147–2152, 2012.

[18] J. C. Knight, S. Richter, M. Wuest, J. D. Way, F. Wuest, and "Synthesis a, "nd evaluation of an ^{18}F-labelled norbornene derivative for copper-free click chemistry reactions," *Organic & Biomolecular Chemistry*, vol. 11, no. 23, pp. 3817–3825, 2013.

[19] B. D. Zlatopolskiy, R. Kandler, F. M. Mottaghy, and B. Neumaier, "C-(4-[^{18}F]fluorophenyl)-N-phenyl nitrone: a novel ^{18}F-labeled building block for metal free [3+2]cycloaddition," *Applied Radiation and Isotopes*, vol. 70, no. 1, pp. 184–192, 2012.

[20] B. D. Zlatopolskiy, R. Kandler, D. Kobus, F. M. Mottaghy, and B. Neumaier, "Beyond azide-alkyne click reaction: easy access to ^{18}F-labelled compounds via nitrile oxide cycloadditions," *Chemical Communications*, vol. 48, no. 57, pp. 7134–7136, 2012.

[21] B. D. Zlatopolskiy, P. Krapf, R. Richarz, H. Frauendorf, F. M. Mottaghy, and B. Neumaier, "Synthesis of ^{18}F-labelled β-lactams by using the kinugasa reaction," *Chemistry: A European Journal*, vol. 20, pp. 4697–4703, 2014.

[22] R. Schirrmacher, C. Wängler, and E. Schirrmacher, "Recent developments and trends in ^{18}F-radiochemistry: syntheses and applications," *Mini-Reviews in Organic Chemistry*, vol. 4, no. 4, pp. 317–329, 2007.

[23] M. Glaser and E. G. Robins, ""Click labelling" in PET radiochemistry," *Journal of Labelled Compounds and Radiopharmaceuticals*, vol. 52, no. 10, pp. 407–414, 2009.

[24] T. L. Ross, "The click chemistry approach applied to fluorine-18," *Current Radiopharmaceuticals*, vol. 3, no. 3, pp. 202–223, 2010.

[25] M. Pretze, D. Pietzsch, and C. Mamat, "Recent trends in bioorthogonal click-radiolabeling reactions using fluorine-18," *Molecules*, vol. 18, no. 7, pp. 8618–8665, 2013.

[26] J. Marik and J. L. Sutcliffe, "Click for PET: rapid preparation of [^{18}F]fluoropeptides using CuI catalyzed 1,3-dipolar cycloaddition," *Tetrahedron Letters*, vol. 47, no. 37, pp. 6681–6684, 2006.

[27] D. H. Kim, Y. S. Choe, K.-H. Jung et al., "A ^{18}F-labeled glucose analog: synthesis using a click labeling method and in vitro evaluation," *Archives of Pharmacal Research*, vol. 31, no. 5, pp. 587–593, 2008.

[28] D. H. Kim, Y. S. Choe, and B.-T. Kim, "Evaluation of 4-[^{18}F]fluoro-1-butyne as a radiolabeled synthon for click chemistry with azido compounds," *Applied Radiation and Isotopes*, vol. 68, no. 2, pp. 329–333, 2010.

[29] S. H. Hausner, J. Marik, M. K. J. Gagnon, and J. L. Sutcliffe, "In vivo positron emission tomography (PET) imaging with an $\alpha_v\beta_6$ specific peptide radiolabeled using ^{18}F-"click" chemistry: evaluation and comparison with the corresponding 4-[^{18}F]fluorobenzoyl- and 2-[^{18}F] fluoropropionyl-peptides," *Journal of Medicinal Chemistry*, vol. 51, no. 19, pp. 5901–5904, 2008.

[30] T. L. Ross, M. Honer, P. Y. H. Lam et al., "Fluorine-18 click radiosynthesis and preclinical evaluation of a new ^{18}F-labeled folic acid derivative," *Bioconjugate Chemistry*, vol. 19, no. 12, pp. 2462–2470, 2008.

[31] M. Glaser and E. Årstad, ""Click labeling" with 2-[^{18}F]fluoroethylazide for positron emission tomography," *Bioconjugate Chemistry*, vol. 18, no. 3, pp. 989–993, 2007.

[32] D. Kobus, Y. Giesen, R. Ullrich, H. Backes, and B. Neumaier, "A fully automated two-step synthesis of an ^{18}F-labelled tyrosine kinase inhibitor for EGFR kinase activity imaging in tumors," *Applied Radiation and Isotopes*, vol. 67, no. 11, pp. 1977–1984, 2009.

[33] G. Smith, M. Glaser, M. Perumal et al., "Design, synthesis, and biological characterization of a caspase 3/7 selective isatin labeled with 2-[^{18}F]fluoroethylazide," *Journal of Medicinal Chemistry*, vol. 51, no. 24, pp. 8057–8067, 2008.

[34] M. Glaser, M. Solbakken, D. R. Turton et al., "Methods for ^{18}F-labeling of RGD peptides: comparison of aminooxy [^{18}F] fluorobenzaldehyde condensation with "click labeling" using 2-[^{18}F]fluoroethylazide, and S-alkylation with [^{18}F] fluoropropanethiol," *Amino Acids*, vol. 37, no. 4, pp. 717–724, 2009.

[35] F. Pisaneschi, Q.-D. Nguyen, E. Shamsaei et al., "Development of a new epidermal growth factor receptor positron emission tomography imaging agent based on the 3-cyanoquinoline core: synthesis and biological evaluation," *Bioorganic and Medicinal Chemistry*, vol. 18, no. 18, pp. 6634–6645, 2010.

[36] M. Glaser, J. Goggi, G. Smith et al., "Improved radiosynthesis of the apoptosis marker ^{18}F-ICMT11 including biological evaluation," *Bioorganic & Medicinal Chemistry Letters*, vol. 21, no. 23, pp. 6945–6949, 2011.

[37] U. Ackermann, G. O'Keefe, S.-T. Lee et al., "Synthesis of a [^{18}F]fluoroethyltriazolylthymidine radiotracer from [^{18}F]2-fluoroethyl azide and 5-ethynyl-2′-deoxyuridine," *Journal of Labelled Compounds and Radiopharmaceuticals*, vol. 54, no. 5, pp. 260–266, 2011.

[38] L. Iddon, J. Leyton, B. Indrevoll et al., "Synthesis and in vitro evaluation of [^{18}F]fluoroethyl triazole labelled [Tyr3]octreotate analogues using click chemistry," *Bioorganic & Medicinal Chemistry Letters*, vol. 21, no. 10, pp. 3122–3127, 2011.

[39] R. Fortt, G. Smith, R. O. Awais, S. K. Luthra, and E. O. Aboagye, "Automated GMP synthesis of [^{18}F]ICMT-11 for in vivo imaging of caspase-3 activity," *Nuclear Medicine and Biology*, vol. 39, no. 7, pp. 1000–1005, 2012.

[40] G. Smith, R. Sala, L. Carroll et al., "Synthesis and evaluation of nucleoside radiotracers for imaging proliferation," *Nuclear Medicine and Biology*, vol. 39, no. 5, pp. 652–665, 2012.

[41] D. Zhou, W. Chu, C. S. Dence, R. H. Mach, and M. J. Welch, "Highly efficient click labeling using 2-[^{18}F]fluoroethyl azide and synthesis of an ^{18}F-N-hydroxysuccinimide ester as conjugation agent," *Nuclear Medicine and Biology*, vol. 39, no. 8, pp. 1175–1181, 2012.

[42] E. Laurens, S. D. Yeoh, A. Rigopoulos et al., "Radiolabelling and evaluation of novel haloethylsulfoxides as PET imaging agents for tumor hypoxia," *Nuclear Medicine and Biology*, vol. 39, no. 6, pp. 871–882, 2012.

[43] R. Bejot, L. Carroll, K. Bhakoo, J. Declerck, and V. Gouverneur, "A fluorous and click approach for screening potential PET probes: evaluation of potential hypoxia biomarkers," *Bioorganic and Medicinal Chemistry*, vol. 20, no. 1, pp. 324–329, 2012.

[44] J. Li, L. Shi, L. Jia et al., "Radiolabeling of RGD peptide and preliminary biological evaluation in mice bearing U87MG tumors," *Bioorganic & Medicinal Chemistry*, vol. 20, no. 12, pp. 3850–3855, 2012.

[45] E. Galante, B. W. Schoultz, M. Koepp, and E. Arstad, "Chelator-accelerated one-pot "click" labeling of small molecule tracers with 2-[^{18}F]fluoroethyl azide," *Molecules*, vol. 18, no. 5, pp. 5335–5347, 2013.

[46] K. K. S. Sai, C. Huang, L. Yuan et al., "^{18}F-AFETP,^{18}F-FET, and ^{18}F-FDG imaging of mouse DBT gliomas," *Journal of Nuclear Medicine*, vol. 54, no. 7, pp. 1120–1126, 2013.

[47] A. Haslop, A. Gee, C. Plisson, and N. Long, "Fully automated radiosynthesis of [1-(2-[^{18}F]fluoroethyl),1H[1,2,3]triazole 4-ethylene] triphenylphosphonium bromide as a potential positron emission tomography tracer for imaging apoptosis," *Journal of Labelled Compounds and Radiopharmaceuticals*, vol. 56, no. 6, pp. 313–316, 2013.

[48] L. Jia, Z. Cheng, L. Shi et al., "Fluorine-18 labeling by click chemistry: multiple probes in one pot," *Applied Radiation and Isotopes*, vol. 75, pp. 64–70, 2013.

[49] R. Bejot, J. Goggi, S. S. Moonshi, and E. G. Robins, "A practical synthesis of [^{18}F]FtRGD: an angiogenesis biomarker for PET," *Journal of Labelled Compounds and Radiopharmaceuticals*, vol. 56, no. 2, pp. 42–49, 2013.

[50] U. Sirion, H. J. Kim, J. H. Lee et al., "An efficient F-18 labeling method for PET study: huisgen 1,3-dipolar cycloaddition of bioactive substances and F-18-labeled compounds," *Tetrahedron Letters*, vol. 48, no. 23, pp. 3953–3957, 2007.

[51] Z.-B. Li, Z. Wu, K. Chen, F. T. Chin, and X. Chen, "Click chemistry for ^{18}F-labeling of RGD peptides and microPET imaging of tumor integrin $\alpha_v\beta_3$ expression," *Bioconjugate Chemistry*, vol. 18, no. 6, pp. 1987–1994, 2007.

[52] N. K. Devaraj, E. J. Keliher, G. M. Thurber, M. Nahrendorf, and R. Weissleder, "^{18}F labeled nanoparticles for in Vivo PET-CT imaging," *Bioconjugate Chemistry*, vol. 20, no. 2, pp. 397–401, 2009.

[53] H. S. Gill and J. Marik, "Preparation of ^{18}F-labeled peptides using the copper(I)-catalyzed azide-alkyne 1,3-dipolar cycloaddition," *Nature Protocols*, vol. 6, no. 11, pp. 1718–1725, 2011.

[54] C.-M. Lee, H.-J. Jeong, D. W. Kim, M.-H. Sohn, and S. T. Lim, "The effect of fluorination of zinc oxide nanoparticles on evaluation of their biodistribution after oral administration," *Nanotechnology*, vol. 23, no. 20, Article ID 205102, 2012.

[55] H. Schieferstein, T. Betzel, C. R. Fischer, and T. L. Ross, "^{18}F-click labeling and preclinical evaluation of a new ^{18}F-folate for PET imaging," *EJNMMI Research*, vol. 3, article 68, pp. 1–10, 2013.

[56] T. Ramenda, R. Bergmann, and F. Wuest, "Synthesis of ^{18}F-labeled neurotensin(8-13) via copper-mediated 1,3-dipolar [3+2]cycloaddition reaction," *Letters in Drug Design and Discovery*, vol. 4, no. 4, pp. 279–285, 2007.

[57] T. Ramenda, T. Kniess, R. Bergmann, J. Steinbach, and F. Wuest, "Radiolabelling of proteins with fluorine-18 via click chemistry," *Chemical Communications*, no. 48, pp. 7521–7523, 2009.

[58] T. Ramenda, J. Steinbach, and F. Wuest, "4-[^{18}F]Fluoro-N-methyl-N-(propyl-2-yn-1-yl)benzenesulfonamide ([^{18}F]F-SA): a versatile building block for labeling of peptides, proteins and oligonucleotides with fluorine-18 via Cu(I)-mediated click chemistry," *Amino Acids*, vol. 44, no. 4, pp. 1167–1180, 2013.

[59] J. A. H. Inkster, B. Guérin, T. J. Ruth, and M. J. Adam, "Radiosynthesis and bioconjugation of [^{18}F]FPy5yne, a prosthetic group for the ^{18}F labeling of bioactive peptides," *Journal of Labelled Compounds and Radiopharmaceuticals*, vol. 51, no. 14, pp. 444–452, 2008.

[60] A. C. Valdivia, M. Estrada, T. Hadizad, D. J. Stewart, R. S. Beanlands, and J. N. Dasilva, "A fast, simple, and reproducible automated synthesis of [^{18}F]FPyKYNE-c(RGDyK) for $\alpha_v\beta_3$ receptor positron emission tomography imaging," *Journal of Labelled Compounds and Radiopharmaceuticals*, vol. 55, no. 2, pp. 57–60, 2012.

[61] P. Daumar, C. A. Wanger-Baumann, N. Pillarsetty et al., "Efficient ^{18}F-labeling of large 37-amino-acid pHLIP peptide analogues and their biological evaluation," *Bioconjugate Chemistry*, vol. 23, no. 8, pp. 1557–1566, 2012.

[62] G. Vaidyanathan, B. J. White, and M. R. Zalutsky, "Propargyl 4-[^{18}F]fluorobenzoate: a putatively more stable prosthetic group for the fluorine-18 labeling of biomolecules via click chemistry," *Current Radiopharmaceuticals*, vol. 2, no. 1, pp. 63–74, 2009.

[63] Y. Li, Y. Liu, L. Zhang, and Y. Xu, "One-step radiosynthesis of 4-[^{18}F]flouro-3-nitro-N-2-propyn-1-yl-benzamide ([^{18}F]FNPB): a new stable aromatic porosthetic group for efficient labeling of peptides with fluorine-18," *Journal of Labelled Compounds and Radiopharmaceuticals*, vol. 55, no. 6, pp. 229–234, 2012.

[64] D. Thonon, C. Kech, J. Paris, C. Lemaire, and A. Luxen, "New strategy for the preparation of clickable peptides and labeling with 1-(azidomethyl)-4-[^{18}F]-fluorobenzene for PET," *Bioconjugate Chemistry*, vol. 20, no. 4, pp. 817–823, 2009.

[65] F. Mercier, J. Paris, G. Kaisin et al., "General method for labeling siRNA by click chemistry with fluorine-18 for the purpose of PET maging," *Bioconjugate Chemistry*, vol. 22, no. 1, pp. 108–114, 2011.

[66] J. Flagothier, G. Kaisin, F. Mercier et al., "Synthesis of two new alkyne-bearing linkers used for the preparation of siRNA for labeling by click chemistry with fluorine-18," *Applied Radiation and Isotopes*, vol. 70, no. 8, pp. 1549–1557, 2012.

[67] J.-H. Chun and V. W. Pike, "Single-step radiosynthesis of "^{18}F-labeled click synthons" from azide-functionalized diaryliodonium salts," *European Journal of Organic Chemistry*, vol. 2012, no. 24, pp. 4541–4547, 2012.

[68] S. Maschauer and O. Prante, "A series of 2-O-trifluoromethylsulfonyl-d-mannopyranosides as precursors for concomitant ^{18}F-labeling and glycosylation by click chemistry," *Carbohydrate Research*, vol. 344, no. 6, pp. 753–761, 2009.

[69] S. Maschauer, J. Einsiedel, R. Haubner et al., "Labeling and glycosylate of peptides using click chemistry: a general approach to ^{18}F-glycopeptides as effective imaging probes for positron emission tomography," *Angewandte Chemie International Edition*, vol. 49, no. 5, pp. 976–979, 2010.

[70] C. R. Fischer, C. Müller, J. Reber et al., "[^{18}F]fluoro-deoxyglucose folate: a novel PET radiotracer with improved in vivo properties for folate receptor targeting," *Bioconjugate Chemistry*, vol. 23, no. 4, pp. 805–813, 2012.

[71] S. Maschauer, R. Haubner, T. Kuwert, and O. Prante, "^{18}F-Glyco-RGD peptides for PET imaging of integrin expression: efficient radiosynthesis by click chemistry and modulation of biodistribution by glycosylation," *Molecular Pharmaceutics*, vol. 11, no. 2, pp. 505–515, 2014.

[72] O. Boutureira, F. D'Hooge, M. Fernández-González et al., "Fluoroglycoproteins: ready chemical site-selective incorporation of fluorosugars into proteins," *Chemical Communications*, vol. 46, no. 43, pp. 8142–8144, 2010.

[73] S. Maschauer, K. Michel, P. Tripal et al., "Synthesis and in vivo evaluation of an ^{18}F-labeled glycoconjugate of PD156707 for imaging ETA receptor expression in thyroid carcinoma by positron emission tomography," *Americam Journal of Nuclear Medicine and Molecular Imaging*, vol. 3, no. 5, pp. 425–436, 2013.

[74] F. Pisaneschi, R. L. Slade, L. Iddon et al., "Synthesis of a new fluorine-18 glycosylated "click" cyanoquinoline for the imaging of epidermal growth factor receptor," *Journal of Labelled Compounds and Radiopharmaceuticals*, vol. 57, no. 2, pp. 92–96, 2014.

[75] Y. Li, J. Guo, S. Tang, L. Lang, X. Chen, and D. M. Perrin, "One-step and one-pot-two-step radiosynthesis of functional imaging," *American Journal of Nuclear Medicine and Molecular Imaging*, vol. 3, no. 1, pp. 44–56, 2013.

[76] Y. Li, Z. Liu, C. W. Harwig et al., "^{18}F-click labeling of a bombesin antagonist with an alkyne-^{18}F-ArBF3-: in vivo PET imaging of tumors expressing the GRP-receptor," *American Journal of Nuclear Medicine and Molecular Imaging*, vol. 3, no. 1, pp. 57–70, 2013.

[77] Z. Liu, Y. Li, J. Lozada et al., "Stoichiometric Leverage: rapid ^{18}F-aryltrifluoroborate radiosynthesis at high specific activity for click conjugation," *Angewandte Chemie*, vol. 125, no. 8, pp. 2359–2363, 2013.

[78] M. Pretze and C. Mamat, "Automated preparation of [^{18}F]AFP and [^{18}F]BFP: two novel bifunctional ^{18}F-labeling building blocks for Huisgen-click," *Journal of Fluorine Chemistry*, vol. 150, pp. 25–35, 2013.

[79] M. Fani, X. Wang, G. Nicolas et al., "Development of new folate-based PET radiotracers: preclinical evaluation of 68Ga-DOTA-folate conjugates," *European Journal of Nuclear Medicine and Molecular Imaging*, vol. 38, no. 1, pp. 108–119, 2011.

[80] N. K. Devaraj, G. M. Thurber, E. J. Keliher, B. Marinelli, and R. Weissleder, "Reactive polymer enables efficient in vivo bioorthogonal chemistry," *Proceedings of the National Academy of Sciences of the United States of America*, vol. 109, no. 13, pp. 4762–4767, 2012.

[81] V. V. Rostovtsev, L. G. Green, V. V. Fokin, and K. B. Sharpless, "A stepwise huisgen cycloaddition process: copper(I)-catalyzed regioselective "Ligation" of azides and terminal alkynes," *Angewandte Chemie*, vol. 114, no. 14, pp. 2708–2711, 2002.

[82] C. W. Tornøe, C. Christensen, and M. Meldal, "Peptidotriazoles on solid phase: [1,2,3]-triazoles by regiospecific copper(I)-catalyzed 1,3-dipolar cycloadditions of terminal alkynes to azides," *Journal of Organic Chemistry*, vol. 67, no. 9, pp. 3057–3064, 2002.

[83] M. V. Gil, M. J. Arévalo, and Ó. López, "Click chemistry—what's in a name? Triazole synthesis and beyond," *Synthesis*, no. 11, pp. 1589–1620, 2007.

[84] K. D. Hänni and D. A. Leigh, "The application of CuAAC "click" chemistry to catenane and rotaxane synthesis," *Chemical Society Reviews*, vol. 39, no. 4, pp. 1240–1251, 2010.

[85] Y. Hua and A. H. Flood, "Click chemistry generates privileged CH hydrogen-bonding triazoles: the latest addition to anion supramolecular chemistry," *Chemical Society Reviews*, vol. 39, no. 4, pp. 1262–1271, 2010.

[86] C. O. Kappe and E. Van Der Eycken, "Click chemistry under non-classical reaction conditions," *Chemical Society Reviews*, vol. 39, no. 4, pp. 1280–1290, 2010.

[87] J. E. Hein and V. V. Fokin, "Copper-catalyzed azide-alkyne cycloaddition (CuAAC) and beyond: new reactivity of copper(i) acetylides," *Chemical Society Reviews*, vol. 39, no. 4, pp. 1302–1315, 2010.

[88] S. K. Mamidyala and M. G. Finn, "In situ click chemistry: probing the binding landscapes of biological molecules," *Chemical Society Reviews*, vol. 39, no. 4, pp. 1252–1261, 2010.

[89] R. A. Decréau, J. P. Collman, and A. Hosseini, "Electrochemical applications. How click chemistry brought biomimetic models to the next level: electrocatalysis under controlled rate of electron transfer," *Chemical Society Reviews*, vol. 39, no. 4, pp. 1291–1301, 2010.

[90] A. H. El-Sagheer and T. Brown, "Click chemistry with DNA," *Chemical Society Reviews*, vol. 39, no. 4, pp. 1388–1405, 2010.

[91] W. H. Binder and R. Sachsenhofer, ""Click" chemistry in polymer and materials science," *Macromolecular Rapid Communications*, vol. 28, no. 1, pp. 15–54, 2007.

[92] P. L. Golas and K. Matyjaszewski, "Marrying click chemistry with polymerization: expanding the scope of polymeric materials," *Chemical Society Reviews*, vol. 39, no. 4, pp. 1338–1354, 2010.

[93] A. Michael, "Über die Einwirkung von Diazobenzolimid auf Acetylendicarbonsäure-methylester," *Journal für Praktische Chemie*, vol. 48, no. 1, pp. 94–95, 1893.

[94] S. Maschauer and O. Prante, "Sweetening pharmaceutical radiochemistry by ^{18}F-fluoro-glycosylation: a short review," *BioMed Research International*, vol. 2014, Article ID 214748, 30 pages, 2014.

[95] Z. Liu, Y. Li, J. Lozada et al., "Stoichiometric leverage: rapid ^{18}F-aryltrifluoroborate radiosynthesis at high specific activity for click conjugation," *Angewandte Chemie International Edition English*, vol. 56, no. 8, pp. 2303–2307, 2013.

[96] G. J. Brewer, "Copper toxicity in the general population," *Clinical Neurophysiology*, vol. 121, no. 4, pp. 459–460, 2010.

[97] P. Mäding, F. Füchtner, and F. Wüst, "Module-assisted synthesis of the bifunctional labelling agent N-succinimidyl 4-[^{18}F]fluorobenzoate ([^{18}F]SFB)," *Applied Radiation and Isotopes*, vol. 63, no. 3, pp. 329–332, 2005.

[98] M. M. Herth, V. L. Andersen, S. Lehel, J. Madsen, G. M. Knudsen, and J. L. Kristensen, "Development of a 11C-labeled tetrazine for rapid tetrazine-trans-cyclooctene ligation," *Chemical Communications*, vol. 49, no. 36, pp. 3805–3807, 2013.

[99] M. S. Haka, M. R. Kilbourn, G. L. Watkins, and S. A. Toorongian, "Aryltrimethylammonium trifluoromethanesulfonates as precursors to aryl [^{18}F]fluorides: improved synthesis of [^{18}F]GBR-13119," *Journal of Labelled Compounds and Radiopharmaceuticals*, vol. 27, no. 7, pp. 823–833, 1989.

Hindawi Publishing Corporation
BioMed Research International
Volume 2014, Article ID 153741, 13 pages
http://dx.doi.org/10.1155/2014/153741

Review Article

Bimodal Imaging Probes for Combined PET and OI: Recent Developments and Future Directions for Hybrid Agent Development

Uwe Seibold,[1,2] Björn Wängler,[2] Ralf Schirrmacher,[3] and Carmen Wängler[1]

[1] *Biomedical Chemistry, Department of Clinical Radiology and Nuclear Medicine, Medical Faculty Mannheim of Heidelberg University, Theodor-Kutzer-Ufer 1-3, 68167 Mannheim, Germany*
[2] *Molecular Imaging and Radiochemistry, Department of Clinical Radiology and Nuclear Medicine, Medical Faculty Mannheim of Heidelberg University, 68167 Mannheim, Germany*
[3] *McConnell Brain Imaging Centre, Montreal Neurological Institute, McGill University, Montreal, QC, Canada H3A 2B4*

Correspondence should be addressed to Carmen Wängler; carmen.waengler@medma.uni-heidelberg.de

Received 11 February 2014; Accepted 18 March 2014; Published 16 April 2014

Academic Editor: Patrick Riss

Molecular imaging—and especially positron emission tomography (PET)—has gained increasing importance for diagnosis of various diseases and thus experiences an increasing dissemination. Therefore, there is also a growing demand for highly affine PET tracers specifically accumulating and visualizing target structures in the human body. Beyond the development of agents suitable for PET alone, recent tendencies aim at the synthesis of bimodal imaging probes applicable in PET as well as optical imaging (OI), as this combination of modalities can provide clinical advantages. PET, due to the high tissue penetration of the γ-radiation emitted by PET nuclides, allows a quantitative imaging able to identify and visualize tumors and metastases in the whole body. OI on the contrary visualizes photons exhibiting only a limited tissue penetration but enables the identification of tumor margins and infected lymph nodes during surgery without bearing a radiation burden for the surgeon. Thus, there is an emerging interest in bimodal agents for PET and OI in order to exploit the potential of both imaging techniques for the imaging and treatment of tumor diseases. This short review summarizes the available hybrid probes developed for dual PET and OI and discusses future directions for hybrid agent development.

1. Introduction

Within the last decades, the development of new radiotracers for PET imaging has experienced an enormous progress due to its enormous specificity and sensitivity in the visualization of target tissues. Thus, a rising number of valuable compounds applicable in cardiologic, neurologic, and especially oncologic imaging were developed. However, PET alone displays a limited spatial resolution of 1–3 mm in clinical practice and also is not able to allow a morphological correlation of the tracer accumulation which is however especially crucial in case of tumor diagnosis, localization, and staging. Thus, almost all clinical PET systems sold within the last years are combinations of PET and computed tomography (CT) systems, integrating the strengths of both modalities: the high specificity and sensitivity of PET making already functional changes in tissues visible at a very early stage of disease and the detailed morphologic information provided by CT [1]. Most recently, also combined clinical PET/MRI (magnetic resonance imaging) systems are commercially available. The MRI modality provides an even higher resolution and soft tissue contrast than CT, allowing for a functional imaging without causing any additional radiation burden to the patient. In combination with the very high sensitivity and specificity of PET, an almost ideal combined imaging modality is obtained for the whole-body imaging of patients [2] although the number of hybrid agents applicable in PET/MR imaging is very limited so far.

Despite these favorable properties of PET/CT and also PET/MRI systems in whole-body imaging for the identification of target structures, these modalities exhibit certain limitations: after having specifically identified and localized a tumor target tissue, the resection of the tumor mass is difficult due to the intricate intraoperative identification of tumor margins and small metastases. Additionally, the identification of the sentinel lymph node (SLN) which is often resected for histology is not trivial. For this purpose, another combination of imaging modalities could be of special interest, namely, the combination of PET with optical imaging (OI).

Although OI is a modality with restricted applicability for whole-body *in vivo* imaging due to the limited tissue penetration of the light emitted by the fluorescent probe, it is a valuable methodology for surface imaging applications such as intraoperative image-guided surgery due to its favorable spatial resolution and sensitivity [3–5]. Thus, a combined bimodal imaging consisting of an initial PET scan using γ-radiation with a high tissue penetration range to identify and localize tumor lesions throughout the body and a subsequent intraoperative OI in order to identify tumor margins and infected lymph nodes can result in a significant clinical improvement [6–8]. Especially in breast and prostate carcinomas as well as melanomas, the prognosis strongly depends on the presence of lymph node metastases [9–11]. However, the secure intraoperative identification of sentinel and infected lymph nodes is crucial for efficient diagnosis and treatment but is difficult if the surgeon can only rely on abnormal visual appearance and palpation to discriminate between lymph nodes and surrounding tissues or to identify infected nodes. The use of a specific tumor-accumulating agent which can be visualized during surgery by optical imaging techniques emitting light which can penetrate tissue in a reasonable range (so that a target node can be detected even if not already fully surgically exposed) would mean a significant improvement for surgery (Figure 1).

The development of new combined imaging techniques however also requires the development of the respective hybrid imaging agents that are suitable for all involved imaging modalities. Thus, considerable research has been conducted in this field of hybrid contrast agents over the last years [3, 4, 12–15].

For combined PET and optical imaging, in principle, the use of two separate molecular markers, one for PET and one for OI (instead of using a hybrid imaging agent), would also be possible. However, this is no optimal approach as both agents are likely to exhibit differing biodistribution and pharmacokinetic properties (especially in cases of relatively small, specifically accumulating biomolecules such as peptides). Hence, to achieve reliable results that are comparable between both imaging modalities, a hybrid marker has to be applied.

It has to be kept in mind that optical imaging is not fully quantifiable as it is surface-weighted due to absorbance and scattering of the photons by tissue penetration (especially when imaging deep tissues exhibiting a low imaging agent accumulation) and thus cannot be fully correlated to PET imaging data [16–19]. As PET, however, is fully quantifiable and used for whole-body imaging whereas OI is used for intraoperative imaging purposes only in order to identify tumor tissues (tumor margins, small metastases, and infected lymph nodes), the quantification of optical signals is no critical criterion.

For OI, different classes of reporter probes detectable by optical imaging techniques can in principle be used in a hybrid PET/OI agent: (i) fluorescent proteins that can be detected by bioluminescence imaging (BLI), (ii) γ-emitting radionuclides that can be visualized by Cherenkov luminescence imaging (CLI: luminescence that can be observed when a particle travels faster than light in the examined medium), (iii) fluorescent small dye molecules that can ideally emit near infrared light, and (iv) quantum dots which are semiconductor nanocrystals consisting of Cd/Te or Cd/Se materials and whose emission characteristics can be tailored by particle size. For all these probes that can be used in the development of a hybrid PET/OI agent, substances emitting light of the near-infrared and infrared spectrum (700–900 nm) are most useful, as light of these wavelengths exhibits the highest tissue permeability of several mm to cm *in vivo* [20, 21].

Large proteins such as GFP (green fluorescent protein) or RFP (red fluorescent protein) are in principle applicable in the synthesis of a hybrid compound. However, they are structurally demanding and would most possibly have a severe impact on the pharmacokinetic properties of the resulting imaging agent. Thus, it is only conceivable to use these compounds in combination with particle carriers. Furthermore, the quantum yield of these proteins is rather limited and they do not enable near-infrared photon emissions [22], further restricting the use of fluorescent proteins in hybrid optical imaging agents.

In contrast, CLI using different positron-emitting radionuclides has been proposed as a favorable optical imaging technique for imaging-guided surgery [23]. This technique does not require the conjugation of an additional fluorescent compound in order to obtain a bimodal imaging agent. This is favorable as an additionally conjugated fluorescent dye can—if susceptible to the radiolabeling conditions applied—interfere with the radiosynthesis or result in a significant alteration of the pharmacokinetic properties of the resulting hybrid compound. Unfortunately, using the Cherenkov luminescence imaging approach, one of the most valuable properties of combined PET/OI probes to be applied in intraoperative imaging, namely, the consecutive detection via PET and the subsequent later resection of the tumor, cannot be utilized. Using a hybrid compound consisting of a fluorescent dye in addition to a radionuclide, the optical intraoperative imaging can be performed delayed in time after identifying and localizing the tumorous tissue by a whole-body PET scan. By this procedure, the radionuclide at least partially decayed before surgery, resulting in no or only low radiation burden to the surgeon during intraoperative imaging and resection. In contrast, using CLI for intraoperative imaging can result in a significant radiation burden as is indicated by a recent study, systematically investigating the potential of CLI in a preclinical setting. In this work—when imaging an ^{124}I activity depot located subcutaneously in 4 mm depth—an

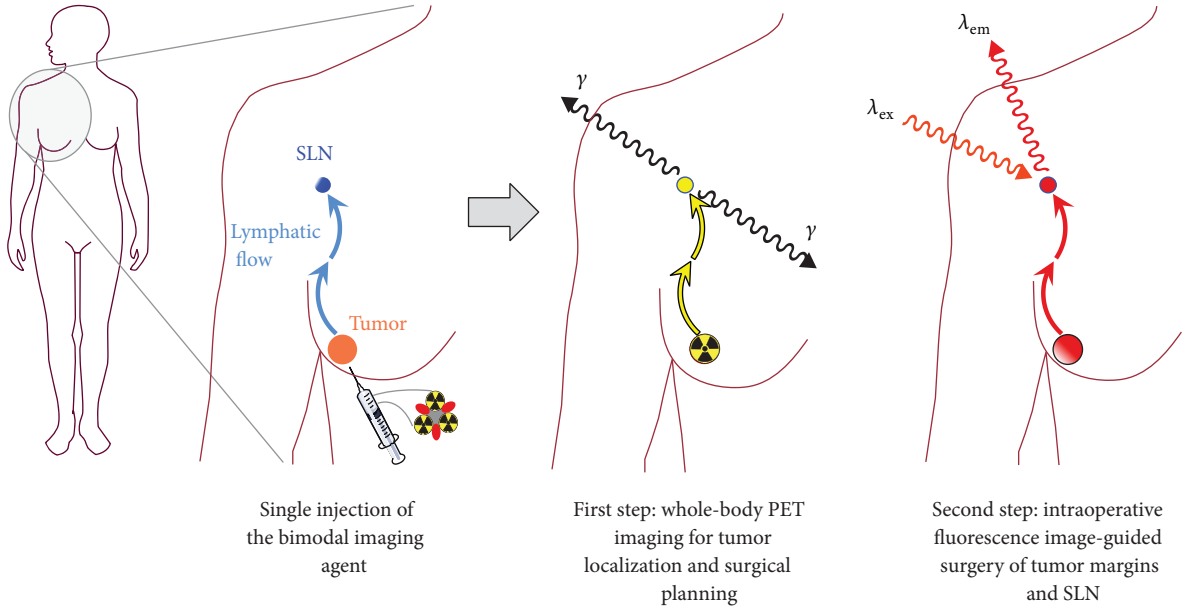

Figure 1: Schematic depiction of the operation principle of a PET/OI hybrid compound. After being applied to the patient in a single injection, an initial whole-body PET scan is performed, identifying and localizing tumor and potential metastases, thus serving as a tool for surgery planning. During the following surgical intervention, the same compound—having accumulated in the target tumor areas over time—can be used as a marker for intraoperative image-guided surgery of the respective malignant tissues.

activity concentration of at least 0.3 mCi/mL (11.1 MBq/mL) was necessary to obtain a detectable signal [24].

In most of the reported bimodal hybrid compounds for PET/OI, small fluorescent dyes or quantum dots are thus applied as they produce no ionizing radiation and are relatively stable under physiological conditions [25–27]. This allows for an image-guided surgery even after the decay of the radionuclide. In addition, small fluorescent dye molecules exhibit the advantage of being relatively small in size and thus result in a less prominent influence on the binding parameters of the carrier molecule which is especially important for the derivatization of small and medium-sized biomolecules.

2. Examples of Dually Labeled Agents Applicable in Hybrid *In Vivo* PET and Optical Imaging

Besides hybrid agents for combined PET/OI, also markers for dual SPECT/OI have been developed over the last years, comprising dually labeled antibodies [28, 29], peptides [30–35], a nontargeted small molecule [36], and nanoparticles [37–40]. However, as PET is—in contrast to SPECT—fully quantifiable and exhibits a much higher sensitivity than the latter, the main focus in this young field of bimodal probe development for use in nuclear medicine and optical imaging lies on the development of PET/OI agents, having a greater potential for a possible clinical application.

2.1. Nontargeted Small Molecules. Apart from targeted and nontargeted probes based on different biomolecule or nanoparticle carriers developed for a mostly tumor target-specific accumulation, the synthesis of several small molecule-based bimodal labels was reported. These are intended to be used directly without any further targeting for imaging (Figure 2, **1**–**3**) or could serve as a basis for a future bimodal labeling of biologically active compounds such as antibodies and other proteins (Figure 2, **5**–**8**).

The imaging agents **1**–**3** [41–44] depicted in Figure 2 are based on porphyrin or phthalocyanine derivatives which can show a significant accumulation in tumor tissues and can be used as photosensitizers thus being applicable in photodynamic therapy. These porphyrin and phthalocyanine derivatives were radiolabeled with ^{124}I and ^{64}Cu in different positions, respectively, and subjected to tumor xenograft mice for *in vivo* evaluation of their PET and/or optical imaging characteristics. Due to the missing tumor targeting entity, the observed tumor accumulations were faint and also a high unspecific accumulation of the compounds in nontarget organs such as liver, spleen, gut, lung, and blood was observed [41, 42, 44], limiting the usefulness of these compounds for *in vivo* tumor imaging. The ^{18}F-labeled Cy5.5 derivative **4** was synthesized in a proof of concept approach to demonstrate the applicability of a new secondary ^{18}F-labeling precursor for the radiolabeling of even sensitive molecules such as cyanine dyes and was thus not investigated regarding its *in vivo* characteristics. It could however be useful as hybrid label if functionalized for a bioconjugation and introduced into a targeting vector [45].

In contrast to compounds **1**–**4**, hybrid agents **5**–**8** [46–49] are not intended to be used directly for an *in vivo* application but for conjugation to a specifically accumulating agent such as a peptide, antibody, or antibody fragment by different reactive functional groups (active esters, maleimide,

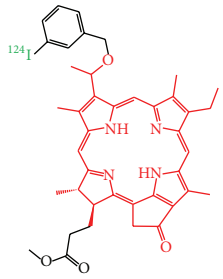

^{124}I-PS4
1

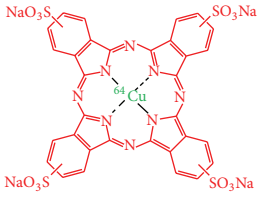

^{64}Cu-PcS$_4$
2

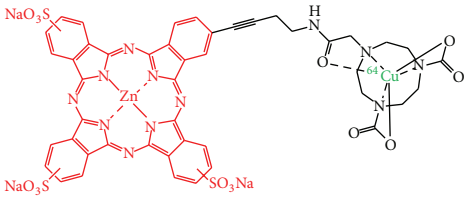

^{64}Cu-NOTA-C4-Zn-PcS$_3$
3

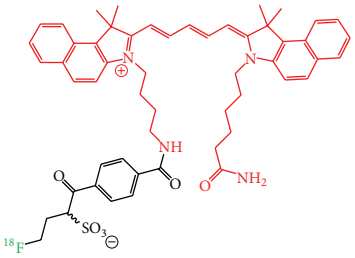

^{18}F-Cy5.5
4

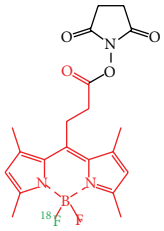

^{18}F-BODIPY N-hydroxysuccinimide ester
5

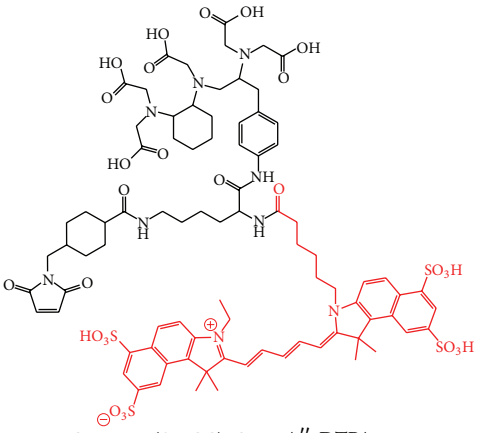

Cy5.5-Lys(SMCC)-CHX-A″-DTPA
6

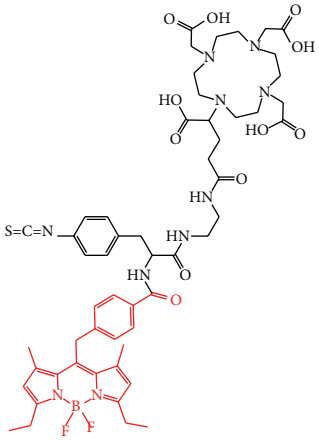

BODIPY-DOTAGA-isothiocyanate
7

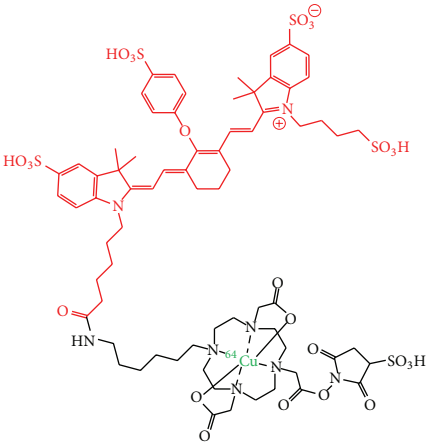

^{64}Cu-DO2A-IRDye800CW
8

Figure 2: Structures of small molecule-based bimodal labels developed for hybrid imaging with PET and OI (fluorescent dyes are depicted in red and PET nuclides in green).

and isothiocyanate). By this approach, the concomitant introduction of the radio- and the fluorescent label into the biomolecule is enabled and the resulting hybrid probe can be used in a targeted *in vivo* imaging application. However, the application of such a hybrid label for the derivatization of a specifically accumulating carrier molecule as well as the subsequent radiolabeling and *in vivo* evaluation of the so obtained dually labeled imaging probe was so far only shown for **8**. For this purpose, an anti-EpCAM antibody was first reacted with DO2A-IRDye800CW-sulfo NHS ester,

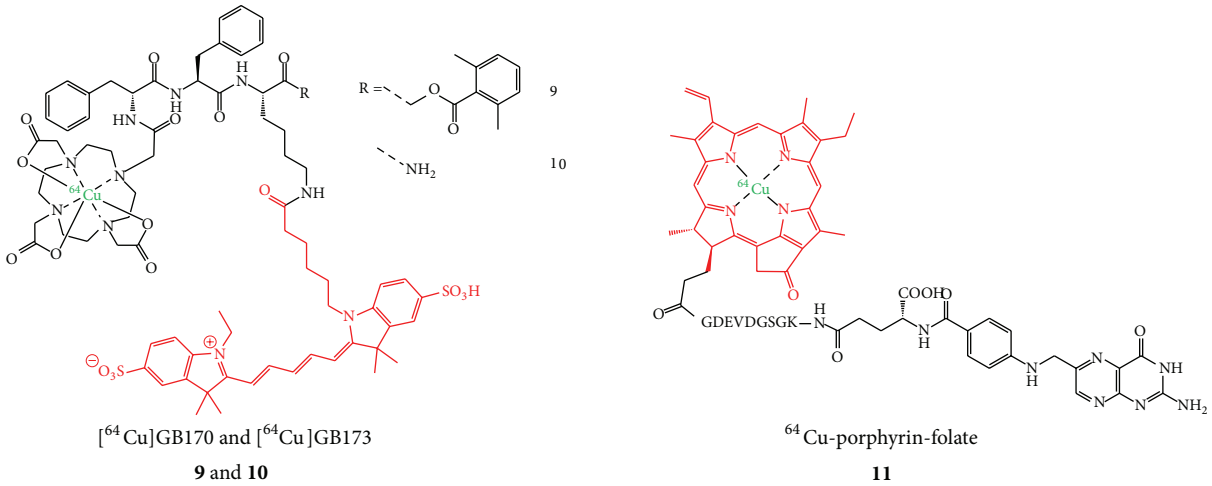

Figure 3: Structures of hybrid small molecule agents intended for specific accumulation in tumor tissues.

radiolabeled with ^{64}Cu (**8**), and finally evaluated in a proof of concept study in PC-3 xenograft mice [49]. Unfortunately, only near-infrared fluorescence imaging (NIR-FI) whole-body *in vivo* images and no PET data were shown in this study which is most probably attributable to the foreseeable insufficient stability of the ^{64}Cu-DO2A complex [50], resulting in very high liver and blood accumulations of the radionuclide compromising the *in vivo* PET data. In addition, also the NIR-FI data point to a predominant liver and also high kidney as well as lung accumulation at 40 h p.i. of the dual-labeled antibody, limiting its potential for hybrid *in vivo* tumor imaging. Thus, though not directly applicable *in vivo*, these small molecule-based hybrid imaging probes reflect the high interest in this relatively new field of hybrid PET/OI agent development.

2.2. Dually Labeled Small Molecules and Peptides Intended for Target-Specific Accumulation and Bimodal Target Visualization by PET/OI. The introduction of a fluorescent dye together with a radiolabel (which is either covalently attached or complexed by a chelator system) can result in a significant structural alteration especially in case of rather small target-specific molecules. Nevertheless, attempts have been made to synthesize such dually labeled small molecules and peptides, as they usually display fast pharmacokinetics and target accumulations and a rapid clearance from nontarget tissues, in principle resulting in favorable high-contrast images.

Especially for the studied small molecules (Figure 3, **9**–**11**), the structural change by introducing two labels was shown to result in high background and low specific tumor accumulations. The main excretory organ was in all cases the liver, for which a very pronounced uptake of the radiolabeled substances was observed, but also kidneys, spleen, and intestines showed high accumulations of the tracers, hampering a high tumor uptake and thus efficient tumor visualization with PET [51, 52].

Interestingly, it could be shown in the study dealing with the dually labeled cysteine cathepsin substrates [^{64}Cu]**9** and [^{64}Cu]**10** that the introduction of the NIR dye can result in a favorable prolonged circulation compared to the ^{64}Cu-DOTA-modified analog not comprising a fluorescent dye [52]. This positive effect of fluorescent dye conjugation could be confirmed by another study [16]. This prolonged circulation was described to result not only in a higher unspecific accumulation in all organs but also in a significantly higher and at least in part specific tumor accumulation [52] presumably due to a higher interaction probability of the hybrid agent with its target.

Despite the disappointing results obtained with PET imaging of the ^{64}Cu-labeled porphyrin-folate conjugate **11**, a clear tumor visualization was possible with fluorescence imaging (FI) after 24 h p.i. which can be attributed to the fact that the tumors were rather large and located directly under the skin. Furthermore, the tumors were—from all tissues—located nearest to the detector system, minimizing the absorbance and scattering of the fluorescent light emitted from the tumors whereas the photons emitted from the excretory organs were most probably strongly attenuated [51].

Due to their larger molecular size, peptides are in principle more likely to tolerate a derivatization with two different labels in terms of receptor binding and *in vivo* pharmacokinetics. This theoretical tendency seems in fact to be reflected in the results obtained for dually labeled peptides. From the dually labeled PET radionuclide and fluorescent dye comprising peptides available for tumor imaging so far (**12**–**16**, Figure 4), 4 compounds, namely, **13**–**16**, were evaluated *in vivo* regarding their biodistribution properties and tumor visualization abilities [16, 17, 25, 26, 53].

The results obtained in these studies seem to point to a more favorable biodistribution together with higher tumor to background ratios and higher tumor targeting specificity in case of larger dually labeled peptidic targeting vectors. It could, for example, be shown that for Tyr^3-octreotate (TATE), derivatized at the N-terminus with ^{64}Cu-DOTA and at the C-terminus with a NIR dye (**13**), on the one hand encouraging *in vitro* binding results to A427-7 tumor cell

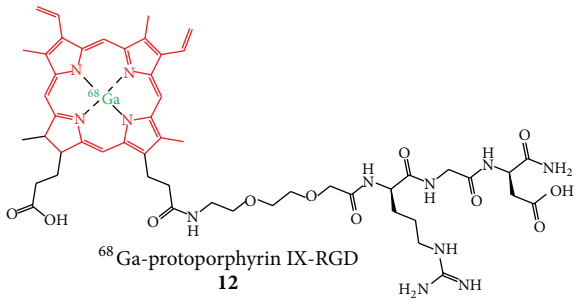

^{68}Ga-protoporphyrin IX-RGD
12

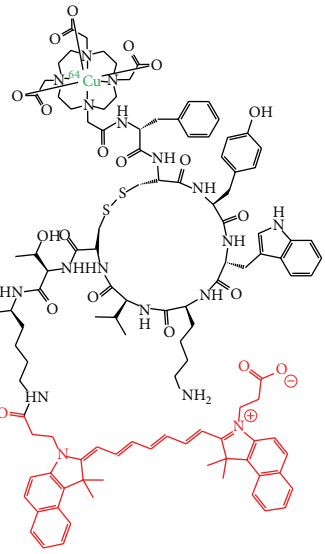

^{64}Cu-DOTA-TATE-Lys(cypate)-NH$_2$
13

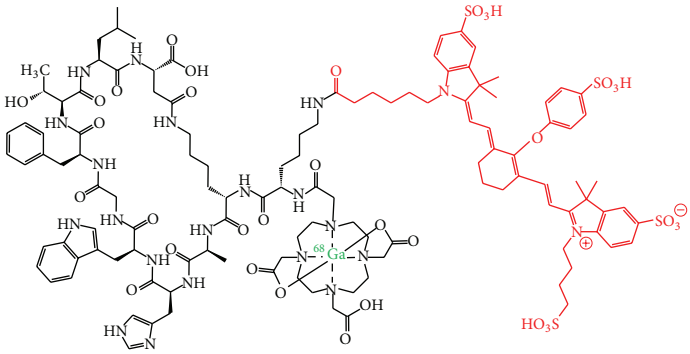

^{68}Ga-DOTA-IRDye800CW-HWGF
14

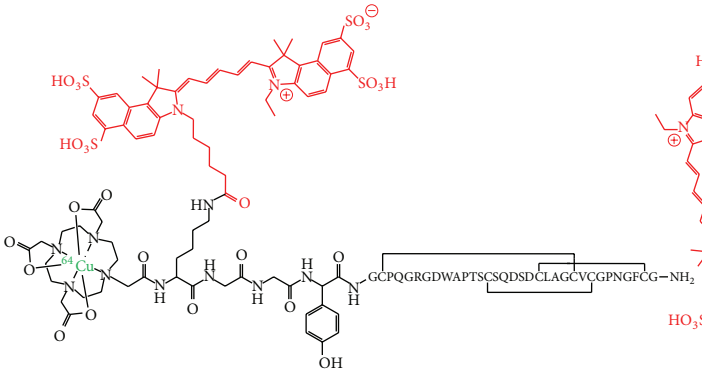

^{64}Cu-DOTA-Lys(Cy5.5)-Gly-Gly-Tyr-2.5D
15

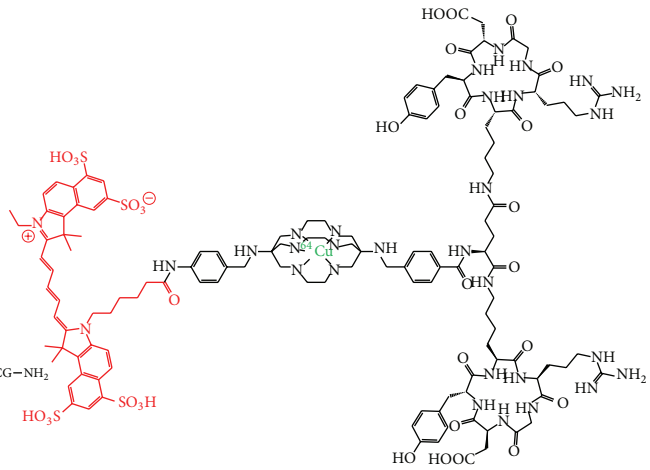

^{64}Cu-BaAnSar-RGD$_2$-Cy5.5
16

Figure 4: Structures of dually labeled PET radionuclide and fluorescent dye comprising peptides developed for *in vivo* tumor imaging with PET and OI.

membranes with K_i values of 0.43 nM for TATE and 11.5 nM for ^{nat}Cu-**13** could be obtained but that the agent was on the other hand not able to visualize the respective A427-7 tumor *in vivo* in xenograft mice at 24 h p.i. with FI [26]. Moreover, the low tumor uptake (only reaching a tumor-to-blood ratio of about 2) could not be blocked by cold peptide in biodistribution studies with ^{64}Cu-**13**, pointing to an unspecific tumor accumulation caused by the EPR effect (enhanced permeability and retention effect: a passive tumor-targeting process that results in an unspecific uptake of compounds due to a more permeable tumor vasculature and efficient diffusion through the tumor interstitium). Overall, a significant accumulation of this compound could only be observed in liver (16.824 ± 1.520%ID/g), spleen (8.069 ± 1.808%ID/g), and lung (1.428 ± 0.738%ID/g) after 1 h p.i. (for comparison: tumor accumulation was 0.287 ± 0.046%ID/g), pointing to a too pronounced overall lipophilicity of the compound for a successful *in vivo* application.

Similar effects were shown for **14**, which was developed to visualize MMP2 and 9 *in vivo* [25]. However, in a heterotopic ossification model activating MMP9, a target visualization could not be achieved by PET imaging. Using NIR-FI, the ossification site could be visualized, but no whole-body images were shown limiting the informative value of these images.

In contrast to these latter studies, two examples of very promising peptidic hybrid compounds for PET and OI were reported. One of these—consisting of an $\alpha_v\beta_3$ and $\alpha_v\beta_5$-affine knottin peptide targeting tumor angiogenesis, derivatized with Cy5.5 and DOTA via an amino acid spacer—was radiolabeled with ^{64}Cu (**15**) and successfully used for specific *in vivo* PET and NIR-FI of an integrin-positive U87MG tumor in xenograft mice [17]. These favorable results were achieved although the *in vitro* binding data indicated an adverse influence of the derivatization of the peptide with NIR dye and chelator compared to a monolabeling with DOTA or NIR dye alone. Interestingly, comparing the ^{64}Cu-DOTA-monolabeled knottin peptide with the dual-labeled one regarding *in vivo* biodistribution with PET, both compounds achieve tumor-to-background ratios (TBR) of ~ 4.5. However, these comparable ratios were found at different time points: the ^{64}Cu-DOTA-monolabeled peptide reaches this TBR already at 4 h p.i. whereas the same TBR is achieved by the dually labeled peptide **15** at 24 h p.i., indicating—as described before—a retention-prolonging effect of the conjugated NIR dye. This is confirmed by the corresponding NIR-FI experiment comparing the NIR-monolabeled peptide with the dually-labeled one **15** which both reach the TBR of ~4.5 at 24 h p.i.

A very encouraging example of a dually labeled hybrid compound was described recently, consisting of a cRGD-dimer (serving as tumor-targeting vector) and Cy5.5 which is connected to the peptidic part via a sarcophagine-derived chelator used for ^{64}Cu-labeling [16]. The radiolabeled compound ^{64}Cu-**16** was successfully used for the *in vivo* imaging of integrin-rich U87MG tumors in a xenograft mouse model, showing a high tumor uptake together with a stable tumor retention (6.41 ± 0.28, 6.51 ± 1.45, and 5.92 ± 1.57%ID/g at 1, 4, and 20 h *p.i.*, resp.), resulting in the highest tumor-to-background ratios of ~7 at 20 h p.i. As described before, this NIR dye-labeled compound ^{64}Cu-**16** showed a prolonged circulation together with a higher tumor accumulation compared to the corresponding, nonfluorescent-labeled derivative [16]. Furthermore, ^{64}Cu-**16** was used for image-guided resection of the tumor in the same animal model and showed—in contrast to the PET images displaying a homogeneous tumor areal due to the physically limited spatial resolution of ^{64}Cu—the presence of a metastasis near the primary tumor, impressively demonstrating the advantages of intraoperative optical imaging and the synergistic effects of PET combined with OI.

These favorable *in vivo* imaging results found for **15** and **16** are probably a result of two different effects: the large size of the peptidic targeting vector relative to both labels and also the introduction of both labels in only one position of the peptidic moiety, limiting their influence on the overall biodistribution compared to two labels introduced in different positions of the peptide. Thus, due to the strong potential influence of two labeling moieties introduced, the ligand design has to be carefully considered especially when derivatizing peptides.

2.3. Fluorescent and Radiolabeled Antibodies for Combined PET/OI. Antibodies with their slow pharmacokinetics and very high target specificity should be well suited as targeting vectors for a dual-labeling approach with a PET nuclide and a NIR dye as they exhibit a more complex structure than small molecules and peptides resulting in a less strong alteration of structure, binding characteristics, and thus biodistribution properties by the concomitant conjugation of two labels. Several different antibodies have been derivatized with desferrioxamine [54–56] for ^{89}Zr-labeling, NOTA [57] or DOTA [18, 58, 59] for ^{64}Cu-labeling, and the NIR dyes 800CW [54–59] or Alexa Fluor 750 [18] (Figure 5).

In all studies, it could be demonstrated that the number of introduced derivatization sites has a crucial effect on the biodistribution characteristics of the obtained hybrid compounds. One study, for example, describes the derivatization of an anti-CD20 IgG with ~10 chelators and ~2 fluorescent dyes, resulting in an unfavorable biodistribution of the hybrid compound in lymphoma-bearing mice, showing a very high liver and spleen accumulation of the antibody. Consequently, only a moderate tumor uptake was observed resulting in only poor tumor visualization *in vivo* [18]. Reducing the number of introduced labels, radionuclide chelator and fluorescent dye, to ~2 per trastuzumab molecule, improved results could be obtained in 4T1.2neu/R tumor-bearing xenograft mice, allowing for a tumor visualization with PET as well as NIR-FI at 24 h p.i., although tumor-to-muscle ratios of only ~2.5 were obtained [58]. Reducing the number of both labeling moieties to 1 per anti-CD105 antibody molecule, the tumor-to-muscle ratios could be improved to ~7 in 4T1 tumor xenograft mouse models [56]. However, besides a tumor uptake of ~10%ID/g, high liver, spleen, and blood uptakes of ~16%ID/g, ~8%ID/g, and ~11%ID/g were observed at 48 h p.i., respectively, impairing the *in vivo* imaging results.

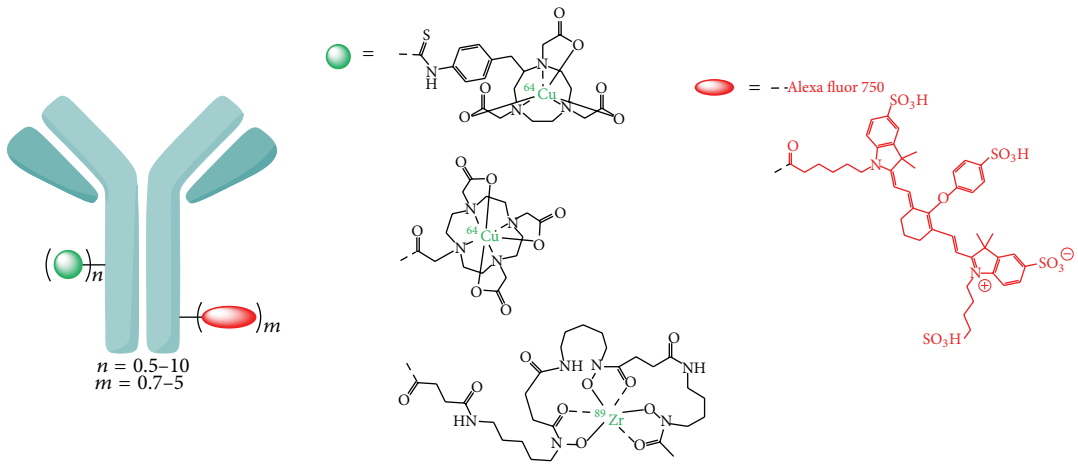

Figure 5: Schematic depiction of dually labeled antibodies developed for *in vivo* hybrid PET/OI of tumors.

Nevertheless, the observed tumor uptakes were no result of the EPR effect alone but also of a specific binding, as they could be blocked by about 50% by coapplication of unlabeled antibody.

Other studies, limiting the number of introduced labels to a minimum of 0.5–0.9 equivalents of each labeling moiety per antibody, found even more favorable biodistribution properties such as a slowed clearance, lower liver, and higher and prolonged tumor uptakes resulting in a clear visualization of the tumor mass *in vivo* at 48 h p.i. with PET as well as NIR-FI [54, 57]. Besides the observed impaired biodistribution properties of high liver and spleen uptake *in vivo* when conjugating several fluorescent dye molecules per antibody, a conjugation of several dyes also results in a fluorescence quenching effect and thus a decreased overall fluorescence intensity, being detrimental to a successful *in vivo* NIR-FI of the target tissue [54, 57]. These studies furthermore investigated the correlation between organ uptakes determined by *in vivo* PET and *in vivo* or *ex vivo* NIR-FI. The PET data in these studies served as reference parameters as PET is fully quantifiable. It was found that the deviations in measured organ uptakes were higher for the NIR-FI data obtained *in vivo* than obtained *ex vivo*. Also, the deviations were higher for deeper tissues, pointing to a significant scattering and absorbance of the NIR light, limiting the quantification of tissue uptakes by fluorescence imaging and necessitating the quantification of organ uptakes by PET. This is, however, no limitation for optical imaging in terms of intraoperative imaging settings where only qualitative images are required for a successful tumor resection.

Besides the described general findings regarding the negative influence of a high number of conjugated labeling moieties on the biodistribution properties of derivatized antibodies, one study systematically investigated the influence of the number of conjugation sites on the biodistribution of dual-labeled antibodies [55]. There, the EGFR and VEGF targeting antibodies cetuximab and bevacizumab were initially derivatized with on average 0.5 desferrioxamine chelators, followed by an introduction of 0.5 to 5 800CW NIR dyes, and the biodistribution of the resulting hybrid imaging compounds was determined *in vivo* after ^{89}Zr-radiolabeling. It could be shown that the antibody uptake into the liver proportionally increased with the number of conjugated dyes, whereas the tumor accumulation decreased to the same extent.

Thus, in order to achieve optimal imaging results using a dually labeled hybrid antibody for PET and NIR fluorescence imaging, the development of a small molecule serving as a dual-label would be of advantage. This molecule could consist of a chelator for radiometal labeling, the NIR dye, and a functionality enabling a concomitant conjugation of both labels in only one position of the antibody, thus limiting its structural change to an absolute minimum.

2.4. Nanoparticles as a Platform for Hybrid PET/OI Agents. Nanoparticles—in contrast to biomolecules—exhibit the advantage of possessing a large surface which can easily be modified with functional groups for the conjugation of targeting vectors, radiolabels, and fluorescent dyes. On the other hand, they also face several problems: (i) they necessitate a stable coating for functionalization, (ii) exhibit a long tissue retention, (iii) only insufficient knowledge is available about their toxicity (especially in case of quantum dots, consisting of Cd ions and other potentially toxic metals), metabolism, and excretion, and (iv) they strongly accumulate in the reticuloendothelial system (RES) and thus in liver, spleen, bone marrow, and lymph nodes. Furthermore, the stoichiometry of the conjugated moieties is difficult to control or quantify after reaction. Nevertheless, most of the hybrid compounds developed for dual PET and OI so far are based on nanoparticles as carriers.

The group of nanoparticles applicable as structural basis for hybrid PET/OI agents consists of several different subgroups: polymer-based nanoparticles [60], lipid-based particles such as micelles [61] and liposomes [62], carbon-based systems such as nanotubes [63], and also metal-based nanoparticles such as iron oxide [5, 27, 64–67], silica [8], and upconversion nanoparticles [68, 69] as well as quantum dots (QDs) [70–73].

QDs are fluorescent semiconductor nanocrystals whose fluorescent properties can be influenced by the particle size and composition. Furthermore, they exhibit high quantum yields and photostability [74], making them interesting fluorophores for the development of compounds for hybrid PET/optical imaging when stably radiolabeled with a positron-emitter (Figure 6(a)). Superparamagnetic iron oxide nanoparticles on the other hand are detectable by MRI, enabling a triple-modality imaging with PET/OI and MRI when derivatized with fluorescent dyes and radionuclides (Figures 6(b) and 6(c)) [27, 64]. QDs as well as iron oxide nanoparticles have to be coated with biocompatible materials to render them amenable for an *in vivo* application. This coating can consist of different materials such as SiO_2 or other inorganic material, dextran, micelles, or polyethylene glycols (PEGs) and furthermore enables a chemical modification of the surface of the particles with dyes, radiolabels, and targeting vectors allowing for a target-specific accumulation (Figures 6(d) and 6(e)). An alternative to the approach of chemical modification of the coating of a nanoparticle with NIR dyes in order to obtain a fluorescent agent is the encapsulation of the fluorophore within the particle coating (Figure 6(b)) which has been shown to result in a much higher fluorescence signal and photostability of the fluorescent dye than a surficial dye conjugation (Figure 6(c)) [8, 27].

An important factor in the design of particles intended for *in vivo* imaging purposes is their sufficient stability over the duration of the examination. Thus, also the radiolabel has to be stably introduced by covalent conjugation (in case of nonmetallic isotopes such as ^{18}F or iodine isotopes) or stable complex formation (in case of radiometal ions). As the development of hybrid agents for combined PET and OI is still in the beginning, nanoparticles which do not exhibit a stable radionuclide introduction have also been reported. In these cases, the particles were only incubated with the radionuclide, "trapping" the respective radioisotope by proteins used for coating of the particle surface [61], functional groups such as primary amines [64], ionic interactions for ^{18}F-labeling [68, 69], or the use an suboptimal chelator for the applied radiometal [65]. In these cases, liberation of the radionuclide was inevitable, resulting in the expectable unfavorable biodistribution characteristics of the radiolabel and thus low image quality. In other cases, the potential of the labeled nanoparticles was not demonstrated as the agents were applied via intratumoral injection [62] or incubated with tumor cells that in the following could be visualized in animals directly after implantation of the labeled cells [66].

In contrast, also well-designed hybrid nanoparticle probes were described, showing highly promising results and giving directions for further developments.

As already mentioned, the particle coating allows not only for the conjugation of fluorescent dyes and radiolabels but also for modification with a targeting vector such as peptides or proteins for enabling a tumor-specific accumulation and imaging, but only few examples of such targeted particles can be found. Two of them describe the surface-modification of ^{64}Cu-labeled QDs with VEGF and c(RGDyK) for *in vivo* imaging of angiogenesis and, in both cases, a $VEGFR_2$ and $\alpha_v\beta_3$ receptor-specific binding could be demonstrated *in vitro* and *in vivo* [70, 71]. Although the major fraction of the particles was shown to rapidly accumulate in the reticuloendothelial system (which is attributed to their size of about 20 nm), both particles allow a visualization of the tumor entity in the respective tumor xenograft mouse models. Furthermore, they show a targeting-vector dependent accumulation as the respective particles without a VEGF or c(RGDyK) derivatization show only a background level tumor accumulation. Another even more favorable example of a hybrid nanoparticle was described very recently. Small silica particles of 6-7 nm in diameter comprising encapsulated NIR dye Cy5.5 were PEG-coated in order to achieve a higher biocompatibility and lower liver accumulation. These particles were further derivatized on their surface with c(RGDyK) and radiolabeled with ^{124}I on the tyrosine moiety of the peptide. These particles were successfully used for whole-body PET imaging for tumor and multiple metastases visualization (showing a very favorable biodistribution without accumulation the RES) as well as intraoperative imaging guidance in a spontaneous melanoma miniswine model [8]. The intraoperative imaging was performed using a hand-held fluorescence imaging camera allowing for real-time fluorescence imaging and surgical guidance. By this, it was possible to identify sentinel lymph nodes and to discriminate between metastatic tumor infiltration and inflammatory processes during surgery. This example of presurgical whole-body PET imaging together with subsequent intraoperative optical image-guided surgery in a larger animal shows the very high clinical potential of this approach.

In order to overcome the short circulation half-life and rapid RES accumulation of nanoparticles, resulting in a very low interaction probability of the imaging agent with the tissue to be visualized, the use of smaller particles (<12 nm) has been proposed [71, 73]. Furthermore, PEGs can be attached to the particle surface. This modification slows the particle resorption by liver and spleen [72, 73] but can in return result in a higher bone marrow uptake of the compounds *in vivo* [71, 73]. Particles comprising no targeting vector showing a rapid accumulation in the RES can however also be useful, especially for sentinel lymph node (SLN) mapping (Figure 1) [27, 60].

3. Conclusion

So far, the obtained results for hybrid PET/OI agents are variable. Nevertheless, some examples already show the high potential of these substances for target visualization with both imaging modalities. Future developments of dually labeled hybrid imaging agents for PET/OI exhibiting a favorable *in vivo* biodistribution and being applicable in a multimodal clinical setting face the challenge to introduce a radiolabel as well as a fluorescent reporter probe by at the same time preserving the favorable pharmacokinetic properties enabling a successful and specific target visualization.

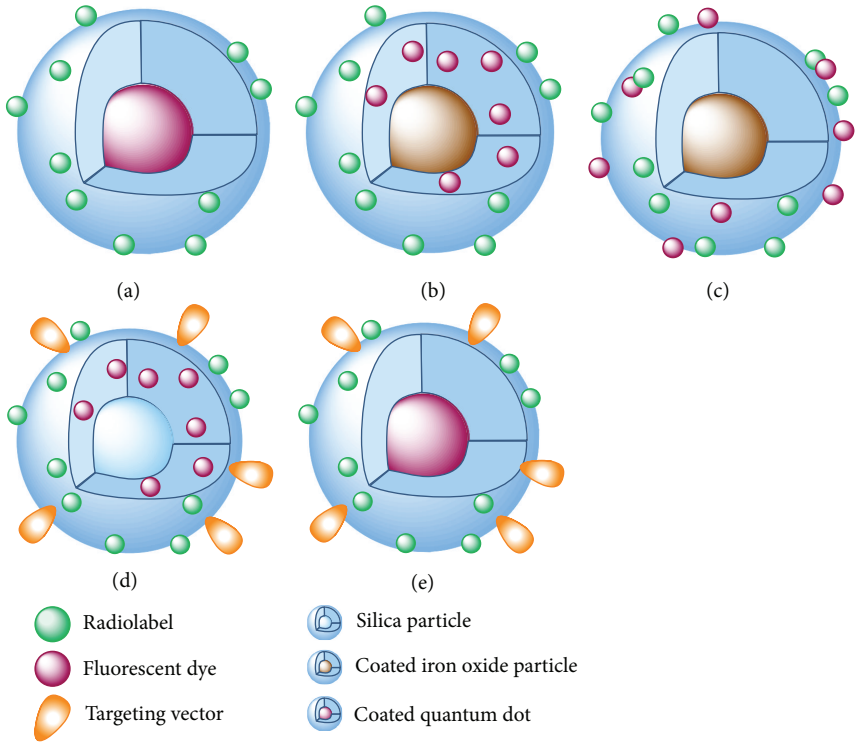

Figure 6: Schematic representation of different kinds of labeled nanoparticles that were already used as hybrid compounds for PET and OI: (a) coated quantum dot loaded with chelating agent for radiometal introduction, (b) coated iron oxide particle with encapsulated fluorescent dye and derivatized on its surface with a chelator for radiolabeling, (c) coated iron oxide particle derivatized on the surface with fluorescent dye and chelator for radiometal labeling, (d) silica nanoparticles with encapsulated fluorescent dye and surficial derivatization with radionuclide and targeting vector, and (e) coated quantum dot loaded with chelating agent for radiometal introduction and a targeting vector.

Promising probes developed so far comprise dually labeled nanoparticles, antibodies, and peptides although the agents based on each of these substance classes require a careful optimization regarding the overall biodistribution of the hybrid agents. Thus, one focus of future developments could be the design of small molecules comprising the radionuclide as well as the NIR dye enabling the ideally site-specific, one-step dual-labeling of biomolecules, exerting only a minor structural alteration to the targeting vector and thus only a minor effect on its bioactivity resulting in highly potent compounds for hybrid imaging. In case of nanoparticles, the pharmacokinetic properties need to be optimized in order to minimize their uptake by the RES and to maximize their target-specific accumulation. Such developments could then result in hybrid imaging agents having a significant impact on whole-body *in vivo* target detection by PET as well as subsequent optical imaging-guided intraoperative curative surgery.

Conflict of Interests

The authors declare that there is no conflict of interests regarding the publication of this paper.

Acknowledgments

The authors acknowledge the financial support by Deutsche Forschungsgemeinschaft and Ruprecht-Karls-Universität Heidelberg within the funding programme Open Access Publishing.

References

[1] S. R. Cherry, "Multimodality *in vivo* imaging systems: twice the power or double the trouble?" *Annual Review of Biomedical Engineering*, vol. 8, pp. 35–62, 2006.

[2] S. R. Cherry, "Multimodality imaging: beyond PET/CT and SPECT/CT," *Seminars in Nuclear Medicine*, vol. 39, no. 5, pp. 348–353, 2009.

[3] J. Cheon and J. H. Lee, "Synergistically integrated nanoparticles as multimodal probes for nanobiotechnology," *Accounts of Chemical Research*, vol. 41, no. 12, pp. 1630–1640, 2008.

[4] T. Buckle, P. T. K. Chin, and F. W. B. van Leeuwen, "(Non-targeted) radioactive/fluorescent nanoparticles and their potential in combined pre-and intraoperative imaging during sentinel lymph node resection," *Nanotechnology*, vol. 21, no. 48, pp. 482001–482010, 2010.

[5] M. Nahrendorf, E. Keliher, B. Marinelli et al., "Hybrid PET-optical imaging using targeted probes," *Proceedings of the*

National Academy of Sciences of the United States of America, vol. 107, no. 17, pp. 7910–7915, 2010.

[6] G. M. van Dam, G. Themelis, L. M. A. Crane et al., "Intraoperative tumor-specific fluorescence imaging in ovarian cancer by folate receptor-α targeting: first in-human results," *Nature Medicine*, vol. 17, no. 10, pp. 1315–1319, 2011.

[7] P. T. Chin, C. A. Beekman, T. Buckle, L. Josephson, and F. W. van Leeuwen, "Multispectral visualization of surgical safety-margins using fluorescent marker seeds," *The American Journal of Nuclear Medicine and Molecular Imaging*, vol. 2, pp. 151–162, 2012.

[8] M. S. Bradbury, E. Phillips, P. H. Montero et al., "Clinically-translated silica nanoparticles as dual-modality cancer-targeted probes for image-guided surgery and interventions," *Integrative Biology*, vol. 5, pp. 74–86, 2013.

[9] E. J. T. Rutgers, "Sentinel node biopsy: interpretation and management of patients with immunohistochemistry-positive sentinel nodes and those with micrometastases," *Journal of Clinical Oncology*, vol. 26, no. 5, pp. 698–702, 2008.

[10] C. M. Balch, S.-J. Soong, J. E. Gershenwald et al., "Prognostic factors analysis of 17,600 melanoma patients: validation of the American Joint Committee on Cancer melanoma staging system," *Journal of Clinical Oncology*, vol. 19, no. 16, pp. 3622–3634, 2001.

[11] L. Vermeeren, R. A. Valdés Olmos, W. Meinhardt et al., "Value of SPECT/CT for detection and anatomic localization of sentinel lymph nodes before laparoscopic sentinel node lymphadenectomy in prostate carcinoma," *Journal of Nuclear Medicine*, vol. 50, no. 6, pp. 865–870, 2009.

[12] J. Kuil, T. Buckle, and F. W. van Leeuwen, "Imaging agents for the chemokine receptor 4 (CXCR4)," *Chemical Society Reviews*, vol. 41, pp. 5239–5261, 2012.

[13] J. C. Knight and F. R. Wuest, "Nuclear (PET/SPECT) and optical imaging probes targeting the CXCR4 chemokine receptor," *Medicinal Chemistry Communications* , vol. 3, pp. 1039–1053, 2012.

[14] K. Yan, P. Li, H. Zhu et al., "Recent advances in multifunctional magnetic nanoparticles and applications to biomedical diagnosis and treatment," *RSC Advances*, vol. 3, pp. 10598–10618, 2013.

[15] A. Louie, "Multimodality imaging probes: design and challenges," *Chemical Reviews*, vol. 110, no. 5, pp. 3146–3195, 2010.

[16] S. Liu, D. Li, C. W. Huang et al., "Efficient construction of PET/fluorescence probe based on sarcophagine cage: an opportunity to integrate diagnosis with treatment," *Molecular Imaging and Biology*, vol. 14, pp. 718–724, 2012.

[17] R. H. Kimura, Z. Miao, Z. Cheng, S. S. Gambhir, and J. R. Cochran, "A dual-labeled knottin peptide for PET and near-infrared fluorescence imaging of integrin expression in living subjects," *Bioconjugate Chemistry*, vol. 21, no. 3, pp. 436–444, 2010.

[18] P. Paudyal, B. Paudyal, Y. Iida et al., "Dual functional molecular imaging probe targeting CD20 with PET and optical imaging," *Oncology Reports*, vol. 22, no. 1, pp. 115–119, 2009.

[19] R. Weissleder and U. Mahmood, "Molecular imaging," *Radiology*, vol. 219, no. 2, pp. 316–333, 2001.

[20] K. Shah and R. Weissleder, "Molecular optical imaging: applications leading to the development of present day therapeutics," *NeuroRx*, vol. 2, no. 2, pp. 215–225, 2005.

[21] J. V. Frangioni, "*In vivo* near-infrared fluorescence imaging," *Current Opinion in Chemical Biology*, vol. 7, no. 5, pp. 626–634, 2003.

[22] J. M. Park and S. S. Gambhir, "Multimodality radionuclide, fluorescence, and bioluminescence small-animal imaging," *Proceedings of the IEEE*, vol. 93, no. 4, pp. 771–782, 2005.

[23] J. P. Holland, G. Normand, A. Ruggiero, J. S. Lewis, and J. Grimm, "Intraoperative imaging of positron emission tomographic radiotracers using cerenkov luminescence emissions," *Molecular Imaging*, vol. 10, no. 3, pp. 177–186, 2011.

[24] J. C. Park, M. K. Yu, G. I. An et al., "Facile preparation of a hybrid nanoprobe for triple-modality optical/PET/MR imaging," *Small*, vol. 6, no. 24, pp. 2863–2868, 2010.

[25] A. Azhdarinia, N. Wilganowski, H. Robinson et al., "Characterization of chemical, radiochemical and optical properties of a dual-labeled MMP-9 targeting peptide," *Bioorganic & Medicinal Chemistry*, vol. 19, no. 12, pp. 3769–3776, 2011.

[26] W. B. Edwards, B. Xu, W. Akers et al., "Agonist—antagonist dilemma in molecular imaging: evaluation of a monomolecular multimodal imaging agent for the somatostatin receptor," *Bioconjugate Chemistry*, vol. 19, no. 1, pp. 192–200, 2008.

[27] J. S. Kim, Y.-H. Kim, J. H. Kim et al., "Development and *in vivo* imaging of a PET/MRI nanoprobe with enhanced NIR fluorescence by dye encapsulation," *Nanomedicine*, vol. 7, no. 2, pp. 219–229, 2012.

[28] L. Sampath, S. Kwon, S. Ke et al., "Dual-labeled trastuzumab-based imaging agent for the detection of human epidermal growth factor receptor 2 overexpression in breast cancer," *Journal of Nuclear Medicine*, vol. 48, no. 9, pp. 1501–1510, 2007.

[29] L. Sampath, W. Wang, and E. M. Sevick-Muraca, "Near infrared fluorescent optical imaging for nodal staging," *Journal of Biomedical Optics*, vol. 13, no. 4, Article ID 041312, 2008.

[30] J. Kuil, T. Buckle, J. Oldenburg et al., "Hybrid peptide dendrimers for imaging of chemokine receptor 4 (CXCR4) expression," *Molecular Pharmaceutics*, vol. 8, no. 6, pp. 2444–2453, 2011.

[31] J. Kuil, T. Buckle, H. Yuan et al., "Synthesis and evaluation of a bimodal CXCR4 antagonistic peptide," *Bioconjugate Chemistry*, vol. 22, no. 5, pp. 859–864, 2011.

[32] W. Wang, S. Ke, S. Kwon et al., "A new optical and nuclear dual-labeled imaging agent targeting interleukin 11 receptor alpha-chain," *Bioconjugate Chemistry*, vol. 18, no. 2, pp. 397–402, 2007.

[33] J. P. Houston, S. Ke, W. Wang, C. Li, and E. M. Sevick-Muraca, "Quality analysis of *in vivo* near-infrared fluorescence and conventional gamma images acquired using a dual-labeled tumor-targeting probe," *Journal of Biomedical Optics*, vol. 10, no. 5, Article ID 054010, 2005.

[34] W. B. Edwards, W. J. Akers, Y. Ye et al., "Multimodal imaging of integrin receptor-positive tumors by bioluminescence, fluorescence, gamma scintigraphy, and single-photon emission computed tomography using a cyclic RGD peptide labeled with a near-infrared fluorescent dye and a radionuclide," *Molecular Imaging*, vol. 8, no. 2, pp. 101–110, 2009.

[35] C. Li, W. Wang, Q. Wu et al., "Dual optical and nuclear imaging in human melanoma xenografts using a single targeted imaging probe," *Nuclear Medicine and Biology*, vol. 33, no. 3, pp. 349–358, 2006.

[36] Z. Zhang, K. Liang, S. Bloch, M. Berezin, and S. Achilefu, "Monomolecular multimodal fluorescence-radioisotope imaging agents," *Bioconjugate Chemistry*, vol. 16, no. 5, pp. 1232–1239, 2005.

[37] C. A. Boswell, P. K. Eck, C. A. S. Regino et al., "Synthesis, characterization, and biological evaluation of integrin $\alpha v\beta 3$-targeted PAMAM dendrimers," *Molecular Pharmaceutics*, vol. 5, no. 4, pp. 527–539, 2008.

[38] D. R. Vera, D. J. Hall, C. K. Hoh, P. Gallant, L. M. McIntosh, and R. F. Mattrey, "Cy5.5-DTPA-galactosyl-dextran: a fluorescent probe for *in vivo* measurement of receptor biochemistry," *Nuclear Medicine and Biology*, vol. 32, no. 7, pp. 687–693, 2005.

[39] N. Mitchell, T. L. Kalber, M. S. Cooper et al., "Incorporation of paramagnetic, fluorescent and PET/SPECT contrast agents into liposomes for multimodal imaging," *Biomaterials*, vol. 34, pp. 1179–1192, 2013.

[40] Z. Yang, S. Zheng, W. J. Harrison et al., "Long-circulating near-infrared fluorescence core-cross-linked polymeric micelles: synthesis, characterization, and dual nuclear/optical imaging," *Biomacromolecules*, vol. 8, no. 11, pp. 3422–3428, 2007.

[41] S. K. Pandey, A. L. Gryshuk, M. Sajjad et al., "Multimodality agents for tumor imaging (PET, fluorescence) and photodynamic therapy. A possible "see and treat" approach," *Journal of Medicinal Chemistry*, vol. 48, no. 20, pp. 6286–6295, 2005.

[42] E. R. Ranyuk, N. Cauchon, H. Ali, R. Lecomte, B. Guérin, and J. E. Van Lier, "PET imaging using64Cu-labeled sulfophthalocyanines: synthesis and biodistribution," *Bioorganic & Medicinal Chemistry Letters*, vol. 21, no. 24, pp. 7470–7473, 2011.

[43] R. Lebel, N. Zarifyussefian, M. Letendre-Jauniaux et al., "Ultra-high sensitivity detection of bimodal probes at ultra-low noise for combined fluorescence and positron emission tomography imaging," vol. 8574 of *Proceedings of SPIE*, pp. 8574–8580, 2013.

[44] E. Ranyuk, R. Lebel, Y. Berube-Lauziere et al., "(68)Ga/DOTA- and (64)Cu/NOTA-phthalocyanine conjugates as fluorescent/PET bimodal imaging probes," *Bioconjugate Chemistry*, vol. 24, pp. 1624–1633, 2013.

[45] T. Priem, C. Bouteiller, D. Camporese et al., "A novel sulfonated prosthetic group for [F-18]-radiolabelling and imparting water solubility of biomolecules and cyanine fluorophores," *Organic & Biomolecular Chemistry*, vol. 11, pp. 469–479, 2013.

[46] J. A. Hendricks, E. J. Keliher, D. P. Wan, S. A. Hilderbrand, R. Weissleder, and R. Mazitschek, "Synthesis of [F-18]BODIPY: bifunctional reporter for hybrid optical/positron emission tomography imaging," *Angewandte Chemie International Edition*, vol. 51, pp. 4603–4606, 2012.

[47] H. Xu, K. Baidoo, A. J. Gunn et al., "Design, synthesis, and characterization of a dual modality positron emission tomography and fluorescence imaging agent for monoclonal antibody tumor-targeted imaging," *Journal of Medicinal Chemistry*, vol. 50, no. 19, pp. 4759–4765, 2007.

[48] C. Bernhard, M. Moreau, D. Lhenry et al., "DOTAGA-anhydride: a valuable building block for the preparation of DOTA-like chelating agents," *Chemistry—A European Journal*, vol. 18, pp. 7834–7841, 2012.

[49] S. C. Ghosh, P. Ghosh, N. Wilganowski et al., "Multimodal chelation platform for near-infrared fluorescence/nuclear imaging," *Journal of Medicinal Chemistry*, vol. 56, pp. 406–416, 2013.

[50] B. Wängler, R. Schirrmacher, P. Bartenstein, and C. Wängler, "Chelating agents and their use in radiopharmaceutical sciences," *Mini Reviews in Medicinal Chemistry*, vol. 11, pp. 968–983, 2011.

[51] T. W. Liu, J. M. Stewart, T. D. MacDonald et al., "Biologically-targeted detection of primary and micro-metastatic ovarian cancer," *Theranostics*, vol. 3, pp. 420–427, 2013.

[52] G. Ren, G. Blum, M. Verdoes et al., "Non-invasive imaging of cysteine cathepsin activity in solid tumors using a64Cu-labeled activity-based probe," *PLoS ONE*, vol. 6, no. 11, Article ID e28029, 2011.

[53] B. Behnam Azad, C.-F. Cho, J. D. Lewis, and L. G. Luyt, "Synthesis, radiometal labeling and in vitro evaluation of a targeted PPIX derivative," *Applied Radiation and Isotopes*, vol. 70, no. 3, pp. 505–511, 2012.

[54] Y. Zhang, H. Hong, G. W. Severin et al., "ImmunoPET and near-infrared fluorescence imaging of CD105 expression using a monoclonal antibody dual-labeled with 89Zr and IRDye 800CW," *The American Journal of Translational Research*, vol. 4, pp. 333–346, 2012.

[55] R. Cohen, M. A. Stammes, I. H. de Roos, M. Stigter-van Walsum, G. W. Visser, and G. A. van Dongen, "Inert coupling of IRDye800CW to monoclonal antibodies for clinical optical imaging of tumor targets," *European Journal of Nuclear Medicine and Molecular Imaging Research*, vol. 1, no. 31, 2011.

[56] H. Hong, Y. Zhang, G. W. Severin et al., "Multimodality imaging of breast cancer experimental lung metastasis with bioluminescence and a monoclonal antibody dual-labeled with Zr-89 and IRDye 800CW," *Molecular Pharmacology*, vol. 9, pp. 2339–2349, 2012.

[57] Y. Zhang, H. Hong, J. W. Engle et al., "Positron emission tomography and optical imaging of tumor CD105 expression with a dual-labeled monoclonal antibody," *Molecular Pharmaceutics*, vol. 9, no. 3, pp. 645–653, 2012.

[58] L. Sampath, S. Kwon, M. A. Hall, R. E. Price, and E. M. Sevick-Muraca, "Detection of cancer metastases with a dual-labeled near- infrared/positron emission tomography imaging agent," *Translational Oncology*, vol. 3, no. 5, pp. 307–318, 2010.

[59] M. A. Hall, M. B. Aldrich, A. Azhdarinia et al., "Quantifying multimodal contrast agent biological activity using near-infrared flow cytometry," *Contrast Media & Molecular Imaging*, vol. 7, no. 3, pp. 338–345, 2012.

[60] R. Ting, T. A. Aguilera, J. L. Crisp et al., "Fast18F labeling of a near-infrared fluorophore enables positron emission tomography and optical imaging of sentinel lymph nodes," *Bioconjugate Chemistry*, vol. 21, no. 10, pp. 1811–1819, 2010.

[61] X. Lin, J. Xie, G. Niu et al., "Chimeric ferritin nanocages for multiple function loading and multimodal imaging," *Nano Letters*, vol. 11, no. 2, pp. 814–819, 2011.

[62] S. H. Li, B. Goins, L. J. Zhang, and A. D. Bao, "Novel multifunctional theranostic liposome drug delivery system: construction, characterization, and multimodality MR, near-infrared fluorescent, and nuclear imaging," *Bioconjugate Chemistry*, vol. 23, pp. 1322–1332, 2012.

[63] A. Ruggiero, C. H. Villa, E. Bander et al., "Paradoxical glomerular filtration of carbon nanotubes," *Proceedings of the National Academy of Sciences of the United States of America*, vol. 107, no. 27, pp. 12369–12374, 2010.

[64] L. Stelter, J. G. Pinkernelle, R. Michel et al., "Modification of aminosilanized superparamagnetic nanoparticles: feasibility of multimodal detection using 3T MRI, small animal PET, and fluorescence imaging," *Molecular Imaging and Biology*, vol. 12, no. 1, pp. 25–34, 2010.

[65] M. Nahrendorf, H. Zhang, S. Hembrador et al., "Nanoparticle PET-CT imaging of macrophages in inflammatory atherosclerosis," *Circulation*, vol. 117, no. 3, pp. 379–387, 2008.

[66] D. W. Hwang, H. Y. Ko, S.-K. Kim, D. Kim, D. S. Lee, and S. Kim, "Development of a quadruple imaging modality by using nanoparticles," *Chemistry—A European Journal*, vol. 15, no. 37, pp. 9387–9393, 2009.

[67] J. Xie, K. Chen, J. Huang et al., "PET/NIRF/MRI triple functional iron oxide nanoparticles," *Biomaterials*, vol. 31, no. 11, pp. 3016–3022, 2010.

[68] Q. Liu, M. Chen, Y. Sun et al., "Multifunctional rare-earth self-assembled nanosystem for tri-modal upconversion luminescence /fluorescence /positron emission tomography imaging," *Biomaterials*, vol. 32, pp. 8243–8253, 2011.

[69] J. Zhou, M. Yu, Y. Sun et al., "Fluorine-18-labeled Gd3+/Yb3+/Er3+ co-doped NaYF4 nanophosphors for multimodality PET/MR/UCL imaging," *Biomaterials*, vol. 32, no. 4, pp. 1148–1156, 2011.

[70] K. Chen, Z.-B. Li, H. Wang, W. Cai, and X. Chen, "Dual-modality optical and positron emission tomography imaging of vascular endothelial growth factor receptor on tumor vasculature using quantum dots," *European Journal of Nuclear Medicine and Molecular Imaging*, vol. 35, no. 12, pp. 2235–2244, 2008.

[71] W. Cai, K. Chen, Z.-B. Li, S. S. Gambhir, and X. Chen, "Dual-function probe for PET and near-infrared fluorescence imaging of tumor vasculature," *Journal of Nuclear Medicine*, vol. 48, no. 11, pp. 1862–1870, 2007.

[72] F. Ducongé, T. Pons, C. Pestourie et al., "Fluorine-18-labeled phospholipid quantum dot micelles for *in vivo* multimodal imaging from whole body to cellular scales," *Bioconjugate Chemistry*, vol. 19, no. 9, pp. 1921–1926, 2008.

[73] M. L. Schipper, Z. Cheng, S.-W. Lee et al., "MicroPET-based biodistribution of quantum dots in living mice," *Journal of Nuclear Medicine*, vol. 48, no. 9, pp. 1511–1518, 2007.

[74] X. Michalet, F. F. Pinaud, L. A. Bentolila et al., "Quantum dots for live cells, *in vivo* imaging, and diagnostics," *Science*, vol. 307, no. 5709, pp. 538–544, 2005.